UNIVERSITY OF BIRMINGHAM

Development and application of high-field asymmetric waveform ion mobility spectrometry and mass spectrometry for the investigation of fibroblast growth factor signalling

by

Hongyan Zhao

A thesis submitted to the University of Birmingham for the degree of
DOCTOR OF PHILOSOPHY

School of Biosciences
The University of Birmingham
September 2016

Acknowledgment

I would like to thank my supervisors, Professor Helen Cooper and Professor John Heath for their constant support and help throughout the course of my studies. It was a great opportunity to get to work with experienced experts in related field. Many thanks go to Dr Andrew Creese and Dr Debbie Cunningham who always unselfishly share their expertise and experience.

I am grateful for Jinglei Yu and Cleidiane Zampronio for providing practical assistance. A special thanks go to colleague Gloria Ulasi who accompany me through various instrument troubleshooting. Thanks to all in Cooper Mass Spectrometry group and friends on 5th floor, Biosciences, for making my time at the university so pleasurable.

I would like to acknowledge Chinese Scholarship Council for funding my PhD.

To Yu, thank you for raising me up so I can see the mountains.

Abstract

The deregulation of FGF signalling is closely linked to many human diseases, including cancer. Through phosphorylation and dephosphorylation processes, FGF signalling is finely controlled. The thesis presented focuses on applying mass spectrometry tools to investigate FGF signalling using the breast carcinoma SUM52 cell line.

High-Field Asymmetric Waveform Ion Mobility Spectrometry (FAIMS) is a technique that separates and focuses ions at atmospheric pressure. It has been demonstrated that the application of LC-FAIMS-MS/MS results in increased signal-to-noise ratios and improved dynamic range in the analysis of complex proteomics samples. The LC-FAIMS-MS/MS method for large-scale quantitative analysis was optimized and the performance of LC-MS/MS and LC-FAIMS-MS/MS was compared. Results showed the two techniques shared good complementarity. The incorporation of FAIMS resulted in an increase in identifications of novel phosphosites and an increase in the identification of multiply-phosphorylated peptides. Next, a modified FAIMS interface was evaluated for proteomic analyses. This novel FAIMS device exhibited potential in enhancing proteomic analysis showing an increase in peak capacity and proteome coverage and a lower level of redundancy. Next, SRM was applied for accurate quantitation of 75 phosphopeptides in a time-resolved way. These candidates were selected from kinases in response to FGFR inhibition in a SILAC experiment performed on SUM52 and MFM233 cells, with peptides containing multiple sites of phosphorylation also included. The data revealed that these phosphorylation sites showed different associations with FGF1 stimulation. Expression patterns were clustered into early, mid- and late stage response.

Results presented in this work range from the large-scale investigation of phosphorylation events involved in FGF signalling, the application of a novel FAIMS interface and a targeted quantitation profile of the key phosphorylation events in FGF signalling, which would benefit both understanding and the potential mechanisms of FGF signalling.

Table of contents

List of figures and tables

Tables

Abbreviations

CID, collision induced dissociation

CV, compensation voltage

Da, Daltons

DV, dispersion voltage

EGFR, epidermal growth factor receptor

ESI, electrospray ionization

ETD, electron transfer dissociation

FAIMS, field asymmetric ion mobility spectrometry

FGFR, fibroblast growth factor receptor

GRB2, growth-factor-receptor-bound protein 2

IMS, ion mobility spectrometry

IS, internal standard

LC, liquid chromatography

MS/MS, tandem mass spectrometry

PDGF, platelet-derived growth factor receptor

PI3K, phosphoinositide 3-kinase

PLCγ, phospholipase Cγ

PTM, posttranslational modification

QqQ, triple quadrupole mass analyser

Ras/MAPK, rat sarcoma/mitogen-activated protein kinase

RTK, receptor tyrosine kinase

SCX, strong cation exchange

SFK, Src family kinase

SILAC, stable isotope labelling of amino acids in cell culture

S/N signal-to-noise ratio

SOS, Son of Sevenless

SRM, selected reaction monitoring

VEGFR, vascular Endothelial Growth Factor Receptor

CHAPTER 1

INTRODUCTION

1.1 Overview

Fibroblast growth factor (FGF) ligands and receptors play important roles in the regulation of cell growth, cell division, angiogenesis and tumour growth. Accumulating evidence demonstrates that deregulation of FGF signalling is closely related to many human diseases including cancer. Through phosphorylation and dephosphorylation processes, FGF signalling is propagated through a series of receptor proteins, scaffolding proteins and signal mediators, leading to activation of multiple downstream pathways.

Tandem mass spectrometry (MS/MS) combined with pre-fractionation and phosphoenrichment is a well-established workflow for large-scale quantitative phosphoproteomic analysis. One of the major challenges in phosphoproteomic research is to map sites of modification in multiply-phosphorylated peptides. In recent years, ion mobility spectrometry has emerged as an attractive technique for specific and global proteome profiling. Field asymmetric waveform ion mobility spectrometry (FAIMS) is a gas phase separation technique based on the differences in ion mobility in high and low electric fields. Coupled with liquid chromatography (LC)-MS/MS, FAIMS has been shown to enhance proteomic analyses by extending proteome coverage, improving signal-to-noise and separating isomeric peptides.

Following the discovery phase provided by a shotgun strategy, a targeted quantitation method is needed for biological interpretation. For sensitive detection and accurate quantitation of selected peptides, selected reaction monitoring (SRM) has emerged as the method of choice that complements the discovery capabilities of shotgun approach. Consistently identified and precisely quantified data across multiple samples provide the basis for a system biology interpretation, a requirement that can be achieved by SRM.

The aim of this chapter is to provide background on current research and development in FGF signalling (section 1.2), an overview of mass spectrometry (section 1.3), proteomics by mass

spectrometry (section 1.4) and FAIMS (section 1.5), which forms the basis for the work presented in this thesis: investigation of the application of FAIMS to increase phosphoproteomic coverage in FGF signalling (Chapter 4) and the employment of targeted approaches for accurate quantitation (Chapter 6).

1.2 Fibroblast growth factor (FGF) and FGF signalling

Fibroblast growth factor was first discovered in bovine pituitary extracts by Armelin *et al.* in 1973 and it was found to introduce the proliferation of fibroblasts[1]. Over forty years, extensive research has been carried out in order to reveal the functions of FGF and the signal transduction of FGF pathway[2]. It has been shown that FGF and the FGF signalling pathway play diverse roles in cell division, cell growth and maturation, angiogenesis, wound healing and tumour growth[3]. Accumulating evidence suggests the deregulation of FGF signalling has been associated with many human diseases, including cancer[4].

1.2.1 FGFs

FGFs are glycoproteins that bind to cell surface receptors to initiate signalling. The mammalian FGF family comprises 23 members[5]. They are structurally related and all share a highly conserved region of 120 amino acids, which is responsible for the interaction with FGF receptors[2]. This conserved region forms 12 anti-parallel β-strands, which fold into a cylindrical barrel. Many FGFs contain a signal peptide region for secretion into the extracellular environment.

An important feature of FGF family is that they have a strong affinity for heparin and heparin-like glycosaminoglycans (HLGAGs). Current understanding holds that the binding to heparin

and HLGAGs could protect FGFs from degradation, leading to FGFR dimerization and subsequent activation of the intracellular kinase domain[6]. Although not all members are receptor activating (except FGF11, 12, 13 and 14), or have fibroblast stimulation activities (FGF-7), they are still clustered as FGF family members as they are structurally related.

Generally, FGFs are secreted glycoproteins that are localized to the extracellular matrix[7]. Most FGFs (except FGF1 and FGF2) are produced in endoplasmic reticulum (ER) and utilize the signal peptide for secretion into extracellular matrix. In order to signal, FGFs are released from the extracellular matrix and free FGFs can bind with low-affinity receptors, such as heparin. Heparin can guide FGFs to FGFR and stabilize the ligand-receptor complex. Some FGF members, such as FGF1 and FGF2, have also been found in nucleus and nucleolus in addition to their extracellular and transmembrane locations[8]. FGF1 and FGF2 contain a nuclear localization signal (NLS), which regulates their translocation of FGFs after internalization. This provides a novel mechanism for FGF-mediated nuclear events, which are regulated through a direct interaction with nuclear effectors[9].

1.2.2 FGFR

1.2.2.1 Structure

FGFs activate FGF signalling by binding with four tyrosine kinase receptors (FGFR1, FGFR2, FGFR3 and FGFR4), which are responsible for transmitting the extracellular signal to cytoplasmic environment. The members of FGFR family are composed of an extracellular ligand-binding domain, a transmembrane spanning domain, and an intracellular domain containing a protein tyrosine kinase (TK) core. The extracellular portion contains three immunoglobulin (Ig)-like domains. The second and third Ig domains interact directly with the FGF ligand[10]. The intracellular region possesses a juxtamembrane domain, two tyrosine kinase

domains (which are split by a kinase insert sequence) and a C-terminal tail. This protein structure places FGFR in the Ig superfamily of receptors and the family of receptor tyrosine kinase (RTK), such as EGFR family (epidermal growth factor receptor), PDGF family (platelet-derived growth factor receptor)[11].

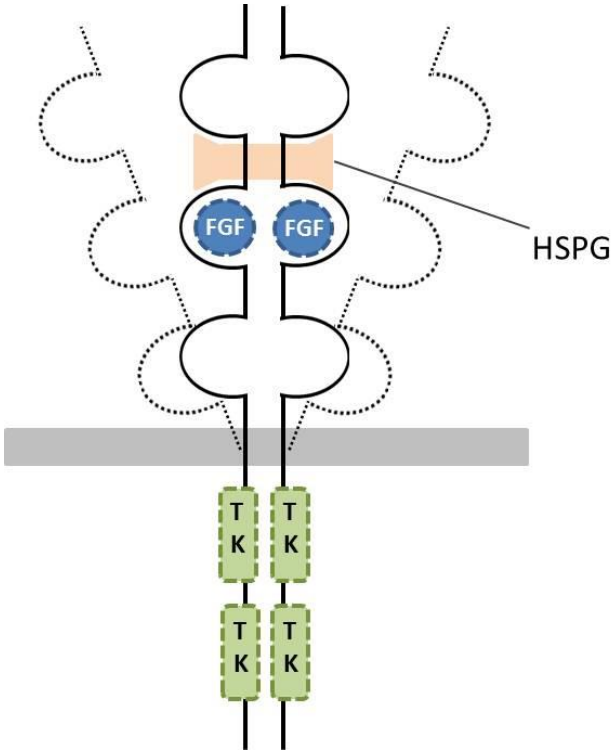

Figure 1.1 Schematic structure of FGFRs (Adapted from Turner *et al.*[12])
FGFR consists of extracellular domain, transmembrane domain and tyrosine kinase (TK) domain. The dotted lines indicates FGFR in monomer status.

1.2.2.2 FGFR specificity

FGFR isoforms, arising from various alternative splicing events occurring both in the extracellular and the intracellular domain of receptors, are crucial in modulating ligand-binding specificity and receptor activity[13]. Generally, each receptor can be activated by different FGFs and most of the FGFs can bind with multiple receptors (with the exception of FGF3, 7 and 9 which can bind with one FGFR member). Differences in splice variants in the extracellular domain are often associated with the specificity of the receptor. For instance, shortened FGFR2

splice variants in the C-terminal tail were observed in several cancer cell lines. It was established that the C-terminal deletion is able to induce conformational changes in the receptor, leading to accumulated level of the receptor at cell surface and thus enhanced signalling capacity[14].

Also, the spatial and temporal expression patterns of FGF and FGFR are jointly responsible for regulation of the specificity of the FGF-FGFR interaction[15]. For instance, the FGFR IIIb and FGFR IIIc splice isoforms in Ig-like domain III are regulated in a tissue-specific manner. The FGFR IIIb isoform is expressed exclusively in epithelial tissues and the FGFR IIIc isoform is preferentially expressed in mesenchymal tissues[16].

1.2.2.3 Phosphorylation of receptor

Receptor tyrosine kinase (RTK) represents a family of cell-surface proteins that can be activated by ligands in cell signalling processes. Like other RTKs, the intracellular tyrosine domain of FGFR catalyses autophosphorylation of the receptor itself and phosphorylation of RTK substrates (see Figure 1.2). For FGFR, this was first suggested by the finding that an elevated expression level of tyrosine phosphorylation was observed upon FGF-1 and FGF-2 stimulation in 3T3 fibroblasts, by Western blot using phosphotyrosine antibody[17]. FGF stimulation is able to induce an immediate response in phosphorylation of the receptor and tyrosine phosphorylation of FGFR was found to occur within 30 seconds of FGF stimulation[18].

In FGFR1, seven phosphotyrosine sites have been identified in the cytoplasmic domain (Figure1.2): Y463 in juxtamembrane (JM) domain, Y583 and Y585 in the kinase insert (KI) domain, Y653 and Y654 in the activation loop of the second tyrosine kinase domain[19], Y730 and Y766 in the C-terminal tail[20]. The activation of FGFR1 has been described as a temporal phosphorylation mechanism occurring in the intracellular domain[21]. Of these seven tyrosine

sites, the phosphorylation of Y653 serves as the initiation reaction, which activates the kinase by 50-100 fold, and the phosphorylation of Y654 can increase kinase activity by up to 500-1000 fold. Followed by the activation of two tyrosine sites in the activation loop, juxtamembrane region Y463, kinase insert Y586/Y588, and in the C-terminal region Y769 are also phosphorylated to promote further receptor activation or serve as the recruitment site for downstream signalling proteins.

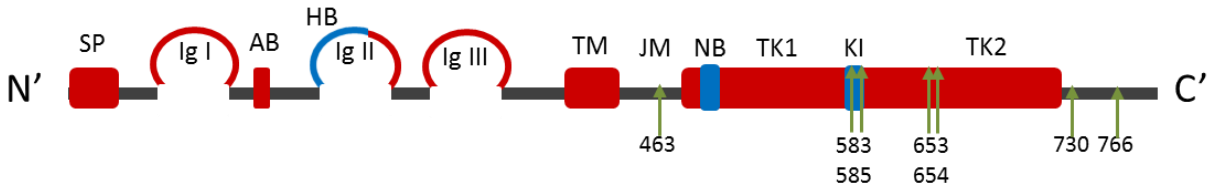

Figure 1.2 Structure and phosphorylation sites of FGFR1
FGFR1 comprises an extracellular domain, a transmembrane domain (TM) and a cytoplasmic domain. Signal peptide (SP) sits in N-terminal. There are 2 or 3 Ig-like domains in the extracellular domain. The acid box (AB) locates between Ig-I and Ig-II. Heparin binding domain is in Ig-II. Followed by juxtamembrane domain (JM) are two tyrosine kinase (TK) subdomains, including a nuclear binding domain (NB) and a short kinase insert (KI). Seven tyrosine phosphorylation sites have been identified so far: Tyr463 in JM, Tyr582 and Tyr585 in KI, Tyr653 and Tyr654 in TK2, Tyr730 and Tyr766 in C-terminal tail.

1.2.3 FGF signalling

1.2.3.1 Activation of FGF signalling

The FGF signalling is a typical RTK-induced signalling cascade (see Figure 1.3). The FGFs exert their biological functions through the binding with Ig-like domain (II and III) of FGFR, with the assistance of heparin[22]. Binding of FGFs to receptors induces dimerization of the receptors, which will cause a conformational shift in the intracellular domain of the receptor. In contrast to the non-dimerized form, the conformational change opens the kinase domain for ATP binding. It activates FGFR and leads to *trans*-autophosphorylation reaction in the receptor, where phosphorylation occurs through the other kinase in the dimer. Following phosphorylation in the activation loop (e.g. Y653 and Y654 in FGFR1), the activated FGFR is capable of catalysing the phosphorylation of multiple tyrosine residues in the kinase domain.

The phosphorylated tyrosine residues on the receptor can function as regulation sites or docking sites for adaptor proteins. FGFR substrate 2 (FRS2), a key adapter protein in FGF signalling, are recruited to the FGF-FGFR complex in this step[23]. FRS2 binds with the juxtamembrane region of FGFR. The recruitment of FRS2 initiates the phosphorylation of itself and FRS2 can further recruit downstream molecules and adaptor proteins via phosphorylation events.

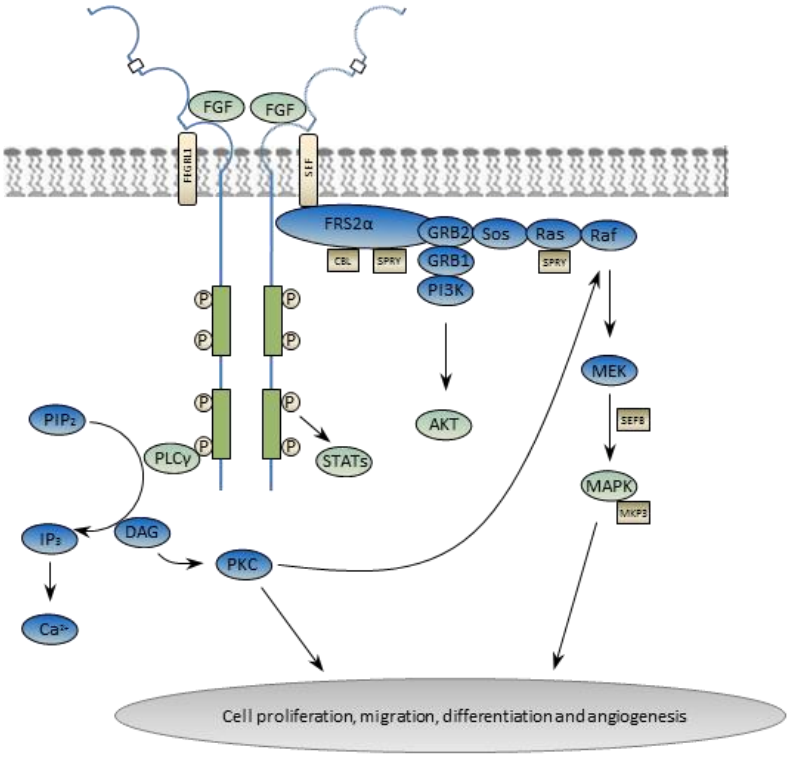

Figure 1.3 FGFR signalling network (Adapted from Turner and Grose[12])
Upon ligand binding, FGFRs at plasma membrane dimerise and trans-autophosphorylate, thus triggering series of phosphorylation and dephosphorylation events in various signalling proteins.

Phosphorylation events hold the key to understand the signalling events downstream of FGFR. For instance, phosphorylation of the active sites of kinases often significantly alter the binding capacity for substrates[24]. At the next level, specificity is regulated by the interaction between the docking motif of the substrate and the kinase. In some cases, recruitment of substrates to kinases require phosphorylation of an adjacent or distant residue from the active site[25].

One of the most widely accepted models for FGF signal transduction is the diffusion-based model (also termed canonical model)[26]. It proposes the receptors are monomers in the absence

of ligands, and dimerise and trans-phosphorylated each other upon ligand binding. The other model postulates that FGF receptors form dimers even in the absence of ligands, but ligand binding triggers the structural changes of the dimers and significantly increases FGFR phosphorylation. Also, different ligand binding (e.g. FGF1 and FGF2) can cause different effects on the receptor structure, therefore induce specific biological responses[27].

1.2.3.2 Downstream of FGF signalling

The main downstream pathways of FGF signalling include the Ras/MAPK (rat sarcoma mitogen-activated protein kinase) pathway whose activation is mediated by growth-factor-receptor-bound protein 2 (GRB2) and Son of Sevenless (SOS), the PI3K (phosphoinositide 3-kinase)/AKT pathway activated by GRB2, and the Src pathway that initiated directly by FRS2[28–30]. In addition, instead of propagating the signal through FRS2, the tyrosine site (e.g. Y766 in FGFR1) in the kinase domain of FGFR can directly act as the recruiting site for PLCγ (phospholipase Cγ), leading to the recruitment of more partner proteins. These signalling cascades form a complex network, which regulates a wide array of biological processes and also mediates the FGF signal transduction by regulation of phosphorylation of downstream signalling molecules.

In humans, the activation of the Ras/MAPK pathway is a highly conserved mechanism in response to FGFs, while activation of other downstream pathways is subject to cell type or tissue. The maintenance of certain levels of phosphorylation of Ras and MAPKs is critical to enable phosphorylation of target substrates. A number of inhibitors, targeting upstream proteins (e.g. FGFRs or Ras), were developed to block the activation of Ras/MAPK pathway.

Another complex activated through GRB2 is the PI3K/AKT pathway, which further activates AKT-dependent anti-apoptotic pathway. The PI3K/AKT pathway also responds to a wide

variety of stimuli, such as RTKs, B/T cell receptors, integrin, G-protein-coupled receptors and other receptors that catalyse the production of phosphatidylinositol (3,4,5) trisphosphate (PIP3) by PI3K[31]. Downstream effects of AKT are primarily associated with the regulation of cell cycle, cell survival and metabolism via mTOR pathway[32].

Non receptor Src family kinases (SFKs) are regulators of FGF signalling[33]. Of Src family, Src, Fyn and Yes are found universally expressed in human cells while other members are expressed in specific tissues or particular development stages. In addition to FGF signalling, SFKs are involved in signalling by many RTKs, including PDGF receptor (PDGF-R)[34], epidermal growth factor receptor (EGFR)[35] and insulin-like growth factor-1 receptor (IGF-1R)[36]. Their participation is particularly important in the regulation of DNA synthesis and endocytosis. It has been shown the elevated levels of dephosphorylation of Tyr527 in Src, which has been detected in various cell lines, transforms Src to become abnormally active.

An important aspect of FGFR-induced cellular events is through PLCγ-mediated mitogenesis. Activation of PLCγ is through direct binding to a conserved phosphotyrosine residue in C-terminal tail of FGFR[37]. PLC then hydrolyses phosphotidylinositol-4,5-diphosphate to inositol-1,4,5-trisphosphate (IP3) and diacylglycerol (DAG). IP3 stimulates intracellular calcium release, while DAG activates protein kinase C (PKC)[38].

1.2.4 FGF signalling and cancer

1.2.4.1 Current understanding of FGF signalling and cancer

FGFR2 has been extensively examined in its relationship with breast, gastric and bladder cancer [39–42]. The FGFR2 gene is located on human chromosome 10 and it encodes FGFR2 protein which shares highly conservative sequence with the FGFR family members. Due to

splicing of the third Ig-like domain, there are two natural isoforms of FGFR2: FGFR2IIIb and FGFR2IIIc. The IIIb isoform is expressed exclusively in epithelial tissue and the IIIc isoform is preferentially expressed in mesenchymal tissue. Triple-negative breast cancer (TNBC) cell lines, for example SUM52 and MFM223, show FGFR2 amplification. FGFR2 amplifications have also been described in approximately 3% -10% of primary gastric cancers patients and usually associated with the poor prognosis and low survival rate[43]. Decreased levels of FGFR2-IIIb have also been reported in a number of bladder cancer cases, which suggests the potential role of FGFR2 as a tumour suppressor in bladder carcinomas[44,45].

A genome-wide association study (GWAS) has identified several SNPs (single nucleotide polymorphism) in FGFR family as novel breast cancer susceptibility loci[46]. Eight SNPs located in intron 2 of FGFR2 have attracted extensive attention. They change binding affinity of transcription factors directly downstream of FGFR[47]. A SNP in FGFR4 has been shown to contribute to more aggressive behaviour and poor prognosis in several types of cancer, including breast cancer[48].

Mutated FGFRs have also been found to be associated with several developmental syndromes, including cancer[49]. Mutations in cytoplasmic and tyrosine kinase domain of FGFR1 and FGFR2 have been discovered in endometrial cancer, which alter the ligand specificity and kinase activity respectively[50]. In some circumstances, mutation can cause loss-of-function[51].

As a result of gene splicing, novel splice variants of FGF family are identified to be associated with cancer. For example, an FGFR2 variant with a shortened C-terminus has been identified in several cancer cell lines. The study of rat osteosarcoma cell line has shown the alteration of C-terminus resulted from the fusion of FGFR2 to a novel protein due to chromosomal rearrangement. The fusion protein acts as dimer leading to the autophosphorylation of tyrosine domain. Therefore this protein can cause continuous signalling in the absence of FGFs and thus enhanced signalling capacity[52].

1.2.4.2 Therapeutic development

Upstream intervention of FGF signalling primarily involves inhibiting ligand-receptor binding. FGF ligand traps (*e.g.* FP1039), a fusion protein comprised of the extracellular domain of FGFR fused with the Fc region of IgG, was developed and is being tested for clinical application[53]. Another approach to inhibit ligand binding is to use peptide mimics, which is particularly useful for patients with FGFR amplification[54].

A number of tyrosine kinase inhibitors targeting FGFR activity are in early clinical development. These inhibitors are multi-targeting ATP-competitive inhibitors. As kinase domains of RTKs are similar in structure, these inhibitors are not specific and activity of VEGFRs and PDGFRs could also be affected[51]. Dovitinib is a potent TKI with anti-angiogenic activity through the inhibition of FGFR, VEGFR, and PDGFR. Dovitinib is in phase II clinical trials for advanced breast and endometrial cancers and phase III clinical trial for renal cell carcinoma. The second generation inhibitors target FGFRs with selectivity over other kinases. For example, AZD 4547 shows affinity with FGFRs approximately 120-fold higher than VEGFRs. AZD4547 is in phase II clinical trial for breast cancer[55]. SU5402 is one of the compounds that have been designed as FGFR specific inhibitors[56]. SU5402 occupies the same region in FGFRs as ATP to inhibit FGFR tyrosine phosphorylation and does not affect kinase activity of VEGFRs and PDGFRs. It should be noted that the selective inhibitors also exhibits toxicities, including hypertension, cardiovascular events and some FGFR-specific toxicities[57]. The development of specific toxicity management protocols is required and a few projects are on the way[58]. Monoclonal antibodies are an alternative to avoid the side effects of multi-targeting inhibitors. Antibodies targeting FGFR1-IIIc and FGFR3 are in preclinical development[55].

Proteins downstream of FGFRs also participate in multiple signalling, therefore it is difficult to target them to inhibit FGF signalling. Thus, targeting downstream effectors is aiming at more specific processes or pathways. In this thesis, to inhibit Src family kinase, dasatinib is used. Dasatinib is a small molecule inhibitor of Src and Abl proteins and has already been used in treatment of imatinib refractory chronic myelogenous leukemia (CML)[59]. It is not clear whether it can be used as breast tumour suppressor, but its association with FGF signalling has made it promising for clinical trial for breast cancer patients.

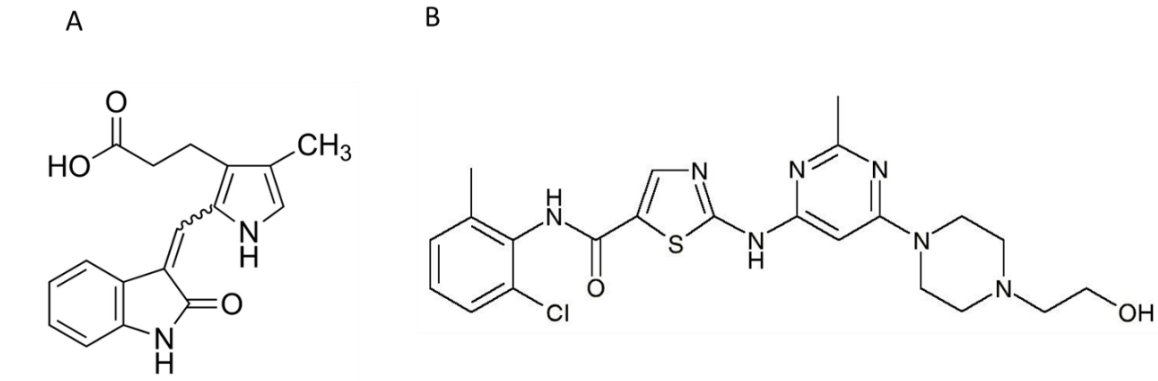

Figure 1.4 Chemical structures of (A) SU5402 and (B) dasatinib

Previous studies have provided a valid rationale to further explore the potency of FGFR-targeting drugs in their targeting specificity, toxicity and anti-tumour activity. Although the most effective anti-tumour activity was observed with multi-targeting kinase inhibitors, selective inhibitors present less toxicity and non-FGF related problems. In addition to small molecule inhibitor, the application of small interfering RNAs, the combination of FGFR and other kinase inhibitors has shown preliminary progress in targeting specific FGFR events[60].

1.2.4.3 Future prospects

Progress is being made in understanding the association between FGF signalling and development of cancer, and therapeutic strategy, e.g. key signalling molecules responsible for cancer pathogenesis and progression, response of FGF signalling to chemotherapy and

development of FGFR inhibitor in combination with conventional therapies. However, this is still the early phase of understanding of how FGF signalling can be targeted in development of cancer. Understanding the mechanism underlying intracellular responses induced by FGF signalling requires knowledge of receptor activation, signal transduction cascades and the downstream regulation of gene expression, which are modulated by phosphorylation and dephosphorylation at different levels.

Functional interpretation of these phosphorylation events requires detailed analysis of specific residues or combinations of residues. Much attention has been focused on individual residues and multiple/combinatorial phosphorylation events have attracted less attention because it is harder to identify these peptides. Current understanding suggests that it is more challenging to detect doubly- and multiply-phosphorylated peptides than singly-phosphorylated peptides due to their low stoichiometry and poor binding ability to chromatographic columns. Whereas, deciphering the mechanisms of FGFR signalling requires knowledge of multiply-phosphorylated peptides as the adjacent phosphosites may play regulatory roles. Thus, one of the major challenges in intracellular cell signalling research is to map sites of modification in multiply-phosphorylated peptides.

Liquid chromatography coupled with tandem mass spectrometry, combined with pre-fractionation and phosphoenrichment is a well-established workflow for large-scale quantitative phosphoproteomic analysis[61]. Although progress has been made, low phosphoproteome coverage, limited dynamic range and co-elution of peptide isomers still remain a challenge. With the development in phosphopeptide enrichment protocols, liquid chromatography, combinations of MS/MS approaches and development of novel data handling software, a more profound understanding of FGF signalling and its role in cancer development will emerge.

1.3 Mass spectrometry

Mass spectrometry (MS) is an analytical technique that enables identification and quantitation of molecules by their measuring mass-to-charge ratio (*m/z*)[62]. As it is a sensitive technique that offers both low detection limits and high mass accuracy, mass spectrometry is an invaluable tool for study in a range of fields, including organic chemistry, proteomics, metabolomics and clinical testing etc. In addition, high throughput analysis is possible by mass spectrometry[63].

In mass spectrometric analysis, samples are ionised and subject to gas phase environment for separation based on *m/z* values. Tandem mass spectrometry (MS/MS) technique allows the multiple stages of isolation and fragmentation in time and space. Charged ions (termed precursor ions) are isolated according to their *m/z* values, typically by subjecting them and accelerating them into an electric field. Therefore, the isolation and fragmentation of the precursor ions occurs in multiple stages. MS/MS results will be displayed in spectra with the relative abundance of detected fragment ions and a function of the *m/z* ratio. Mass spectrometers comprise three parts: an ion source that ionizes the sample, mass analyser that separates ions based on *m/z* ratios and detector that records the signal. Modern mass spectrometers have undergone immense technological innovations during recent decades allowing for applications in analyses of drugs, peptides, proteins, carbohydrates, DNA and many other biologically relevant molecules[64–66]. Separation techniques combined with mass spectrometry have been widely used to enhance resolving power in the analysis of complex samples. Increasing application of mass spectrometry to complex biological samples has driven data analysis software development. In the following text, instrumentations and applications of mass spectrometry will be introduced in more detail.

1.3.1 Ionization

The ionization process enables molecules to acquire a negative or positive charge through interactions with chemicals, light or electrons. The earliest ionization techniques were electron ionization (EI)[67] and chemical ionisation (CI)[68], which tend to induce fragmentation thus limiting formation of stable molecular ions. These two techniques are primarily used in the analysis of organic molecules. Fast atom bombardment (FAB) is a soft ionization technique, which yield little or no fragmentation, thus allowing the analysis of molecules larger than 25,000 Da. It uses a beam of high energy atoms to desorb ions from a surface[69]. When highly energetic ions are used instead of atoms, this method is also known as liquid secondary ion mass spectrometry (LSIMS)[70]. More recent techniques, matrix-assisted laser desorption ionization (MALDI)[71] and electrospray ionization (ESI)[72] are also soft ionization techniques, similar to FAB. The key feature of MALDI is the use of a matrix to assist desorption. Prior to MALDI ionization, the sample is mixed with an organic matrix on a metal plate. The mixture is dried and the matrix co-crystallised with the sample. A laser beam at a specific wavelength is then directed at the sample-matrix mixture, causing the matrix to absorb energy, which enables protons to be transferred from matrix to the sample and ionise the sample. In 2002, the developers of MALDI (Koichi Tanaka) and ESI (John Fenn) were awarded Nobel Prize in Chemistry 'for their development of soft ionization methods for mass spectrometric analyses of biological macromolecules'. Currently, MALDI is routinely used in tissue imaging and identification of a wide variety of analytes in tissues[73].

ESI is suitable for both organic and biological molecules and was used in the work presented herein. In ESI, samples are usually dissolved in a mixture containing volatile organic solvents (e.g. methanol or acetonitrile) and an acidic buffer. Typically, the sample will go through three major stages. First, the sample solution becomes charged when passing through a thin metal capillary at a certain voltage. Second, as the surface tension of the droplet overcome the

electrostatic repulsion, the charged droplets become unstable when Rayleigh limits is reached, leading to evaporation of solvent from the charged droplets and formation of decreasing charged droplets. There are two main models describing the third stage of ESI process (see Figure 1.5): the charge residue model (CRM)[74] and the ion evaporation model (IEM)[75]. The CRM model suggests as the remaining solvent evaporates, the gas phase ions are produced as the size of the droplet decreases into a droplet containing only one macromolecule. The IEM model proposes that as the droplet decreases to a radius of 10 nM, the strength at the surface of the droplet can assist the field desorption and allow the formation of gas phase ions. The exact mechanism of ESI is still under debate. However, there is a consensus among scientists that a combination of these two models occur during ESI.

ESI is able to preserve multiply charged ions, facilitating the identification of large molecules. Due to multiple charging, the m/z values of multiple charged ions become lower and fall into the mass range of common mass analysers. Thus, analysis of protein and macromolecules is made possible by applying ESI in modern mass spectrometer.

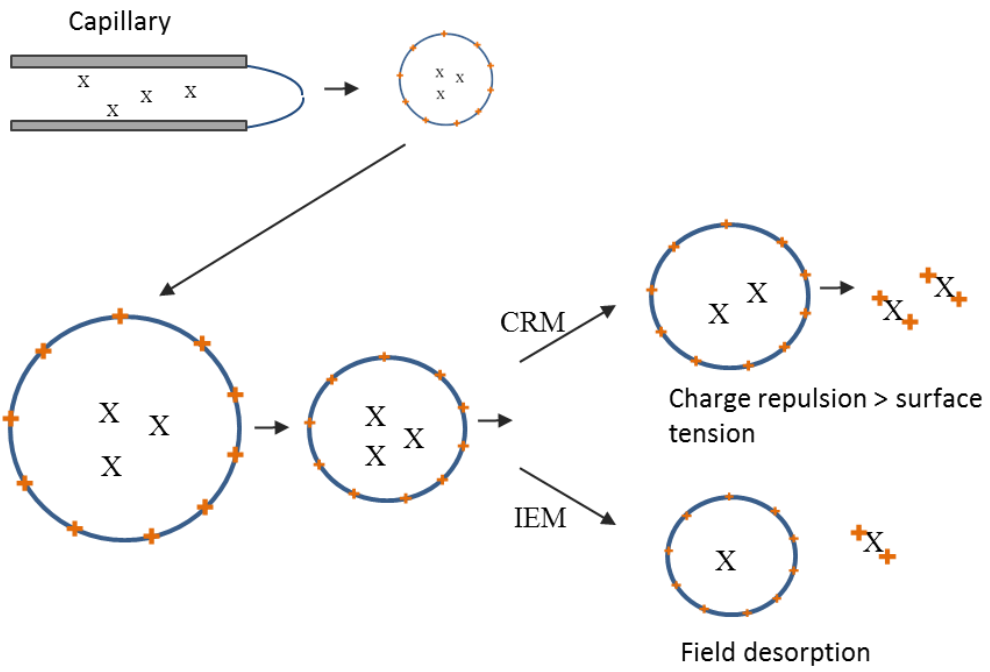

Figure 1.5 Electrospray ionisation: the proposed model of CRM and IEM、

1.3.2 Mass analysers

Once in the gas phase, ions are transferred to the mass analyser for isolation or/and separation based on *m/z* values. Several types of mass analysers that utilise different mechanisms to separate ions, either by static or dynamic electric or/and magnetic fields or in combination, have been developed. There are three main classes of mass analyser. One type of mass analyser separates ions in space according to their *m/z* values, i.e., the time-of-flight (TOF)[76] analyser. Another type of mass analyser scans for a particular *m/z* value while removing all the other ions, such as the quadrupole mass analyser[77]. Thirdly, mass analysers can measure the resonant oscillations of ions in electric/magnetic fields, such as the linear ion trap[78], 3D ion trap[79], Fourier transform ion cyclotron resonance (FTICR)[80] and orbitrap[81] mass analyser. The mass analysers which have been employed in this work are the dual-pressure linear ion trap, the Orbitrap mass analyser and the triple-quadrupole mass analyser and a detailed introduction is given in Section 1.3.4.1 and 1.3.4.2.

1.3.3 Tandem mass spectrometry

Tandem mass spectrometry (MS/MS) enables characterisation of the structure of an analyte, and is especially useful in the analysis of peptides, intact proteins and post-translational modifications. In mass spectrometry-based proteomic analyses, MS/MS of a peptide provides information on peptide sequence and structure. There are different fragmentation techniques available. The most commonly used are collision induced dissociation (CID)[82,83], electron capture dissociation (ECD)[84] and electron transfer dissociation (ETD)[85]. CID and ETD are the most widely used fragmentation techniques in proteomics and solely used in this thesis, and therefore are discussed further below.

1.3.3.1 Collision induced dissociation

In CID (also referred to as collision activated dissociation, CAD), precursor ions are accelerated by electric potentials to high kinetic energy and collided with inert gas (typically helium, nitrogen or argon). During the collision, a certain amount of kinetic energy is converted into internal energy resulting in bond breakage and fragmentation of molecules. The mobile proton model proposed by Gaskell and Wysocki best describes the mechanism of CID fragmentation on peptides and proteins[86,87]. The model proposes that a proton is mobile between various protonation sites and the actual fragmentation site is the result of competition between various fragmentation pathways. The energy required for proton mobility depends on gas-phase basicity of the group. The proton is preferentially mobilised to N-terminal or basic site, e.g. lysine or arginine, over non-basic amino acid, leading to charge-directed fragmentation. Therefore, as the proton migrates to amide nitrogen, which leads to weakening of the amide bond and makes the adjacent carbonyl group susceptible to attack, peptides tend to undergo N-Co breakage along the peptide backbone, which produces a series of *b* and *y* fragment ions (Figure 1.6)[88,89].

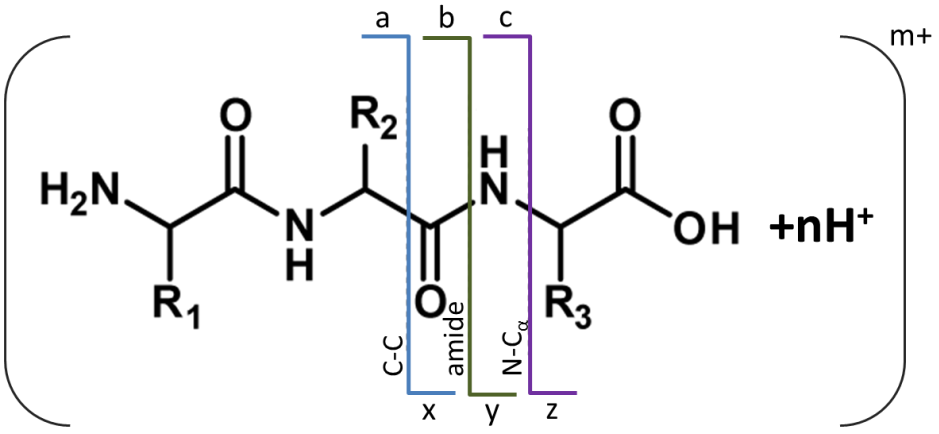

Figure 1.6 Dissociation products of protonated peptides
CID produces *b* and *y* type anions by heterolytic amide bond breakage. ETD and ECD produces *c* and *z* type ions by homolytic bond cleavage.

1.3.3.2 Electron transfer dissociation

ETD induces fragmentation by transferring electrons to positively charged precursor ions to induce specific N-Cα breakage along the peptide backbone, while the side chains and peptide modifications are left intact[85,90]. The ETD radical anions (e.g. anthracene or fluoranthene) are required as strong bases or/and reagents for proton abstraction.

The ETD fragmentation mechanism can be described by the Utah-Washington mechanism, developed independently by two groups[91,92]. In a peptide, the electron attachment to amide π* orbital makes it a strong base with a strong affinity to protons. The amide group is then able to participate in proton abstraction, leading to the breakage of N-Cα bond and generation of *c* and *z* ions, as shown in Figure 1.7. The proton abstraction is where the two mechanisms differ. The Washington mechanism proposes the initial electron capture takes place at a charge site. However, the Utah mechanism suggests that capture occurs directly in a stabilised orbital (S-S σ* or amide π* orbital), leading to peptide fragmentation.

ETD has been seen as a complementary technique to CID fragmentation, as ETD (a) favours fragmentation of large peptides and intact proteins, and (b) is able to preserve labile PTMs on backbone fragments for PTM characterisation. Combinations of CID and ETD fragmentation and alternating CID/ETD fragmentation methods both proved to improve sequence coverage and PTM identification than individual CID and ETD fragmentation alone[93].

1.3.4 Hybrid instruments

1.3.4.1 Hybrid Orbitrap mass spectrometer

The LTQ Orbitrap Velos ETD mass spectrometer is a hybrid mass spectrometer comprising a dual-pressure linear ion trap (the linear trap quadrupole, LTQ) and the Orbitrap analyser[94]. Figure1.8 shows the schematic diagram of an LTQ Orbitrap Velos ETD mass spectrometer.

The LTQ is used for for ion trapping, ion selection, ion fragmentation and low resolution scanning. In the LTQ, ions are trapped (and fragmented) in the first ion trap with high gas (helium) pressure (-5×10^{-3} Torr) before passed to the second ion trap with low gas pressure (-4×10^{-4} Torr) for fast scanning. The LTQ comprises linear ion traps (LIT) which create two dimensional (2-D) quadrupole fields[95]. The 2-D ion trap uses an oscillating field (radio frequency field, RF field) to trap ions radially and a static electric field applied to the tip of the rods to trap ions axially in two dimensions. A 2-D ion trap comprises of four parallel electrode rods and an opposite electrical potential applied to the end electrodes with the same polarity. In the 2-D trap, the ions collide with inert gas and travel along the *z* axis through the centre of rods owing to the application of a balanced dipolar field. In the *xy* plane, the ions are oscillated due to a RF potential on the rods. The application of DC voltage to the rods allows the ions to be trapped. Within an LIT, ions can be ejected between the rods and the exit lens either axially or radially by applying an AC voltage. The toroidal shape of the ion trap increases the ion trapping capacity, as well as increased the scanning speed.

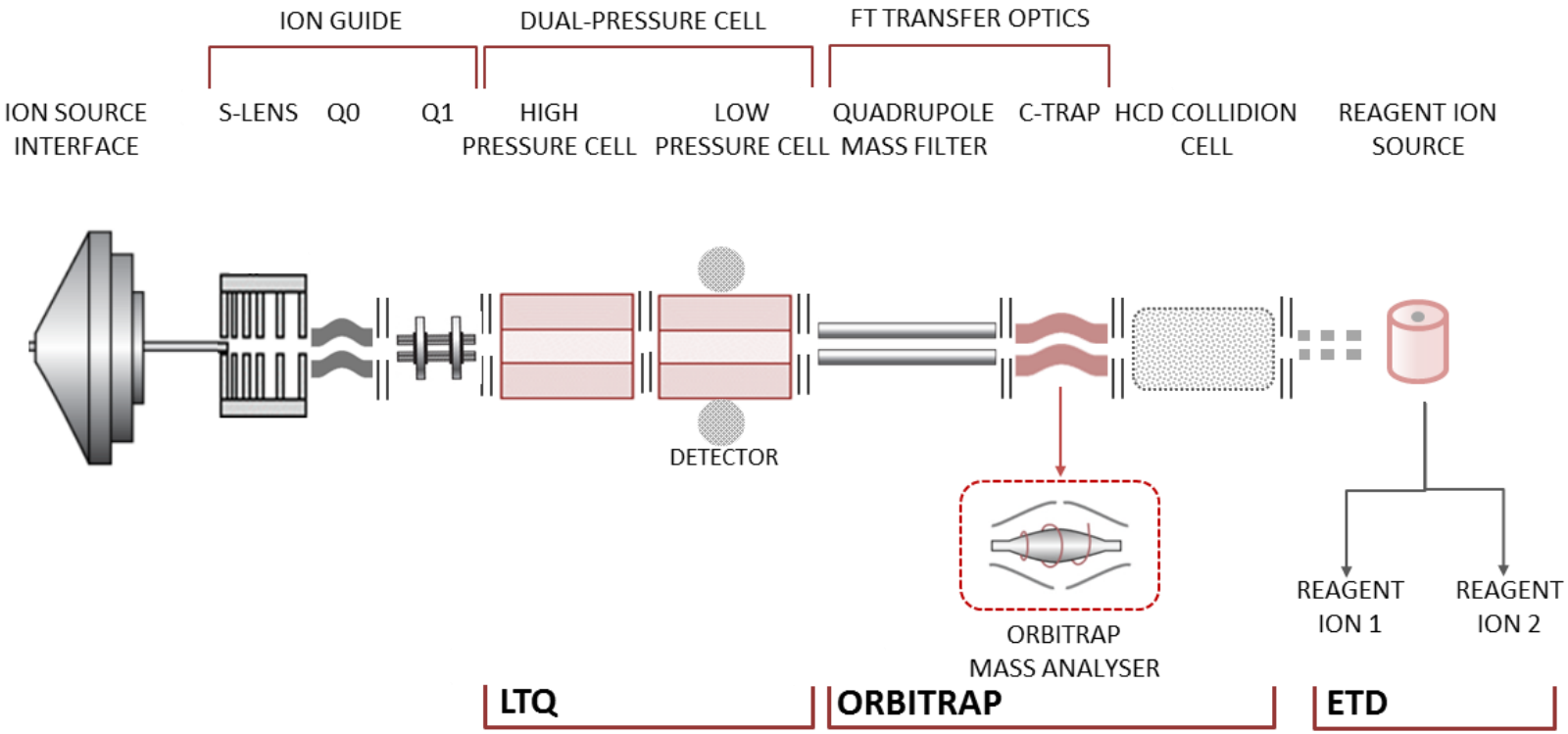

Figure 1.7 Schematic of LTQ Orbitrap Velos ETD mass spectrometer (Adapted from Thermo Scientific)
Based on Thermo Scientific, 2009. It comprises of an ion guide for collimating ion beam and enhancing ion transmission; a dual-pressure ion trap, which isolates ions according to *m/z* value and fragment ions; an Orbitrap mass analyser coupled with a C-trap and HCD collision cell for high-resolution MS scan and HCD fragmentation; and an ETD unit that provides ETD fragmentation.

Developed by Makarov in 1996[81], Orbitrap mass analyser is the modification of ion trap, which is made of an electrically isolated barrel-like outer cylindrical electrode and a spindle-shape inner electrode (see Figure 1.7). In Orbitrap, ions are ejected tangentially into the interstice while an electrostatic voltage is applied to the inner electrode and the outer electrode is at the ground potential. As ions enter the trap, they start to oscillate around the inner electrode under the electrostatic attraction. Due to properties of quadro-logarithmic potential, ion motion in the axial direction is harmonic. To stabilize the ions in a stable spiral radius around the inner electrode and to prevent unwanted collisions with the outer electrode, the potential of inner electrode is set at around -3200 V for positive ions to provide kinetic energy. The axial frequency (*w*) of ion oscillation can be described as:

$$\omega = \sqrt{\left(\frac{q}{m}\right)k}$$

q: total charge; *m*: ion mass; *k*: force constant of the potential

This equation shows the axial frequency is dependent on the *m/q* ratio. Therefore, ions of different *m/z* ratios will oscillate along the inner electrode at a specific frequency. The image current induced by the oscillating ions can be detected on the outer electrode and converted to frequencies and intensities by Fourier transform algorithm, yielding the mass spectrum.

LTQ and Orbitrap work in parallel in data dependent acquisition: Orbitrap is performing MS1 scan while LTQ is isolating and fragmenting ions detected in MS1 spectrum. This combination allows for acquirement of high resolution MS spectra with excellent mass accuracy in the Orbitrap and rapid MS/MS scan (several Hz) in the ion trap. A pre-defined number of precursor ions will be selected according to their abundance and reported back to LTQ for selection and fragmentation. MS/MS scan can be acquired in either CID or ETD mode in LTQ. In addition, HCD fragmentation is introduced in HCD collision cell to overcome the drawback of low mass

resolution and accuracy when performing fragmentation of LTQ. For highly complex samples, the high resolution of hybrid LTQ/Orbitrap instrument maximizes the number of ions analysed, which is particularly advantageous for bottom-up proteomic analysis. Initial reports showed the resolution of Orbitrap spectrum can achieve 60,000 at m/z in 1 second of scan time and the increases of resolution are proportional to the allowed scan time and inversely proportional to the square root of *m/z* values. In proteomics, these features make it ideal for analysis of intact protein, complex peptide mixtures and their PTMs. Coupled with nanoLC and electrospray, LTQ Orbitrap is one of the most commonly used mass spectrometers in large scale proteomics analysis. The LTQ Orbitrap Velos mass spectrometer was used in Chapter 3 and 4; LTQ Orbitrap Elite mass spectrometer was used in Chapter 5.

1.3.4.2 Triple-quadrupole mass spectrometer

TSQ Vantage Triple Quadrupole Mass Spectrometer (referred to as QqQ in the thesis), introduced by Thermo Scientific, is a triple quadrupole (QqQ) mass spectrometer featuring a QqQ mass analyser. QqQ mass analyser primarily used in study of drug metabolism, environmental studies and targeted proteomic quantitation[96].

QqQ analyser is made of four cylindrical or hyperbolic rods in parallel[97]. In a quadrupole, ions are separated based on the stability of their trajectories in oscillating electric fields which are applied to the rods. Each rods pair is connected electrically. Paul and Steinwegen described the principle of the quadrupole[98].

$$\varphi_0 = +(U - V\cos\omega t)/r_0$$

ϕ represents the potential applied to the rods, w is the angular frequency, U is the DC voltage and V is the amplitude of RF voltage.

Ions travelling between the quadrupole rods are subjected to a RF field superposed on a constant field (DC voltage) that is applied to one pair of the rods or the other. The principle of ion motion in a quadrupole field can be described by Mathieu equation:

$$\frac{d^2u}{d\xi^2} + (a_u - 2q_u cos2\xi)u = 0$$

u represents *x*, *y* and *z* coordinates, a_u and q_u are dimensionless trapping parameters, and ζ is a dimensionless trapping parameter equal to Ωt/2 (Ω is frequency and time).

While travelling along the z axis, ions are also exposed to *x* and *y* accelerations induced by the electric field:

$$F_x = md^2x/dt^2 = -z\,(\delta\Phi/\delta x)$$

$$F_y = md^2y/dt^2 = -z\,(\delta\Phi/\delta y)$$

Φ the quadrupolar potential:

$$\varphi_{(x,\,y)} = \varphi_0\,(x^2-y^2)/r_0 = (x^2-y^2)(U - V\cos\omega t)/r_0$$

Thus, we can deduce:

$$U = a_u \frac{m}{z}\frac{\omega^2 r_0^2}{8e} \qquad V = q_u \frac{m}{z}\frac{\omega^2 r_0^2}{e}$$

Both U and V are constant for a given quadrupole instrument. Thus, each ion has a specific a_u and q_u, resulting in the difference in field influence. At a given ratio of voltages, only the ions of a certain *m/z* value are allowed to travel through the poles and reach the detector. By varying the applied DC voltage, selection of ions within a particular *m/z* window can be achieved.

In this thesis, QqQ mass spectrometer was used predominantly in Chapter 6 in selected reaction monitoring (SRM)[99] mode. Figure 1.8 shows the schematic design of the QqQ mass spectrometer. Ions are focused into the instrument via the S-Lens, through quadrupoles and

reached the channel electron multiplier (CEM) for detection. QqQ analyser is comprised of three quadrupoles: Q1 and Q3 act as mass filters and Q2 is the collision cell.

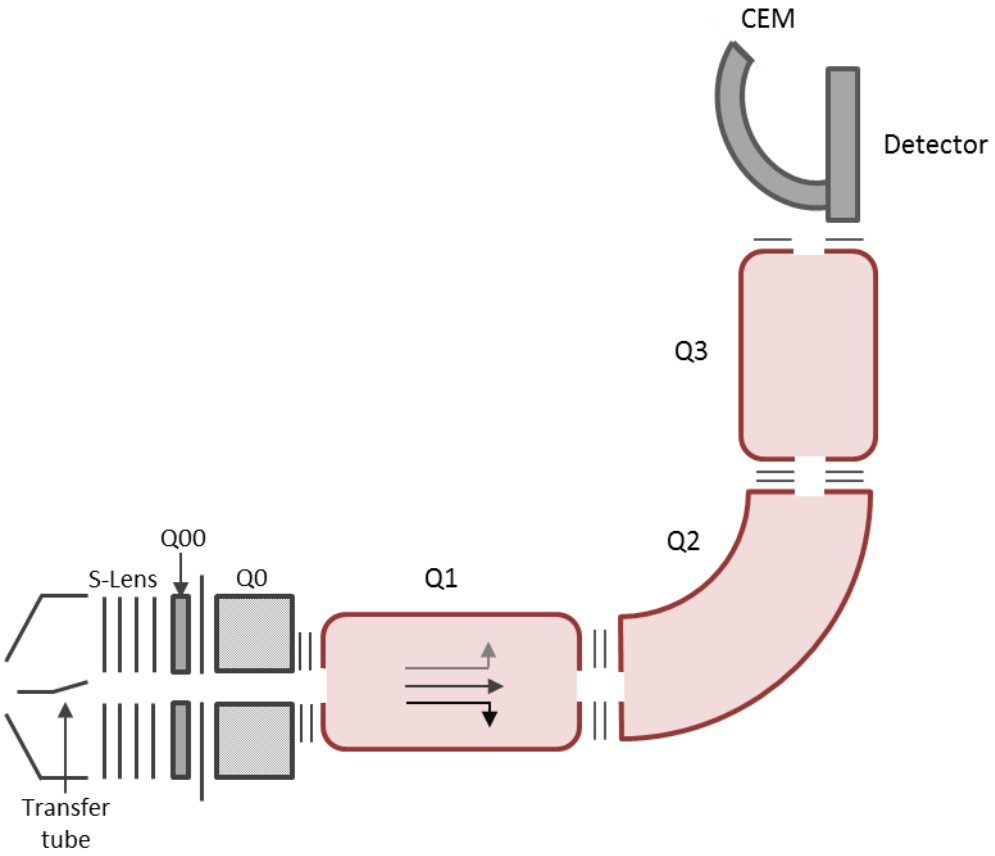

Figure 1.8 Schematic of TSQ Vantage Triple Quadrupole Mass Spectrometer (Thermo Scientific)
Based on Thermo Scientific, 2009. It comprises of an S-lens, an ion guide for collimating ion beam and enhancing ion transmission; a quadrupole mass filter (Q1), which filters ions according to m/z value; a collision cell for fragmentation of selected ions; and a linear ion trap that can also function as a mass filter.

The design of QqQ analyser allows the mass analysis to happen in a sequential manner[100]. QqQ analyser can operate in full scan mode, product ion mode, precursor ion mode and neutral loss mode *etc*, as shown in Figure 1.9. In full scan mode, Q1 and Q3 quadrupoles are set to scan the full mass range, which is used to detect unknown products in a sample. Product ion scan mode selects a particular ion, passes it into Q2 for fragmentation and full mass range of fragment ions is scanned in Q3. SRM scan mode has two stages of mass selection. Q1 quadrupole is responsible for filtering the precursor ions according to their m/z ratio. Q2 acts as collision cell

and Q3 is then set to filter the pre-set fragment ions, allowing only the selected fragment ions to reach detector. If Q1 or Q3 is set to scan more than a single mass, this method is referred to multiple reaction monitoring (MRM).

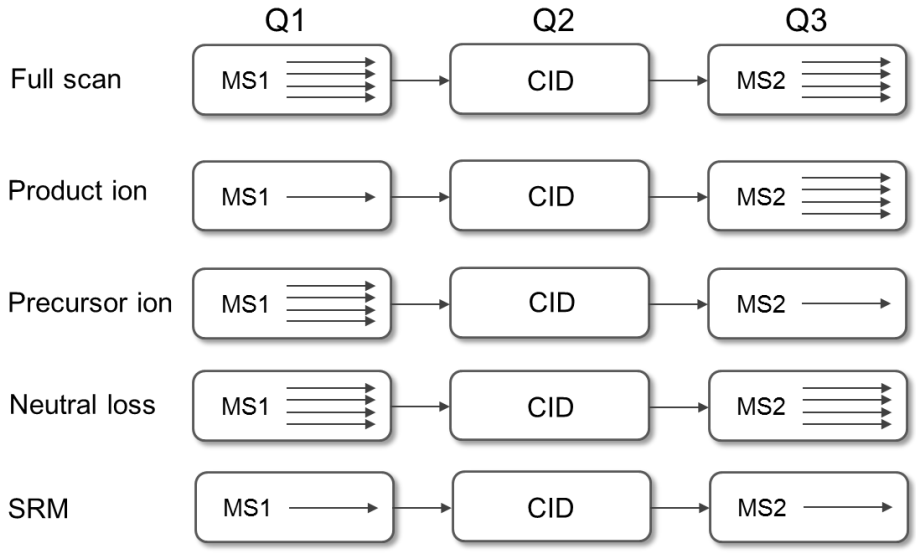

Figure 1.9 Scan modes of QqQ mass analyser

1.4 Proteomics by mass spectrometry

Proteomics is an established field focusing on study of proteins hugely aided by the development of mass spectrometry. Proteomics aims to understand the molecular mechanism of biological processes and diseases from the study of peptide or protein structure, expression, protein-protein interaction and post-translational modification etc[101].

There are two complementary strategies in MS-based proteomics: bottom-up and top-down [102]. The bottom-up approach focuses on MS/MS analysis of tryptic digested peptides for protein identification. This approach usually requires pre-separation prior to MS analysis, such as high performance liquid chromatography (HPLC). The peptide sequence identified in the bottom-

up analysis can be searched against protein databases and limited sequence coverage is required for unambiguous identification. An alternative approach is top-down, which analyses intact proteins without proteolytic digestion and preserves the labile structural characteristics which are likely to be destroyed in bottom-up strategy. However, the application of top-down approach is limited to certain types of proteins and instruments and is faced with technical challenges such as electrospray efficiency, instrument sensitivity and detection limit.

Proteomic profiling of a biological process or cellular network is typically achieved by bottom-up approaches. Especially within the last decade, owing to technological advances the scale of our understanding has been expanded with great accuracy and depth, from identification and structure of proteins to creation of a comprehensive proteomic network. Subsequently, to determine the candidate arising from discovery experiment, a targeted quantitation method is required. Selected reaction monitoring (SRM, also known as MRM, multiple reaction monitoring) has emerged as the method of choice[103]. This method is well-established for quantitative MS/MS analysis, offering high selectivity and high-throughput ability. SRM has been applied in small molecules quantitation for several decades[104]. More recently, researchers employed SRM approach in environmental compounds, drug metabolites and it is being increasingly applied in peptide quantitation in complex biological samples.

1.4.1 Bottom-up proteomics workflow

1.4.1.2 Bottom-up proteomics workflow

Complex samples, such as whole cell lysate and protein complexes, often require pre-separation prior to LC-MS/MS analysis in bottom-up approach. Coupled with high scanning speed of mass spectrometry, this approach is able to recover hundreds to thousands of peptides

in a single analysis. The work in this thesis used the bottom-up approach. Figure 1.10 summarises the typical workflow of a bottom-up proteomic analysis.

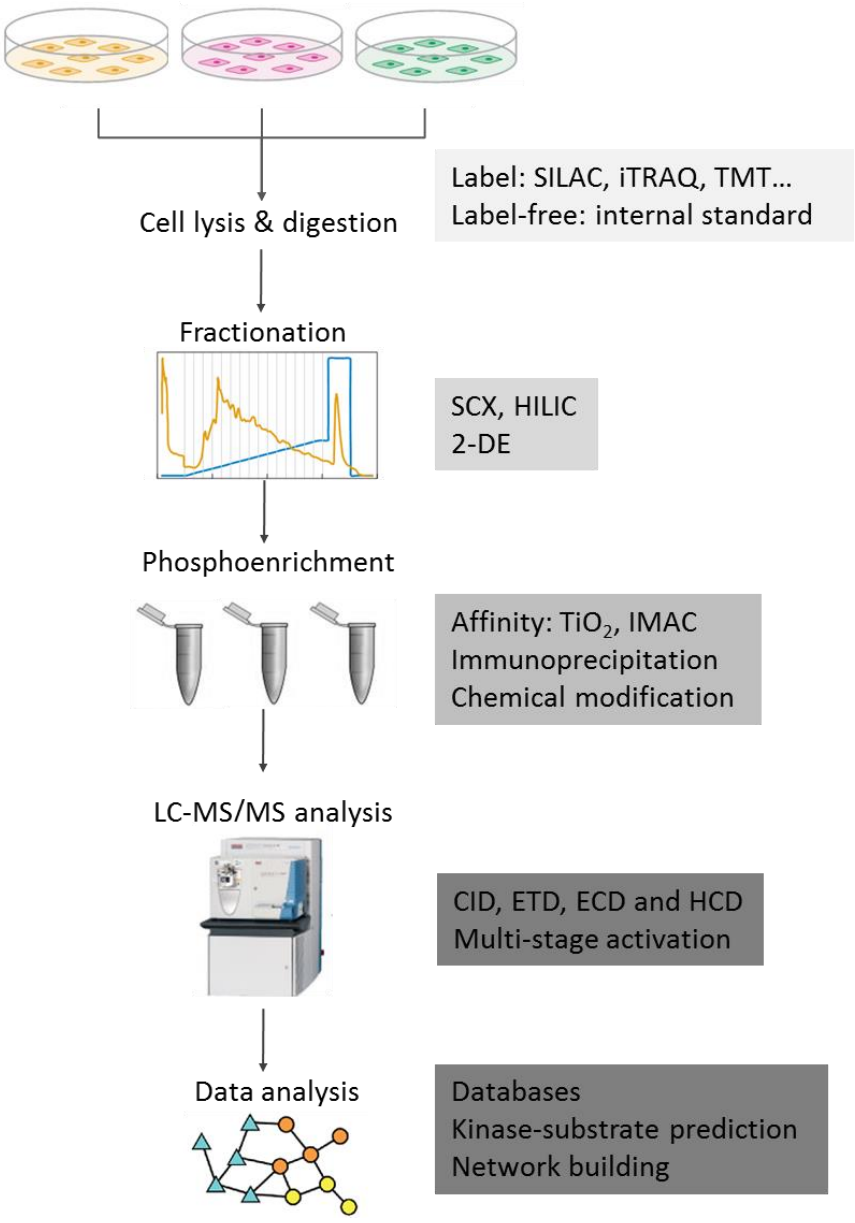

Figure 1.10 Typical bottom-up proteomics workflow

Bottom-up proteomic analysis requires the following: (1) cell labelling or label-free strategies for quantitative analysis (if quantitation is required); (2) proteolytic digestion of proteins; (3) separation and fractionation; (4) for identification of phosphopeptides, further purification using affinity enrichment or chromatography methods; (5) characterisation of peptides and proteins using mass spectrometry; (6) database search using software for peptide identification

and site specific identification. The development and application of these aspects are discussed in detail in the following sections.

1.4.1.3 Data scan mode

The extreme complexity of biological samples typically requires mass spectrometers with faster scanning speeds, better resolution and broader dynamic range. Traditionally MS/MS data are acquired through data-dependent acquisition (DDA) mode, where a full mass spectrum dictates which peptide ions are selected for fragmentation. Data-independent acquisition (DIA) performed fragmentation on all peptides in a defined *m/z* window, and this process can be repeated to map the desired *m/z* range. This approach is not biased towards the peptides with the strongest signal and has been proved efficient in the identification of low abundance precursors, with at least 5-fold increase in precursor selectivity[105].

Another research area that attracts attention is ion mobility mass spectrometry (IMS). IMS is a gas phase separation technique that can either be used prior to MS detection or as an integrated part of mass spectrometer. Drift tube IMS, travelling wave IMS and differential IMS have been applied as an additional dimension of separation/fractionation technique and have shown potential in enhancing separation/identification.

1.4.2 Phosphoproteomics by mass spectrometry

Phosphoproteomics is a branch of proteomics that focuses on identification and quantitation of specific and global phosphorylation events. As the most common mechanism of regulation of protein function and signal transduction, the interpretation of protein phosphorylation in the context of human diseases is an area of intense research[106]. Phosphorylation has been extensively investigated with small-scale protein approaches (e.g. immuno-detection and

kinase activity assays) and high throughput mass spectrometry approaches. Developments in enrichment strategies, sample labelling methods, and mass spectrometry methods have all contributed to the rapid progress of phosphoproteomics in recent years[107].

1.4.2.1 Enrichment and fractionation

Efficient isolation of phosphopeptides from a complex biological mixture, *e.g.* whole cell lysate or serum, is the initial step in phosphoproteomics analysis. Currently, the immunoaffinity-based approach is the most commonly used methods for phosphopeptide and phosphoprotein enrichment[108]. Table 1.1 summarises the main methods used in phosphoproteomic studies.

Incorporation of additional reagents, such as citric acid[109] and aliphatic hydroxy acid[110] in enrichment protocols has been shown to enhance enrichment efficiency, especially for multiply phosphorylated peptides. The former has been used in the work presented here. New affinity materials (e.g. TiO_2, Fe_2O_3[111] and SiO_2[112]) that exhibit complementary enrichment performance are being used in combination in phosphoproteomic studies.

Table 1.1 Summary of the classic enrichment methods used in phosphoproteomic studies
(Adapted from Thingholm *et al.*[108])

Name	Principle	Reference
Immunoprecipitation (IP)	Isolation of phosphoproteins by binding to antibodies (e.g. anti-phosphotyrosine antibodies)	113
Immobilised Metal ion Affinity Chromatography (**IMAC**)	Purifying phosphoproteins and phosphopeptides from complex samples by their affinity toward positively charged metal ions (Fe^{3+} or Al^{3+})	114
Titanium dioxide (**TiO_2**) chromatography	Highly selective enrichment of phosphopeptides from complex samples by their affinity toward TiO_2-coated beads packed in a micro-column	115
Sequential elution from IMAC (**SIMAC**)	Method in which mono-and multi-phosphorylated peptides are enriched from highly complex samples and separated prior to MS/MS analysis	116
Phosphoramidate Chemistry (**PAC**)	To link phosphate groups to immobilised iodoacetyl groups for purification	117

Fractionation methods, e.g. strong cation exchange chromatography (SCX) and hydrophilic interaction chromatography (HILIC), provide an extra dimension of separation prior to MS/MS analysis. Alternatively, two-dimensional gel electrophoresis (2-DE) can be used for the separation of proteins and phosphoproteins in proteomic analysis. Combinations of enrichment and fractionation methods are used widely in current phosphoproteomic strategies to maximize phosphoproteome coverage (see Table 1.2).

Table 1.2 Summary of fractionation methods used in phosphoproteomic studies

Name	Principle	Reference
Strong cation exchange chromatography (**SCX**)	Phosphopeptides will be eluted prior to non phosphopeptides with higher charge states at pH 2.7; SCX is an efficient fractionation tool prior to subsequent phosphopeptide enrichment (e.g. TiO_2 chromatography)	107
Hydrophilic Interaction Chromatography (**HILIC**)	For fractionation of peptides based on hydrophilicity prior to phosphopeptide enrichment	260
Two-dimensional gel electrophoresis (**2-DE**)	Separation of proteins based on their charge state and molecular weight	259

1.4.2.2 Quantitation strategy

Strategies based on differential stable isotope labelling are frequently used in quantitative phosphoproteomic analyses. Mass spectrometric isotope dilution was first introduced by Moore *et al.*, a MS-based quantitation strategy to determine the concentration by adding known amount of isotopic standards[118]. This concept has since been applied to quantitation of a large number of biological analytes, such as glucose and cholesterol[119,120]. A quantitation approach in complex biological mixtures using isotope-coded affinity tags (ICAT) tag was described by Gygi and co-workers in 1999[121]. The ICAT tag specifically target reduced cysteine residues and the tag can result in a mass difference of either 8 Da. Samples carrying light or heavy

isotope labels are mixed prior to trypsin digestion, minimising the variance arising from sample preparation procedures. Using this strategy, they investigated the protein expression level in *Saccharomyces cerevisiae* under glucose-repressed conditions. ICAT method has been widely used and the concept of ICAT strategy has been adapted and modified to a number of isotope labelling methods, such as Isotope-coded protein labels (ICPL)[122], Isobaric tags for relative and absolute quantitation (iTRAQ)[123] and tandem mass tags (TMT)[124].

In stable isotope labelling by amino acids in cell culture (SILAC)[125] approach, cells are cultured in a medium containing differentially isotopically labelled amino acids (usually lysine and arginine). Lysates with different labels are mixed prior to digestion and sample preparation. As a result, peptides with the same amino acid sequence and different isotopic labels can be distinguished by mass spectrometry; relative abundance can be obtained by calculating the ratio of differentially labelled peptides. For example, using the SILAC-based method combined with SCX and TiO_2 enrichment, 6600 unique phosphorylation sites from 2244 proteins were successfully identified in EGF-stimulated HeLa cells[107]. More recently, Olsen *et al.* showed that quantification of 20,443 phosphorylation sites from 6027 proteins was achieved in a study of the phosphoproteome of the cell cycle and a specific kinase motif was identified at various stages in the cell cycle[126]. Hinsby *et al.* applied SILAC in the phosphoproteomics workflow to study protein phosphorylation in response to FGF1 stimulation in the human 293T cell line. An antibody was used to isolate binding proteins of a specific phosphoprotein and 28 binding partners were identified that were involved in stimulation by FGF1[127]. A novel component of FGF signalling, for example insulin receptor substrate 4 (IRS4), was identified and a novel tyrosine phosphorylation site (Tyr915) in IRS4 was found to directly interact with several proteins in FGF signalling cascade. More recently, the SILAC approach has been not only limited to cell culture systems, but also available to *in vivo* experiments in mice[128].

Label-free quantitation methods typically require the use of an internal standard. Methods were developed using peak height, spectral count or fragment-ion intensities to normalize the peptide signal [129,130]. These methods are increasingly popular, as they are especially valuable for samples that are not suitable for *in vitro* labelling. Langlais *et al.* investigated the site-specific phosphorylation of Insulin Receptor Substrate-1 with a label-free method and were able to relatively quantify isobaric phosphopeptides within one protein[131]. Old *et al.* performed global profiling using a label-free quantitation method to identify the phosphorylation events involved in oncogenic B-Raf signalling. Ninety phosphorylation events were revealed to be sensitive to MEK1/2 inhibitor. Multiple phosphorylation sites of an uncharacterised protein were subjected to detailed investigation and its phosphorylation was shown to be involved in controlling melanoma cell invasion[132].

1.4.2.3 Mass spectrometry analysis

CID and ETD are the most frequently used fragmentation techniques in proteomics[133]. Some reports suggest ETD can identify a larger number of phosphopeptides than CID, especially for multiply charged peptides[134]. An alternative strategy is to combine CID and ETD results or alternate CID/ETD in one analysis. Electron capture dissociation (ECD)[135] and higher energy collision activated dissociation (HCD)[136] are also used in large-scale localization of phosphorylation.

Phosphopeptides in complex mixtures often escape standard mass spectrometry detection because of their low abundance and inadequate fragmentation patterns. Neutral loss scanning, in which the mass range is continuously scanned for ions with a mass shift of 98 Da (H_3PO_4), can be used in sequential fragmentation to partially address these issues[137]. In ion traps, MS^3 will be triggered if a 98 Da mass shift is detected. A drawback of this approach is tyrosine-

phosphorylated peptides typically lose HPO_3 rather than H_3PO_4 thus the product ion is the unmodified amino acid, which may limit the identification of tyrosine-phosphorylated peptides

Combinations of multiple fragmentation methods have been employed to exploit their complementarity. Frese and co-workers coupled multi-enzyme digestion and alternate CID and ETD tandem mass spectrometry for the characterisation of caseins[138]. They concluded that the complementary information provided by CID (peptide sequencing and identification of single-point modification) and ETD (PTMs) was crucial for complete protein sequencing, where an average 32% increase of sequence coverage was observed in alternating CID/ETD approach compared to CID or ETD alone.

1.4.2.4 Data analysis

The three main databases in phosphoproteome research, which store biochemically verified and mass spectrometry identified protein phosphorylation data are PhosphoSitePlus (www.phosphosite.org), Phospho.ELM (http://phospho.elm.eu.org) and Phosida (www.phosida.com). Phosphoproteome data of model organisms and various species are available through their websites.

Annotation of phosphorylation is the first step towards the interpretation of protein function. While phosphoproteomics has greatly broadened the knowledge of phosphorylation events in various biological processes, the need to characterise the regulatory relationship between kinases and phosphorylation substrates has expanded. Software focusing on motif analysis, e.g. Scansite (http://scansite.mit.edu), NetWorkin (http://networkin.info) and iGPS (http://igps.biocuckoo.org), have been developed to identify the upstream kinases responsible for identified phosphorylation sites. Results from bioinformatic mining are powerful in

revealing the protein family, pathway or biological function related to a group of phosphorylation substrates[139].

Software based on consensus motif to predict upstream kinases are popular in deciphering high-throughput phosphoproteomic data. Pawson and co-workers showed with Networkin kinase prediction was able to assign 60-80 % of substrate from an *in vivo* study[139]. Although this marked huge progress in phosphoproteome software, it still points out limitation of current bioinformatic tools. It should be noted that the prediction does not provide direct evidence of specific kinase-substrate information and further validation is required. In addition, the knowledge of novel phosphorylation sites is limited in context of their function and consensus motif, which offers another direction of future bioinformatic innovation.

1.4.2.5 Future prospects

Owing to the huge role played by phosphorylation in signal transduction, phosphoproteomics is becoming one of the fastest-growing areas in the study of signal transduction pathways. Many studies have focused on the temporal dynamics of regulated phosphorylation events in cell signalling or various biological processes. In recent years, the large-scale phosphoproteomics workflow is able to map phosphorylation events in considerable depth, from a few hundreds of phosphorylation sites up to thousands of sites in one single analysis. A huge emphasis has also been placed from discovery-driven to site-specific analysis that focuses on interpretation of specific biological connections.

Phosphopeptide identification capacity is still limited by enrichment methods, instrument performance and data interpretation methods. For tryptic peptides, singly modified peptides constitute the majority of the total phosphopeptides identified by current technologies[140]. Current understanding holds that it is more challenging to identify doubly- and multiply-

phosphorylated peptides than singly-phosphorylated peptides. Nevertheless, deciphering the mechanisms of cell signalling requires knowledge of multiply-phosphorylated peptides as these adjacent phosphorylation sites may play important regulatory roles. Therefore, one of the crucial challenges in cell signalling research is to map modification sites in multiply-phosphorylated peptides.

Although significant progress has been made, low phosphoproteomic coverage, limited dynamic range and co-elution of peptide isomers still remain a challenge. The development of phosphoproteomics required the advances in sample preparation, multiplexed MS techniques and novel data handling software in the future.

1.4.3 Targeted proteomics-selected reaction monitoring

1.4.3.1 Overview

Large-scale proteome analysis has been extensively applied in biomarker discovery and the development of shotgun approaches greatly increased proteome coverage[141]. Accurate quantitation and validation is a necessary step for further characterisation. Conventional methods, e.g. Western blot and enzyme-linked immunosorbent assay (ELISA) provide good sensitivity and reproducibility. However, antibody is not always available for such assays. SRM has emerged as an alternative approach with high reproducibility and throughput. Also, in combination with LC-MS/MS, the detection limit in attomole level can be routinely achieved by SRM[142,143].

Unlike full MS scan mode, where data are collected by summing up signal intensity over all *m/z* to a total-ion chromatogram (TIC), SRM data is collected to form an extracted ion chromatogram (XIC), where *m/z* values are extracted from the full mass range to build an

elution profile for a given analyte. In SRM analysis, mass spectrometer only selects a set of target ions within the given *m/z* range and allow them for fragmentation. The relative abundance of specified fragment ions is indicative of the abundance of peptides in the sample. In some cases, peptides with similar *m/z* or isobaric peptides may appear in the same mass window in SRM selection[144]. Thus, monitoring a single precursor mass is not sufficient to define a unique analyte. Then, targeting a specific precursor as well as multiple fragment ions may provide highly specific signal to minimize the incidence of false positive detection.

SRM assay typically makes use of a QqQ mass analyser. The most widely used instruments are QqQ mass spectrometer, quadrupole-time of flight (Q-TOF) mass spectrometer and quadrupole-TRAP mass spectrometer. TSQ Vantage Triple Quadrupole Mass Spectrometer used in this thesis was described in detail in Section 1.3.4.2.

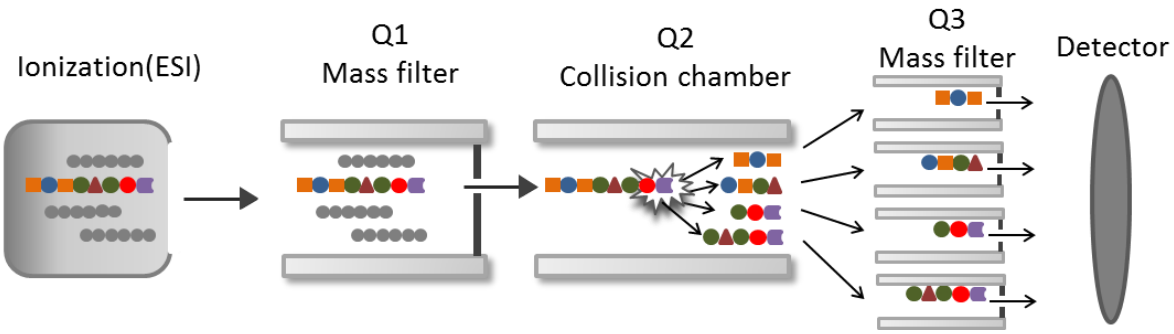

Figure 1.11 Selected reaction monitoring technique

As a targeted method, SRM has to be hypothesis-driven; therefore, knowledge of the analyte is required from previously acquired discovery data[145]. Based on information of precursor/fragment ions obtained from discovery data, a transition (pair of product ion and fragment ion) list can be built to ensure accurate and specific quantitation. This underlying mechanism of SRM makes it an ideal validation platform, complimentary to the results obtained from the discovery-based method.

1.4.3.2 SRM experiment design

As SRM-based quantitation approach does not allow peptide *de novo* sequencing. Knowledge of the MS/MS behaviour of the peptides is required. The selection of target peptides and transitions are crucial for accuracy and precision of the SRM assays, especially for complex biological samples.

The target peptides are usually referred to as signature peptides or proteotypic peptides (PTPs)[146]. The signal intensity of different peptides of the same protein can differ by up to 100-fold in intensity[147]. There are several factors and empirical rules affecting the choice of peptides. First, peptides with the most intense MS response are promising targets for SRM assay, such as the highly detectable peptides derived from previous shotgun experiments or peptides predicted by computational tools[148]. Second, the signature peptides can be uniquely identified only in one protein or one isoform. Third, for peptides with post-translational modification, it is important to distinguish the unmodified and modified form as in most cases they tend to show different responses.

The selection of signature peptides is then followed by the selection of a set of fragment ions. There are a number of public available databases of MS/MS spectra and validated SRM assays to provide empirical guides to assay development and transition selection[149–151]. An alternative way to optimize the transition selection is to directly infuse the target peptide and select the unique fragments with the most intense signals. Fragments with similar masses should be avoided. To study PTM peptides, the fragment losing the modified group, e.g. phosphate group, is necessary in order to distinguish them from unmodified peptides. Commonly, 2 to 4 fragment ions are selected for each peptide due to the limitation of the number of transitions that can be measured per LC-MS/MS analysis. If measuring too many transitions in one run, the cycle time will be prolonged, thus there will not be enough data points to build the chromatographic

elution profile of the targeted peptides. However, the number of transitions analysed per LC-MS/MS run can be increased by scheduling SRM transitions[152]. A retention time window can be set to scan for a specific peptide, therefore a higher number of peptides can be measured in one LC-MS/MS run.

To improve the accuracy and precision of SRM assay, pre-fractionation is usually necessary depending on the complexity of sample. The most widely used approach is to couple LC with SRM tandem mass spectrometry[153]. Selective enrichment procedures following enzyme digestion could be employed for the investigation of peptides with PTM[154,155]. It is reported the combination of enrichment and fractionation is able to enrich the target peptide by up to 3 orders of magnitude[104]. However, it is worth mentioning that the introduction of sample processing procedures will potentially affect the reproducibility and precision of SRM assay. SRM has also been coupled with ion mobility separation[156].

1.4.3.3 Absolute quantitation

SRM can perform relative and absolute quantitation. Relative (differential) quantitation by SRM is straightforward and can be used to determine the relative quantities between two samples. In some cases, the amount of biomarkers present in a sample or a parallel comparison of peptide quantities is needed among multiple samples, thus the relative quantitation information is insufficient. Absolute quantitation can be achieved, combined with isotope labelling or label-free approach.

1.4.3.3.1 Isotope-based quantitation

The widespread and frequently used absolute quantitation approach employs an internal standard (IS) with isotope labelling[154]. First, a calibration curve needs to be established by

infusing stable-isotope labelled IS peptides. IS peptides can be synthesised by solid-phase peptide synthesis to incorporate heavy labelled amino acids. Then, IS peptides of known amount can be spiked into the isotopic labelled endogenous peptides. The amount of IS peptide required can be determined in a pilot experiment for the individual peptide. The absolute amount of endogenous peptides can then be derived from the relative signal intensity of endogenous peptides compared with that of the IS peptides. The introduction of isotopic labels as internal standards has enabled absolute peptide quantitation and data replication. Although labelling the endogenous peptides and synthesis of IS peptide are cost-intensive, it is compensated by better accuracy and more precise quantitation[157].

1.4.3.3.2 Label-free quantitation

Label-free SRM is based on quantitation of a single or a group of IS peptides as the reference standard to measure all the target endogenous peptides[158]. Although the label-free approach is experimentally simple, variations in the signal intensity among LC-MS/MS analyses or within a single LC-MS/MS pose a challenge to the accuracy of quantitation assay. To minimize these fluctuations, normalization is performed to ensure there is no global shift in the ion intensities.

The need for absolute quantitation information and reducing the cost of an experiment has increased the demand for label-free quantitation strategies. The QconCAT[159] strategy employs a pool of signature internal standard peptides and enables absolute parallel quantitation of multiple samples. A recently developed label-free approach uses internal standard peptides with a quantitation tag[160]. The tag is added via the trypsin cleavage site to all peptides, which can then be used to normalize the amount of internal standard peptides.

1.4.3.4 Applications of SRM

The specificity of SRM assay depends on the uniqueness of the peptide sequence and the response of the fragment ions of each peptide. Highly sequence-homologous proteins and mutant proteins, which cannot be distinguished by traditional affinity-based methods, can be unambiguously identified by SRM. Wang *et al.* demonstrated the applicability of SRM in the measurement of peptides with somatic mutations of Ras, with peptides differing by only one amino acid[161]. The capability of site-specific quantitation opens up opportunities for SRM-based diagnostic applications.

Large-scale proteomics and genomics screen can generate a list of proteins of potential interest. Based on this previous knowledge, SRM-based experiment can then be performed to target these proteins for validation or detailed characterisation. Jovanovic and co-workers used SRM to quantitatively monitor a set of putative target proteins of microRNA *let*-7 in *Caenorhabditis elegans*[162]. These targets were selected from microarray RNAi screen, microRNA target prediction algorithms and literature. Around 50% of proteins of interest were successfully quantified and biologically relevant let-7 interactors were identified. Wolf-Wolf-Yadlin *et al.* investigated previously identified phosphorylation events in EGF signalling[163]. They combined affinity-based enrichment and SRM to study the dynamics of phosphorylation in a time-course manner during EGF simulation. Over 200 hundred phosphorylation profiles were recorded, and early and late phosphorylation responses were identified upon stimulation.

The SRM approach can be applied to identify novel biomarkers for a disease due to its multiplexing capabilities of up to 100 analytes[164]. Anderson and Hunter assessed the precision and dynamic range of SRM technique for multiple quantitations in plasma samples[99]. They used multiplexed SRM to reproducibly quantify 47 out of 53 proteins. These quantitation results yielded a limit of quantification (LOQ) of 0.1 μg/mL and a dynamic range of

approximately 4.5 orders of magnitude. Coupled with affinity enrichment and fractionation, Keshishian *et al.* significantly expanded the detection limit down to 1–10 ng/mL[165]. With this strategy, Cima *et al.* measured 49 candidate biomarkers for prostate cancer from serum samples from more than 100 individuals, from which they proposed a four-protein signature for prostate cancer detection[166].

1.5 High-Field Asymmetric Waveform Ion Mobility Spectrometry (FAIMS)

1.5.1 Ion mobility mass spectrometry

Ion mobility spectrometry (IMS) is a gas-phase analytical technique used to separate and identify ions based on their ion mobility as they travel through an electric field[167]. Separation is not based on *m/z* ratio as it is in conventional mass spectrometry, but on a combination of the mass, charge, size, and shape of an ion. Separation in IMS occurs on a timescale of milliseconds, several orders of magnitudes faster than the seconds to hours in chromatographic separations. The compact design of some IMS devices has allowed the approach to be used in detection of explosives, drugs and chemical weapons. Although it was demonstrated in 1962 that IMS could be coupled with mass spectrometry[168], it was not until 1993 with the advancement of instrumentation that IMS-MS has been used in detection of low abundance chemicals, separation of complex mixtures and characterization of structural information[169].

Types of IMS techniques in mass spectrometry include drift tube ion mobility spectrometry (DTIMS), travelling wave ion mobility spectrometry (TWIMS) and high-field asymmetric ion mobility spectrometry (FAIMS)[170]. Features of these three techniques are shown in Table 1.3.

Table 1.3 Comparison of the three types of IMS

Features	DTIMS	TWIMS	FAIMS
CCS measurement	Direct measurement	Requires calibration against known CCS	None
Duty cycle	Poor duty cycle, 10s of ms	Poor duty cycle, 1/10s of ms	Fastest, μs
Resolving power	Highest resolving power	High resolving power (generally worse than DTIMS)	Less resolving power but 'high separation selectivity'
Sensitivity	Lower sensitivity	High sensitivity	Highest sensitivity
Orthogonality of separation	Poor	Poor	Highly orthogonal to MS
Requirement of mass spectrometer	Require to be integrated into mass spectrometer	Require to be integrated into mass spectrometer	Can be fitted prior to introduction to existing mass spectrometer

Drift tube ion mobility spectrometry makes use of a long, gas-filled (typically helium) drift tube in the presence of a constant electric field. Ions are injected in the opposite direction to the buffer gas and migration time through the drift tube is measured to distinguish analyte ions. The movement of ions in applied electric fields is analogous to electrophoresis in that their movement is delayed by the counter-flow buffer gas. The drift time measurement provides information on chemical structure and three-dimensional conformation of an ion, as the mobility of an ion is related to rotationally-averaged collision cross section (CCS) in a DTIMS cell. The CCS of an ion can be calculated according to Mason–Schamp equation[171]:

$$\Omega = \frac{3ze}{16N}\left(\frac{2\pi}{\mu k_B T}\right)^{1/2}\frac{1}{K_0}$$

z is the charge state, K_0 is the mobility in low field, *e* is the elementary charge, *N* is the number density of the drift gas, μ is the reduced mass of the ion–neutral drift gas pair, k_B is the Boltzmann constant and *T* is the gas temperature.

Together with molecular dynamics simulations, DTIMS technique is useful in providing structural information, which can be compared with data acquired by techniques such as X-ray crystallography and nuclear magnetic resonance (NMR) spectroscopy. Commercially available instruments, e.g. Agilent ion mobility Q-TOF mass spectrometer, featuring a drift tube ion mobility cell are able to provide extra separation and acquire structural information besides routine qualitative and quantitative applications.

The travelling wave ion mobility spectrometry (TWIMS) device is similar to traditional DTIMS but comprised of stacked ring electrodes, to which a radio frequency (RF) is applied[172]. Adjacent rings have opposite RF voltage applied to them, which confines the ions within the cell, whilst the application of a direct current (DC) to each pair of adjacent rings provides the wave that drives the ions through the mobility cell. By tuning RF and DC, separation can be achieved. TWIMS has shown improved duty cycle and better capabilities for multiply charged ions compared with traditional DTIMS[173]. Another advantage of TWIMS is that the ion confinement and accumulation ability does not hugely compromise the sensitivity of mass spectrometer, therefore allowing the application of low abundance analytes. TWIMS is only available in a number of Water SYNAPT family instruments.

FAIMS is exploited in the course of this study. Fundamental theories and applications of FAIMS are described in the following sections.

1.5.2 Fundamentals of FAIMS

FAIMS separates ions according to differences in ion mobility in high and low electric fields. In a FAIMS device, ions are guided by carrier gas into a pair of parallel electrodes to which a radiofrequency waveform voltage is applied. The radiofrequency waveform, termed dispersion

voltage (DV), is asymmetric and alternating between positive and negative field. An equal product of each part for the wave form is maintained but the value of positive field is higher than that of negative field. To produce equal part of waveform, the high-field wave is twice the magnitude and half the duration of the low-field. Ions, exposed to alternating high and low electric fields, travel through electrodes guided by the carrier gas (helium or nitrogen). Ion mobility in an electric field can be described as below[169]:

$$k_h(E) = k_0[1 + f(E/N)] \quad (1)$$

K_h is the ion mobility at high field and K_0 is the ion mobility at zero field. $f(E/N)$ describes the ion mobility as a function of electric field strength (E) and density of gas (N).

At zero/low field, ion drift velocity is proportional to the applied field and K is constant with varying field strength. As field strength increases, the velocity is no longer proportional to the applied field and the increase in K is nonlinear[170]. The dependence of K_h on field strength is the basis of FAIMS separation. When exposed to high electric field, the collision energy between an ion and a carrier gas molecule is different from that in low electric field. Certain ions show increased mobility as field strength increases (type A ions); certain ions show initial increase in ion mobility as field strength increases, follow by decreased mobility as field strength further increases (type B ions); certain types of ions show decreased mobility with increased field strength (type C ions).

The ion mobility can also be influenced by use of gas mixtures. According to Blanc's law, the mobility of an ion in gas mixtures is correlated to the mobility in individual gas and their abundance. Therefore, for a mixture of gas X and gas Y, the mobility of an ion can be calculated as:

$$\frac{1}{K_{XY}} = \frac{x}{K_X} + \frac{y}{K_Y} \quad (2)$$

K_X and K_Y is the ion mobility in gas X and gas Y. *x* and *y* is the relative abundance of gas X and gas Y.

Furthermore, when the ions interact with the carrier gas which is dense enough, the ions will quickly acquire a terminal velocity. The terminal velocity is proportional to the strength of the electric field. This proportionality differs at high and low electric field and allows the separation of FAIMS.

$$V_d = kE \quad (3)$$

V_d represents an ion's terminal velocity, k is the ion's mobility and E is the electric field strength.

Thus, in each cycle of changing waveform the ions will drift towards one of the electrodes. After a couple of cycles, the majority of the ions will end up colliding with one of the electrodes and neutralize. Only the ions with 'balanced' drift will be allowed to pass on and exit the electrode. Figure 1.12 shows the separation trajectory of a FAIMS device.

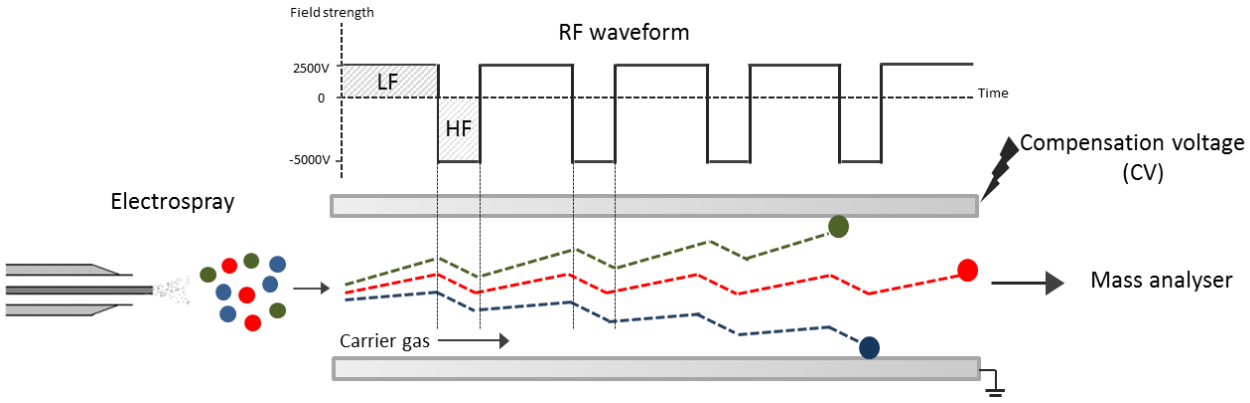

Figure 1.12 Schematic diagram of FAIMS separation

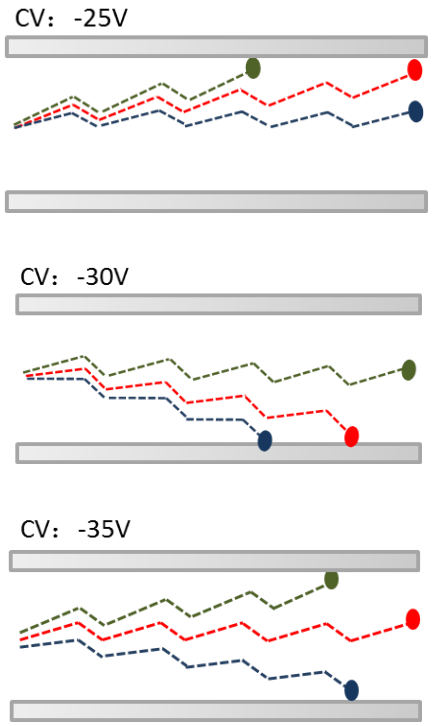

Figure 1.13 FAIMS separation by tuning CVs

By superposing a small direct current (DC), the compensation voltage (CV) to the electrode, the drift induced by the difference in high and low electric field can be compensated or eliminated. Accordingly, by applying different CVs, ions of interest can be selectively transmitted through the device (see Figure 1.13). The CV value of an ion is compound-specific.

To analyse a mixture of ions, separation can be achieved by scanning through CVs. As majority of the chemical noise and short peptide exhibit type C behaviour, they will be largely filtered out during FAIMS cycles. This selective transmission significantly improved signal-to-noise ratio and detection limit of FAIMS technique.

1.5.3 Design of FAIMS electrodes

1.5.3.1 Planar FAIMS

Separation in planar FAIMS is performed between two parallel planar electrodes (see Figure 1.14A). The design of planar FAIMS (p-FAIMS) allows decreased residence time and faster

CV scanning speed, and p-FAIMS can switch between FAIMS and non-FAIMS mode by setting the electrode potential to ground[174]. Another advantage is p-FAIMS can achieve higher resolving power compared to c-FAIMS because the parallel electrodes can produce a uniform electric field without the focusing effect[175]. It was also observed that the sensitivity of p-FAIMS device is limited to the field strength applied[174]. The reason is, within p-FAIMS electrodes, increased field strength causes ions to drift further during each cycle of the waveform and neutralize with the electrodes, decreasing signal.

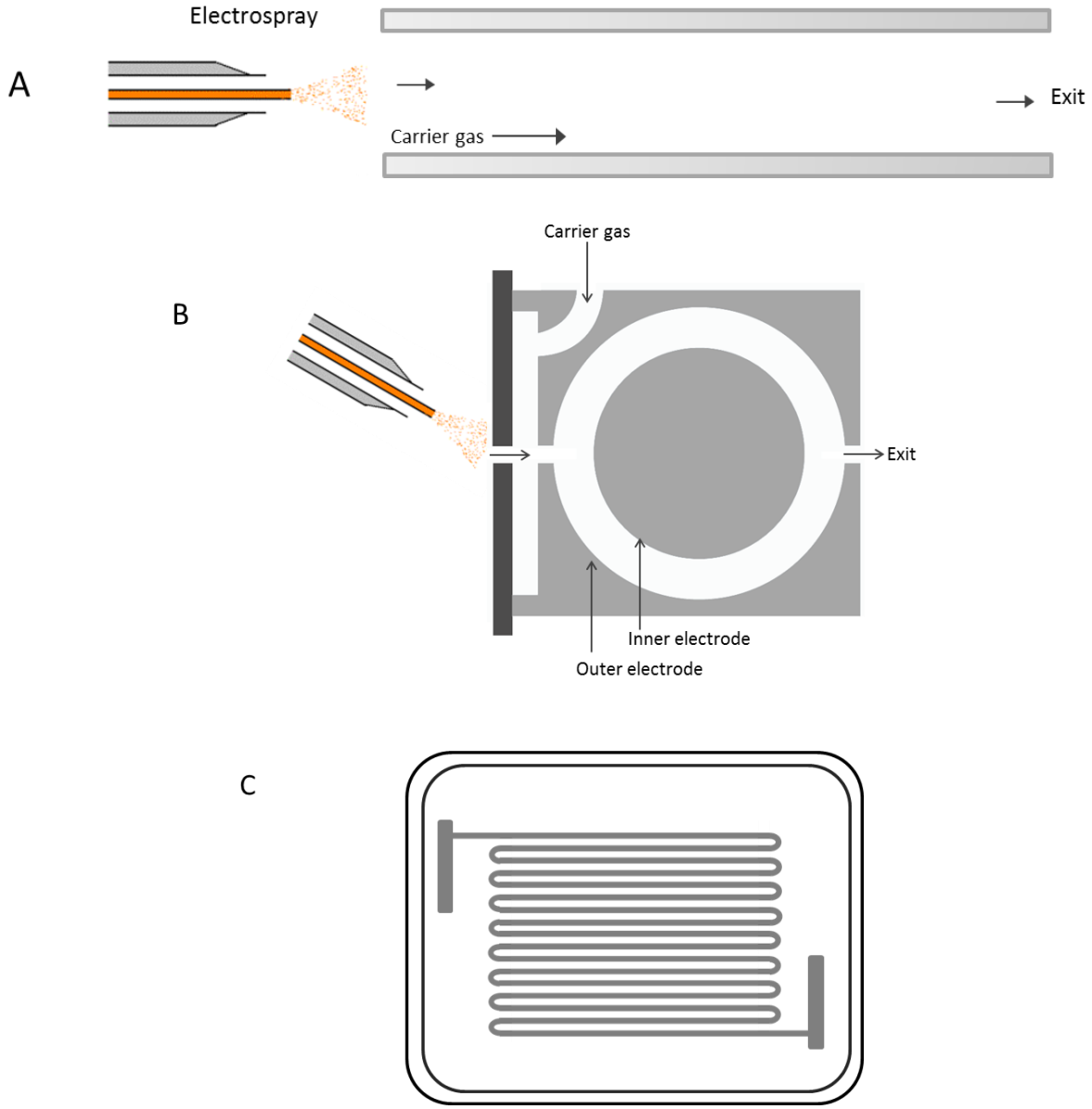

Figure 1.14 Schematic diagrams of (A) p-FAIMS, (B) c-FAIMS and (C) ultra-FAIMS chip.

1.5.3.2 Cylindrical FAIMS

An electrode design of concentric cylinders was first introduced by Carnahan *et al.* and improved by Guevremont *et al*[176]. The prototype design consisted of an inner electrode (cylinder) and an outer electrode, which are coaxially aligned with a 5 mm gap. In this model, ions are focused in the electrode gap, travelling transversely along the electrode. Asymmetric waveform (up to $\pm$3000V) is applied to outer electrode at a frequency of 200 kHz. The cylindrical design creates an inhomogeneous ion focusing effect, where ions with high field dependence will be efficiently focused and transmitted while ions exhibit low field dependence may be poorly focused[177]. A theoretical analysis of the focusing effect was described by Krylov[178]. In contrast to p-FAIMS, the sensitivity of cylindrical FAIMS increases as the field strength increases due to the focusing effect.

In 2005, c-FAIMS device was marketed by Thermo Fisher Scientific (developed by Ionalytics Corporation) with interface to mass spectrometer. Improvements were adopted where ions are introduced into the electrodes in a direction orthogonal to the axis of the electrodes and guided by carrier gas to the exit through an aperture on the opposite side of the electrode (Figure 1.11). In this device, the inner and outer electrode is 13 mm and 18 mm in diameter, with a 2.5 mm gap. Asymmetric waveform is applied to the inner electrode. A high flow ESI probe (New Objective probe, μL/min to mL/min) is compatible with the Thermo c-FAIMS device. Recently, to couple nanoLC with FAIMS, a modified HESI probe (Thermo Scientific) was introduced by Swearingen *et al*. to accommodate a capillary column[179]. This probe also allows the use of sheath gas to assist electrospray. A 33.0% increase in proteome coverage was observed with these modifications. The Thermo c-FAIMS device with a modified HESI was used in the work presented in Chapter 3 and 4.

1.5.3.3 Ultra FAIMS

A multichannel microchip p-FAIMS device (termed ultra-FAIMS) was described by Shvartsburg *et al.*[180] and is manufactured by Owlstone Nanotech. It is constructed with interleaved plates with multiple parallel gaps 35 μm in width and 300 μm in length, as shown in Figure 1.11. Compared with conventional p-FAIMS with field strength of approximate 20 kV/cm, ultra-FAIMS device can raise the field strength up to 60 kV/cm or 180 kV/cm. The drawback of the ultra-FAIMS device is that extreme high fields will decrease transmission efficiency due to increased diffusion, but this loss can be partially offset by the decreased residence time. The scan time of ultra-FAIMS device can be 100-10,000 times faster than previous devices. Dispersion field and compensation field can be varied simultaneously to allow two dimensional FAIMS analysis and identify the optimum conditions for separation of a particular (set of) ion. The chip-based FAIMS device can be attached to suitable mass spectrometers between the ionisation source and MS inlet.

1.5.3.4 Novel cylindrical electrode design

Recently, a modified FAIMS device was described which is based on the Thermo c-FAIMS device[181]. There are two main improvements in the modified FAIMS interface: (1) the gap between inner and outer electrode was reduced gap from 2.5 mm to 1.5 mm; (2) FAIMS inlet was modified to improve ion transmission.

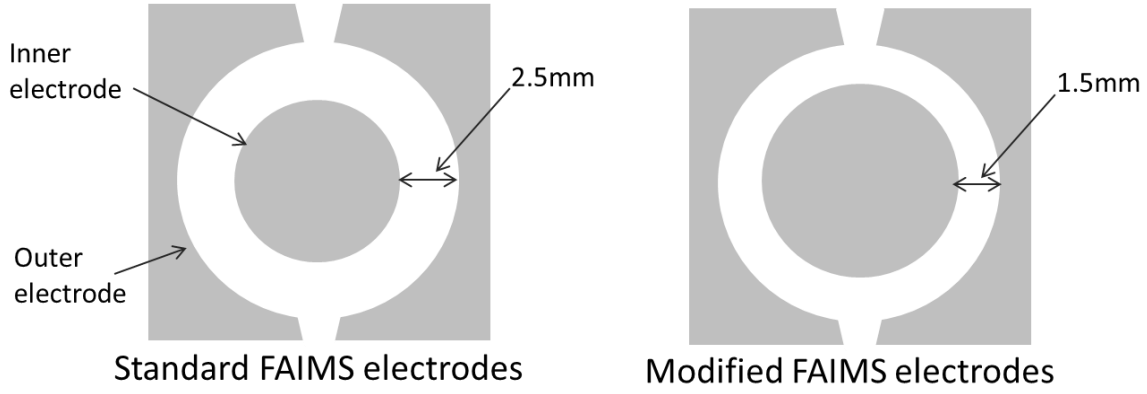

Figure 1.15 Side view comparison of standard and modified FAIMS electrodes

The field strength in a ring-shaped region can be described as in the equation below[174]. The reduction in gap by increasing the radius of the inner electrode allows application of higher field strength at a fixed V_a. The increase in the magnitude of the focusing field could enhance dependence of ion on field strength; therefore enhance ion focusing effect through the electrodes. Separation at low field strength is closely related to *m/z* ratio and therefore separation at low field strength has no particular advantages in resolving similar analytes. Therefore, increasing applied field strength compatible with available instrument becomes a useful separation enhancement tool in optimization of the FAIMS device.

$$E = (-V_a)/[r \ln(a/b)] \quad (4)$$

Va: potential applied to inner electrode; r: radial distance from the inner electrode; a: outer diameter of the inner electrode; b: inner diameter of the inner electrode.

The ion inlet region of the FAIMS device was modified to accommodate two carrier gas inlets, creating a symmetric gas flow and reducing ion loss in the entrance region. Comparison between standard and modified FAIMS showed little improvement in sensitivity but significant improvement in S/N was observed. It has been demonstrated that in analysis of standard peptides the modified FAIMS device resulted in up to ten-fold increase in S/N and simulation analysis showed the ion transmission efficiency was improved of ~9-fold and residence time can be reduced to 13.2 ms (±3.9 ms), compared with 50-100 ms in standard FAIMS. Evaluation of the modified FAIMS for qualitative and quantitative analysis of complex biological samples is presented in Chapter 5.

1.5.4 FAIMS and proteomics

The FAIMS technology has introduced new opportunities into proteomics research. FAIMS can be used to separate ions, either with direct infusion electrospray or with LC, prior to their introduction into mass spectrometer[182]. In 2001, a commercialized c-FAIMS device was first introduced by Ionalytics Corporation, which enabled FAIMS to couple with electrospray ionization (ESI). Thermo Fisher Scientific released the c-FAIMS device based on Ionalytics that interfaced with their instruments in 2005. Since then, an increasing number of studies have been carried out to investigate the potential of FAIMS in proteomics research[179,183,184].

The application of FAIMS in proteomics as a separation technique provides advantages in several aspects: (a) reduced background signal and improved signal-to-noise ratio; (b) increased limits of detection and dynamic range; (c) enhanced separation and identification of isobaric ions.

Venne *et al.* combined FAIMS with a quadrupole time-of-flight (Q-TOF) spectrometer in the study of Glu-fibrinopeptide B[185]. A 6~12-fold improvement of S/N ratio and a 20% increase in peptide identification were observed. They applied an 'internal CV-stepping' FAIMS method: each LC-MS/MS scan was collected at a different CV in a single LC-FAIMS-MS/MS run. With this method, LC-FAIMS-MS/MS provided a 20% increase in the number of peptide ions compared with the conventional LC-MS/MS approach in the analysis of U937 cells.

FAIMS has shown potential in shotgun proteomic analysis, especially when coupled with LC, adding an extra dimension of separation. Canterbury *et al.* coupled FAIMS with a LTQ linear ion trap to analyse a complex tryptic digest of *S. cerevisiae* proteins[186]. The use of FAIMS resulted in a fivefold increase in dynamic range and an eightfold increase in peak capacity. However, a loss of signal of one order of magnitude was reported. They proposed the loss may occur in the ion inlet region of FAIMS device as explained above. Saba *et al.* have

demonstrated the ability of FAIMS to enrich multiply charged peptides and increase dynamic range while reducing the background signal[187]. The 'external CV-stepping' method was used in their study: the CV was kept constant during one LC-FAIMS-MS/MS analysis and multiple CVs were scanned individually (in this case ranging from -22 V to -46 V). With this method, they reported a 46% increase in the number of peptide assignment in analysing tryptic digest of U937 cells.

In early studies, FAIMS was normally operated with nitrogen alone. Recently, several groups have also reported the addition of He to the carrier gas could enhance the peptide detection[188,189]. Shvartsburg *et al.* investigated the effect of He content (as carrier gas with nitrogen) on the separation of 3 mono-phosphorylated peptide isomers[189]. They found increasing helium content from 0 % to 75 % induced a shift in the CV value and a decrease in peak widths, which led to improved isomer separation. Shvartsburg *et al.* have examined 50:50 He:N_2 as the carrier gas and the result showed that it significantly improved peptide transmission and resolving power (2~3 times). The composition of carrier gas can greatly affect the behaviour of ions in high and low electric field. They proposed the addition of He enhanced the ion unfolding in the gas environment, resulting in broader separation space and narrower peaks.

FAIMS also provides us a new angle to improve the performance of LC-MS/MS by addressing some of its instrumental limitations. In the investigation of PTM, the presence of positional isomers and co-eluting peptides of the same mass often lead to ambiguous identification[190]. The separation based on LC alone is limited. Thus, pre-separation is particularly useful for the accurate localization of modifications. Bridon *et al.* have also demonstrated the advantages of FAIMS in PTM identification in the study of *Drosophila melanogaster* Schneider S2 cells, where FAIMS expanded the phosphoproteome coverage by 49%. Meanwhile, 78 potential phospho-isomers were identified by FAIMS. Creese *et al.* applied FAIMS to the analysis of a phosphopeptide library, which comprised of 4000 phosphopeptides with sequence inversions

and structural isomers[191]. The use of the library enabled evaluation of the performance of FAIMS regards the separation ability more accurately. The results showed, combined with SCX, LC-FAIMS-MS/MS analyses exhibited a 2-fold increase in the number of phosphopeptide assignments compared to SCX-LC-MS/MS.

1.6 Aims and objectives

The aim of this thesis was to develop and apply methods to gain a greater insight into the key phosphorylation events of FGF signalling following inhibitor treatments. To achieve this, LC-MS/MS and LC-FAIMS-MS/MS were applied to global phosphoproteomics of FGF signalling together with targeted quantitation of specific phosphorylation events.

The specific aims of the work presented in the following chapters were:

- To evaluate the performance of FAIMS in quantitative proteomic analysis and generate a method suitable for SILAC-based LC-FAIMS-MS/MS analysis (**Chapter 3**).
- To investigate of site-specific phosphorylation in FGFR signalling following chemical inhibitions by LC-MS/MS and LC-FAIMS-MS/MS (**Chapter 4**).
- To evaluate the performance of standard and modified FAIMS interface in proteomic analysis (**Chapter 5**).
- To investigate the dynamics of the key phosphorylation events in the FGF signalling by SRM (**Chapter 6**).

CHAPTER 2

MATERIALS AND METHODS

2.1. Buffers and solutions

2.1.1 General laboratory reagents

- Acetic acid (J. T. Baker)
- Acetonitrile, HPLC grade (J. T. Baker)
- Ammonium bicarbonate (Fisher Scientific)
- Ethylenediaminetetraacetic acid (EDTA) (Fisher Scientific)
- Formic acid (Fisher Scientific)
- Iodoacetamide (Sigma-Aldrich)
- Methanol, HPLC grade (J. T. Baker)
- Potassium chloride (Sigma-Aldrich)
- Potassium dihydrogen phosphate (Sanofi)
- Trifluoroacetic acid (TFA) (Sigma-Aldrich)
- Water, HPLC grade (J. T. Baker)

2.1.2 Cell culture

- Phosphate buffered saline (PBS): PBS pH 7.2 tablets (Oxoid) made up according to manufacturers' instructions
- RPMI 1640 medium (Life technologies)
- RPMI 1640 medium for SILAC (Life technologies)
- SILAC labels: L-arginine and L-lysine (R0K0) (Sigma-Aldrich)
- SILAC labels: $^{13}C_6$ L-arginine and 4,4,5,5-D4 L-lysine (R6K4) (Goss Scientific)
- SILAC labels: $^{13}C_6$ 15N4 L-arginine and $^{13}C_6$ $^{15}N_2$ L-lysine (R10K8) (Goss Scientific)
- 0.1 mg/mL streptomycin and 100 I.U./ml penicillin (Sigma-Aldrich)
- 0.5 mg/mL proline (Sigma-Aldrich)

- 10 % Fetal bovine serum, FBS (Biosera)
- 10 % dialyzed FBS (Labtech International)
- 20 ng/mL FGF1 (BioLegend)
- 10 mg/mL heparin (Sigma-Aldrich)
- 1μM dasatinib (Sellek Chemicals)
- Cell lysis buffer: 0.05 M tris-HCl (Thermo Fisher Scientific), 0.15 M NaCl (Thermo Fisher Scientific), 1 % Triton X-100 (Sigma-Aldrich) (v/v), complete protease inhibitor cocktail tablets (Roche Applied Science): 1 tablet per 10 mL (contains EDTA; final concentration 0.001 M)
- Complete Mini, Protease Inhibitor Cocktail Tablets (Roche Diagnostics)

2.1.3 Sample preparation

- C18 Zip-Tip (Millipore)
- Coomassie protein assay kit (Fisher Scientific)
- Trypsin Gold-Mass spectrometry grade (Promega)
- TitansphereTM Phos-TiO2 kit (GL Sciences)
- NuPAGE 4-12% pre-cast Bis-Tris gels (Life technologies)

2.1.4 Fractionations

Strong cation exchange (SCX) chromatography:

- 100×2.1 mm polysulfoethyl aspartamide column (5 μm particle size, 20 nm pore size)
- Mobile phase A (5 mM KH_2PO_4, 20 % (v/v) acetonitrile, pH 3.0)
- Mobile phase B (5 mM potassium dihydrogen phosphate, 20 % (v/v) acetonitrile, 250 mM potassium chloride, pH 3 with phosphoric acid)

Phosphoenrichment :

- Buffer A (0.5% TFA, 80 % acetonitrile)
- Buffer B (25% lactic acid and 75% Buffer A)
- 5 % ammonia hydroxide (Sigma-Aldrich)
- 5% pyrrolidine (Sigma-Aldrich)

2.1.5 Mass spectrometry

- LTQ Velos ESI Positive Ion Calibration Solution (Life technologies)
- Protein Mixture Digest (Dionex)
- MS Qual/Quant QC Mix (Sigma-Aldrich)
- Substance P (Sigma-Aldrich)

2.2 Methods

2.2.1 Cell culture

2.2.1.1 Cell culture

SUM52PE breast cancer cell lines were kindly provided by Dr. Simon Cook, Babraham Institute. SUM52PE cells were grown in RPMI1640 media supplemented with 10% foetal bovine serum (FBS), 0.2 U/ml penicillin, 0.1 mg/ml streptomycin and 2 mM L-glutamine. Cells were cultured at 37 ℃ with 5% CO_2.

2.2.1.2 Cell labelling

For SILAC labelling, SUM52PE cells were grown in amino acid deficient media (RPMI1640) supplemented with 0.1 mg/mL L-Lysine and L-Arginine, "medium" $^{13}C_6$ L-Lysine and $^{13}C_6$ $^{15}N_2$ L-Arginine or "heavy" $^{13}C_6$ L-Lysine and $^{13}C_6$ $^{15}N_4$ L-Arginine, 10% dialyzed FBS, 0.1 mg/mL streptomycin, 0.2 U/mL penicillin and 2 mM L-Glutamine. Cells were cultured for at least five doublings in order for the cells to fully attain complete labelling[192].

2.2.1.3 Cell treatment: SILAC

Prior to treatment, cells grown to 80-90% confluence were serum-starved for 4 hours. After serum starvation, "light" cells were treated with 20 ng/mL FGF1 and 10 mg/mL heparin for 30 min; "medium" cells were treated with 20 μM SU5402 for 30 min followed by treatment of 10 mg/mL heparin and 20 ng/mL FGF1 for 30 min; cells cultured in "heavy" media were treated with 1 μM dasatinib for 30 min followed by a 30-minute treatment of 20 ng/mL FGF1 and 10 mg/mL heparin.

2.2.1.4 Cell treatment: SRM

Prior to treatment, SUM52PE cells were serum-starved for 4 hours. Cells were treated with 20 ng/mL of FGF1 and 10 ng/μL of heparin for 0 s, 20 s, 40 s, 1 min, 3 min, 5 min, 10 min, 20 min, 30 min and 60 min individually.

2.2.1.5 Cell lysis

Prior to cell lysis, cells cultured in 100 mM dish were washed twice with cold PBS and incubated at 4 ℃ for at least 30 min in 800 μL lysis buffer (50 mM Tris-HCl pH 7.4, 150 mM NaCl, 1% Triton TX-100, 1 tablet of protease inhibitor cocktail and 1 tablet of phosphatase

inhibitor cocktail per 10 mL of buffer). Protein concentration was determined using the Coomassie Protein Assay Kit according to manufacturers' instructions. Lysates were adjusted to the desired concentration prior to further experiments.

2.2.1.6 Trypsin digestion

Samples were suspended in 50 mM ammonium bicarbonate. For SILAC samples, equal amount of "light", "medium" and "heavy" lysates were pooled prior to trypsin digestion. Reduction was performed at 56 ℃ in the presence of 8 mM dithiothreitol (DTT) for 45 min. Sample was then alkylated in 25 mM iodoacetamide at room temperature in the dark for 45 min. After reduction and alkylation, proteins were digested by trypsin at an enzyme: protein ratio of 1:100 at 37 ℃ overnight. The digestion was terminated by the addition of 0.5% (v/v) formic acid.

2.2.2 Fractionations

2.2.2.1 Peptide desalting using Sep-Pak Cartridges

Sep-Pak Cartridges were wet with 4 mL of acetonitrile. Cartridges were then conditioned with 1.5 mL of 50% acetonitrile/0.5% acetic acid and 4 mL of 0.1% TFA. Sample was loaded through the cartridges twice. Wash with 4 mL of 0.1% TFA. Cartridges were conditioned with 1 mL of 0.5% acetic acid. Peptides were eluted by use of 2 mL of 50% acetonitrile. Elution was dried by vacuum centrifugation.

2.2.2.2 Peptide desalting using Macro-trap

Sample was resuspended in 20 µL of 1% TFA. Trap was wet with 200 µL of 50% acetonitrile and washed with 100 µL of 0.2% TFA. Sample was loaded twice. Trap was washed with 300

μL of 0.1% TFA. Sample was eluted with 300 μL of 70% acetonitrile. Elution was dried by vacuum centrifugation.

2.2.2.3 Peptide desalting using Ziptip

Sample was resuspended in 20 μL of 1% TFA. Tip was wet with 10 μL 100% acetonitrile (repeat twice) and conditioned with 10 μL of 0.1% TFA (repeat three times). Sample was loaded by aspirating and dispensing the solvent 7-8 times. Tip was washed with 10 μL of 0.1% TFA (repeat three times). Peptides was eluted by aspirating and dispensing in 10 μL of 70% acetonitrile. Elution was dried by vacuum centrifugation.

2.2.2.4 Strong cation exchange (SCX) chromatography

Peptides were resuspended in 100 μL of mobile phase A and loaded onto a 100×2.1 mm polysulfoethyl aspartamide column at a flow rate of 200 μL/min. Separation gradient started from 0 % mobile phase B and increased to 50 % mobile phase B in 30 min, increased from 50% to 100 % mobile phase B in 5 minutes and returned to 100 % mobile phase A to equilibrate. Fractions with 750 μL were collected throughout the run.

2.2.2.5 Phosphoenrichment

Phosphoenrichment was performed using Phos-TiO_2 Phosphopeptide Enrichment Kit according to manufacturers' instructions. Spin tips were conditioned sequentially with 20 μL of Buffer A and 20 μL of Buffer B by centrifugation (3000 ×g, 2 min). Samples were re-suspended in 50 μL of Buffer B and loaded onto the tip for centrifugation (1000 ×*g*, 10 min). Repeat this step and centrifuge again to maximize the binding. Column was washed with 20

μL of Buffer B and 20 μL of Buffer A sequentially and subjected to centrifugation (3000 ×*g*, 2 min). Phosphopeptides were eluted with 5 % ammonium hydroxide and 5% pyrrolidine solution upon centrifugation individually (1000 ×*g*, 5 min). Elution was dried by vacuum centrifugation.

2.2.3 LC-MS/MS analysis

2.2.3.1 Orbitrap Velos mass spectrometer (Chapter 3 and 4)

Experiments were performed on an Orbitrap Velos ETD mass spectrometer, equipped with a Dionex Ultimate 3000 Nano-LC system. Samples were loaded onto a 15 cm C_{18} Acclaim PepMap100 column in mobile phase A (0.1% formic acid) and separated by a gradient from 3.2% to 44% mobile phase B (acetonitrile in 0.1 % formic acid) in 30 min, followed by a 10-minute wash of 90% mobile phase B and a 15 min re-equilibration of 3.2% mobile phase B. Peptides were eluted via a TriVersa Nanomate chip-based electrospray device into the mass spectrometer. For both CID and ETD analyses, the mass spectrometer performed a 'top 7' method comprising a full FT-MS scan (*m/*z 380–1600) at a resolution of 30,000 in the Orbitrap with a 1×10^6 automatic gain control (AGC) target and a 1 s maximum fill time. The seven most abundant precursor ions was isolated for MS/MS scans in ion trap. For CID, MS/MS analysis of the seven most abundant precursor ions above 1000 was performed with a normalized collision energy of 35% (AGC target 5×10^4 charges, maximum fill time 100 ms). For ETD, MS/MS analyses of the seven most abundant precursor ions above a threshold of 5000 was performed with 100 ms activation time (AGC target 5×10^4 charges, maximum fill time 100 ms, reagent AGC target 1×10^5). The precursor isolation window was 2 *m/z*. Only multiply charged precursors were selected for fragmentation. Dynamic exclusion was applied for 60 s.

2.2.3.2 Orbitrap Elite mass spectrometer (Chapter 5)

The mass spectrometer performed a 'top 7' method comprising a full FT-MS scan (*m/*z 380–1600) at a resolution of 30,000 (*m/z* 400) in the Orbitrap with an AGC target of 1×10^6 charges and a maximum fill time of 1 s. The seven most abundant precursor ions detected was isolated for MS/MS scans in ion trap. For CID, MS/MS analyses of the seven most abundant precursor ions above a cut-off of 1000 with a 35% normalized collision energy was performed (AGC target: 5×10^4 charges and maximum fill time 100 ms). Width of the precursor isolation window was 2 *m/z*. Only multiply charged precursors were subjected to fragmentation. Dynamic exclusion was applied for 60 s.

2.2.4 LC-FAIMS-MS/MS analysis

2.2.4.1 Standard FAIMS analysis

The standard FAIMS device was used in Chapter 3, 4 and 5. The standard FAIMS device with a 2.5mm electrode gap width was operated under the following conditions: carrier gas flow rate 2.9 L/min and carrier gas composition 50/50 He:N_2, dispersion voltage (DV) -5 kV, and the inner and outer electrodes temperatures 70 ℃/90 ℃. Liquid chromatography method was as described above. To couple nanospray, the HESI-II source was modified to accommodate the 360 μm O.D. fused silica capillary, with 2 arbitrary units sheath gas to assist electrospray, similar to that described by Swearingen *et al*[179]. The 'external CV stepping' method was used in which the CV is kept constant throughout the LC-MS/MS analysis. Therefore, each analysis is performed at a fixed and separate CV. Liquid chromatography method and MS/MS methods were as described above.

2.2.4.2 Modified FAIMS analysis

The modified FAIMS device was used in Chapter 5. The modified FAIMS device with a 1.5 mm electrode gap width (Thermo Fisher Scientific) was operated under the following conditions: carrier gas (He) flow rate 2.0 L/min, dispersion voltage -5 kV, and the inner and outer electrodes temperatures 70 ℃/90 ℃. To couple nanospray, an in-house nanospray source was modified to accommodate the 360 μm O.D. fused silica capillary. The 'external CV stepping' method was used in which the CV is kept constant throughout the LC-MS/MS analysis. Therefore, each analysis is performed at a fixed and separate CV. Liquid chromatography method and MS/MS methods were as described above.

2.2.5 LC-SRM-MS/MS analysis

2.2.5.1 Synthesis of internal standard peptides

The phosphopeptides selected for SRM analysis were synthesised by GenicBio Limited, Shanghai, China. The phosphopeptides were synthesised without isotope labels by solid phase peptide synthesis. The quantity of each phosphopeptide is 1 mg and the purity of all phosphopeptides is above 95%. Synthetic peptides were resuspended in 50% ACN, 0.1% formic acid to a concentration of 2 pmol/μL. A pool of phosphopeptides was generated by mixing phosphopeptides at the concentration of 2 pmol/μL and stored at -20 ℃ until further use.

2.2.5.2 Selection of transitions

Synthesized phosphopeptides were directly infused into Orbitrap Velos mass spectrometer to assess the purity of each phosphopeptide and optimize the SRM parameters. Specifically, each peptide was prepared at a concentration of 2 pmol/μL in 30% ACN, 0.1% FA.

To assess the quality of each peptide, the total ion MS profile of each peptide was acquired within the mass range *m/z* 380–1800 and the MS/MS profile of each peptide was acquired. Fragment ions with the highest intensity were selected, along with the neutral loss fragment ions for Ser and Thr-containing peptides. To allow comparable quantitation, the same transitions were selected corresponding to endogenous (heavy-labelled) peptides and internal standard (unlabelled) peptides (see Appendix 2).

2.5.5.3 Scheduling of SRM peptides

Scheduling retention time of the phosphopeptides was performed using a Dionex 3000 UHPLC coupled to a TSQ Vantage triple stage quadrupole mass spectrometer. Synthetic phosphopeptides pool (2 picomole/uL) were prepared for LC-SRM-MS/MS analysis. An LC gradient of 3.2-44% ACN over 20 min was delivered, followed by a 5-minute wash of 90% mobile phase B and a 10 min re-equilibration of 3.2% mobile phase B. The SRM transitions were scheduled around their expected elution times. Due to the large number of transitions in this assay (450 transitions for endogenous labelled) and IS peptides), 3 identical methods with different transition sets were created.

2.5.5.4 Establishment of calibration curve

For absolute quantitation, a calibration curve is required to determine the absolute expression level of a peptide. Calibration curves were prepared for each phosphopeptide using synthetic version. A 6-point calibration curve was produced using the following concentrations: 100 attomole, 500 attomole, 1 femtomole, 10 femtomole, 50femtomole and 250 femtomole. Three runs were performed individually in order to accommodate large number of transitions. Three technical replicates were performed in different days.

2.5.5.5 LC-SRM-MS/MS

Peptide mixtures were separated at a flow rate of 352 nL/min in Dionex UHPLC system equipped with 1:300 splitter cartridge to provide nano flow. Samples were loaded onto a 150 mm Acclaim PepMap100 C_{18} column in mobile phase A (0.1% formic acid) and separated by a 20-minute gradient from 3.2% to 44% in mobile phase B (acetonitrile, 0.1 % formic acid), and followed by a 10-minute wash of 90% mobile phase B and re-equilibration (10 min) with 3.2% mobile phase B. Peptides were eluted via a TriVersa Nanomate chip-based electrospray device into the mass spectrometer and a spray voltage of 1.7 kV was used.

All peptides were analysed by TSQ Vantage Triple Quadrupole mass spectrometer. The TSQ Vantage was operated with an ion source temperature of 275 ℃, a unit/unit resolution of 0.7 Da in Q1 and Q3, and a scan width of 0.002 *m/z* for all SRM transitions.

2.2.6 Data analysis

2.2.6.1 SILAC data analysis (Chapter 3 and 4)

Mass spectra were collected using Xcalibur 2.2 and processed by the MaxQuant (version 1.4.1.3).[193] Data were searched against SwissProt human database containing common contaminants and reverse sequence (175242 protein entries) with Mascot (Matrix Science). The search parameters were: minimum peptide length 6, cleavage enzyme trypsin, missed cleavages 2, peptide tolerance 20 ppm and mass tolerance 0.5 Da. Carbamidomethyl (C) was set as a fixed modification. Oxidation (M), acetylation (N-term) and phosphorylation (STY) were set as variable modifications. The appropriate SILAC labels were selected and the maximum labelled amino acids was set to 3. FDR for peptide, protein and site identification was set to 0.01. FDR was calculated as Global FDR at spectral level. Within the Maxquant

output, phosphorylation sites with a Localization Score above 0.75 were considered localized accurately and the accurately localized phosphorylation sites were selected for further analysis.

2.2.6.2 Peptide identifications (Chapter 5)

Data were searched by the Proteome Discoverer 2.1 using the SEQUEST and Mascot algorithms. The following parameters were used: no spectral grouping; fully tryptic, 2 missed cleavages allowed; precursor ion *m/z* tolerance ±10 ppm; fragment ion *m/z* tolerance ±0.8 Da; Carbamidomethyl (Cys) was set as a fixed modification; N-terminal acetylation, oxidation (Met) and phosphorylation (Ser, Thr, and Tyr) were set as variable modifications. Data were filtered to 1 % peptide FDR. For data search of 6 standard proteins, a database containing the 6 proteins and containing common contaminants and reverse sequences were used. For data search of SUM52PE lysates, the SwissProt human database containing common contaminants and reverse sequences were used.

2.2.6.3 SRM data analysis (Chapter 6)

SRM data were acquired using Xcalibur 3.0 and loaded into Skyline 3.1[194] for data analysis. In Skyline, peak detection was manually inspected to ensure retention time of relative transitions were similar and correct peaks were detected. The SRM peak area of synthetic peptides was used to generate calibration curves. The SRM peak area of endogenous peptides was used to generate correlation profiles.

A logarithm transform approach was adopted to combine inter-day calibration data. The mean of triplicate measurements was calculated for further analysis. Next, transform all data and the value of concentration by taking the log base 2 value. Then, calculate the slope and intercept of each peptide in each assay. Next, calculate the mean of slope and intercept of each peptide in inter-day assays. Calculate the R-squared value and the mean of R-squared value of each

peptide. The calibration of data with a less than 0.9 R-squared value will be excluded from further analysis. Convert the data to linear scale and construct calibration curve.

2.2.6.4 Motif-X analysis

The sequence window with the centred phosphorylation sites were submitted for Motif-X analysis. Search parameters were: width 13, occurrences 20, significance 0.000001 and background IPI Human Proteome.

2.2.7 Workflow of SILAC experiment

The schematic diagram of sample preparation process is shown in Figure 2.1. Equal amounts of light, medium and heavy labelled peptides were mixed, digested and then desalted using Sep-pak cartridges. Peptides were re-suspended for SCX fractionation. In SCX, 53 fractions were collected and these fractions were combined into 12. The combined fractions were desalted using Macro-trap cartridges. Phosphoenrichment were performed for the 12 fractions. Following phosphoenrichment, each of the 12 fractions was subsequently split into two. One half of each of the fractions was destined for LC-MS/MS analyses. Ziptip desalting was performed prior to mass spectrometry analyses. For the LC-FAIMS-MS/MS analyses, the remaining twelve half-fractions were pooled and divided equally into 12 aliquots. Each of these 12 aliquots was then analysed at a separate CV. Each of the 24 samples (12 x half-fractions for LC-MS/MS and 12 x aliquots for LC-FAIMS MS/MS) was split into four to allow 2 x CID MS/MS analyses and 2 x ETD MS/MS analyses.

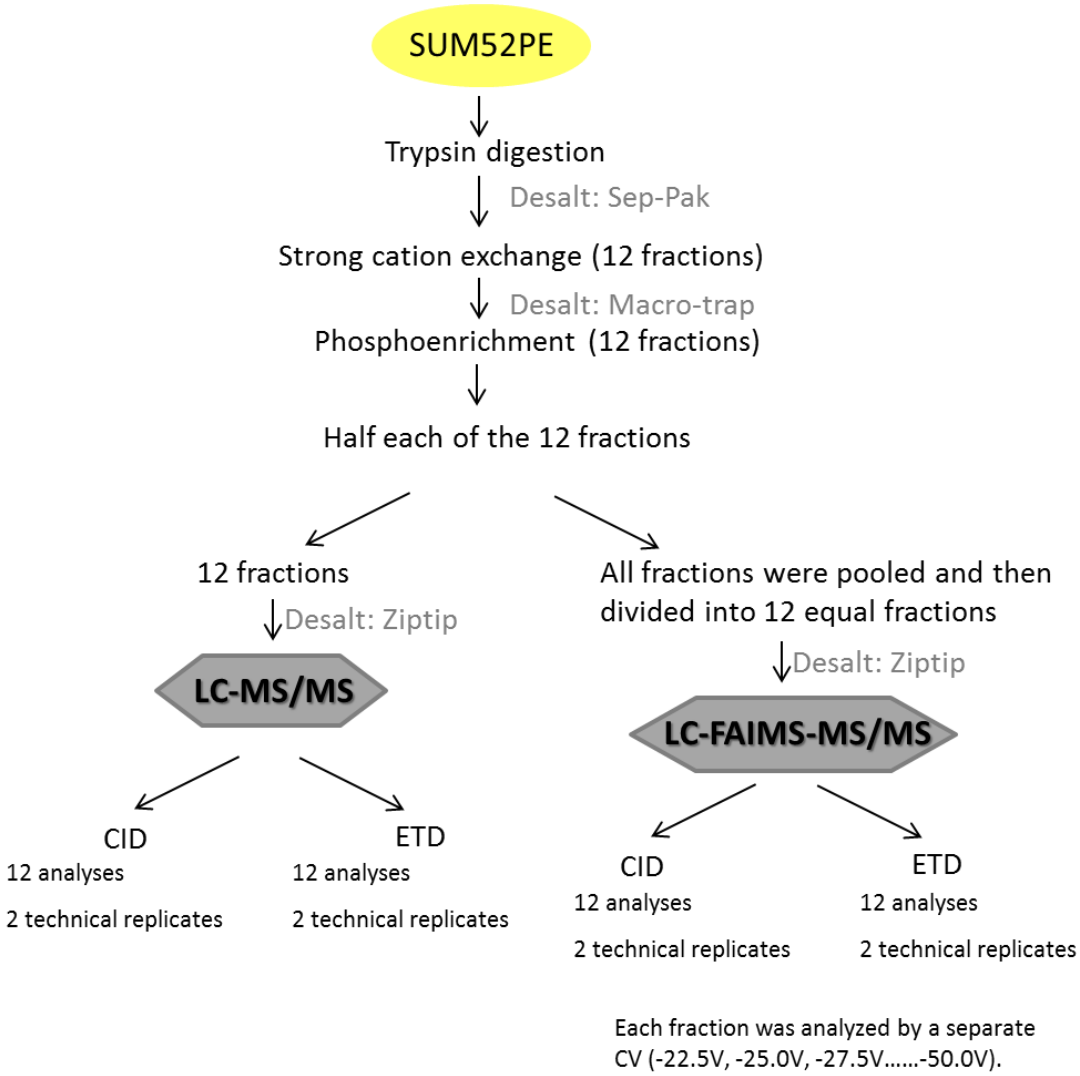

Figure 2.1 Schematic diagram of the sample preparation procedure

2.2.8 Workflow of SRM experiment

In this SRM assay, an absolute quantitation strategy was employed (see Figure 2.2). To obtain absolute quantitation information, internal standard peptides were synthesised corresponding to the peptides of interest. Each IS peptide is identical to native peptides except from their isotopic labels with a difference of 6-10 Da in molecular weight. A known amount (20 fmol) of an IS peptide was spiked to SUM52 cell digests, desalted by Ziptip and analysed by LC-SRM-MS/MS. The quantity of native peptide was calculated using peak ratios in Skyline.

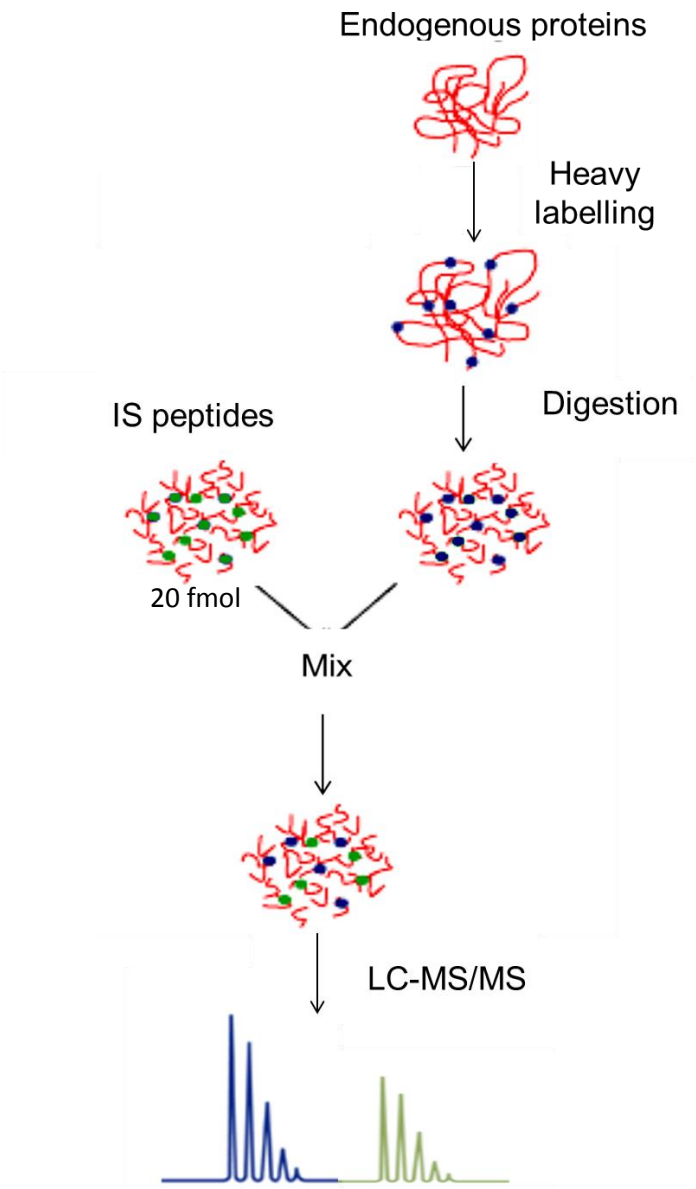

Figure 2.2 Strategy for absolute SRM quantitation assay

CHAPTER 3

OPTIMIZATION OF PHOSPHOPROTEOMIC ANALYSIS BY LC-FAIMS-MS/MS

3.1 Introduction

The aim of the work presented in this chapter was to establish a method that can be used in SILAC-based LC-FAIMS-MS/MS analysis. In this thesis, SILAC was used for quantitative analysis of FGF signalling. In SILAC, cells cultured in different media are labelled by light, medium and heavy isotopic labels. It has been shown, by Shvartsburg *et al*, that different peptides are transmitted at various compensation voltages (CVs) ranges in FAIMS device[195]. It was unclear whether peptides with different isotope labels would be transmitted over different CV ranges, leading to discrepancies in quantitative results. In order to couple SILAC with FAIMS, it was first necessary to evaluate the transmission behaviour of stable isotopic labels in FAIMS device. Secondly, in order to ensure maximum proteome coverage, a pilot experiment was set up to determine the appropriate workflow for SILAC FAIMS using 293T cells and explore the optimum CV range for phosphoproteomics analysis of SU5402 whole cell lysate.

3.2 Results

3.2.1 Quantitation analysis by LC-FAIMS-MS/MS

MS Qual/Quant QC Mix (Sigma-Aldrich) is an "injection-ready" standard and is typically used to monitor quantitation performance. MS Qual/Quant QC Mix contains a set of 14 peptides with light and heavy isotopic labels from 6 pre-digested proteins. These peptides span a 25-fold range of concentration, which makes it ideal for quantitation assessment. A volume of 2 μL of resuspended solution was subjected to LC-FAIMS-MS/MS analyses. Four separate analyses were performed at CVs of -25.0 V, -30.0 V, -35.0V and -40.0V. Results are shown in Table 3.1. The values shown in the table were the average of the four CV steps.

Table 3.1 Quantitation results of Qual/Quant Mix by LC-MS/MS and LC-FAIMS-MS/MS

Ratio of light/heavy peptides by LC-MS/MS analysis was shown in grey ; ratio of light/heavy peptides by LC-FAIMS-MS/MS analysis was shown in yellow ; SD indicates the standard deciation among FAIMS analysis

Sequence	Theoretical Ratio L/H	LC-MS/MS Ratio L/H	LC-FAIMS-MS/MS Ratio L/H	-25V	-30V	-35V	-40V	SD
GGPFSDSYR	1	1.08	1.07		1.093	1.027	1.097	0.038
VLDALQAIK	2	2.18	2.25	2.718	2.066	2.140	3.998	0.452
AVQQPDGLAVLGIFLK	10	10.26	7.44		8.455	6.791	7.065	0.892
SADFTNFDPR	50	33.82	31.46		38.629	28.342	27.418	6.224
EGHLSPDIVAEQK	1	0.84	0.82	0.842	0.804			0.027
ALIVLAHSER	2	1.00	0.93	0.949	0.923	0.923	0.882	0.028
ESDTSYVSLK	10	10.66	-					
GYSIFSYATK	50	44.56	42.67		41.062		43.672	1.846
FEDENFILK	0.5	0.29	0.23				0.233	-
VSFELFADK	1	0.56	0.59		0.577	0.580	0.600	0.013
TAENFR	2	-	-					-
GAGAFGYFEVTHDITK	0.2	0.18	0.19	0.183	0.203	0.171	0.181	0.013
FSTVAGESGSADTVR	10	1.15	1.10	1.143		1.065		0.055
NLSVEDAAR	50	42.31	-					-

The results show that when peptides were selected at different CVs (-25 V, -30 V, -35 V and -40 V), FAIMS was not altering the transmission efficiency of peptides with isotope labels, as indicated by the standard deviation between LC-MS/MS and LC-FAIMS-MS/MS analyses. Comparison of the ratio of light/heavy peptide between LC-MS/MS and LC-FAIMS-MS/MS analyses demonstrated LC-FAIMS-MS/MS was capable of performing quantitative analysis. A few peptides failed to be identified in FAIMS or both of the methods, which is possibly due to their poor capacity to bind columns, low abundance in the mixture or inadequate CV steps. Figure 3.1 shows the MS/MS spectrum of 2+ peptide ALIVLAHSER obtained via LC-MS/MS and LC-FAIMS-MS/MS at CV of -25.0 V and -30.0 V.

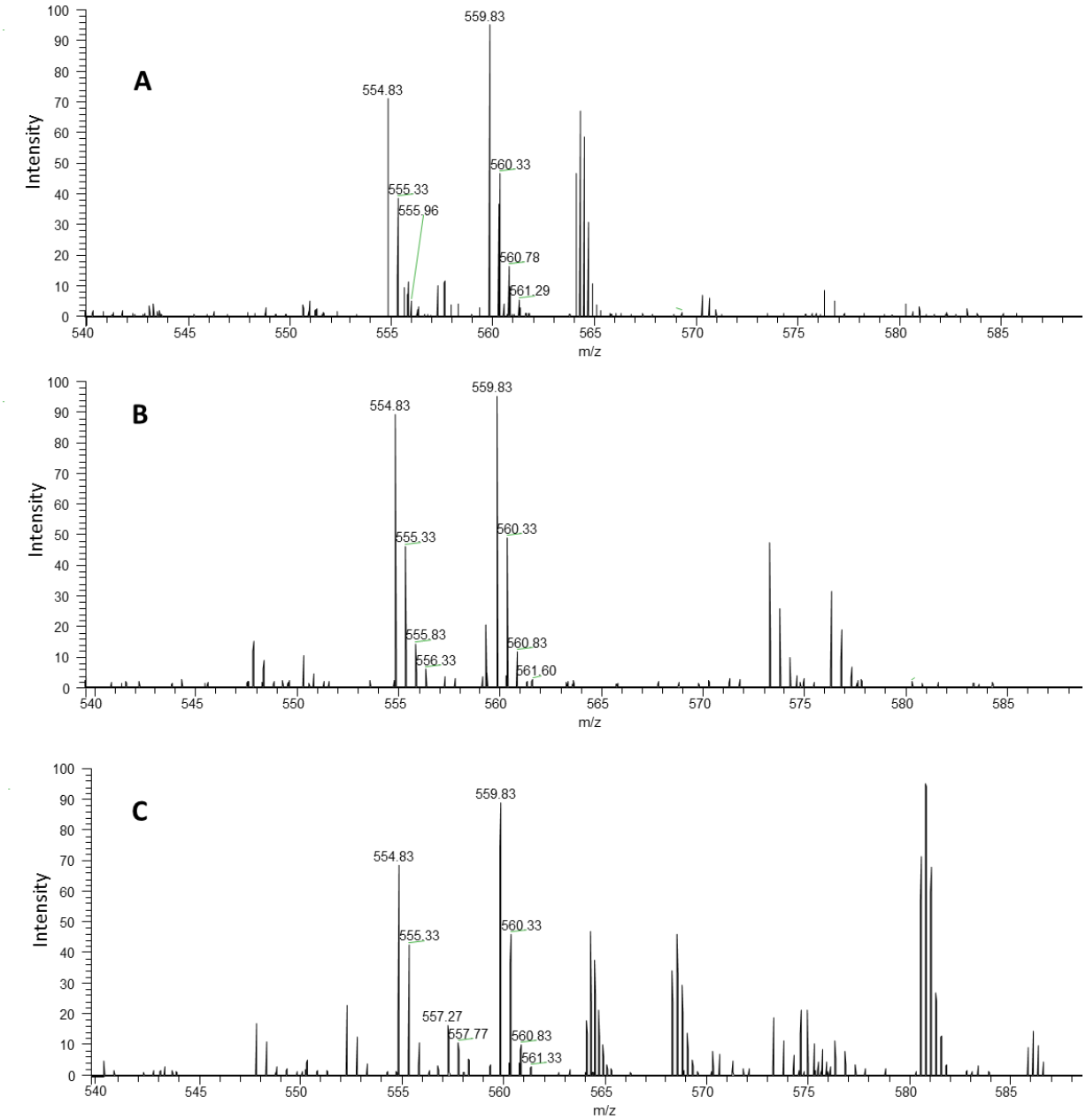

Figure 3.1 MS/MS spectrum of 2+ peptide ALIVLAHSER
A: LC-FAIMS-MS/MS, CV -25 V; B: LC-FAIMS-MS/MS, CV -30 V; C: LC-MS/MS

3.2.2 Phosphoproteomic analysis of 293T cells by LC-MS/MS and LC-FAIMS-MS/MS

3.2.2.1 Workflow

The whole cell lysate of 293T cells was digested, as described in Chapter 2.2.1. For LC-MS/MS analysis, peptides were separated by SCX, following by phosphoenrichment. Previous

experiments conducted within the laboratory suggested that the optimum CV range for proteomic analysis ranged from -20 V to -50 V. Therefore, a CV range of -20 V to -50V was selected. For LC-FAIMS-MS/MS, 13 separate analyses were performed and for each the CV remained constant throughout (CV -20 V, -22.5 V, -25 V…-50 V), as described in Chapter 2.2.4.1.

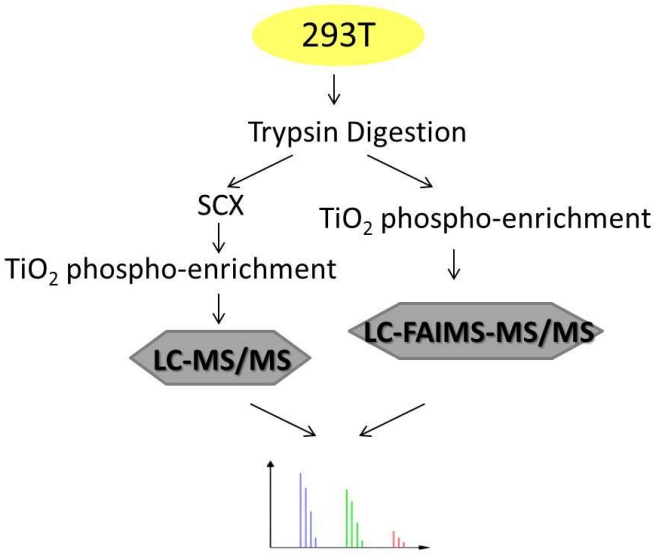

Figure 3.2 Workflow of phosphoproteomics analysis of 293T cells
293T cells lysates were halved after trypsin digestion. For LC-MS/MS analysis, peptides were fractionated by SCX, enriched and submitted for 12 LC-MS/MS runs. For LC-FAIMS-MS/MS analysis, peptides were enriched and analysed at 12 individual CVs.

3.2.2.2 Results

Table 3.2 Number of peptides and proteins identified

MS	**SCX-LC-MS/MS**	**LC-FAIMS-MS/MS**	**Overlap**
Phosphopeptide	2034	340	155
Protein	939	184	96

Table 3.2 shows the number of non-redundant phosphopeptides identified from the two analyses. A total of 2034 non-redundant phosphopeptides were identified by LC-MS/MS (duplicate), compared to 340 by FAIMS analysis (one replicate). LC-MS/MS outperformed FAIMS in terms of the number of identifications. Due to instrument failure, only one set of

FAIMS analysis was performed, which has limited the identification number to some extent. It is also possible that the phosphoenrichment before FAIMS was not efficient. Moreover, these data may indicate further optimization of FAIMS is necessary. It should be noted that although limited information was obtained, 54.4% of the identification by FAIMS was missed by LC-MS/MS approach, which implied FAIMS has the potential to augment proteome research.

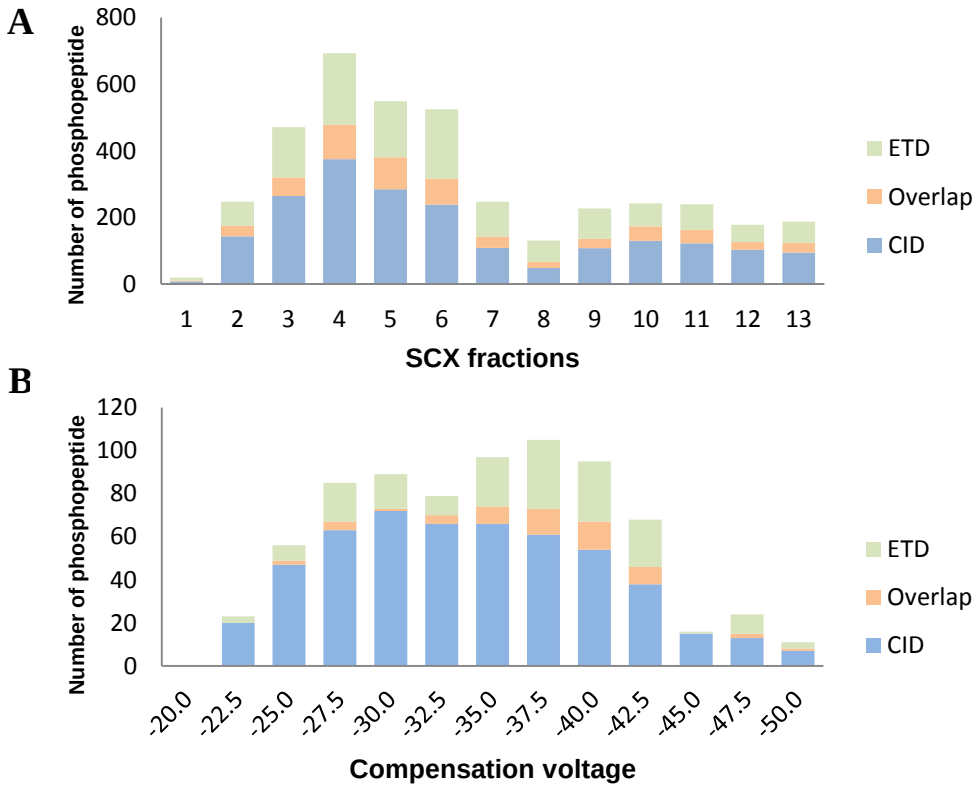

Figure 3.3 (A) Number of phosphopeptides identified in LC-MS/MS per SCX fraction and (B) number of phosphopeptides identified in LC-FAIMS-MS/MS per CV step.

Figure 3.3 shows the number of phosphopeptides identified per SCX fraction and CV step. In LC-MS/MS analyses, 57.2% phosphopeptides were identified from the fraction 3 to 6. In the latter fractions, non-phosphopeptides started to appear while the number of phosphopeptides has started to decrease, which is in agreement with previous studies[196]. In the FAIMS analyses, the identification of phosphopeptides is more evenly distributed across the CV range and the majority (92.3%) of phosphopeptide are identified from CV ranging from -25.0 V to -42.5 V. These data provided the basis for further optimization of CV range.

3.2.3 Phosphoproteomic analysis of SUM52 cells by LC-MS/MS and LC-FAIMS-MS/MS

3.2.3.1 Workflow

In order to further explore the complementarity of LC-MS/MS and LC-FAIMS-MS/MS in phosphoproteomics, a workflow that directly compared the performance of the two techniques was developed. The whole cell lysate of SUM52 was digested by trypsin, separated by SCX, followed by phosphoenrichment and then split for two analyses.

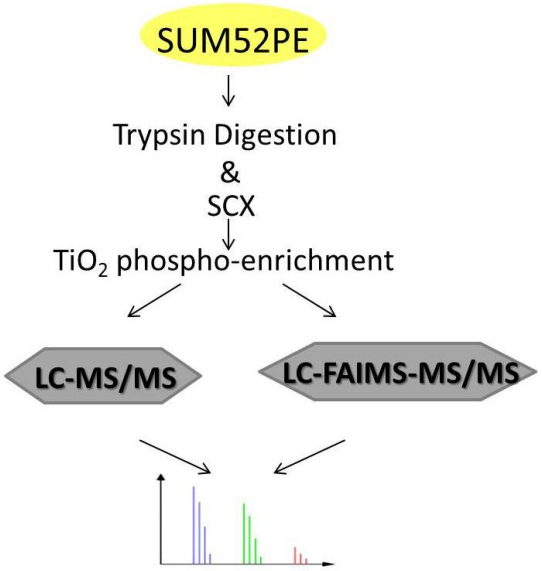

Figure 3.4 Workflow of phosphoproteomics analysis of SUM52
SUM52PE cells were digested, fractionated and enriched prior to MS analyses. For LC-MS/MS, peptides were submitted for 12 LC-MS/MS runs. For LC-FAIMS-MS/MS analysis, peptides were analysed at 12 individual CVs.

3.2.3.2 Results

Table 3.3 Number of peptides and proteins identified

MS	LC	FAIMS
Phosphopeptide	321	331
Peptide	468	515
Protein	350	449

Number of peptides identified is shown in table 3.3. The two approaches have identified a similar number of phosphopeptides and peptides. The composition of phosphorylation status differs greatly, as shown in Figure 3.5. In the FAIMS analyses, 102 multi-phosphorylated peptides were identified (an increase of 65% over those identified by LC-MS/MS analyses). Accordingly, LC-MS/MS has resulted in identification of 195 singly-phosphorylated peptides, an increase of 22% over FAIMS.

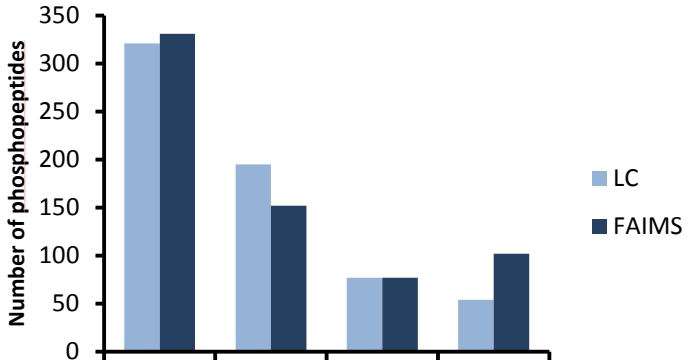

Phosphopeptide	Total	1	2	>3
LC	321	195	77	54
FAIMS	331	152	77	102

Figure 3.5 Phosphorylation status by LC-MS/MS and LC-FAIMS-MS/MS analyses

The overlap in identifications between the workflows is 12 %. In total 73 peptides were identified by both analyses, of which 90% are phosphopeptides. Of the peptides identified only by FAIMS, 18.6% and 21.1% are doubly-phosphorylated and multiply-phosphorylated respectively. In the LC-MS/MS analyses, a relative smaller proportion of doubly-phosphorylated and multiply-phosphorylated peptides are identified (9.6% and 9.2% individually). These data suggest FAIMS has potential in improving proteome coverage, especially for identification of multiply-phosphorylated peptides. This aspect is further explored in Chapter 4.

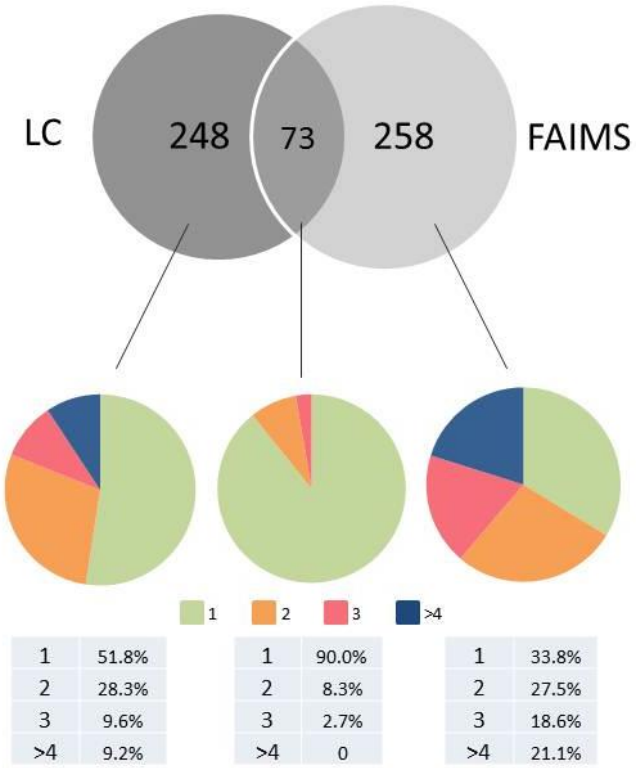

Figure 3.6 Overlap between LC-MS/MS and LC-FAIMS-MS/MS analyses
The table below shows the difference in phosphorylation status

Nevertheless, in this experiment the overall proteome coverage was low and limited information was obtained. This is partly due to the FAIMS workflow needing to be further optimised. It is possible that following SCX, the efficiency of enrichment is limited, which could affect the number of phosphopeptides. Therefore, a replicate experiment was performed with more TiO_2-enrichment tips. As shown in Table 3.4, LC analysis identified 736 phosphopeptides compared to 660 identified by FAIMS.

Table 3.4 Number of peptides and proteins identified in LC-MS/MS and LC-FAIMS-MS/MS analyses

Number of	LC	FAIMS
Phosphopeptide	736	660
Peptide	1271	979
Protein	499	349

3.2.4 Optimization of phosphoenrichment

The Titansphere^{TM} Phos-TiO_2 Kit is based on lactic acid assisted phosphoenrichment using a TiO_2 micro column. Zhao and co-workers developed a two-step separation procedure for sequentially enriching mono- and multi-phosphorylated peptides using citric acid[109] and improvement of multi-phosphorylated peptides identification was observed. In order to evaluate this method and to further apply it to large-scale phosphoproteomic analysis, an experiment comparing the performance of lactic acid and citric acid was performed.

Whole cell lysate of SUM52PE was digested overnight by trypsin. After desalting with Sep-Pak, phosphopeptides were enriched with Titansphere^{TM} Phos-TiO_2 kit using lactic acid and citric acid according to Zhao *et al*. Enriched peptides were desalted using reversed phase C18 Zip-Tip prior to LC-MS/MS analyses.

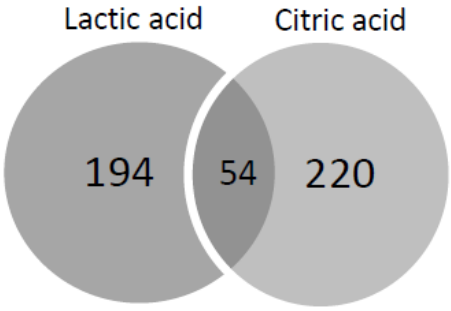

Figure 3.7 Phosphopeptides identified by two enrichment methods (one repeat)

Citric acid-assisted enrichment resulted in a slight increase in the number of phosphopeptides but a very different group of phosphopeptides was identified (see Figure 3.7). Citric acid resulted in a 20.0% increase in the identifications of multiply-phosphorylated peptides compared to lactic acid-assisted enrichment. The two-step method is helpful for the enrichment and purification of phosphopeptide, especially multi-phosphorylated peptides. In this thesis, in order to achieve maximum proteome coverage, phosphoenrichment was performed by lactic acid and two-step citric acid jointly in Chapter 4.

Table 3.5 Peptides identified in phosphoenrichment by lactic acid and citric acid

Number of	Lactic acid	Citric acid
Peptide	340	363
Phosphopeptide	248	274
Multi-phosphor (%)	25.9	46.2

3.3 Conclusion

The performance of LC-FAIMS-MS/MS for quantitative proteomic analysis was evaluated. The use of calibration standards with isotopic labels showed FAIMS did not alter quantitation results compared with the LC-MS/MS method. The method for quantitative LC-FAIMS-MS/MS analysis was established using 293T cells and SUM52 cells. A CV range from -22.5 V to -50 V was selected for further experiments.

CHAPTER 4

FAIMS AND PHOSPHOPROTEOMICS OF FGF SIGNALLING

The content of this chapter has been published in *Journal of Proteome Research*: Zhao H, Cunningham DL, Creese AJ, Heath JK, Cooper HJ. FAIMS and Phosphoproteomics of Fibroblast Growth Factor Signaling: Enhanced Identification of Multiply Phosphorylated Peptides. 2015, *14*(12), 5077-87

4.1 Introduction

By current technologies, singly-phosphorylated peptides constitute the majority of the total phosphopeptides identified[140]. The identification of doubly- and multiply-phosphorylated peptides is more challenging due to their low stoichiometry, poor binding ability to chromatographic columns. Nevertheless, deciphering mechanisms of FGFR signalling requires the knowledge of multiply-phosphorylated peptides as the adjacent phosphorylation sites may play important regulatory roles. Therefore, one of the major challenges in phosphoproteomics research is to map sites of modification in multiply-phosphorylated peptides.

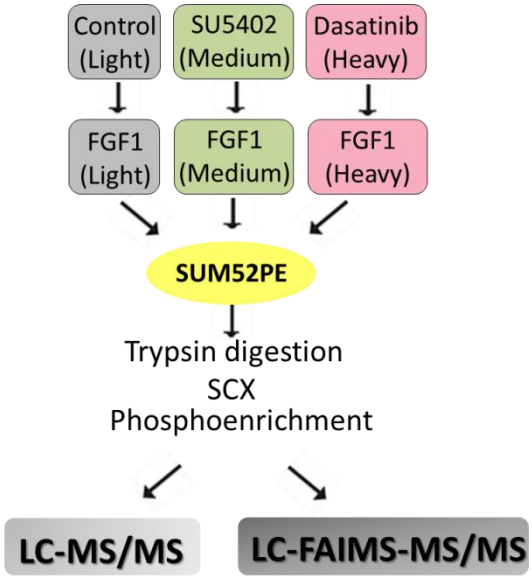

Figure 4.1 Schematic diagram of sample preparation workflow

In this chapter, LC-MS/MS and LC-FAIMS-MS/MS was applied for the investigation of site-specific phosphorylation in FGFR signalling. Previously, quantitative LC-MS/MS was used to identify SFKs-mediated phosphorylation events in FGFR signalling. To further map the key phosphorylation events involved in FGF signalling and SFKs, we used the SILAC approach combined with inhibition of FGFR and SFK. SU5402, a specific FGFR tyrosine kinase inhibitor, and dasatinib, a SFKs inhibitor, were used. Figure 4.1 describes the sample

preparation workflow. SILAC-labelled SUM52 cells were treated with either SU5402 or dasatinib before FGF1 stimulation. Following cell lysis, equal amounts of cell lysates were pooled and digested by trypsin. Next, peptides were fractionated and enriched, and each of the resulting twelve fractions was then divided into two for separate LC-MS/MS and LC-FAIMS-MS/MS analysis. Each LC-FAIMS-MS/MS analysis was performed at a separate and constant compensation voltage (-22.5 V, -25.0 V, -27.5 V…-50.0 V, in 2.5 V steps).

4.2 Results

4.2.1 Phosphopeptide identification by LC-MS/MS and LC-FAIMS-MS/MS

In LC-MS/MS analyses, a total of 3197 non-redundant peptides were identified, of which 2741 were phosphopeptides (85.7%), as shown in Table 4.1. From these phosphopeptides, 2642 phosphosites were identified, of which 1853 phosphosites were accurately localized. Within the well-localised phosphosites, 1542 serine (83.2%), 207 threonine (11.1%) and 104 tyrosine (5.6%) residues were identified.

Table 4.1 Summary of LC-MS/MS and LC-FAIMS-MS/MS analyses

Number of	LC-MS/MS	LC-FAIMS-MS/MS
Non-redundant peptides	3197	1774
Phosphopeptides	2741	1529
Phosphosites	2642	1930
Well-localized phosphosites	1853	1261
Phosphorylated serine (S)	1542 (83.2%)	897 (71.1%)
Phosphorylated threonine (T)	207 (11.1%)	264 (20.9%)
Phosphorylated tyrosine (Y)	104 (5.6%)	100 (7.9%)

In LC-FAIMS-MS/MS analyses, a total of 1774 non-redundant peptides were identified, of which 1529 were phosphopeptides (86.2%). Within these phosphopeptides, a total of 1930

phosphosites were identified and 1261 phosphosites were well localized. The distribution of phosphorylated residues is: 897 (71.1%) serine, 264 (20.9%) threonine and 100 (7.9%) tyrosine. A notable increase in the relative proportion of identified pThr and pTyr phosphorylation sites was observed in the LC-FAIMS-MS/MS dataset.

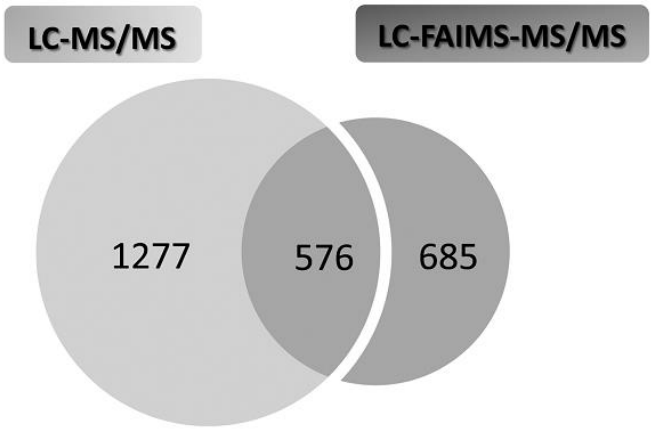

Figure 4.2 Well-localized phosphosites identified via LC−MS/MS and LC−FAIMS−MS/MS

In total, 2538 well-localised phosphorylation sites were identified and the well-localised phosphorylation sites were selected for the following analysis. The two workflows showed good complementarity and the overlapping population comprised 44.0% of the identifications by LC-FAIMS-MS/MS (see Figure 4.2). In order to explore properties of the phosphopeptides identified in LC-MS/MS and LC-FAIMS-MS/MS, the CV distribution, charge state, length and phosphorylation status of these phosphopeptides was examined in the following sections.

4.2.2 CV Distribution

The number of phosphopeptides identified per SCX fraction is shown in Figure 4.3A. In LC-MS/MS analyses, the majority of the peptides identified were derived from the first four SCX fractions (64.7%). In contrast, in the LC-FAIMS-MS/MS analyses (Figure 4.3B), phosphopeptide identification did not show any bias towards a particular (range of) CVs.

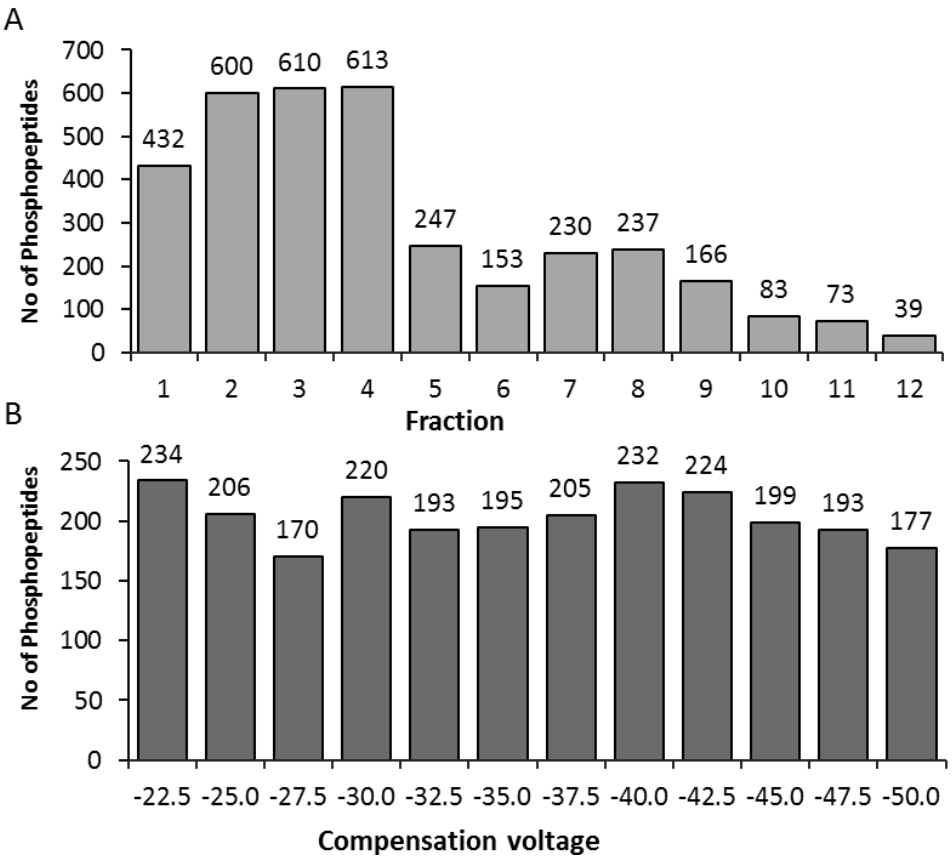

Figure 4.3 Unique peptides identified in (A) LC-MS/MS and (B) LC-FAIMS-MS/MS analyses

4.2.3 Charge state distribution

The distribution of charge states of the identified phosphopeptides is shown in Figure 4.4. Doubly-charged ions (57.7%) constituted the majority of identifications from the LC-MS/MS dataset, with 3+ ions contributing 36.6% of the identifications. For the LC-FAIMS-MS/MS dataset, 26.9% of the total identifications arose from 2+ precursor ions, compared with 63.8% from 3+ ions.

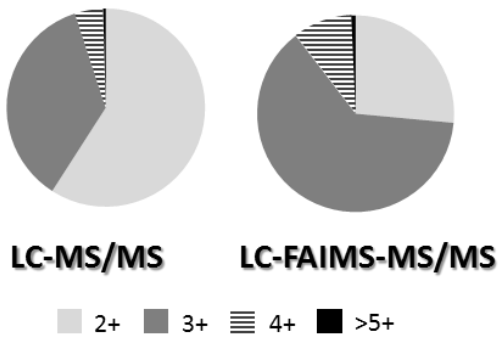

Figure 4.4 Pie chart showing doubly, multiply-charged peptides in LC-MS/MS and LC-FAIMS-MS/MS analyses

Further examination revealed that the majority of the 2+ peptides were identified from the first four fractions, see Figure 4.5. The distribution of triply charged peptides showed a bimodal distribution.

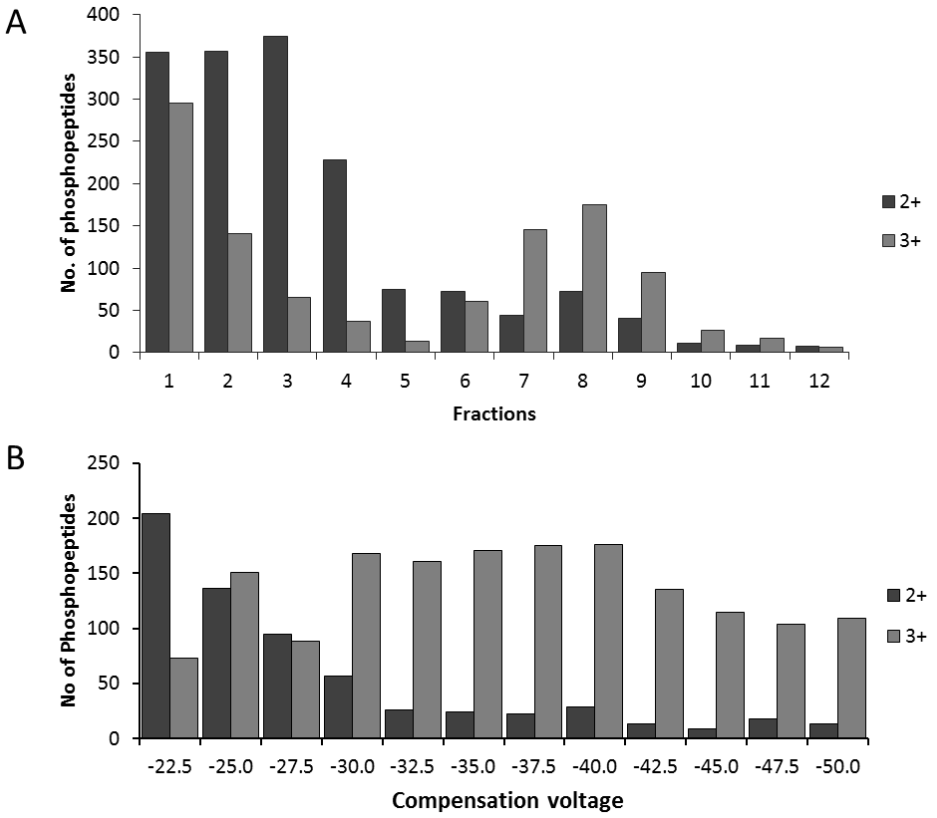

Figure 4.5 Distribution of 2+ and 3+ ions identified in (A) LC-MS/MS and (B) LC-FAIMS-MS/MS

Examination of the LC-MS/MS dataset showed, again, that the majority of ions are identified in the first four fractions (Figure 4.5A). In the LC-FAIMS-MS/MS dataset, 2+ and 3+ ions were identified at distinctly different CV ranges (Figure 4.5B). Doubly-charged ions were mainly observed in CV -22.5 V to -30 V (72.8%); however, 3+ ions were identified throughout all CVs.

4.2.4 Phosphopeptide length

The length of the phosphopeptides identified in the FAIMS dataset ranged from 7 to 40 amino acids and 98.6% were between 7 to 33 amino acids. The distribution of phosphopeptides

according to peptide length (7 to 33 amino acids) and CV is shown in Figure 4.6A. The heat map identified two areas with high incidence of phosphopeptide identification. One is in the CV range -22.5 V to -27.5 V and length 12-18 amino acids. The other area is in the CV range -32.5 V to -47.5 V and length 15-21 amino acids. The two regions overlap with the charge state distribution discussed above: the top-left area is mostly comprised of 2+ phosphopeptides and the middle one is exclusively comprised of 3+ ions. For phosphopeptides identified in LC-MS/MS analyses, 64.7% peptides were identified from the first 4 fractions and 72.5% the peptides were between 11 and 23 amino acid residues (Figure 4.6B).

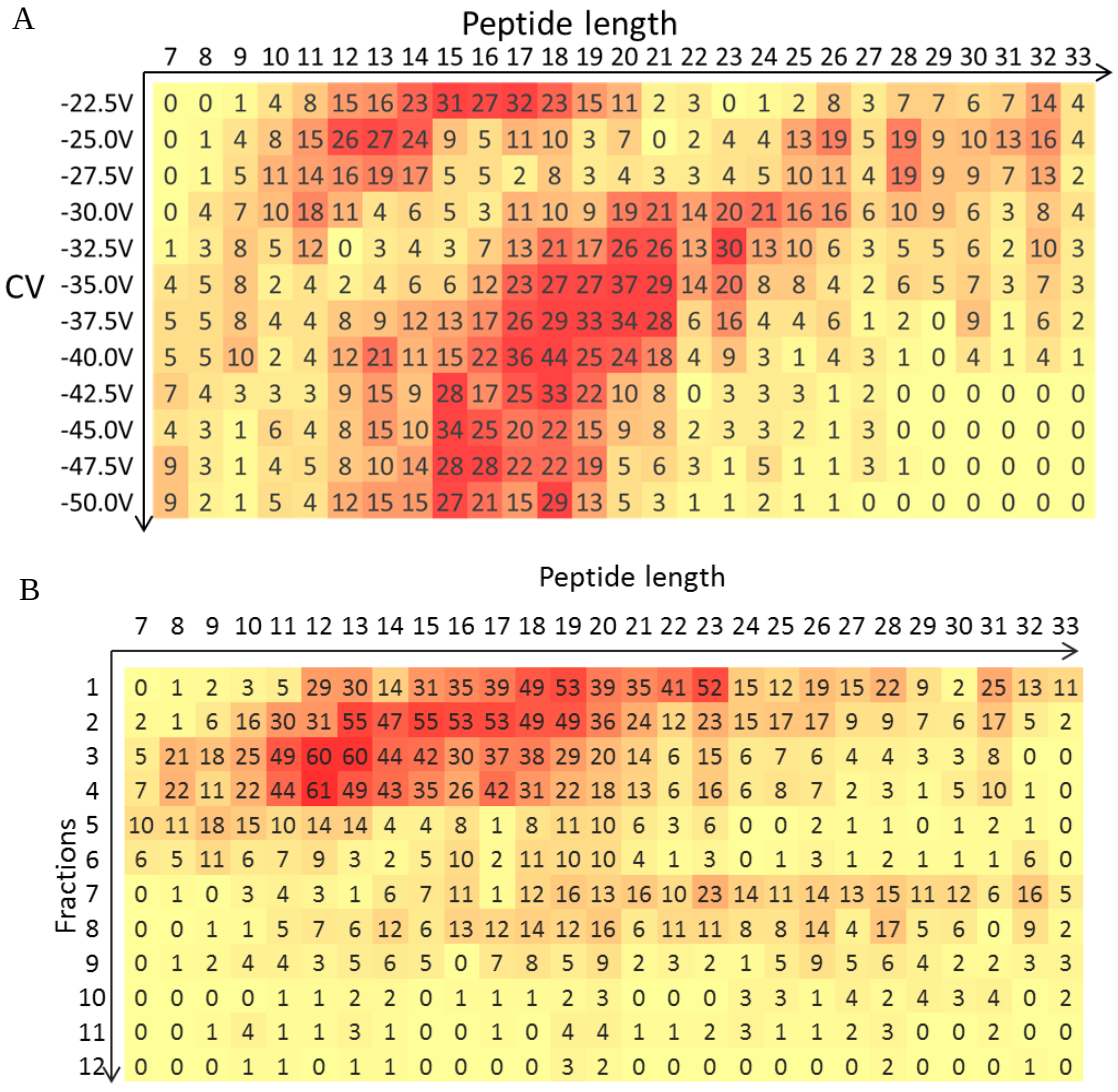

Figure 4.6 Distribution of identified phosphopeptides in (A) LC-MS/MS and (B) LC-FAIMS-MS/MS according to fraction and peptide length (number of amino acid residues). Numbers in each cell represent the number of phosphopeptides identified under the given condition.

4.2.5 Phosphorylation status

The distribution of singly-, doubly- and multiply-phosphorylated peptides is shown in Figure 4.7A. The majority of the phosphopeptide assignments were singly-phosphorylated in both workflows (80.7% in LC-MS/MS dataset and 70.5% in LC-FAIMS-MS/MS dataset). A total of 29.5% of the phosphopeptides identified in the LC-FAIMS-MS/MS analyses were doubly- or multiply-phosphorylated, compared with 19.3% in the LC-MS/MS analyses.

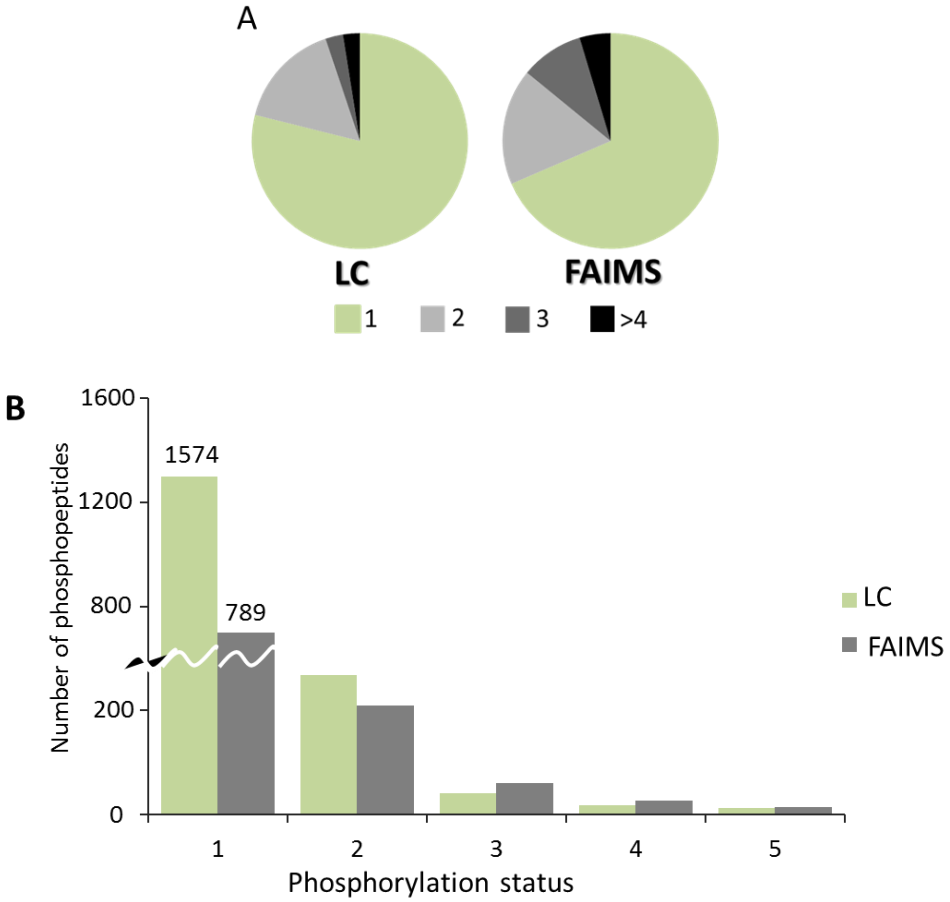

Figure 4.7 (A) Distribution of singly-, doubly- and multiply-phosphorylated peptides. (B) Comparison of singly-, doubly- and multiply-phosphorylated peptides in LC-MS/MS and LC-FAIMS-MS/MS

The distribution of charge states for the doubly- and multiply-phosphorylated peptides identified is shown in Figure 4.8. The multiply-phosphorylated peptides are mainly associated with 3+ ions in the FAIMS dataset compared to non-FAIMS. The enhanced identification of multiply phosphorylated peptides is likely due to the separation of charge states by FAIMS.

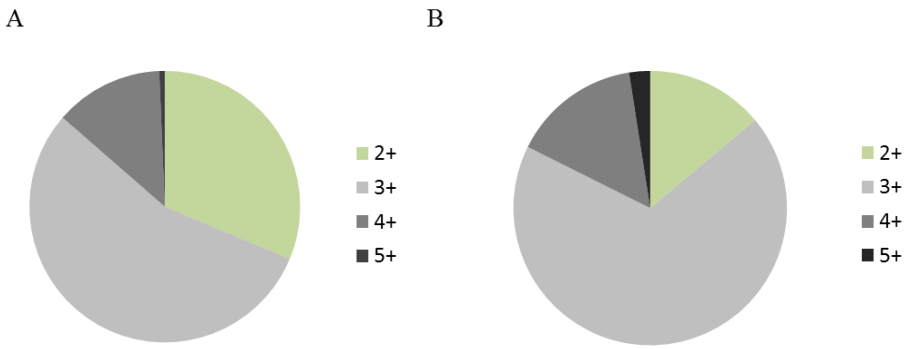

Figure 4.8 Distribution of charge states of doubly- and multiply- phosphorylated peptides in (A) LC-MS/MS analyses and (B) LC-FAIMS-MS/MS analyses

In Figure 4.9, the overlap in identification of doubly-phosphorylated peptide from the two workflows was 21.2%. For multiply-phosphorylated peptides, only 7 of the 188 phosphopeptides were identified by both methods, less than 4% of the total multiply-phosphorylated peptide identifications, emphasizing the complementarity of the two methods, particularly in multiply-phosphorylated peptides.

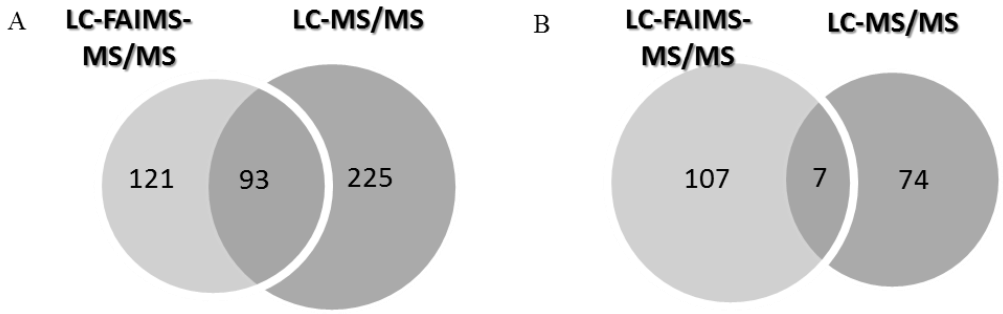

Figure 4.9 Identification of doubly- and multiply-phosphorylated peptides from LC-MS/MS and LC-FAIMS-MS/MS: (A) doubly-phosphorylated peptides and (B) multiply-phosphorylated peptides

4.2.6 Novel phosphorylation sites

To further probe the two datasets, PhosphoSitePlus (http://www.phosphosite.org)[197] was used to identify novel phosphorylation sites from the known sites. In the LC-MS/MS dataset, 75 (4.3%) of the identified phosphosites were novel phosphorylation sites, including 33 pSer sites,

9 pThr sites and 33 pTyr sites. Only three of these sites were also identified in the LC-FAIMS-MS/MS dataset. In contrast, 227 novel phosphosites (19.9%) identified by LC-FAIMS-MS/MS have not been previously reported, comprising of 168 pSer, 42 pThr and 17 pTyr sites. Remarkably, 187 of the novel phosphorylation sites were assigned from multiply-phosphorylated peptides. Details of the novel phosphosites can be found in Appendix 1.

In order to explore the sequence features of the novel sites, Motif-X[198] was used to identify motifs from the novel phosphosites identified in the LC-FAIMS-MS/MS dataset. From 227 novel phosphorylation sites, 3 potential motifs were identified (P<0.0003): SxxT, SxxxT and TxxxxS (see Figure 4.10). SxxxT is a highly conserved motif, recognised by MAPKK supergene family in animals[199]. As promotion and attenuation of FGF signalling requires the involvement of the MAPKK cascade, this observation indicates that substrates of MAPKK with uncharacterised phosphorylation sites may possess interesting properties for further investigation. No consensus motif was identified from the novel phosphosites identified in the LC-MS/MS dataset.

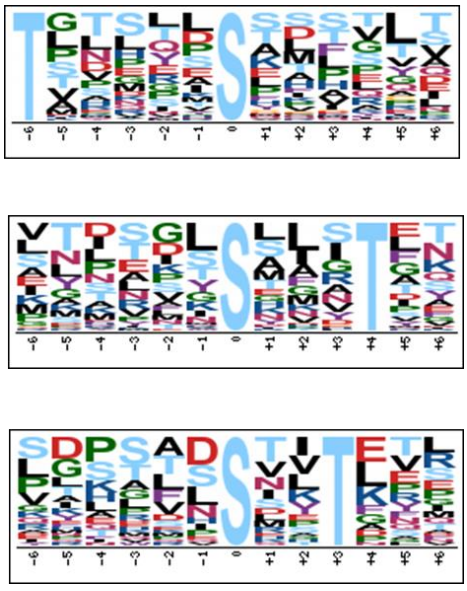

Figure 4.10 Motif analysis of the novel phosphorylation sites in the LC-FAIMS-MS/MS analyses
Motif-X centred on the phosphorylated serine residue. The size of the adjacent amino acid indicates the frequency of the appearance of a particular amino acid.

To determine if the enhancement in identification of novel phosphorylation sites is associated with charge state, the charge state distribution was profiled. In the LC-FAIMS-MS/MS analyses, phosphopeptides with charge states ≥ 3+ represented 91.2% of the novel sites identified compared to 55.3% in LC-MS/MS analyses.

Further analysis by DAVID Functional Classification[200] based on KEGG database revealed a number of highly involved proteins (see Appendix 2). A cluster of G protein-coupled receptors (GPCRs) was enriched in the novel proteins identified in the LC-FAIMS-MS/MS workflow. An example of this is Trem-like transcript 2 (TLT-2) protein, a cell surface receptor protein that may play a role in immune response[201]. A quadruply-phosphorylated peptide MAPAFLLLLLLWPQGCVSGPpSADpSVpYpTK of TLT-2 including the signal peptide region (1-18) was identified at CV of -27.5V. Tandem mass spectrum of the 3+ peptide was shown in Figure 4.11. The signal peptide region is not phosphorylated, but the N-terminus of Ig-like V-set domain (19-268) is highly phosphorylated and this is the first time that phosphorylation sites have been reported within this region.

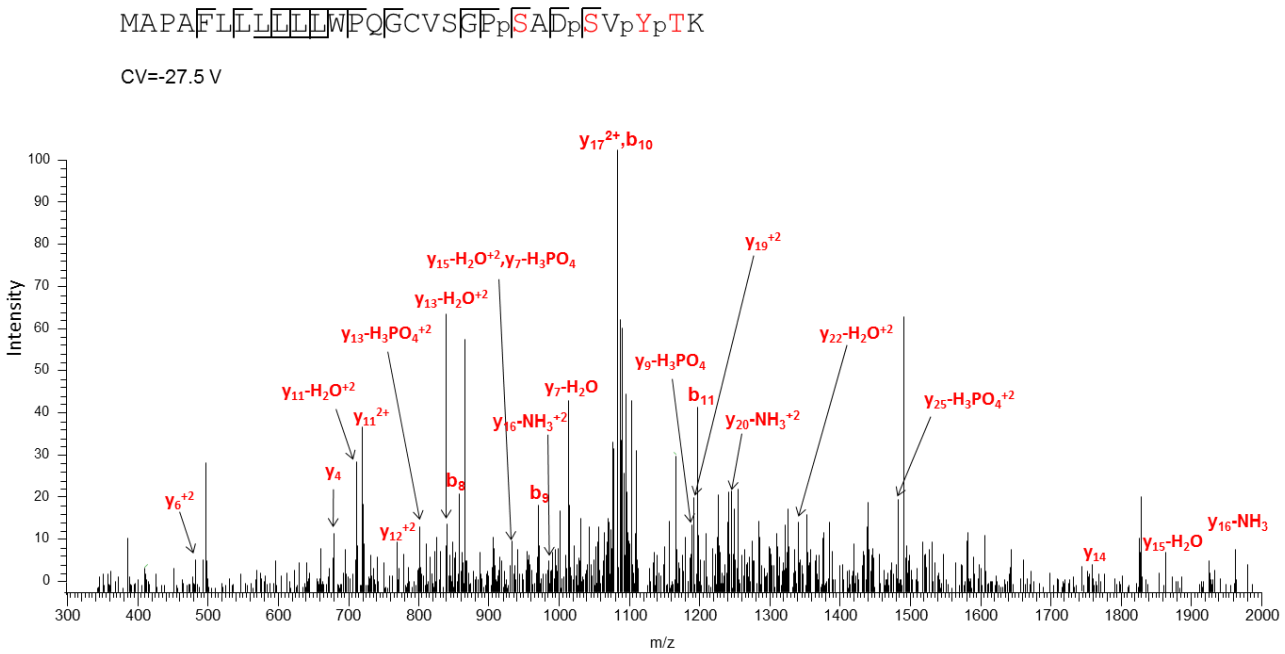

Figure 4.11 CID mass spectrum of $[M+3H]^{3+}$ ions of MAPAFLLLLLLWPQGCVSGPpSADpSVpYpTK at CV of -27.5 V, a multiply-phosphorylated peptide containing previously unobserved phosphosites

4.2.7 FGFR and Src mediated phosphorylation events

4.2.7.1 Initial assessment

To analyse the quantitative response of the phosphosites, an initial assessment was necessary. In the LC-MS/MS dataset, SILAC information on 75.6% of the identified phosphosites were obtained compared to 69.8% in LC-FAIMS-MS/MS dataset. SILAC ratios were normalised (by Maxquant) to avoid unimodal global distribution. The fold change cut-off was applied based on a previous experiment. In that experiment, samples labelled with light, medium and heavy isotopic labels were mixed in equal portions and subjected to LC-MS/MS analysis. The mean SILAC ratios and SD was calculated. For a probability cut-off of p=0.05, the mean ratio ± 2SD was between 0.58 and 1.73. For a more stringent cut-off (p=0.0027), the mean ratio ± 3SD was between 0.44 and 2.23. Therefore, |log2 (FC)|=1 was defined as the boundary of differentially regulated phosphosites to give greater than 95% confidence.

The consistency of quantitation results of the two approaches is shown in Figure 4.12. The quantitation results of the corresponding peptides between the two approaches are in good agreement with 68.6% of the fold-change ratios in the 95% confidence interval.

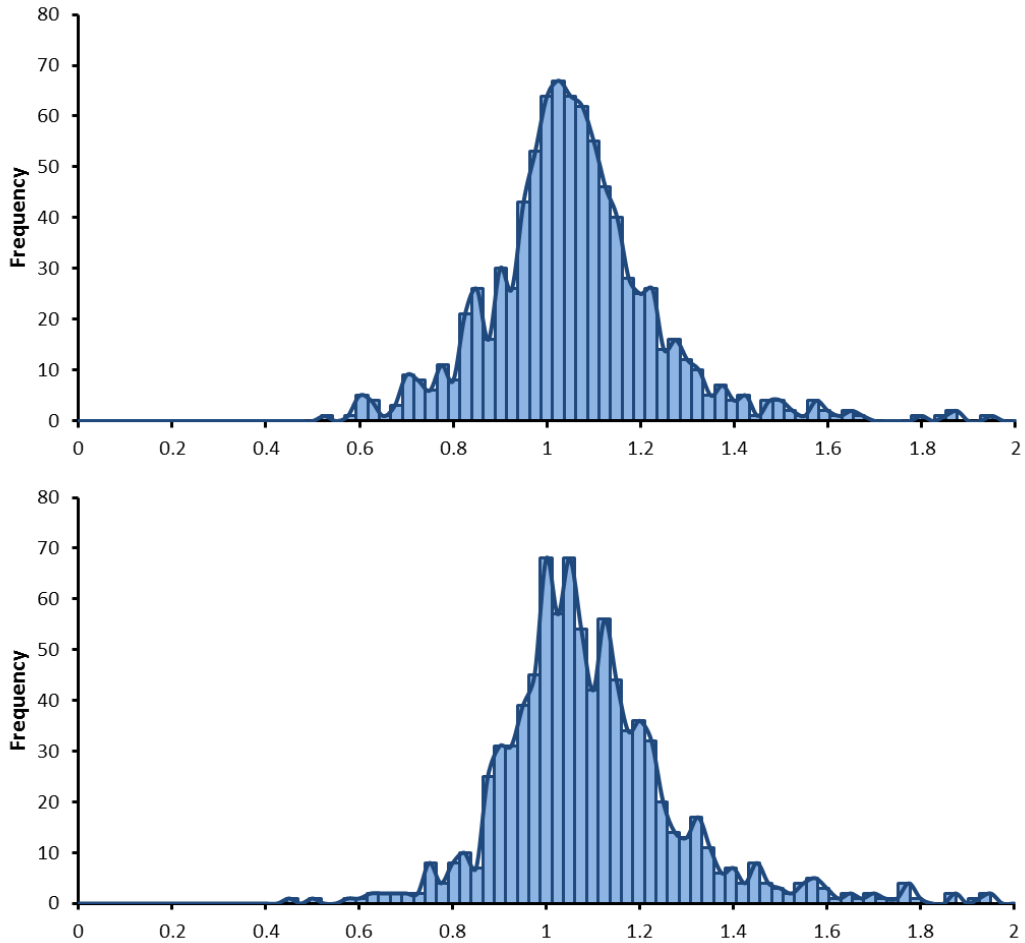

Figure 4.12. Histogram showing the quantitation consistency between LC-MS/MS and LC-FAIMS-MS/MS assays. The frequency was calculated using the ratio of the fold-change of the corresponding peptides of LC-MS/MS against LC-FAIMS-MS/MS assays. (A) Quantitation of SU5402/FGF1; (B) Quantitation of dasatinib/FGF1.

The labelling efficiency of SILAC approach was determined by submitting the light, medium and heavy isotope labelled peptides for individual LC-MS/MS analysis. A manual analysis was performed to ensure the medium and heavy cells were corrected labelled over 98.5%.

4.2.7.2 SU5402 and dasatinib sensitive phosphosites

In order to map the phosphosites regulated by SU5402 and dasatinib, a large-scale quantitative analysis was performed. The comparative analysis of phosphosites responded to SU5402 in LC-MS/MS dataset only, LC-FAIMS-MS/MS dataset only and in both is shown in Figure 4.13.

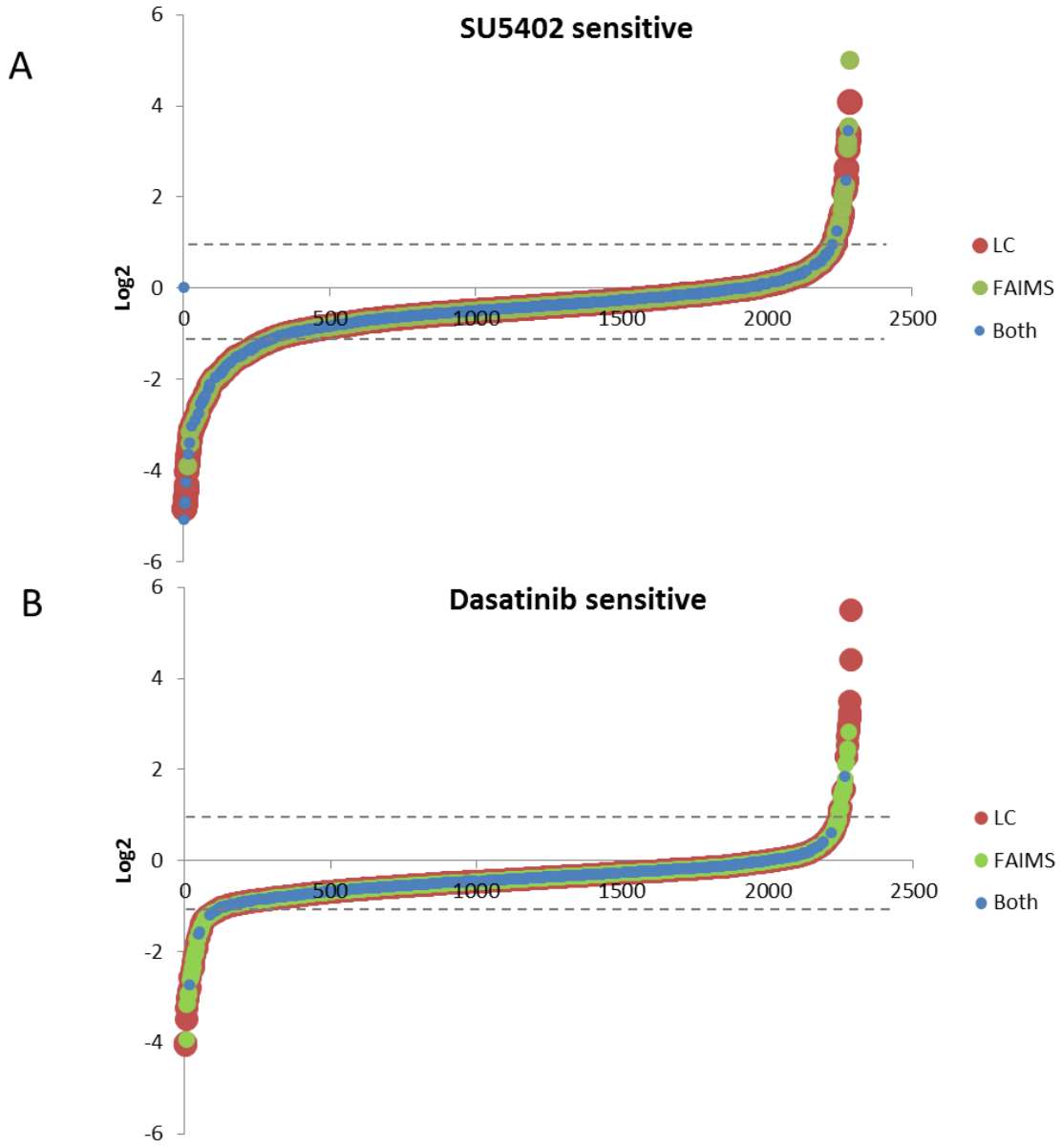

Figure 4.13 (A) Log_2 plot of the ratio of the peptide abundance for SU5402/FGF1 treatments for each phosphopeptide identified; (B) Log_2 plot of the ratio of the peptide abundance ratio for dasatinib/FGF1 treatments for each phosphopeptide identified. Peptides identified by FAIMS only are shown in green and those identified by LC-MS/MS only are shown in red. Peptides identified by both are shown in blue. Dashed lines indicate the cut-off ($log_2 = \pm 1$).

A high occurrence of global down-regulation in phosphorylation levels was observed in the FGF pathway and downstream processes. A total of 256 phosphosites responded to SU5402 ($log_2 \leq -1$ or $log_2 \geq 1$) were detected by both methods (Figure 4.13, shown in blue). LC-MS/MS identified 175 phosphosites (shown in red) and LC-FAIMS-MS/MS identified 153

phosphosites (shown in green) sensitive to SU5402 treatment. There were 186 phosphosites down-regulated due to SU5402 treatment, of which 70 were uniquely identified via the FAIMS workflow. Seventy four phosphosites were up-regulated in response to SU5402, with 29 unique to FAIMS workflow (see Table 4.2).

There are 87 phosphosites sensitive to dasatinib were detected by both methods. LC-MS/MS and LC-FAIMS-MS/MS identified 24 and 60 phosphosites sensitive to dasatinib respectively. A total of 40 phosphosites were down-regulated due to dasatinib treatment, of which 27 were uniquely identified via the FAIMS workflow. Forty-seven phosphosites were found to be up-regulated in response to dasatinib, with 32 unique to the FAIMS workflow.

Table 4.2 Summary of quantitation analysis

Number of	**LC-MS/MS**	**LC-FAIMS-MS/MS**
Well-localized phosphosites	2642	1930
Quantified	1998	1341
SU5402 sensitive	175	153
Dasatinib sensitive	24	60

The LC-MS/MS and LC-FAIMS-MS/MS dataset was further explored to interrogate the coordination between SU5402 and dasatinib treatments. A $\log_2$-$\log_2$ plot was used to visualise the underlying interaction (see Figure 4.14). There are 53 phosphosites sensitive to both SU5402 and dasatinib treatment. LC-FAIMS-MS/MS alone detected 38 phosphosites sensitive to both treatments, 2 of which were found by both methods.

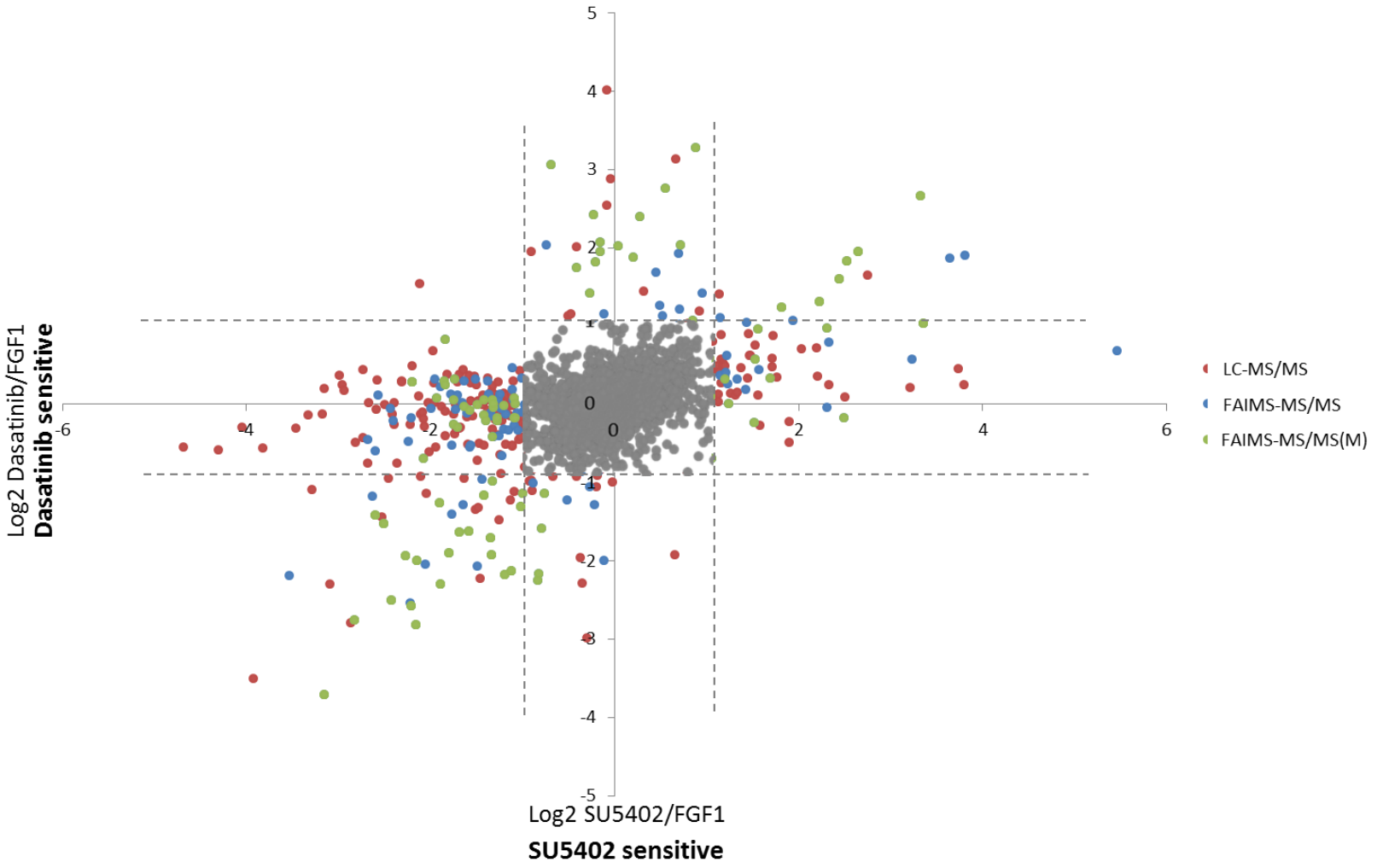

Figure 4.14 (A) Log$_2$-log$_2$ plots to visualise SU5402 and dasatinib sensitive phosphosites.
The ratio of phosphosites abundance of SU5402/FGF1treatment is plotted against the ratio of dasatinib/FGF1 treatments. Phosphosites identified by LC-MS/MS analyses only are shown in red. Phosphosites derived from singly- and multiply-phosphorylated peptides identified by FAIMS only are shown in blue and green respectively. Those identified by both methods are shown in grey. Dashed lines indicate the cut-off (log$_2$ = ±1).

4.2.7.3 SU5402 and dasatinib sensitive proteins

The DAVID Functional Classification tool was used to identify the protein groups in response to SU5402 and dasatinib. The regulated peptides were submitted to DAVID and two groups of protein were enriched in the KEGG database annotation. One is the kinases involved in the cell cycle regulation and translation. For instance, ribosomal protein S6 kinase beta-2 (S6K2) with decreased phosphorylation upon SU5402 and dasatinib inhibition was identified in FAIMS analysis. S6K2 has been previously identified as a downstream effector of FGF signalling[202]. The other group contains a cluster of cell membrane receptors participating in signal transduction, such as LILRB1 and MRG.

Although some of the identified proteins were already known to be associated with FGF signalling, many of the individual proteins or phosphosites identified are novel to this pathway. As an example, breast cancer anti-estrogen resistance protein 3 (BCAR3) acts as an adapter protein for tyrosine kinase-based signalling in breast cancer cells[203]. The FAIMS results revealed a previously unidentified phosphorylation site within this protein (Thr 368). It has been shown BCAR3 enhances cell mobility through interaction with p130 and Src. It has been demonstrated this binding capacity could be greatly reduced when Src activity is affected[204]. The phosphorylation level of T368 site was up-regulated upon SU5402 and dasatinib treatment. Whether or not the up-regulation of T368 is associated with the activity of BCAR3 is yet unknown: this result may provide an entry point to decipher mechanisms of estrogen regulation.

4.2.7.4 Enrichment in multiply-phosphorylated peptides

Table 4.3 Phosphopeptides containing novel phosphosites sensitive to SU5402 or dasatinib

Modified sequence	Novel site	Amino acid	No of phosphosites	Charge	Localization probability
(ac)ATPAAVNPPEMAS(ph)DIPGSVTLPVAPM(ox)AAT(ph)GQVR	29	T	2	4	0.957
(ac)EETMKLAT(ph)M(ox)EDT(ph)VEYCLFLIPDESR	12	T	2	3	0.758
(ac)M(ox)S(ph)S(ph)NSDTGDLQES(ph)LK	3	S	3	3	0.899
(ac)MAS(ph)LS(ph)AAAIT(ph)VPPSVPSR	3	S	3	3	1.000
AS(ph)SPHQAGLGLS(ph)LTPS(ph)PES(ph)PPLPDVSAFS(ph)RGRGGGEGR	2	S	5	4	0.826
AS(ph)SPHQAGLGLS(ph)LTPS(ph)PES(ph)PPLPDVSAFS(ph)RGRGGGEGR	29	S	5	4	0.787
ASLY(ph)VGDLHPEVT(ph)EAM(ox)LY(ph)EK	13	T	3	3	1.000
AT(ph)PLS(ph)STVTLS(ph)M(ox)S(ph)ADVPLVVEY(ph)K	22	Y	5	3	0.987
AT(ph)PLS(ph)STVTLS(ph)M(ox)S(ph)ADVPLVVEY(ph)K	11	S	5	3	0.781
AT(ph)PLS(ph)STVTLS(ph)M(ox)S(ph)ADVPLVVEY(ph)K	13	S	5	3	0.781
DQTAALPLAAEET(ph)ANLPPSPPPSPAS(ph)EQTVT(ph)VEEAS(ph)K	36	S	4	3	0.996
DQTAALPLAAEET(ph)ANLPPSPPPSPAS(ph)EQTVT(ph)VEEAS(ph)K	31	T	4	3	0.831
DS(ph)GQVIPLIVES(ph)CIR	2	S	2	2	1.000
DS(ph)GQVIPLIVES(ph)CIR	12	S	2	2	1.000
DSEDS(ph)LY(ph)NDYVDVFY(ph)NTK	7	Y	3	3	0.989
DSEDS(ph)LY(ph)NDYVDVFY(ph)NTK	5	S	3	3	0.942
EVM(ox)LENY(ph)GNVVS(ph)LGILLR	12	S	2	3	1.000
EVM(ox)LENY(ph)GNVVS(ph)LGILLR	7	Y	2	3	1.000
FPGGSCM(ox)AALTVT(ph)LM(ox)VLSS(ph)PLALAGDTR	13	T	2	3	0.953
GS(ph)FIITLVKIPRMILM(ox)Y(ph)IHS(ph)QLK	2	S	3	3	0.868
GS(ph)T(ph)VHT(ph)AY(ph)LVLSSLAMFT(ph)CLCGM(ox)AGNSMVIWLLGFR	18	T	5	4	0.924
GS(ph)T(ph)VHT(ph)AY(ph)LVLSSLAMFT(ph)CLCGM(ox)AGNSMVIWLLGFR	8	Y	5	4	0.814
LES(ph)Y(ph)LDLM(ox)PNPSLAQVK	3	S	2	3	1.000
LLEPGTHQFAS(ph)VPVR	11	S	3	3	1.000
LLS(ph)HPFLS(ph)THLGSS(ph)M(ox)AR	3	S	2	3	0.957
LPAPLIS(ph)KQQFLS(ph)NS(ph)S(ph)R	7	S	4	3	1.000
LPAPLIS(ph)KQQFLS(ph)NS(ph)S(ph)R	13	S	4	3	1.000
LPVAT(ph)IFTT(ph)HAT(ph)LLGR	5	T	2	3	1.000
M(ox)DIGTLIWDGGPVPNT(ph)HINKCKNY(ph)Y(ph)EVLGVTK	25	Y	2	4	0.915
M(ox)GRTPT(ph)AVQVKS(ph)FTK	12	S	4	3	0.990
M(ox)T(ph)CT(ph)AFGNPKPIVT(ph)WLK	14	T	4	2	1.000
MAPAFLLLLLLWPQGCVSGPS(ph)ADS(ph)VY(ph)T(ph)K	27	T	3	3	0.999
MAPAFLLLLLLWPQGCVSGPS(ph)ADS(ph)VY(ph)T(ph)K	26	Y	3	3	0.999
MAPAFLLLLLLWPQGCVSGPS(ph)ADS(ph)VY(ph)T(ph)K	24	S	3	3	0.998
MAPAFLLLLLLWPQGCVSGPS(ph)ADS(ph)VY(ph)T(ph)K	21	S	3	3	0.839
PLAPPPQPPASPTHS(ph)PS(ph)FPIPDR	17	S	2	3	1.000
PLAPPPQPPASPTHS(ph)PS(ph)FPIPDR	15	S	2	3	0.998
QGQY(ph)S(ph)PM(ox)AIEEQVAVIY(ph)AGVR	17	Y	2	3	1.000
QLEPT(ph)VQSLEMKSKT(ph)AR	15	T	2	3	0.908
QLEPT(ph)VQSLEMKSKT(ph)AR	5	T	2	3	0.908
THNYSM(ox)AIT(ph)Y(ph)Y(ph)EAALK	10	Y	3	3	0.979
TLLTPHT(ph)GVT(ph)S(ph)QVLGVAAAVM(ox)TPLPGGHAAGR	7	T	2	5	0.788
TVTGT(ph)T(ph)M(ox)T(ph)LIPSEMPTPPK	8	T	2	3	0.866
VT(ph)VNYYDEEGS(ph)IPIDQAGLFLT(ph)AIEIS(ph)LDVDADR	2	T	3	4	0.841
VT(ph)VNYYDEEGS(ph)IPIDQAGLFLT(ph)AIEIS(ph)LDVDADR	27	S	2	4	1.000
VT(ph)VNYYDEEGS(ph)IPIDQAGLFLT(ph)AIEIS(ph)LDVDADR	11	S	2	4	0.967
VVLAAASHFFNLM(ox)FT(ph)T(ph)NM(ox)LES(ph)K	16	T	2	3	0.996
VVLAAASHFFNLM(ox)FT(ph)T(ph)NM(ox)LES(ph)K	21	S	2	3	0.990
Y(ph)IWGGFAY(ph)LQDM(ox)VEQGIT(ph)R	18	T	2	3	1.000
Y(ph)IWGGFAY(ph)LQDM(ox)VEQGIT(ph)R	1	Y	2	3	1.000
Y(ph)IWGGFAY(ph)LQDM(ox)VEQGIT(ph)R	8	Y	2	3	1.000

As described above, an enrichment of multiply-phosphorylated peptides was observed in the peptides identified by LC-FAIMS-MS/MS: a total of 67 (55.8%) phosphosites sensitive to SU5402 were from multiply-phosphorylated peptides, compared with 6 from the LC-MS/MS dataset. Similarly, 46 out of 70 phosphosites sensitive to dasatinib originated from multiply phosphorylated-peptides in the LC-FAIMS-MS/MS dataset. Furthermore, among the 67 phosphosites sensitive to SU5402 treatment, 31 were novel phosphosites. The results therefore provide a useful starting point for follow-up functional investigations. A list of novel phosphorylation sites identified from multiply-phosphorylated peptides sensitive to SU5402 or dasatinib treatment is presented in Table 4.3.

4.2.7.5 Kinases involved in FGFR-and Src-regulated phosphorylation events

Based on the kinase-substrate specificity assay, the analysis of regulated phosphosites further reveals how kinases mechanistically affect the changes in a cell. Analysis of amino acid frequency in the phosphorylation sites in FAIMS and non-FAIMS dataset was performed by WebLogo[205] (see Figure 4.15A). The majority of the sequence motif is pSer-derived in both datasets. A higher frequency of serine residues in proximity to the site of phosphorylation in the FAIMS dataset was observed compared to the non-FAIMS because of the multiply phosphorylated peptides.

To identify kinases with putative roles in FGF signalling, bioinformatics tools were used to characterise the phosphorylation motifs identified by FAIMS analysis, non-FAIMS analysis and both methods. Phosphorylation sites sensitive to SU5402 were searched using the kinase prediction tool iGPS 1.0[106] and the number of phosphorylation sites predicted in each method were displayed representatively in the heatmap shown in Figure 4.15. In total, 355 kinases were predicted and the kinases with over 22 substrate matches were shown. Kinases with various

biological functions were identified. Notably, one family that exhibits active kinase activity in response to SU5402 is MAPK family kinase (including Erks, p38 and JNKs).

A closer inspection of the phosphorylation sites in response to SU5402 treatment was analysed by Cytoscape 3.0[206]. The predicted kinases/shared substrates was visualised by nodes/edges relationship. A cluster with a high degree of consensus substrates have been classified. In this cluster, MAP kinases, PLKs and KSRs are fundamental participators *Ras-raf-ERK/MAPK* pathway[207] and these findings indicate the ERK pathway plays an important role in mediating FGF signalling. It is noteworthy that the kinase prediction is based on consensus phosphorylation motif. Therefore, the prediction does not take into consideration interdependence between multiple phosphorylation sites, which make it difficult to correlate the function of these sites to the activity of signalling. Pie charts (representing nodes) were used to display the number of substrates identified in FAIMS analysis, non-FAIMS analysis and both methods, displayed in Figure 4.16.

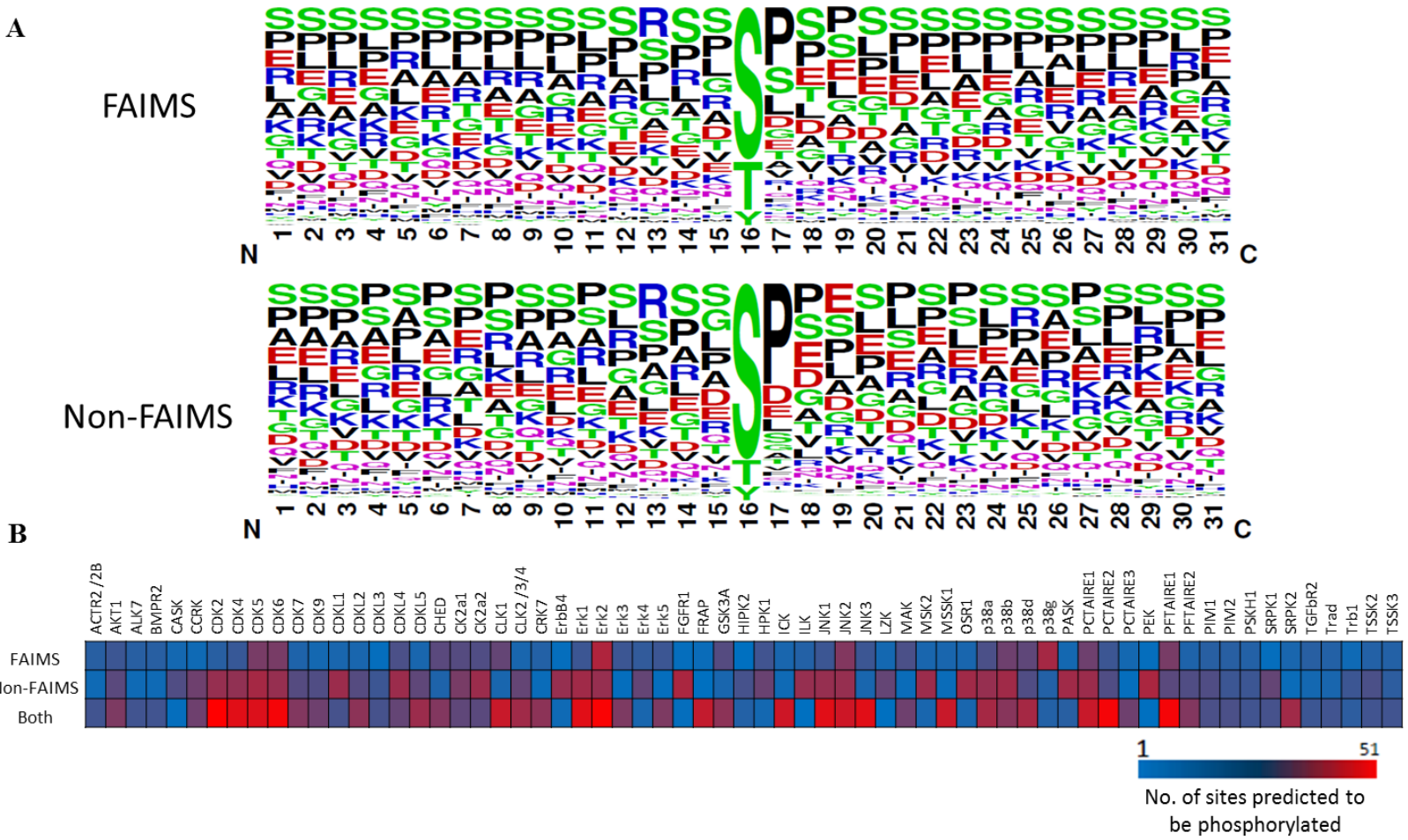

Figure 4.15 (A) Motif analysis of phosphorylation sites in FAIMS and non-FAIMS dataset by WebLogo. (B) Heat map showing proteins and kinases that predicted to phosphorylate substrates in FAIMS and non-FAIMS dataset. Motif analysis centred on the phosphorylated S/T/Y residue. The size of the adjacent amino acid indicates the frequency of the appearance of a particular amino acid. Kinase prediction was performed using iGPS3.0. Kinase predicted with over 22 substrates were shown in the heatmap.

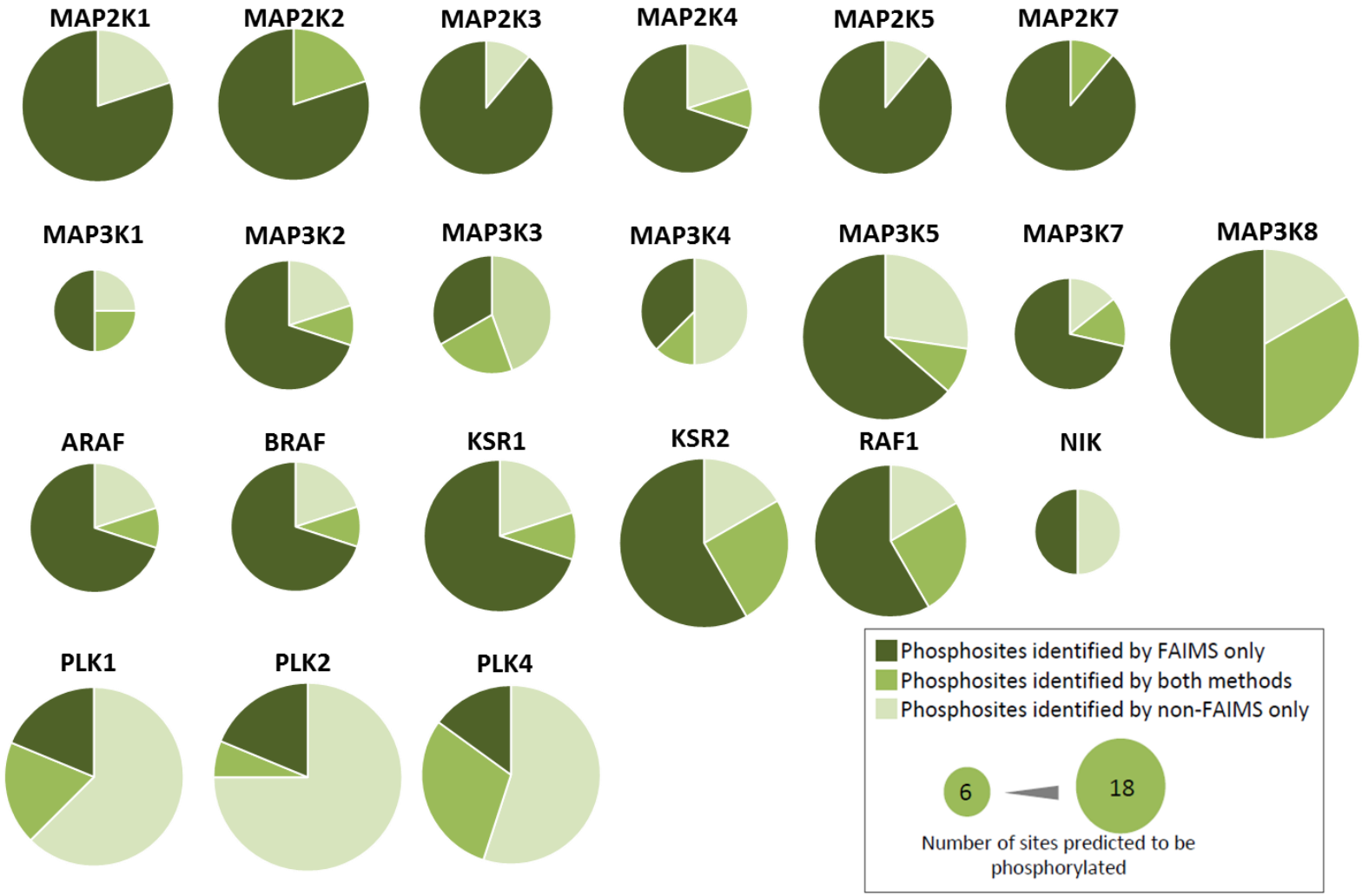

Figure 4.16 A group of kinase predicted to phosphorylate substrates identified by FAIMS, non-FAIMS and both methods. These kinases were identified by Cytoscape 3.0 as a subgroup with shared substrates. Size of pie charts indicate the number of substrate predicted by certain kinase.

4.3 Discussion

4.3.1 Complementarity

The scale of the analyses was not designed to comprehensively map FGF signalling and its downstream pathways, but to generate a complementary set of phosphosites that provide novel insights into the field of phosphoproteomic research. The stochastic nature of LC-MS/MS sampling can result in complementary peptide identifications in technical repeats. Nevertheless, the application of FAIMS identified a distinct set of phosphosites, which is evidenced by a 37.0% increase in the phosphoproteome coverage. Notably, a similar increase in phosphoproteome coverage was observed following multiple replicates (n=2) of LC-MS/MS analyses; however, the properties of the phosphopeptides identified by FAIMS are intrinsically different to those identified by LC-MS/MS in regards to charge state, length and phosphorylation status.

Fewer phosphosites were identified from the FAIMS dataset than the non-FAIMS dataset. This is likely due to low transmission efficiency of FAIMS (typically about 10-20%). In addition, samples analysed by FAIMS were homogenous while samples analysed by the non-FAIMS approach were fractionated by SCX. This difference will contribute to the difference in performance of electrospray ionisation efficiency, LC separation and MS/MS identification.

Note that an increase in the relative proportion of pThr and pTyr sites was observed in the LC-FAIMS-MS/MS dataset. It has been estimated, in eukaryotic cells, the composition of pSer, pThr and pTyr sites is expected to be approximately 86.4%, 11.8% and 1.8%[107]. The successful identification of tyrosine phosphorylation is particularly challenging as it is a substoichiometric modification often occurring on low-abundance proteins[208]. Moreover, knowledge of tyrosine phosphorylation is necessary in deciphering the mechanisms of signal transduction processes and regulation of kinase activity.

4.3.2 CV distribution

In an acidic solution, most tryptic peptides carry ≥2+ charges, however many tryptic phosphopeptides carry 1+ or even negative charges due to the addition of phosphate groups[209]. Therefore in SCX chromatography, peptides are eluted according to their net charge states: multiply-phosphorylated peptides are eluted first due to their negative charge, followed by singly-phosphorylated peptides, missed cleavage phosphopeptides and finally non-phosphopeptides. An enrichment of phosphopeptides was therefore observed in the first few fractions. In the FAIMS analyses, samples from all SCX fractions were pooled to ensure homogeneity, whilst allowing a direct comparison in sample preparation. Thus, the distribution of phosphopeptides in FAIMS analyses is solely based on pre-set CV values.

The extent of proteome coverage is in proportion to the degree of peptide fractionation and resolving power of mass spectrometer. The uneven distribution of phosphopeptides across the 12 LC-MS/MS fractions potentially lowers the efficiency of peptide fractionation, as evidenced by the under-representation of phosphopeptides in the latter eight SCX fractions (35.3% of the total identifications).

4.3.3 Charge state distribution

In MS analysis, one of the difficulties of phosphopeptide detection is low protonation efficiency in the presence of acidic groups (*e.g.* phosphate group). Doubly-charged species are normally the predominant ions following electrospray of tryptic peptides. By coupling FAIMS to LC-MS/MS, an enrichment of 3+ and 4+ ions was observed. These findings suggest that the charge-based selection afforded by the FAIMS device influences the phosphopeptides identified.

In LC-MS/MS analyses, the distributions of peptide charges agree with the pH-dependent elution from SCX cartridges, where phosphopeptides are eluted first as a result of their negative charge, followed by non-phosphopeptides then acidic peptides.

4.3.4 Phosphorylation status

In MS analyses, it is more challenging to detect multiply-phosphorylated peptides due to low ionization efficiency in electrospray process and poor binding to chromatographic columns. The enhancement in identification multiply-phosphorylated peptides is significant in view of their low abundance relative to singly- and non-phosphorylated peptides. This finding may be the result of the improved S/N ratio afforded by FAIMS or charge state differentiation via FAIMS as discussed above. The identification of singly- and multiply-phosphorylated peptides did not show any correlation with the distribution of CV.

Successful identification of multiply-phosphorylated peptides and localization of the phosphorylation sites also has a profound impact on data interpretation, enabling evaluation of the coordination among adjacent phosphorylation sites or investigation of the dynamics between singly- and multiply-phosphorylated peptide forms.

4.3.5 Novel phosphorylation status

The results show that coupling FAIMS to LC-MS/MS in phosphoproteomic analyses not only improves the proteome coverage but also identifies a large set of uncharacterized phosphorylation sites, suggesting that FAIMS has specifically accessed a group of phosphosites not readily accessible by LC-MS/MS. Remarkably, a large number of the novel phosphosites were assigned from multiply-phosphorylated peptides. Again, this finding

highlights the advantages of FAIMS in identification of multiply-phosphorylated peptides. A relationship between the overrepresentation of higher charge state (>3+) and enhanced identification of multiply-phosphorylated peptides is also established, indicating charge-based selection of FAIMS may be responsible for the increase in the number of novel sites.

The peptide MAPAFLLLLLLWPQGCVSGPpSADpSVpYpTK was found to be down-regulated in response to SU5402 but not to dasatinib. Whether these phosphorylation sites in the N-terminus are involved in cleavage of signal peptides or signal recognition is yet unknown. An in-depth analysis is required to establish the cross-talk between these phosphorylation events and perturbation of FGF signalling.

4.3.6 FGFR and Src mediated phosphorylation events

Overall, the results show that chemical inhibition induced significant changes in ~ 17% of the measured phosphosites. The scale of this experiment was not intended to reveal the whole map of FGF signalling, but to provide a unique resource of phosphosites for further study and an example of the utility of FAIMS in phosphoproteomic research.

Activation of FGF signalling can induce diverse cellular response and Erk pathways is one of the four downstream targets of FGF signalling.[210] Activated FGFRs can initiate the downstream cellular response by phosphorylation of specific residues in MAPK family kinases to induce cell differentiation. Previous findings also demonstrated that the activation of Erk1/2 could reduce the FGF-stimulated receptor tyrosine phosphorylation as feedback control.[211] Based on the kinase prediction, our data shows that MAPK pathway exhibits the most prominent perturbation following the inhibition of FGFR activity.

It has been shown, both theoretically and experimentally, that multisite phosphorylation can generate a switch-like temporal profile of response[212] and, when executed in a specific order, dictates the timing of output responses[213,214]. The ability to efficiently define multisite phosphorylation events is of particular biological significance as they represent a significant regulatory mechanism in a variety of settings. However, judged by existing phosphosite databases, the extent and identity of multisite phosphorylation events is poorly defined compared to single site events. Current bioinformatic software, e.g. iGPS and NetWorkin, mainly focuses on interpretation of single sites, rather than interaction of multi-phosphorylation sites. Kinases with a variety of biological functions were identified and FAIMS provides a small and complementary fraction. This is likely because in the FAIMS dataset, 55.8% of regulated phosphosites were identified from multiply-phosphorylated peptides.

Phosphorylation of tyrosine residues is a well-defined mechanism of eliciting protein/protein interaction via sequence specific recognition, such as pTyr binding motifs-SH2 domain[215]. Recognition of pTyr binding motifs can be modified by concurrent phosphorylation of adjacent Ser/Thr that occlude the SH2 binding pocket[216]. This results in the formation/dissolution of protein complexes, which is controlled by the combined action of Tyr and Ser/Thr directed kinases. It is notable that multiply-phosphorylated peptides identified in the FAIMS dataset reveal a significant fraction (58.4%) in which a phosphorylated Tyr is located within ±4 residues of a phospho Ser/Thr. This indicates that the multisite phosphorylation is a prevalent regulatory event which can be preferentially resolved by the application of FAIMS. Besides, this points to the work that can be carried out in the following step, which focuses on the dynamics of key phosphorylation events within FGF signalling. The site-specific analysis of key phosphorylation sites, especially the interdependence among multisite phosphorylation, will be of great significance to determine the downstream network of FGF perturbation.

4.4 Conclusion

The LC-MS/MS and LC-FAIMS-MS/MS analyses have combined SILAC labelling with SCX pre-fractionation and phosphoenrichment. This approach allows us to investigate the regulated phosphorylation events involved in FGF signalling. The two techniques showed complementarity. The application of FAIMS improved the phosphoproteome coverage by 37.0% over that identified with the conventional LC-MS/MS workflow. An enhancement in the identification of multiply phosphorylated peptides and a preference for peptides with high charge states (3+ and above) was observed in the LC-FAIMS-MS/MS dataset. It is also observed that ~20% of the phosphosites identified via FAIMS have not been reported previously. Remarkably, 82.3% of these novel sites are identified from multiply phosphorylated peptides. These properties make FAIMS a valuable addition to phosphoproteomic studies, enhancing the coverage of the phosphoproteome and increasing the confidence of site localisation.

The LC-FAIMS-MS/MS analyses also revealed a substantial number of phosphosites regulated upon inhibitor treatments, especially sites from multiply-phosphorylated peptides. Hence, I propose the LC-FAIMS-MS/MS workflow is a suitable complementary approach in phosphoproteomic analysis. Together, these observations open new possibilities for in-depth characterisation of interesting candidates for their roles in FGF signalling and trafficking.

CHAPTER 5

EVALUATION OF A MODIFIED FAIMS INTERFACE

5.1 Introduction

FAIMS, coupled with LC-MS/MS, has been applied in proteomics studies, and offers advantages including reduced chemical noise and increased signal-to-noise ratio, as described in the introduction. FAIMS can be applied as a complementary tool to augment proteomic analysis.

Recently, a novel FAIMS interface (termed modified FAIMS) was introduced with a reduced electrode gap width (as shown in Figure 1.15) and modified ion inlet design[181]. The standard FAIMS electrode consists of an outer electrode with an inner radius of 9 mm and an inner electrode with a radius of 6.5 mm, forming a 2.5 mm gap. The modified FAIMS electrode is comprised of the standard outer electrode with an enlarged inner electrode (radius of 7.5 mm). The gap between electrodes is reduced from 2.5 mm to 1.5 mm. The reduction in gap allows the application of higher field strength at a fixed DV. The increase in the field magnitude enhances the ion focusing effect through the electrodes. The modification in the ion inlet creates a symmetric gas flow, decreasing the disruption of ion flow and increasing the gas flow to the electrodes. These modifications were reported to enhance the performance of FAIMS (coupled to a triple quadrupole mass spectrometer) by increasing peak capacity without decreasing signal output as shown for bromochlorate anions and six tryptic peptides from bovine serum albumin and enolase[181]. The aim of the work presented in this chapter was to characterise the performance of the standard and modified FAIMS device on an Orbitrap mass spectrometer for proteomic analysis, from a standard peptide to a complex protein digest. The modified FAIMS device was developed by Thermo Fisher and supplied to the University of Birmingham for evaluation.

5.2 Results

5.2.1 Direct infusion of substance P

The operating parameters of the modified FAIMS device were optimised to maintain similar transmission efficiency to that obtained with the standard FAIMS device by tuning the flow rate and composition of carrier gas and spray voltage *etc*. The instrumental parameters used in the following experiments are shown in Table 5.1.

Table 5.1 Comparison of conditions for the standard FAIMS device and the modified FAIMS device

Configuration	Standard FAIMS	Modified FAIMS
Electrode gap (mm)	2.5	1.25
Electrode temperature (inner/outer)	70℃/90℃	70℃/90℃
Dispersion voltage (kV)	-5	-5
Carrier gas	50/50 He:N_2	N_2
Flow rate of carrier gas (L/min)	2.9	2.0
Spray voltage (kV)	2.9	2.9

Substance P was directly infused for FAIMS-MS analysis and a CV scanning experiment was performed to identify the optimum CV range for the 2+ ion of substance P, as shown in Figure 5.1. The CV scanning analysis is performed by collecting MS1 scans at CV ranging from 0 to -60 V, with a 0.3 V minimum CV interval. The optimum CV of 2+ ions of substance P (DV = -5 kV) was -32.09 V for the standard FAIMS device and -39.88 V for the modified FAIMS device, with a shift of 7.79 V. Peak capacity is calculated as the CV peak width at the optimum CV between the lowest and highest CV at half-maximum height. Peak capacity was changed from 7.67 V to 3.68 V, with a 2-fold increase in the modified FAIMS analysis.

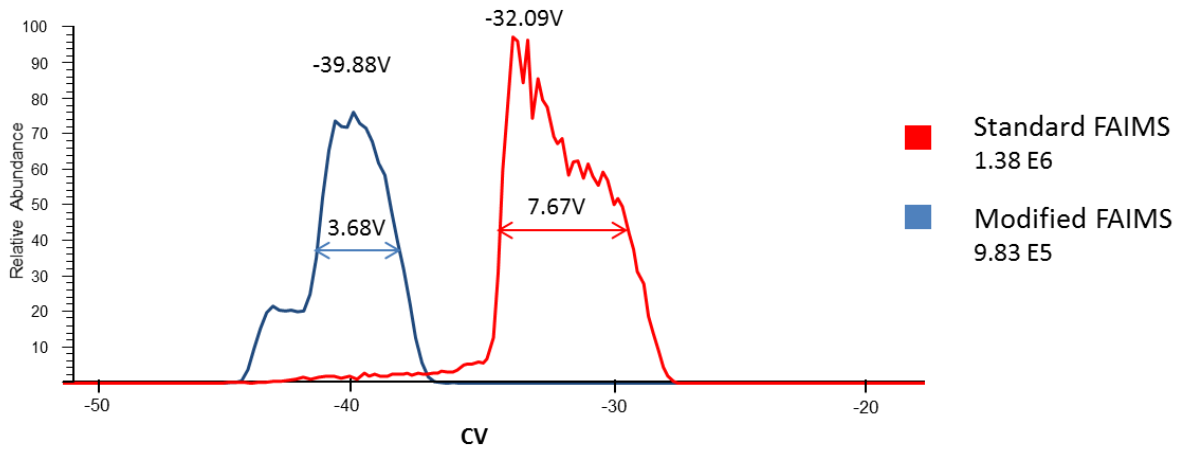

Figure 5.1 Optimum CV of 2+ ions of substance P

5.2.2 Direct infusion of a tryptic digest of six standard proteins

A tryptic digest of six standard proteins (cytochrome c, lysozyme, alcohol dehydrogenase, bovine serum albumin, transferrin and beta-galactosidase) was directly infused for FAIMS analysis. Two representative peptides were selected for CV scanning analysis, as shown in Figure 5.2. For 3+ ions of the peptide GTDKcAcSNHEPYFGYSGAFK (transferrin), the optimum CV shifted from -36.08 V to -47.12 V, an 11.04 V difference. Peak capacity was changed from 10.43 V to 3.98 V, resulting in a 2.62-fold increase in the modified FAIMS analysis. A 68% decrease in the ion signal is observed in the modified FAIMS analysis.

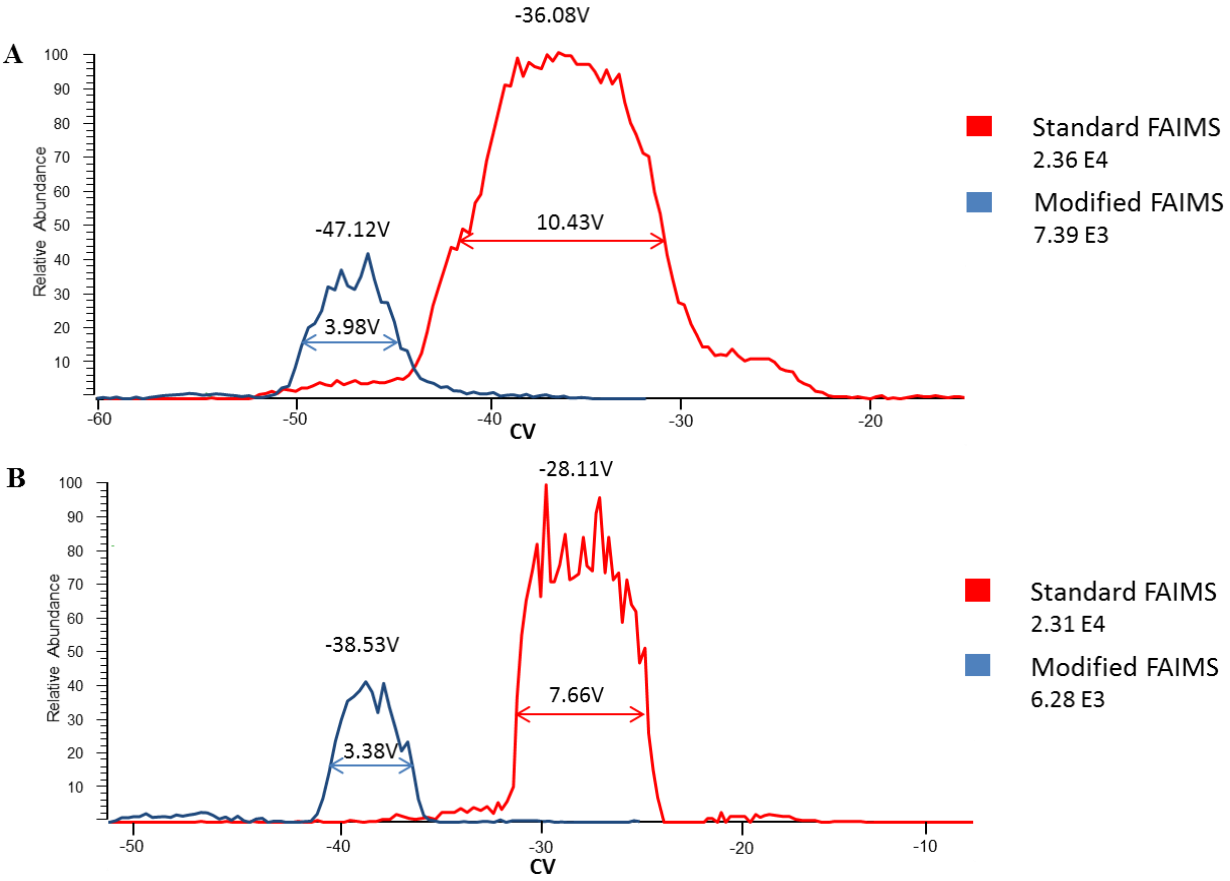

Figure 5.2 Optimum CV of the peptide (A) GTDKcAcSNHEPYFGYSGAFK and (B) FDEFFSAGcAPGSPR

Figure 5.2B shows the CV scanning analysis of 2+ ions of the peptide FDEFFSAGcAPGSPR (transferrin). The optimum CV of this peptide shifted from -28.11 V to -38.53 V from the standard to the modified FAIMS analysis, resulting in a 10.42 V difference. Peak capacity is changed from 7.66 V to 3.38 V, resulting in a 2.26-fold increase in the modified FAIMS analysis. Similarly, a decrease of 72% in the ion signal in the modified FAIMS analysis was observed.

Overall, direct infusion analysis of these two peptides and substance P revealed the optimum CV values for transmission shifted on average by approximately 9.75 V when using the modified FAIMS device. An average increase of 2.32-fold in peak capacity was observed with the modified FAIMS device.

5.2.3 LC-FAIMS-MS/MS analysis of a tryptic digest of six standard proteins

An LC-FAIMS-MS/MS analysis was performed on the tryptic digest of six standard proteins. Based on the direct infusion experiments described above, a different CV range was selected for analyses with the standard and the modified FAIMS device: standard FAIMS CV range = -20 V to -45 V; modified FAIMS CV range = -30 V to -60 V. The 'external CV stepping' method was used in which the CV is kept constant throughout the LC-MS/MS analysis, as described in Chapter 2.2.4.0. The data were searched using the Sequest algorithm in Proteome Discoverer 1.4.

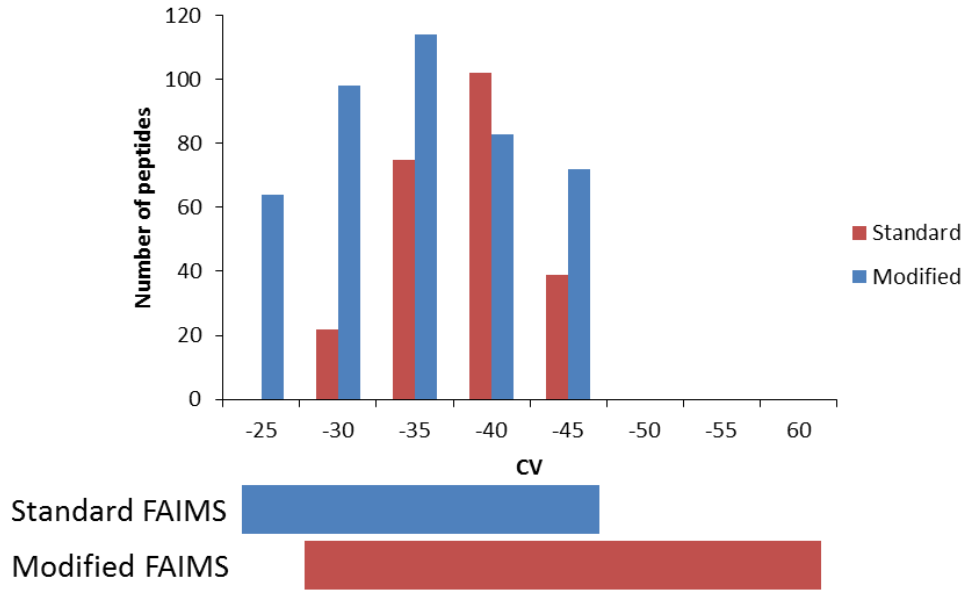

Figure 5.3 Number of peptides identified across CVs:
CV range of the standard FAIMS analysis -25V to -45V; CV range of the modified FAIMS analysis -30V to -60V

Figure 5.3 shows the number of peptides identified in each analysis. For the standard FAIMS analysis, approximately ~70 to ~110 peptides were identified in each analysis with the most identified at CV = -35 V. For the modified FAIMS analysis, the majority of the peptides were identified at CVs -35 V and -40 V; at CVs of -50 V to -60 V, no peptides were identified (see discussion below).

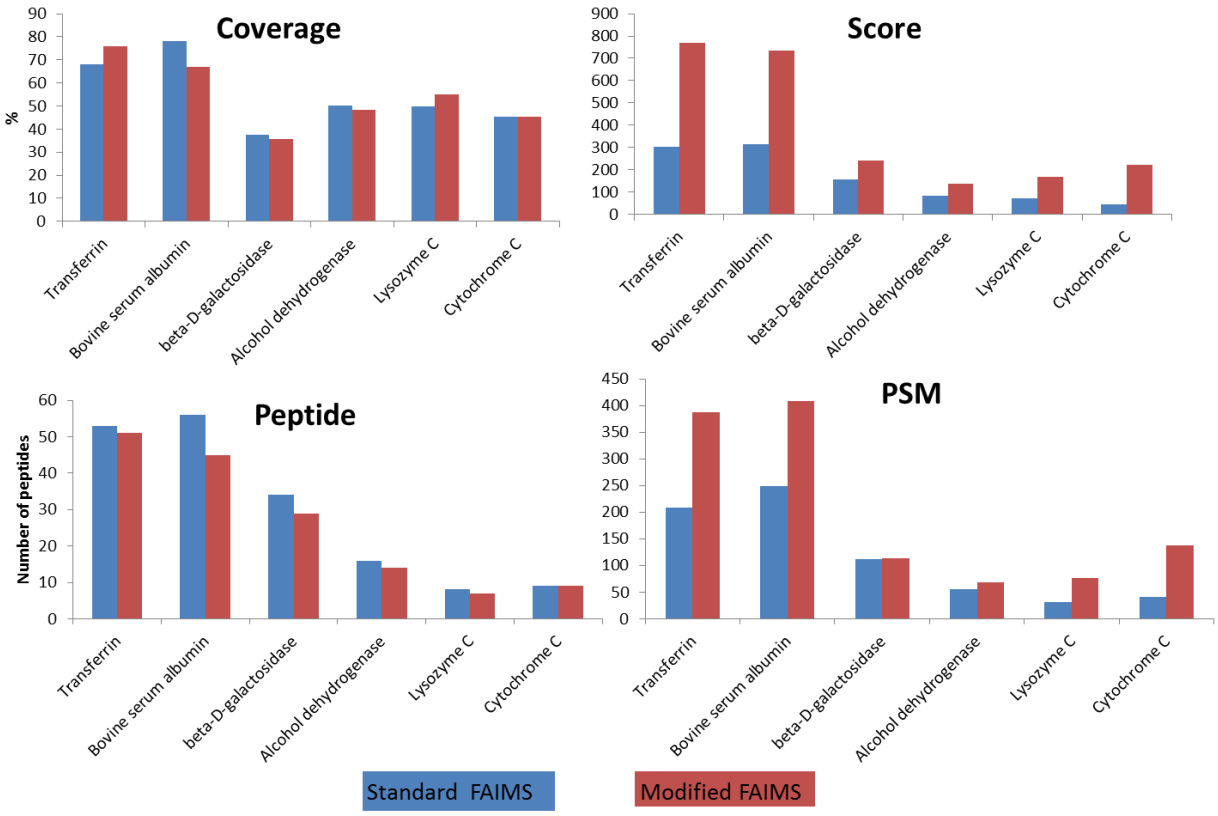

Figure 5.4 Sequence coverage, protein score, number of peptide and PSM in FAIMS analyses

The protein sequence coverage, protein score, number of peptide and peptide spectrum matches (PSM, the number of spectrum matches for the protein) obtained following LC-FAIMS-MS/MS analyses is shown in Figure 5.4. The two devices provided similar results in terms of sequence coverage and the number of peptides identified; however, increased scores and PSMs were observed when using the modified FAIMS device.

5.2.4 LC-FAIMS-MS/MS analysis of SUM52 cell lysate

5.2.4.1 Number of identified peptides

In order to explore the performance of the modified FAIMS device for complex mixtures, SUM52 cells were lysed, and digested for LC-FAIMS-MS/MS analysis, see Chapter 2.2.2.6. The CV range for standard and modified FAIMS was further optimised: for the standard FAIMS device the CV range was -20 V to -45 V; for the modified FAIMS device the CV range

was -30 V to -55 V. Experiments were performed in duplicate. The first replicate analyses were performed on the Orbitrap Velos and the second were performed on the Orbitrap Elite. A higher number of identifications were observed for both FAIMS devices for the analyses performed on the Orbitrap Elite. As shown in Figure 5.5, non-redundant peptide identifications obtained via the two FAIMS devices were complementary, of which 69.4% of the total peptide identifications were identified by both devices.

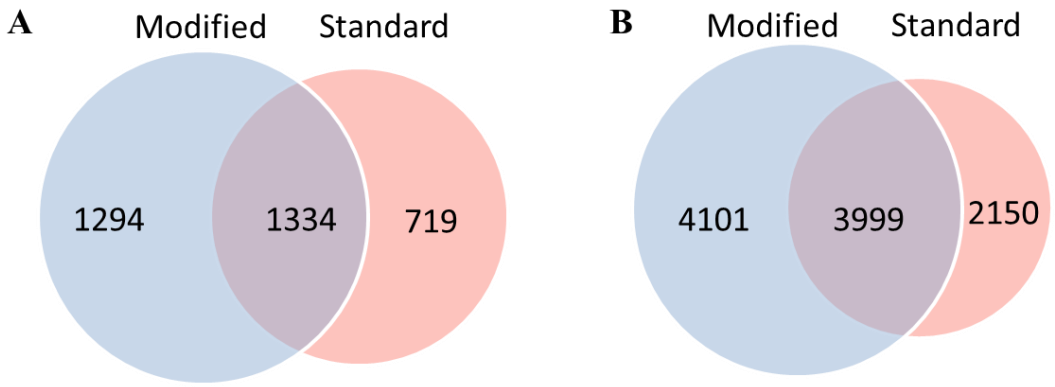

Figure 5.5 Number of peptides identified in the FAIMS analysis (performed by Orbitrap Elite)
(A): replicate 1; (B) replicate 2

5.2.4.2 Distribution of peptides according to CV

In order to visualise the number of peptides across the different CV ranges, Figure 5.6 was plotted. For the standard FAIMS analyses, peptides were uniformly identified across the CV range. In the modified FAIMS analyses, fewer than 100 peptides were identified from CV steps -50 V to -55 V.

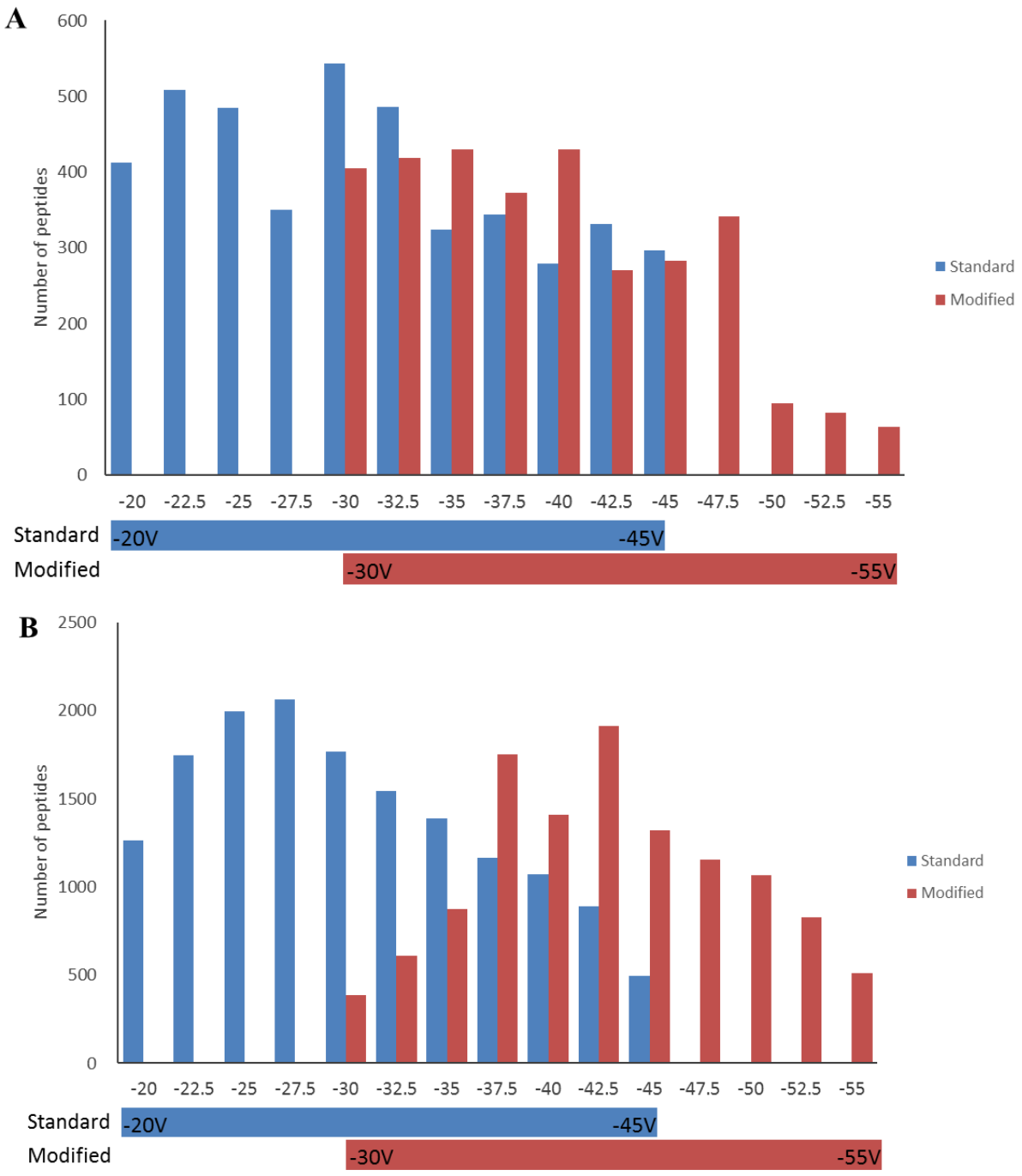

Figure 5.6 Distribution of peptides identified across CV steps in the FAIMS analyses
(A): replicate 1; (B) replicate 2

In the standard FAIMS analyses, e.g. replicate 1, there are 396 peptides identified in each CV analysis on average, compared with 290 identified in modified FAIMS analyses (excluding CV of -52.5 and -55). In replicate 2, 1399 peptides are identified in each CV analysis on average in the standard FAIMS dataset, compared with 1112 identified in the modified FAIMS analyses. Figure 5.5 shows that use of the modified FAIMS device resulted in more identifications than

the standard FAIMS device. This contradiction indicates there might be a lower level of redundant identifications in the modified FAIMS analysis. To that end, the distribution of unique peptides was plotted, see Figure 5.7. In the following, redundant peptides refers to the peptides identified in multiple CV analyses.

5.2.4.3 Redundancy

5.2.4.3.1 Intra-assay redundancy

The intra-assay redundancy was calculated by extracting the matched ions between biological replicate analyses (see Figure 5.7). The number of matched ions is the number of identified ions matched to a specific peptide in a single analysis, therefore indicating the level of redundancy within an assay. The distribution of the number of matched ions between the two analyses shows a small but significant difference of P<0.0001.

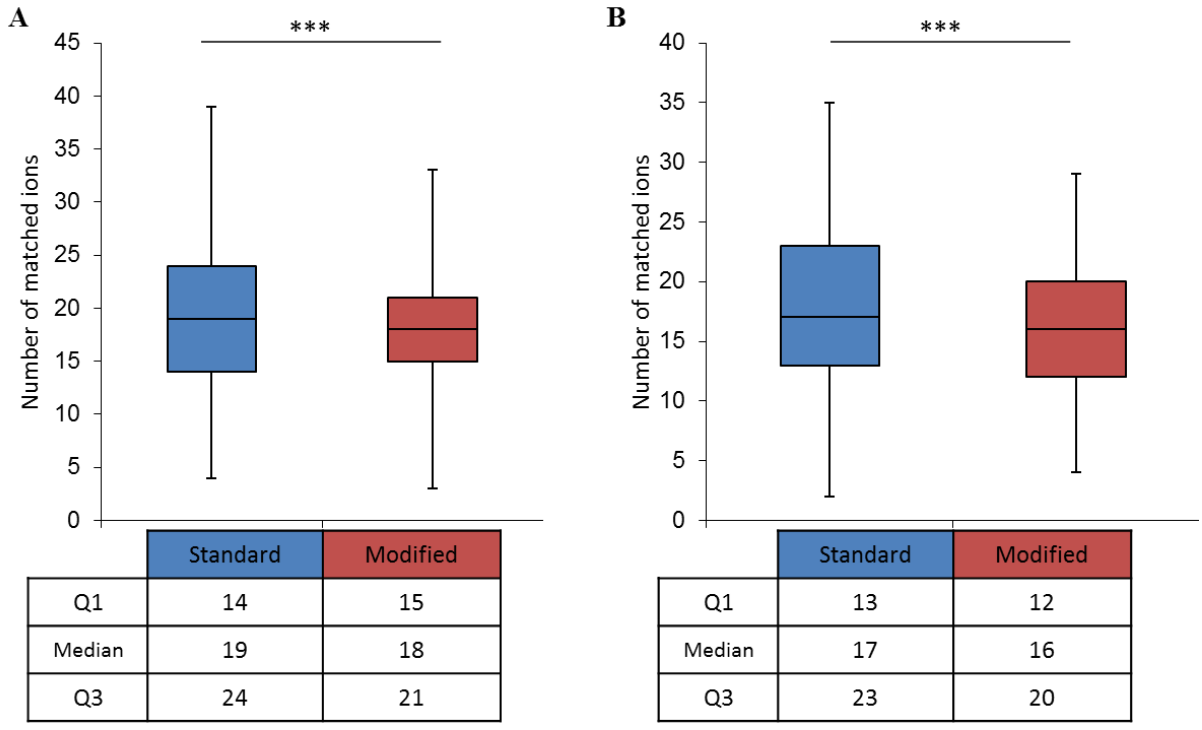

	Standard	Modified
Q1	14	15
Median	19	18
Q3	24	21

	Standard	Modified
Q1	13	12
Median	17	16
Q3	23	20

Figure 5.7 Box plot of the number of matched ions in the FAIMS analyses
The box spans from the Q1 (quartile 1) to Q3 (quartile 3) and median (quartile 2) is shown in the middle. Whiskers above and below the box show the maximum and minimum values. *** indicates a significant difference of P<0.001. (A): replicate 1; (B) replicate 2

5.2.4.3.2 Inter-assay redundancy

Figure 5.8 and Figure 5.9 show the number of unique and redundant peptides identified in each FAIMS analysis. As predicted, a higher level of redundant peptides was identified in standard FAIMS analyses. In replicate 1, for example, the average number of unique peptides in each CV is 98 in the standard FAIMS analyses, while in the modified FAIMS the average number is 153. The increase in unique peptide identification of the modified FAIMS analyses is 1.56-fold over the standard FAIMS.

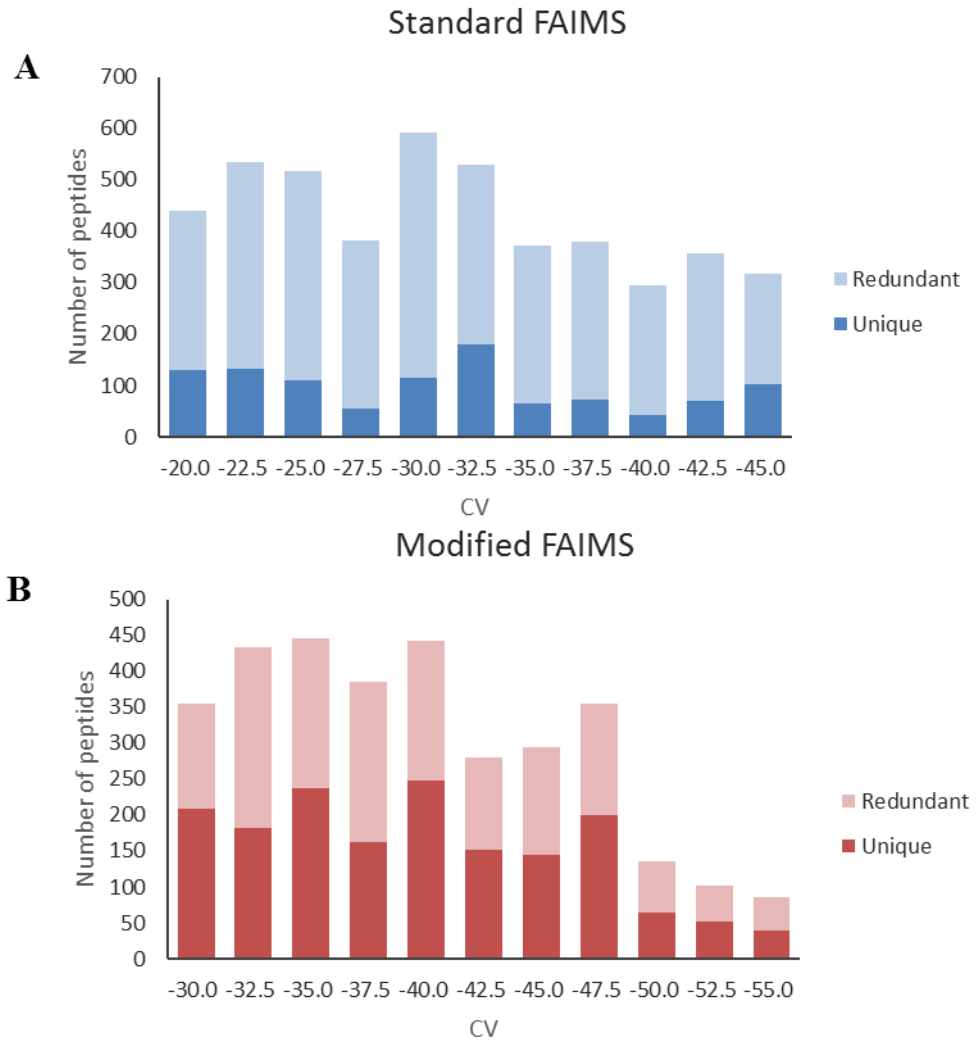

Figure 5.8 Distribution of peptides in the (A) standard and (B) modified FAIMS analysis in replicate 1 Performed by Orbitrap Velos

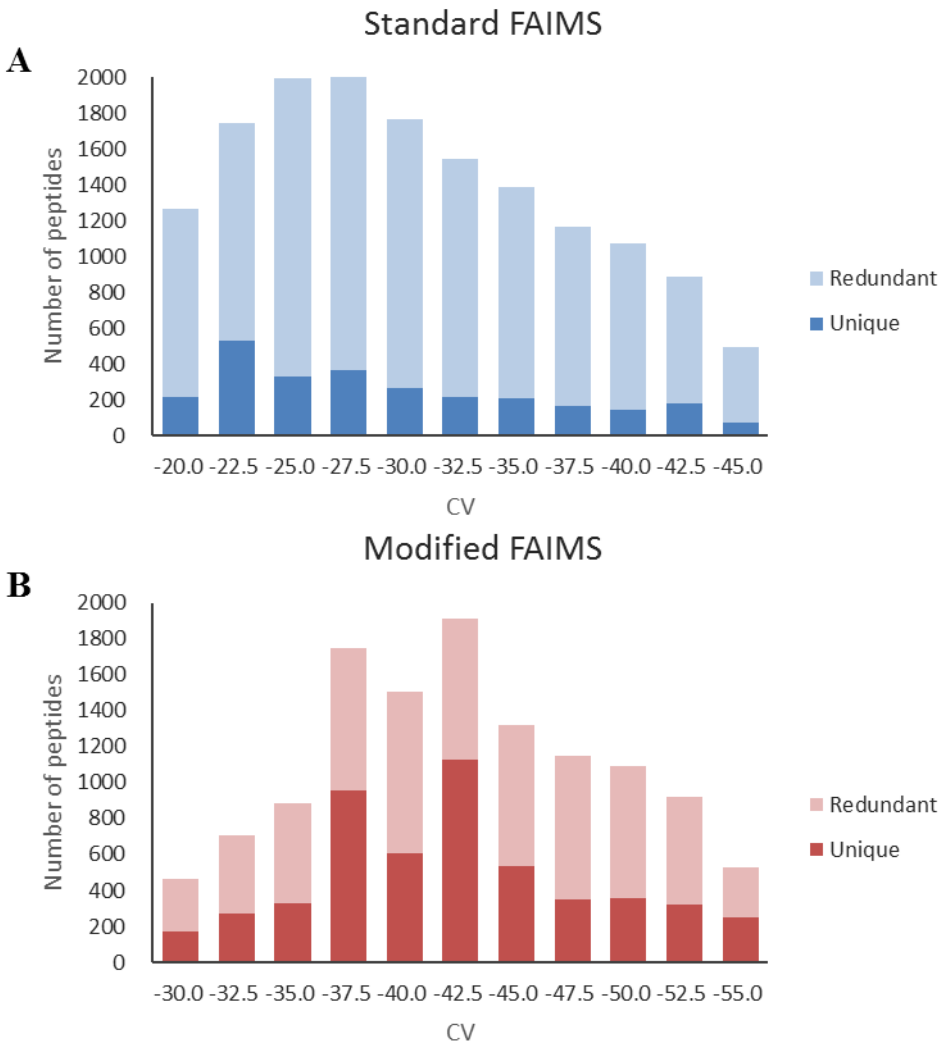

Figure 5.9 Distribution of peptides in the (A) standard and (B) modified FAIMS analysis in replicate 2 Performed by Orbitrap Elite

Figure 5.10 and Figure 5.11 below show the redundancy level in both analyses. The redundancy rate is calculated by dividing the number of redundant peptides against the number of all peptides identified in each CV analysis. In replicate 1, the average redundancy rate of the standard FAIMS analyses is 78.1%, while the redundancy rate of the modified FAIMS analyses is 49.7%. In replicate 2, the average redundancy rate of the standard FAIMS analyses is 83.1% and the redundancy rate of the modified FAIMS analyses is 59.0%.

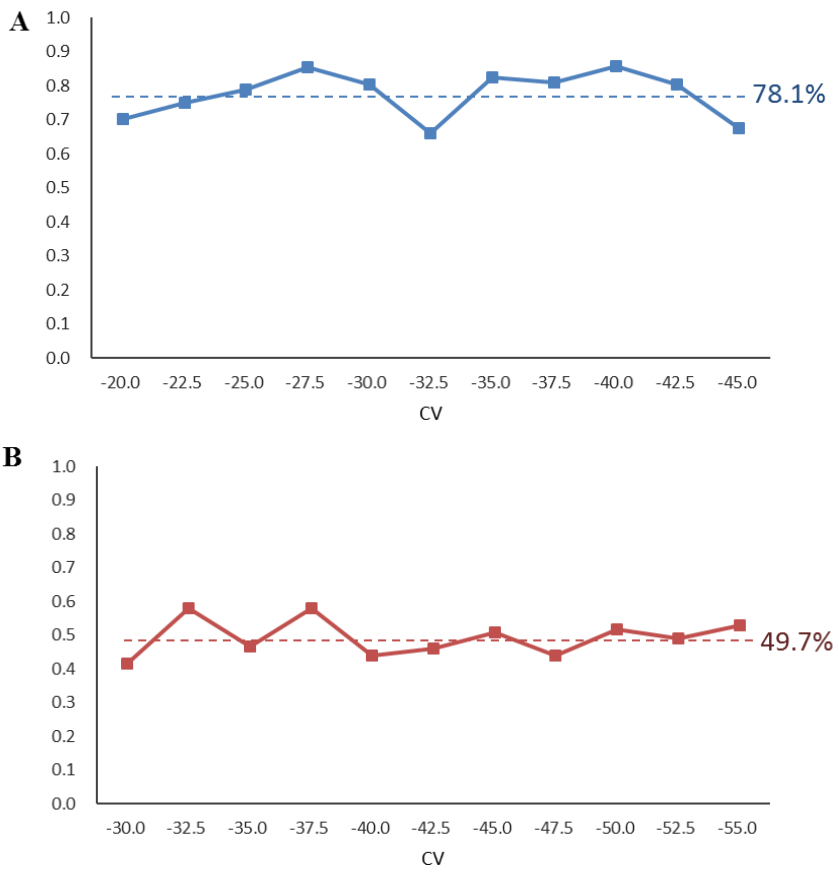

Figure 5.10 Replicate 1: redundancy rate of the (A) standard and (B) modified FAIMS analysis
The dashed line indicates the average redundancy level. Performed by Orbitrap Velos.

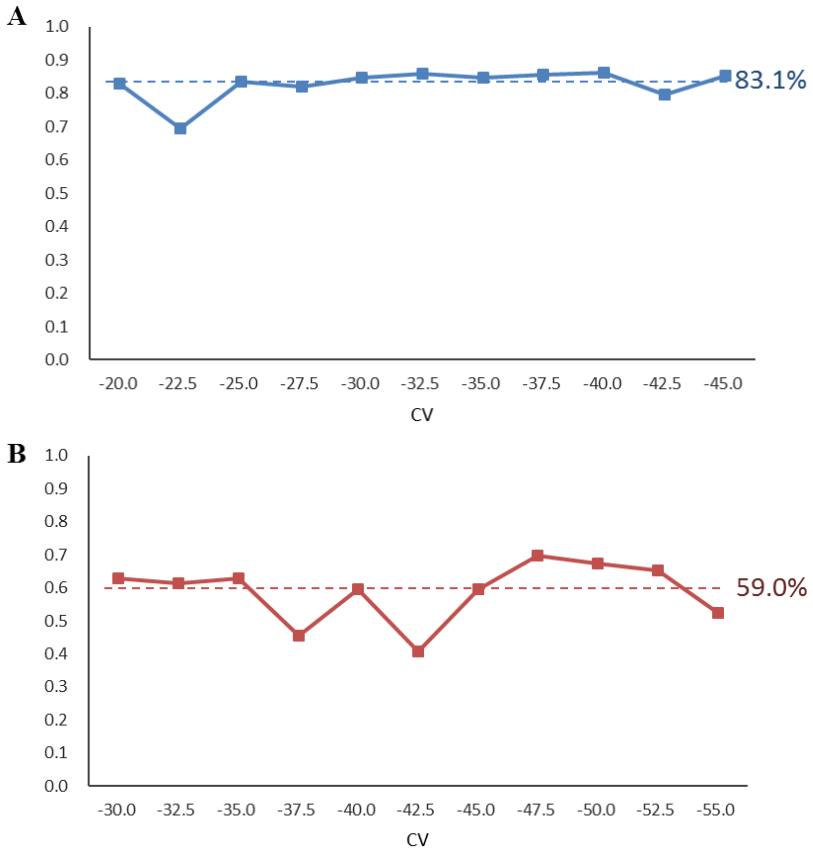

Figure 5.11 Replicate 2: redundancy rate of the (A) standard and (B) modified FAIMS analysis
The dashed line indicates the average redundancy level. Performed by Orbitrap Velos

To further understand the redundancy level, the number of times that a peptide is identified across the whole analysis was investigated, as shown in Figure 5.12. In replicate 1, in the standard FAIMS analyses, peptides identified twice and three times constitute 42.5% of the total identifications. While in the modified FAIMS analyses, peptides identified once alone constitute 49.9% of the total identifications. In replicate 2, in the standard FAIMS analyses, peptides identified twice and three times constitute 50.7% of the total identifications. While in the modified FAIMS analyses, peptides identified once alone constitute 61.8% of the total identifications.

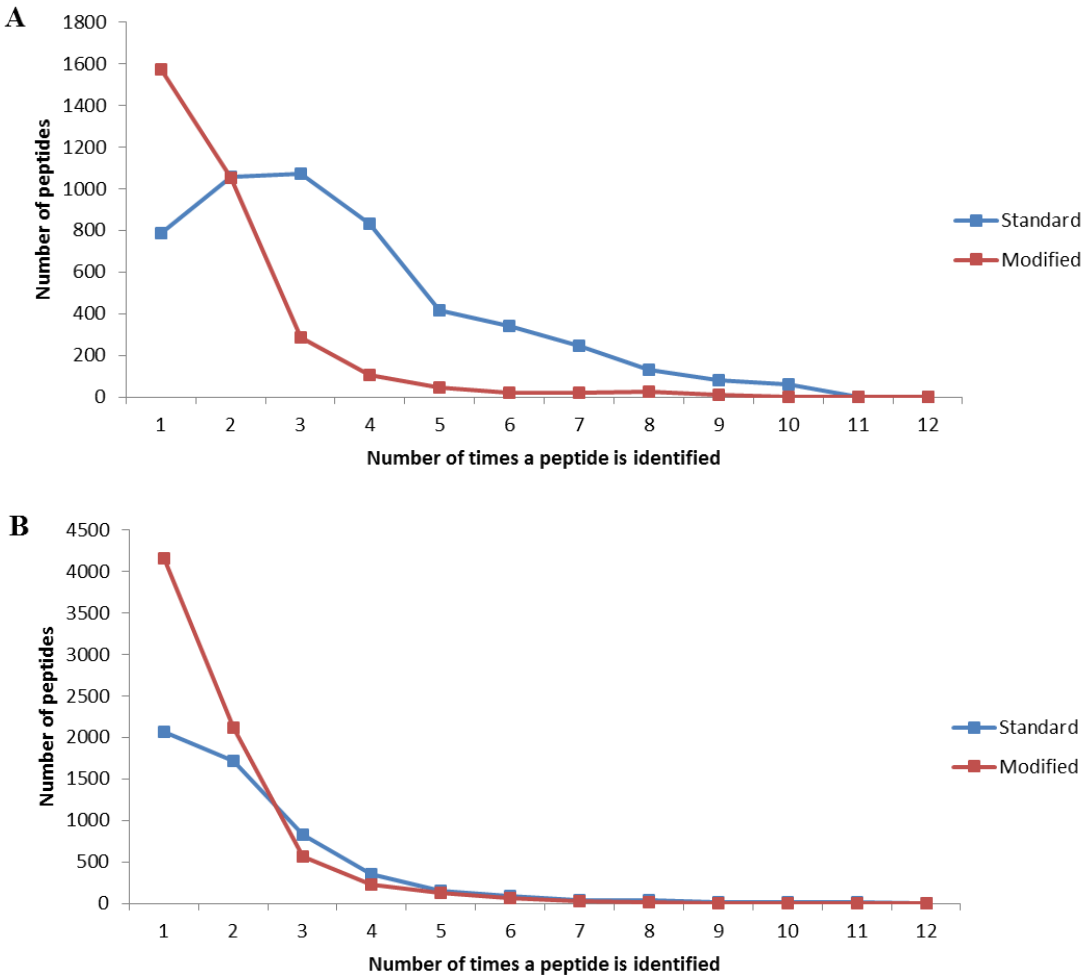

Figure 5.12 Number of times a peptide is identified in the (A) standard and (B) modified FAIMS analysis

5.2.4.4 Charge state

As shown in Chapter 4, the charge-based selection is a feature of FAIMS separation. To explore differences in the charge-based selection in the modified FAIMS device, Figure 5.13 was plotted. In each case 2+ ions constitute the majority of the identifications. In experiment 1, the percentage of 2+ ions is dramatically increased from 58% in the standard FAIMS analyses to 83% in the modified FAIMS analyses. A similar trend was observed in experiment 2, in which 48% of the identifications came from 2+ ions when using the standard FAIMS device compared with 62% with the modified FAIMS device.

To further understand whether this difference relates to the differences in redundancy level, the charge state distribution of uniquely identified ions (ions that have been identified in one CV only) was analysed. A similar trend was observed, where the average proportion of 2+ ions were increased from 52% to 65% from the standard to the modified FAIMS dataset.

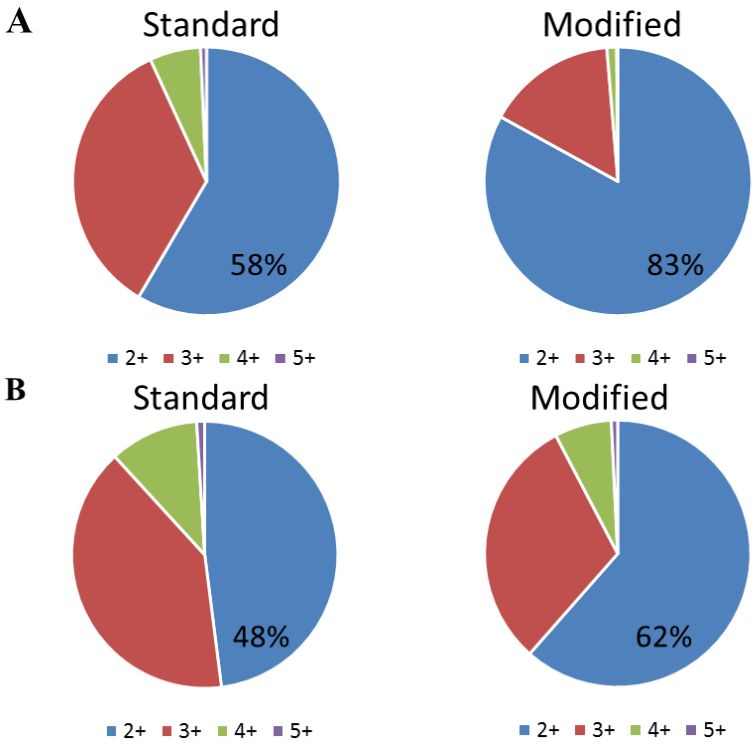

Figure 5.13 Charge state distribution in the standard and modified FAIMS analysis
(A): replicate 1; (B) replicate 2

5.3 Discussion

Although FAIMS has proven beneficial for proteomics in recent years, the wide-spread application has been hindered by poor ion transmission, especially for ions with weak field dependence or ions having extreme low CV. The recently developed modified FAIMS interface was reported to have potential to increase ion transmission efficiency[217]. In the present study, direct infusion experiments and LC-FAIMS-MS/MS analyses were employed to evaluate the performance of the standard and the modified FAIMS device in proteomic applications.

5.3.1 Instrumental and operational parameters

The analytical response of FAIMS is controlled by a fine balance of multiple instrumental and operational parameters. In cylindrical FAIMS, such as that used here, a reduced electrode gap can increase field strength (E) without altering the DV, and enhance the ion focusing effect[218]. For example, by reducing the gap from 2.5 mm to 1.5 mm, the maximum field strength can increase from -23.6 kV/cm to -42.1 kV/cm. This enhancement significantly improves the peak capacity, hence increases separation efficiency. It should be noted that the increase in separation efficiency is at the expense of sensitivity, as shown in Figure 5.2.

The trade-off between sensitivity and resolution has been observed by others and can be partially offset by tuning the gap width, waveform frequency, carrier gas compositions and electrode temperatures[218–220]. By reducing the gap width to 0.5-1 mm, FAIMS becomes more suitable for large multi-charged ions analysis, especially intact protein separation and identification[218]. Barnett and co-workers investigated the effect of temperature and other variables on field strength and ion separation efficiency[220]. By inverting the electrode temperatures (the inner/outer electrode temperature was 70℃/90℃), sensitivity was increased

but peak capacity was reduced. Based on this finding, Swearingen *et al.* tested the performance of a modified FAIMS device with the addition of a gas-phase fractionation within the mass analyser using an unfractionated yeast digest[217]. Their findings were published after our experiments finished in this chapter. Their device used the electrodes with 1.25 mm gap and no ion inlet modification was made. By reducing the electrode gap, better separation was achieved at the expense of a decreased sensitivity, which is in agreement with the results in this chapter. They found the modified FAIMS, operating at DV of -4 kV, improved protein discovery by 86%. Further, by inverting the electrode temperatures, the decrease in sensitivity of modified FAIMS could be partially offset.

Shvartburgs *et al.* found increasing He fractions in carrier gas composition significantly improved resolution[189]. Peak capacity is defined as the ratio of separation space to the peak width at half maximum. The molecular polarizability of He is much lower than that of N_2 and there is greater unfolding in He-rich environments than N_2-rich environments, leading to a higher separation space in He and, thus, improved peak capacity[221]. Barnett and Ouellette demonstrated that using FAIMS with a reduced electrode gap eliminates the He requirement [222]. In the present study, therefore, supplemental He is not required as carrier gas. The benefits of this are reduced costs and risk of He interfering with mass analyser performance of mass analysers, without sacrificing resolution[181].

5.3.2 Direct infusion

Adjustments in electrode gap width were previously reported to alter the gas flow velocities and CV values[222].The results obtained from direct infusion ESI of substance P and tryptic digest of standard proteins also showed the optimum CV range for peptide ion transmission by the modified FAIMS device shifted by approximately 9.75 V. Moreover, the shift of CV of

different ions follows a similar pattern. In the standard FAIMS device, the DV of -5 kV creates a field strength equivalent to -23.6 kV/cm. In the modified FAIMS device, the DV is identical to that in the standard device but due to decrease in the gap width, the field strength is increased to -43.1 kV/cm. As the field strength is different in the two devices, the voltage required to compensate ion shift would be different accordingly.

5.3.3 LC-FAIMS-MS/MS analysis of a tryptic digest of six standard proteins

As the sample is a simple protein mixture, the sequence coverage is expected to be limited by sample purity and instrumental limits. As expected, the two devices achieved similar results for sequence coverage; however, a higher number of PSMs and higher protein scores were observed in the modified FAIMS analyses. The number of PSMs indicates the number of MS/MS spectra matched for any peptide assigned to a particular protein. The results of the modified FAIMS showed more spectrum were unambiguously matched to the identified peptides. When using the Sequest algorithm, the protein score relates to the number of possible peptide matches. Thus, better protein scores were observed in the modified FAIMS analyses.

In the broader CV ranges (from -50 V to 60 V), no peptides were successfully identified. This result is probably due to the CV range from -30 V to -45 V being adequate for transmission of peptides from this simple mixture.

5.3.4 LC-FAIMS-MS/MS analysis of SUM 52 cell lysate

In bottom-up proteomics, protein mixtures are usually enzymatically digested into small peptides and subjected to fractionation and MS analyses. In this manner, identifications yield a series of redundant results within a single LC-MS/MS analysis, as well as across multiple

analyses[223]. Tremendous efforts have been given to enhance the throughput of MS analysis, from prolonged fractionations, multiple replicates and multi-stage MS/MS fragmentations[224]. Yet little consideration has been given to reducing the redundancy in identifications[225].

In the modified FAIMS analyses, the overall reduction in redundant identifications arises through reduced redundancy levels both within an assay and between assays. For intra-assay redundancy, statistical tests showed the distribution of the number of matched ions was significantly lower in the modified FAIMS than that of the standard analyses. For inter-assay redundancy, the modified FAIMS analyses have shown a lower redundancy rate in peptide identifications across multiple CV analyses, as demonstrated in Figure 5.11 and 5.12. This finding can be explained by the reduction in FAIMS peak width in the modified device, as shown in Figure 5.1 and 5.2. That is, the narrower the peak, the less likely a peptide will be observed in multiple CV steps. Therefore, the difference in the inter-assay redundancy seems to have accounted for the overall lower level redundancy.

Typically, FAIMS analyses of complex mixtures are performed at separate CVs, therefore samples need to be split into a number of fractions for each CV analysis. The splitting of samples will result in reduced sample amounts and long instrument hours. Therefore, there is a balance between the number of CV steps and the amount of sample for each analysis. The reduced peak widths observed with the modified FAIMS allows the analyses to be performed with fewer CV steps, potentially increasing the sample amount in each analysis.

5.3.4 Charge state

Comparison of the charge state distribution of the peptide identifications from the standard and modified FAIMS analyses revealed a higher proportion of 2+ peptide ion identification from the modified FAIMS dataset. Chapter 4 shows that charge-based selection is an important

feature of FAIMS separation and, typically, 2+ ions are better transmitted in the non-FAIMS analyses and 3+ ions are the dominant group in the standard FAIMS analyses. The preference for lower charge state ions of the modified FAIMS device resembles that of the non-FAIMS analyses. The extent of charging reflects the compactness of a conformation, where higher charge state typically indicates unfolded structure[226]. The difference in peptide/proteins charge state is also sequence specific. The change in charge state preference in the modified FAIMS device indicates, for a particular range of CV, the change in the preferred structure, which is the possible reason for the difference in the preferred CV range in the modified FAIMS device. The difference in charge state is also likely to contribute to the unique identifications in the modified FAIMS dataset.

5.4 Conclusion

In this chapter, the performance of a novel FAIMS interface developed by Thermo and supplied to the University of Birmingham was evaluated and compared with the commercial Thermo Scientific™ FAIMS device. The direct infusion ESI analysis showed that the modified FAIMS device resulted in a nearly 3-fold increase in the peak capacity and a CV shift of approximately 10 V. Based on this, a different CV range was selected for LC-FAIMS-MS/MS analysis. In analysis of tryptic digest of standard proteins, the two devices showed similar results in sequence coverage but a higher number of PSMs was observed in the modified FAIMS dataset.

In order to further explore the potential of the modified FAIMS in proteomic experiments, a whole cell lysate sample was analysed. An increase in the proteome coverage of 69.4% was observed in the modified FAIMS dataset. The increase in proteome coverage can be attributed to the reduced redundancy in identifications between CV steps in the modified FAIMS analysis, in turn the result of improved resolution.

CHAPTER 6

INVESTIGATION OF DYNAMICS OF THE KEY PHOSPHORYLATION EVENTS IN FGF SIGNALLING BY SELECTED REACTION MONITORING

6.1 Introduction

In a proteomic workflow, the discovery of key proteins is typically initiated by a large-scale shotgun experiment for *de novo* identification of potential biomarkers. A large number of studies have used this methodology for discovery of potential biomarkers involved in a biological process or a disease. The selected reaction monitoring (SRM)-based approach can then be applied for determination and efficient quantitative validation of targeted analytes.

The FGF signalling cascade is the result of protein-protein interactions regulated by specific phosphorylation events. One of the downstream signalling protein family is Src, a non-receptor tyrosine kinase, which has been shown to be recruited by receptor-mediated phosphorylation to the FGF signalling complex to regulate signalling dynamics[227]. Deregulation of FGF signalling, such as overexpression and inhibition, has been associated with many human diseases, including cancer[10]. It has been indicated that the intervention of FGFR activity can be accentuated for therapeutic use[56]. From a clinical view, it is necessary to understand the downstream effect of this inhibition if patients are to receive treatment with FGFR or Src family kinases inhibitors.

Previously, in order to understand the global impact on intracellular phosphorylation events following inhibition of FGFR or Src family kinases, a SILAC experiment was carried out using the triple negative breast cancer cell lines: SUM52 and MFM233 (unpublished, Debbie Cunningham *et al*.,). Results showed that the FGFR dependent phosphorylation events represented a wide variety of biological functions and processes. Therefore, the understanding of the key phosphorylation dynamics is a useful indicator of protein activity and related kinase function.

The aim of the work presented in this chapter was to (1) study the dynamics of key phosphorylation events following activation of FGF signalling, and (2) explore the molecular mechanisms of the FGF signalling cascade in SUM52 cells.

To directly study the downstream dynamics of FGF signalling, we focused on proteins with kinase function. In total, 75 phosphopeptides from kinase were selected for the SRM assay, including 62 singly-phosphorylated peptides and 13 doubly-phosphorylated peptides. These candidates were selected from kinases that contained phosphosites that were sensitive to treatment with the FGFR inhibitor, SU5402, in the SILAC experiment described previously (shown in Table 6.1 and Appendix 2). The phosphorylation profile of these peptides following FGF1 stimulation was studied in a time-resolved way (0 s, 20 s, 40 s, 1 min, 3 min, 5 min, 10 min, 20 min, 30 min and 60 min). An absolute quantitation strategy was employed (see Chapter 2.2.8). To explore the dynamics of the specific phosphorylation events, peptides with differentially phosphorylated versions were investigated individually.

Table 6.1 Overview of selected phosphopeptides for SRM assay

Peptide sequence	Protein	Peptide sequence	Protein
ALGERVSIL	Serine/threonine-protein kinase D1	RLSSTSLASGHSVR	Serine/threonine-protein kinase D2
ATDSFSGRFEDVYQLQEDVLGEGAHAR	MAP kinase-interacting serine/threonine-protein kinase 2	RLSSTSLASGHSVR	Serine/threonine-protein kinase D2
AVLSPGSVFSPGR	Inositol-trisphosphate 3-kinase B	RLSSTSLASGHSVR	Serine/threonine-protein kinase D2
DALDLSDINSEPPRGSFPSFEPR	Membrane-associated tyrosine/ threonine-specific cdc2-inhibitory kinase	RNSFTPLSSSNTIR	6-phosphofructo-2-kinase/fructose-2,6-bisphosphatase 2
DINNIDYYKK	Fibroblast growth factor receptor 2	RNSFTPLSSSNTIR	6-phosphofructo-2-kinase/fructose-2,6-bisphosphatase 2
DINNIDYYKK	Fibroblast growth factor receptor 2	RPHFPQFSYSASGRE	RAC-gamma serine/threonine-protein kinase
DINNIDYYKK	Fibroblast growth factor receptor 2	RPHFPQFSYSASGRE	RAC-alpha serine/threonine-protein kinase
EHIEIIAPSPQR	Eukaryotic translation initiation factor 2-alpha kinase 3	RPHFPQFSYSASGRE	RAC-alpha serine/threonine-protein kinase
EKFSFEPK	Ribosomal protein S6 kinase	RPHFPQFSYSASGTA	RAC-gamma serine/threonine-protein kinase
EYGSPLKAYTPVVVTQWYR	Cyclin-dependent kinase 11B	RPPGMEYSYDINR	Fibroblast growth factor receptor 2
GAILTTM(ox)LVSR	Calcium/calmodulin-dependent protein kinase type II subunit	RPPGMEYSYDINR	Fibroblast growth factor receptor 2
GAQASSGSPALPR	Abelson tyrosine-protein kinase 2	RRSIQDLTVTGTEPGQVSSR	Mitogen-activated protein kinase kinase kinase 7
GFSFVATGLM(ox)EDDGKPR	Ribosomal protein S6 kinase	RSDSASSEPVGIYQGFEK	Protein kinase C delta type
GLCTSPAEHQYFMTEYVATR	Mitogen-activated protein kinase 7	RSDSASSEPVGIYQGFEK	Protein kinase C delta type
GRNSATSADEQPHIGNYR	serine/threonine-protein kinase MARK2	RVSLSEIGFGK	Cyclin-dependent kinase 16
HFM(ox)HQIITGMLYLHSHGILHR	Serine/threonine-protein kinase PLK4	RYSDHAGPAIPSVVAYPK	MAP/microtubule affinity-regulating kinase 3
IADPEHDHTGFLTEYVATR	Mitogen-activated protein kinase 3	SGEQITSSPVSPK	Inositol hexakisphosphate/diphosphoinositol-pentakisphosphate kinase 2
IADPEHDHTGFLTEYVATR	Mitogen-activated protein kinase 3	SGGGDLTLGLEPSEEEAPR	Receptor tyrosine-protein kinase erbB 2
IADPEHDHTGFLTEYVATR	Mitogen-activated protein kinase 3	SHNDFVAILDLPEGEHQYK	5'-AMP-activated protein kinase subunit beta 2
IADPEHDHTGFLTEYVATR	Mitogen-activated protein kinase 3	STVASMMHR	Calcium/calmodulin-dependent protein kinase type II subunit delta
KLPSTTL	Ribosomal protein S6 kinase	SVVGTPAYLAPEVLR	Serine/threonine-protein kinase D1, D3
KLPSTTL	Ribosomal protein S6 kinase	SGSPSDNSGAEEMEVSLAKPK	RAC-alpha serine/threonine-protein kinase
LGSYSGPTSVSR	Pantothenate kinase 2, mitochondrial	STSWHTALR	Triple functional domain protein
LQPFHSTELEDDAIYSVHVPAGLYR	ARF GTPase-activating protein GIT1	TPKDSPGIPPSAGAHQLFR	Ribosomal protein S6 kinase
LSEEAECPNPSTPSK	Serine/threonine-protein kinase 10	TTSFAESCKPVQQPSAFGSM(ox)K	Glycogen synthase kinase-3 beta

NFSAAKSLLNKK	Calcium/calmodulin-dependent protein kinase type II subunit	TTSFAESCKPVQQPSAFGSMK	Glycogen synthase kinase beta 3
NFSAAKSLLNKK	Calcium/calmodulin-dependent protein kinase type II subunit gamma	TTSQCKSEPPLLR	Uridine kinase;Uridine-cytidine kinase-like 1
NFSAAKSLLNKK	Calcium/calmodulin-dependent protein kinase type II subunit gamma	THFPQFSYSASIRE	RAC-beta serine/threonine-protein kinase
NLQSPTQFQTPR	Serine/threonine-protein kinase ULK1	TPKDSPGIPPSAGAHQLFR	Ribosomal protein S6 kinase
NYSVGSRPLKPLSPLR	6-phosphofructo-2-kinase/fructose-2,6-bisphosphatase 2	TPKDSPGIPPSANAHQLFR	Ribosomal protein S6 kinase
NYSVGSRPLKPLSPLR	6-phosphofructo-2-kinase/fructose-2,6-bisphosphatase 2	TPKDSPGIPPSAGAHQLFR	Ribosomal protein S6 kinase
NYSVGSRPLKPLSPLR	6-phosphofructo-2-kinase/fructose-2,6-bisphosphatase 2	TPKDSPGIPPSANAHQLFR	Ribosomal protein S6 kinase
RESVVNLENFRK	Death-associated protein kinase 2	TPKDSPGIPPSAGAHQLFR	Ribosomal protein S6 kinase
RISLSDMPR	Protein kinase C-binding protein 1	VADPDHDHTGFLTEYVATR	Mitogen-activated protein kinase 1
RLNSSPRAPVSPLK	Ribosomal protein S6 kinase beta 2	VADPDHDHTGFLTEYVATR	Mitogen-activated protein kinase 1
RLNSSPRAPVSPLK	Ribosomal protein S6 kinase beta 2	VADPDHDHTGFLTEYVATR	Mitogen-activated protein kinase 1
RLNSSPRAPVSPLK	Ribosomal protein S6 kinase beta 2	VADPDHDHTGFLTEYVATR	Mitogen-activated protein kinase 1
		VTSGGVSESPSGFSK	Serine/threonine-protein kinase Chk1

Table 5.1 (continued)

Phosphorylation sites are shown in red.

Differentially phosphorylated versions of the same peptide are shown in grey.

6.2 Results

The dynamics of specific phosphorylation events in FGF signalling were investigated by SRM in SUM52 cells, as described in Section 2.2.5. The data was collected in a time-dependent profile during FGF1 stimulation (0 s, 20 s, 40 s, 1 min, 3 min, 5 min, 10 min, 20 min, 30 min and 60 min). Three technical replicates and two biological replicates were performed. Phosphopeptides with a peak area count of over 5000 were selected for further analysis. With these criteria, 38 of 75 phosphopeptides were quantified reproducibly.

6.2.1 Initial assessment of SRM assay

To investigate the reproducibility of the quantitation results, precision was assessed using the data from technical replicates (intra-assay precision) and biological replicates (inter-assay precision). In this assay, data from ten time-points following FGF stimulation were collected. Three transitions were selected per phosphopeptide based on the description in Chapter 1.4.3.2. The transitions were monitored in a time-constrained way (termed scheduled), where a small elution time window was specified for transitions of a given peptides (performed by Dr Andrew Creese). In one LC-MS/MS assay, 50 phosphopeptides (25 pairs of IS peptides and endogenous peptides, 150 transitions) were scheduled. Therefore, 3 independent analytical runs were performed for a total of 75 targeted phosphopeptides. Three technical replicates and two biological replicates were performed. Therefore, a total of 6 sets were taken forward for replicate analyses.

6.2.1.1 Technical reproducibility

To assess technical reproducibility, relative standard deviation (% RSD, also known as coefficient of variation) was used to evaluate the variances among three technical replicates (Figure 6.1). RSD was calculated as the standard deviation of peptide measurements over the three replicates divided by the average peptide intensity.

In Figure 6.2, each box displays the distribution of RSD of phosphopeptides detected within each dataset. The red line indicates the 10% cut off of RSD. The medians of RSD of 6 sets of analysis are all below 10%, ranging from 8.01% to 9.87%.

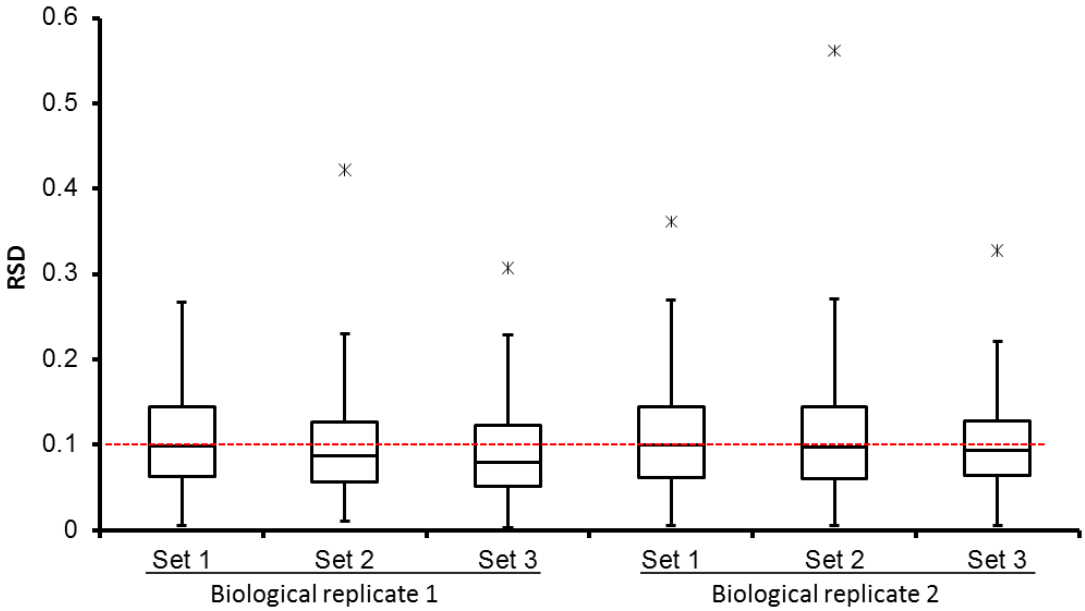

Figure 6.1 Boxplots of RSDs derived from the 3 technical replicates spectra for 2 independent datasets. Box plot shows the RSD for three technical replicates averaged independently for all biological replicates. The number of data point of the 6 datasets are 130,117,119,150,180 and 100 individually. The box spans from the Q1 (quartile 1) to Q3 (quartile 3) and median (quartile 2) is shown in the middle. Whiskers above the box show the maximum values.

For peptide quantitation, a typical SRM assay requires the RSD of technical replicates lower than 10% to 20%, depending on the concentration of peptides[228]. Our results demonstrated good precision among technical replicates, confirming the robustness of the SRM assay.

6.2.1.2 Biological reproducibility

To assess reproducibility in absolute quantitation between independently prepared biological samples, a histogram analysis was performed. For each identified phosphopeptide, the mean of their relative abundance across a time series profile was calculated. Next, the ratios of the mean of relative abundance (endogenous peptide/ IS peptide) between the two biological replicates were calculated, as displayed in Figure 6.2. The distribution shows an approximately normal distribution around the ratio of 1. The variance of 28 phosphopeptides (60.9%) is within ±20%, suggesting the overall absolute quantitation results are within the acceptable level of precision.

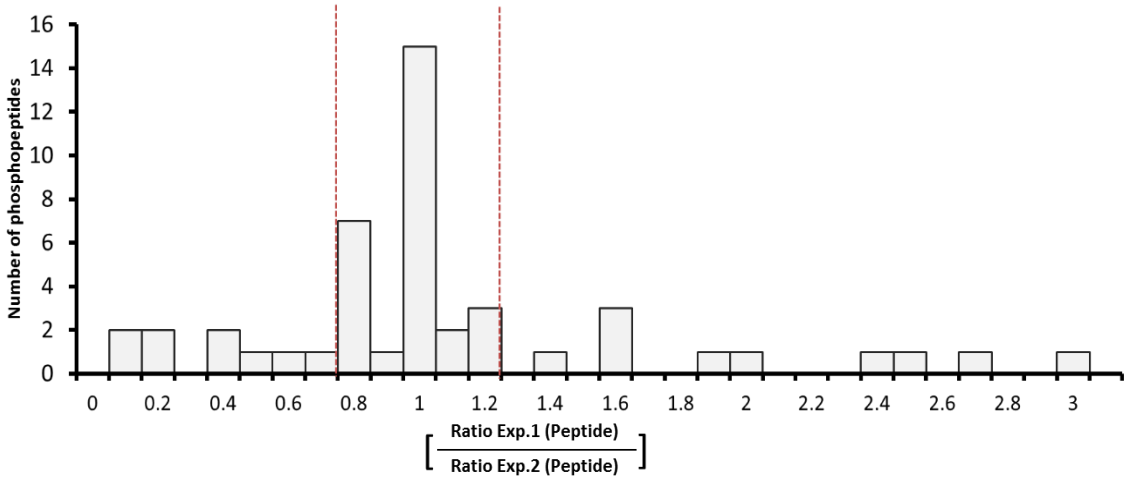

Figure 6.2 Histogram showing the reproducibility of 2 independent biological datasets
X-axis represents the ratio of the values from 2 biological replicates. The dashed lines indicate the ± 20% deviation of the ratio 1.

6.2.2 Overview of SRM-based quantitation of key phosphorylation events in FGF signalling

In order to examine the patterns of phosphopeptide responses following FGF1 stimulation, hierarchical clustering was performed on the phosphopeptides identified reproducibly in the assay. The clustering of phosphopeptides was based on their relative phosphorylation profile and allowed classification of the phosphopeptides from a complex dataset. As shown in Figure 6.3, phosphopeptides were grouped into 4 clusters. The clustering revealed that the phosphopeptides showed different response towards FGF1 stimulation. Different response

patterns were identified: early, mid and late responses. Phosphopeptides with early response type were either down-regulated at early time points (from 20 s to 1 min) after FGF1 treatment or underwent up-regulation followed by rapid down-regulation. Phosphopeptides with mid response pattern were up-regulated from 1min to 10 min following FGF1 treatment. Late response phosphopeptides were up-regulated from 30 min to 60 min of FGF1 stimulation.

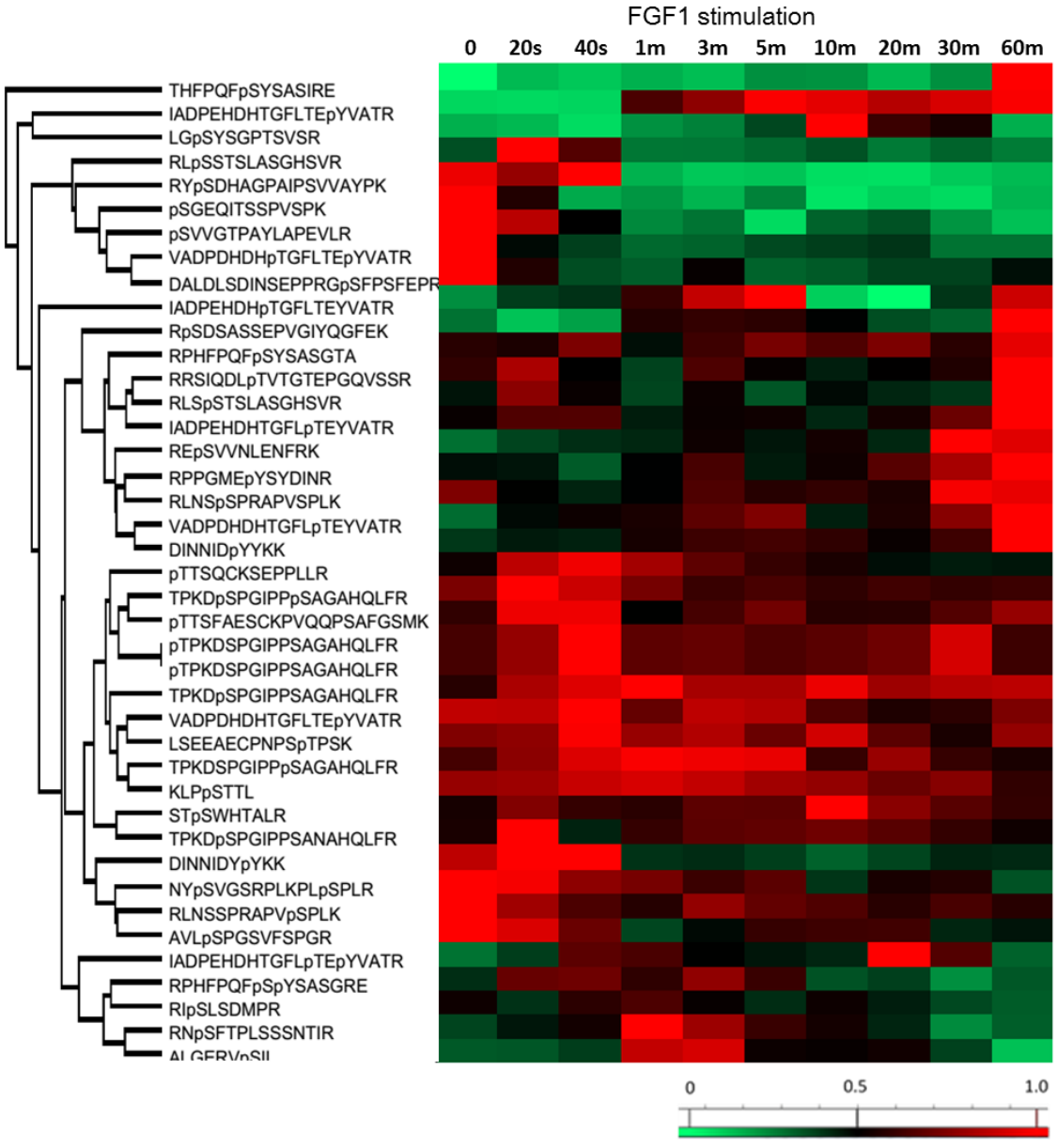

Figure 6.3 Hierarchical clustering of relative phosphorylation profile of key phosphorylation events during FGF1 stimulation. The expression of each phosphopeptide was normalized to a percentage of the highest expression in a time profile (horizontally). The colours in the map display the relative expression of phosphopeptides during FGF1 stimulation. Phosphopeptides with similar expression profiles were grouped together and were connected by clustering tree. Clustering distance was calculated based on Euclidean distance with average linkage by Perseus 1.5.1.6.

6.2.3 Phosphopeptides response to FGF1 treatment

6.2.3.1 Early response phosphopeptides

In total, 12 phosphopeptides were characterised as early response phosphopeptides (0 s to 1 min following FGF1 stimulation), see Table 6.2. There are 10 singly phosphorylated peptides and 2 doubly phosphorylated peptides. Phosphorylation levels of the early response phosphopeptides were down-regulated immediately (except peptide RLSpSTSLASGHSVR which shows the highest expression at 20 s) following the addition of FGF1.

Table 6.2 Early response phosphopeptides

Phosphopeptide	Kinase
AVLSPGSVFSPGR	Inositol-trisphosphate 3-kinase B
DALDLSDINSEPPRGSFPSFEPR	Membrane-associated tyrosine/ threonine-specific cdc2-inhibitory kinase
DINNIDYYKK	Fibroblast growth factor receptor 2
NYSVGSRPLKPLSPLR	6-phosphofructo-2-kinase/fructose-2,6-bisphosphatase 2
RLSSTSLASGHSVR	Serine/threonine-protein kinase D2
RYSDHAGPAIPSVVAYPK	MAP/microtubule affinity-regulating kinase 3
SGEQITSSPVSPK	InsP6 and PP-IP5 kinase 2
SHNDFVAILDLPEGEHQYK	5'-AMP-activated protein kinase subunit beta 2
STVASMMHR	Calcium/calmodulin-dependent protein kinase type II subunit delta
SVVGTPAYLAPEVLR	Serine/threonine-protein kinase D1/D3
TTSQCKSEPPLLR	Uridine kinase;Uridine-cytidine kinase-like 1
VADPDHDHTGFLTEYVATR	Mitogen-activated protein kinase 1

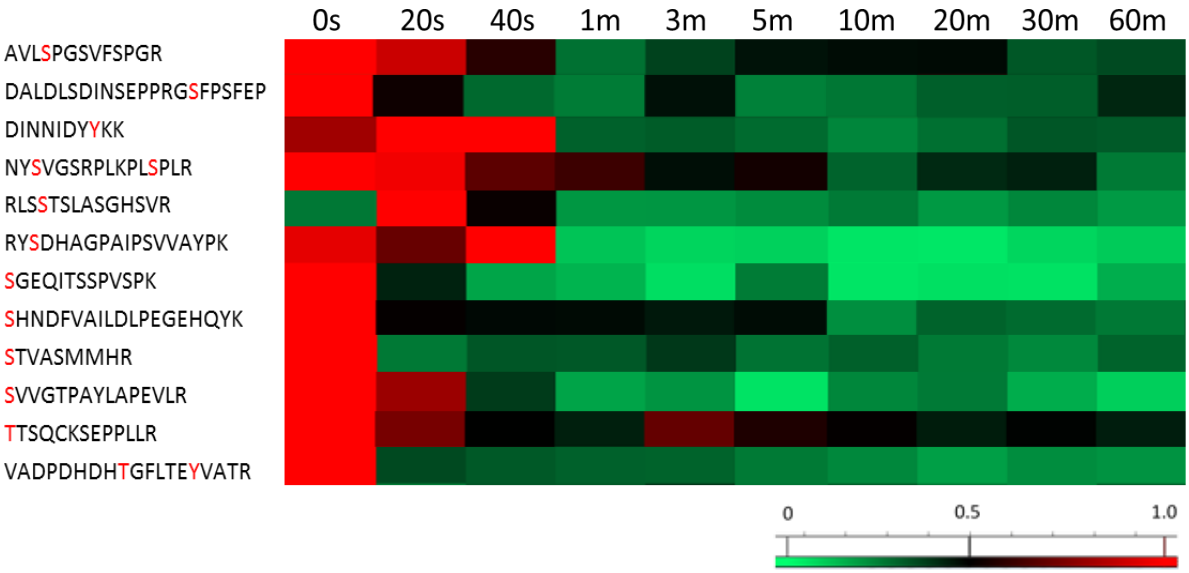

Figure 6.4 Hierarchical clustering of relative phosphorylation profile of early response phosphopeptides. The expression of each phosphopeptide was normalized to a percentage of the highest expression in a time profile (horizontally). The colours in the map display the relative expression of phosphopeptides during FGF1 stimulation. Phosphopeptide sequences were shown on the left of clustering image.

6.2.3.2 Mid response phosphopeptides

In total, 10 phosphopeptides were characterised as mid response phosphopeptides (1 min to 20 min following FGF1 stimulation), shown in Table 6.3. There are 9 singly phosphorylated peptides and 1 doubly phosphorylated peptide. The kinases corresponding to these phosphopeptides include participators of the MAPK pathway, CoA biosynthesis, carbohydrate metabolic process, proliferation and apoptosis. Phosphorylation levels of the mid response phosphopeptides were up-regulated from 1 min to around 20 min following the addition of FGF1.

Table 6.3 Mid response phosphopeptides

Phosphopeptide	Kinase
ALGERVSIL	Serine/threonine-protein kinase D1
IADPEHDHTGFLTEYVATR	Mitogen-activated protein kinase 3
IADPEHDHTGFLTEYVATR	Mitogen-activated protein kinase 3
LGSYSGPTSVSR	Pantothenate kinase 2
RLNSSPRAPVSPLK	Ribosomal protein S6 kinase beta 2
RNSFTPLSSSNTIR	6-phosphofructo-2-kinase/fructose-2,6-bisphosphatase 2
RPHFPQFSYSASGRE	RAC-alpha serine/threonine-protein kinase
SGGGDLTLGLEPSEEEAPR	Receptor tyrosine-protein kinase erbB 2
TPKDSPGIPPSAGAHQLFR	Ribosomal protein S6 kinase
TTSFAESCKPVQQPSAFGSMK	Glycogen synthase kinase-3 beta

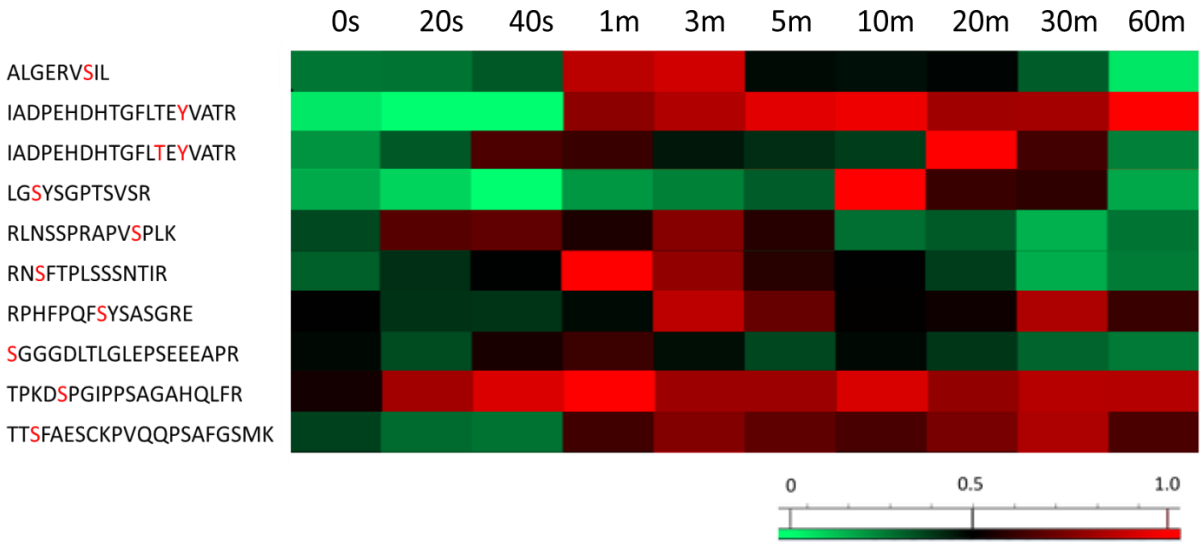

Figure 6.5 Hierarchical clustering of relative phosphorylation profile of mid response phosphopeptides. The expression of each phosphopeptide was normalized to a percentage of the highest expression in a time profile (horizontally). The colours in the map display the relative expression of phosphopeptides during FGF1 stimulation. Phosphopeptides sequences were shown on the left of clustering image.

6.2.3.3. Late response phosphopeptides

In total, 12 phosphopeptides were characterised as late response phosphopeptides (30 min to 60 min following FGF1 stimulation), shown in Table 6.4. There are 10 singly phosphorylated peptides and 2 doubly phosphorylated peptides. The kinases corresponding to these phosphopeptides include participators of transcription, translation, MAPK pathway, calcium metabolic process, proliferation and apoptosis. Phosphorylation levels of the late response phosphopeptides were up-regulated from 30 min to 60 min following the addition of FGF1.

Table 6.4 Late response phosphopeptides

Phosphopeptide	Kinase
DINNIDYYKK	Fibroblast growth factor receptor 2
EHIEIIAPSPQR	Eukaryotic translation initiation factor 2-alpha kinase 3
IADPEHDHTGFLTEYVATR	Mitogen-activated protein kinase 3
NFSAAKSLLNKK	Calcium/calmodulin-dependent protein kinase type II subunit gamma
RESVVNLENFRK	Death-associated protein kinase 2
RISLSDMPR	Protein kinase C-binding protein 1
RLNSSPRAPVSPLK	Ribosomal protein S6 kinase beta 2
RLSSTSLASGHSVR	Serine/threonine-protein kinase D2
RPHFPQFSYSASGRE	RAC-alpha serine/threonine-protein kinase
RPHFPQFSYSASGRE	RAC-gamma serine/threonine-protein kinase
THFPQFSYSASIRE	RAC-beta serine/threonine-protein kinase
VADPDHDHTGFLTEYVATR	Mitogen-activated protein kinase 1

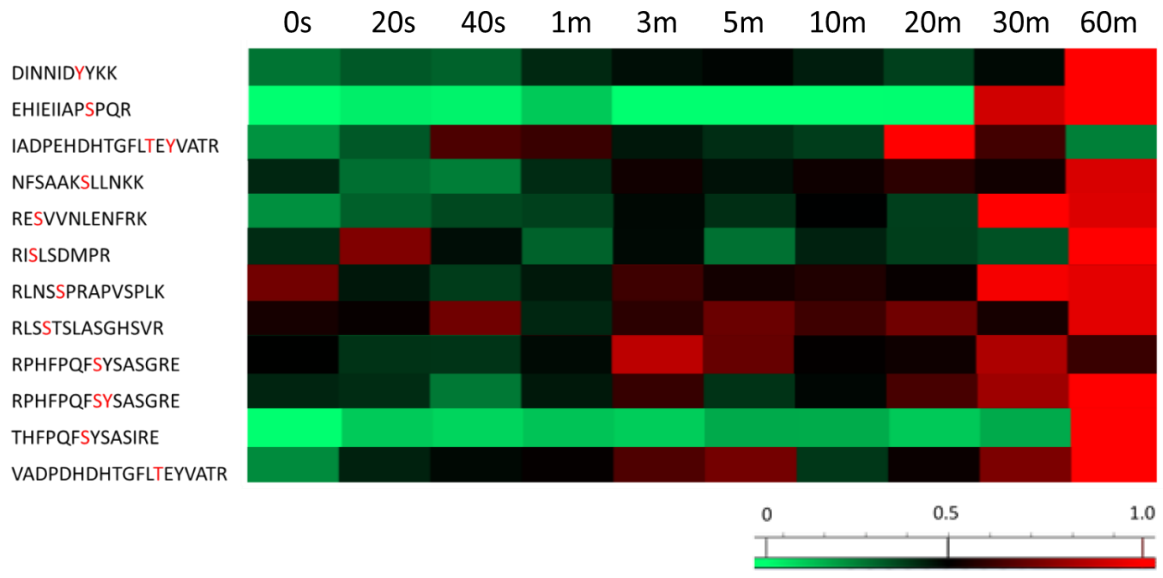

Figure 6.6 Hierarchical clustering of relative phosphorylation profile of late response phosphopeptides. The expression of each phosphopeptide was normalized to a percentage of the highest expression in a time profile (horizontally). The colours in the map display the relative expression of phosphopeptides during FGF1 stimulation. Phosphopeptide sequences were shown on the left of clustering image.

6.2.4 Establishment of calibration curve

For absolute quantitation, a calibration curve is required to determine the absolute amount of a peptide. Calibration curves were prepared for each phosphopeptide using synthetic peptides. A 6-point calibration curve was produced: 100 attomole, 500 attomole, 1 femtomole, 10 femtomole, 50 femtomole and 250 femtomole. Triplicate measurements were performed for each phosphopeptide and three inter-day analyses were performed at the beginning, middle and end of the sample analysis.

When evaluating the reproducibility of the calibration curve assay, the mean of three measurements were used for further analysis; however, the inter-assay variance was observed for experiments performed over a four-week period. Using the mean of three inter-day results could potentially bias the calibration curve as the value of peak area over 6 concentrations can differ by up to 1,000 fold. Therefore, a logarithm transform approach was adopted to combine the inter-day results, as shown in Figure 6.7.

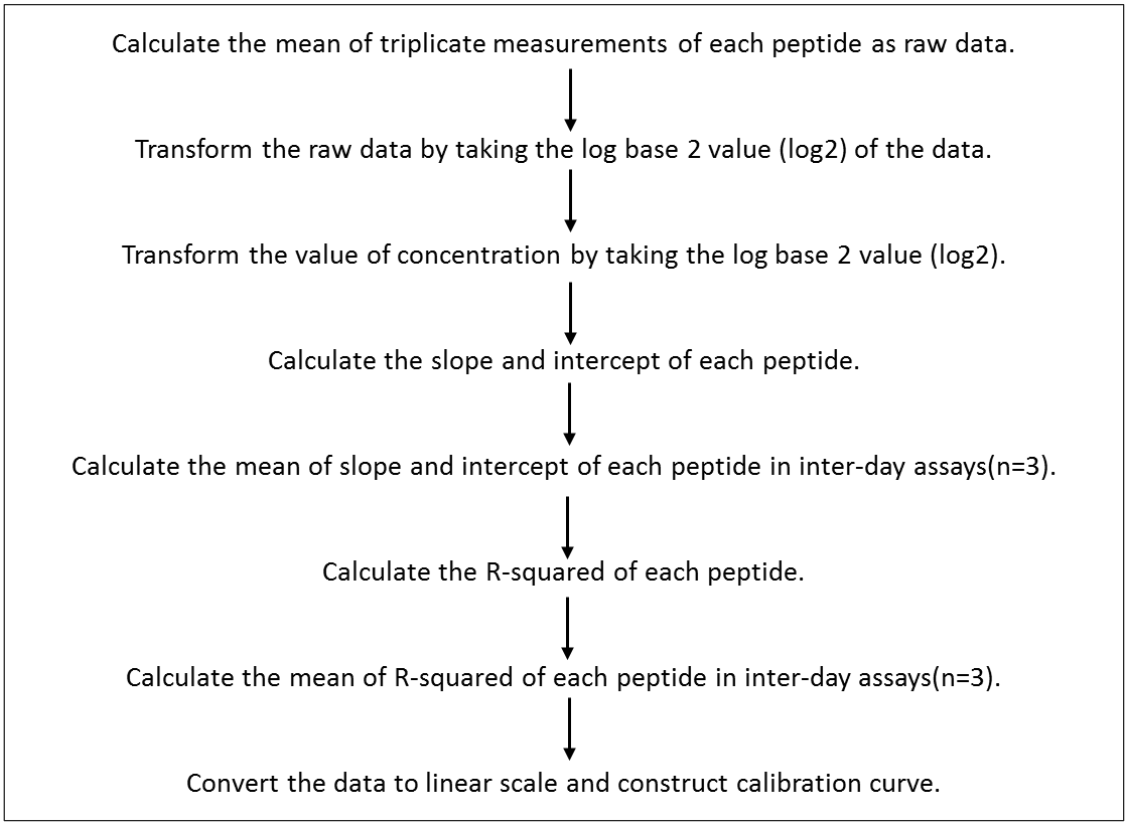

Figure 6.7 Schematic diagram of the logarithm transform approach

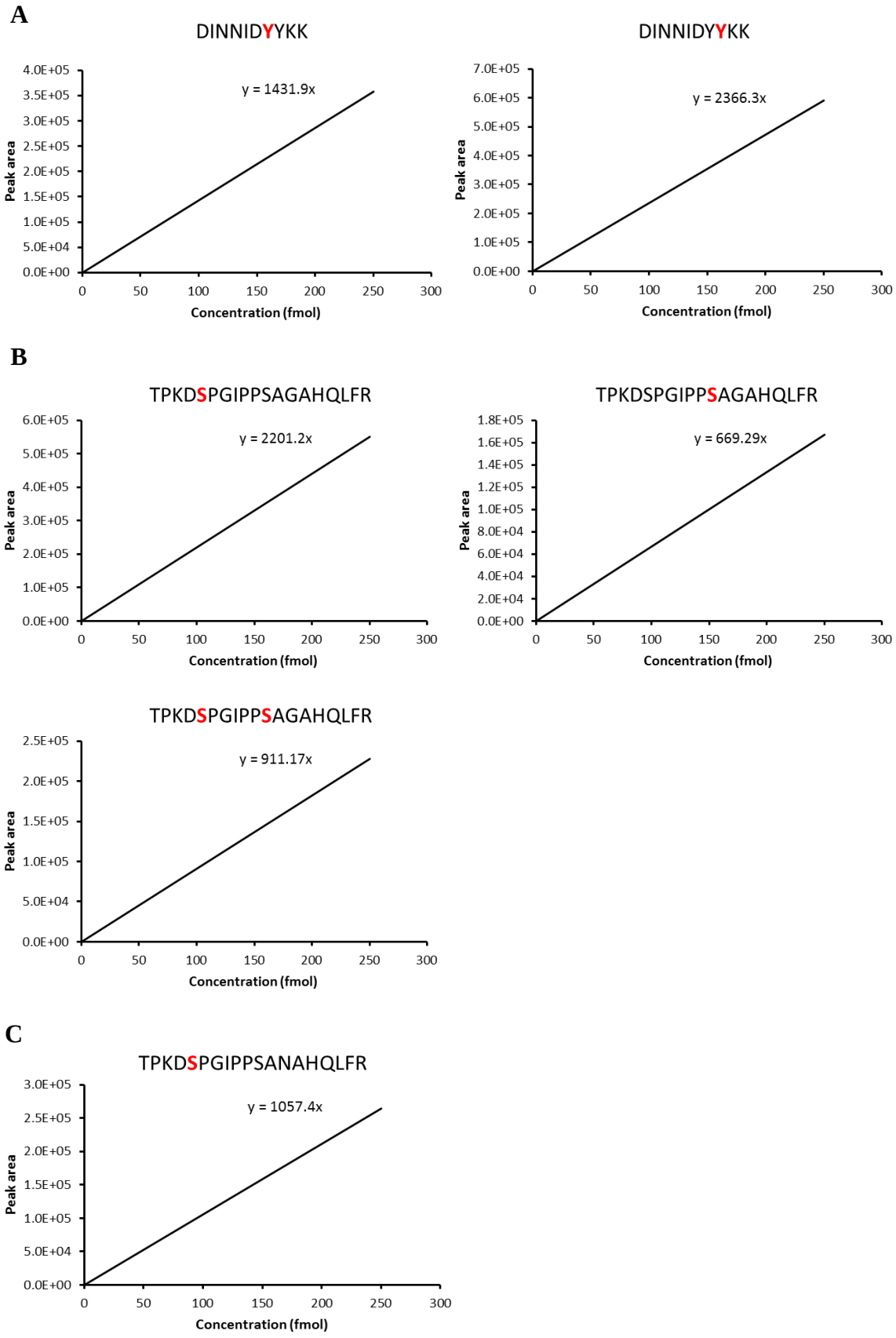

Figure 6.8 Calibration curve of phosphopeptides
(A) DINNIDpYYKK of Fibroblast growth factor receptor 2; (B) TPKDSPGIPPSAGAHQLFR of Ribosomal protein S6 kinase alpha-3; (C) TPKDpSPGIPPSANAHQLFR of Ribosomal protein S6 kinase alpha-1

Figure 6.8 shows a number of calibration curves constructed using the approach described above. The calibration curve with a less than 0.9 R-squared value will be excluded from further analysis. Therefore, 65 phosphopeptides are allowed for absolute quantitation. A representative Skyline output is shown in Figure 6.9.

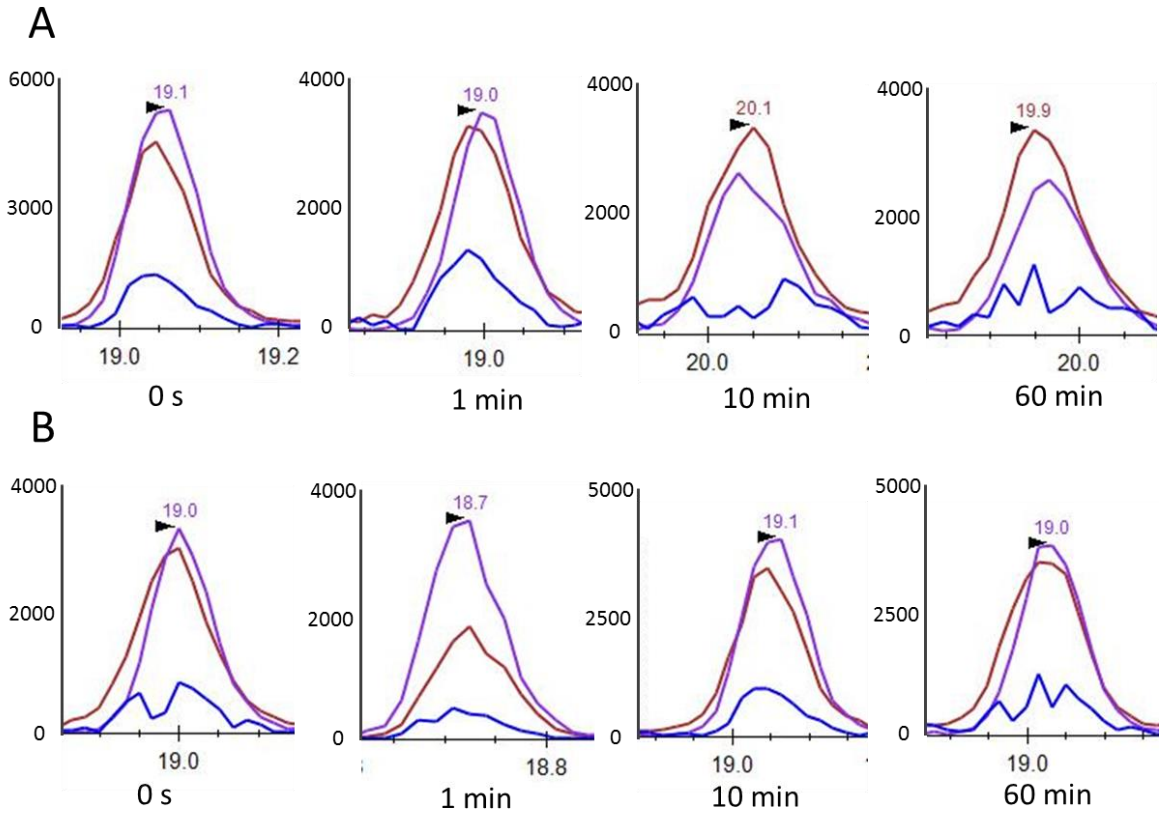

Figure 6.9 Representative Skyline output of 2+ peptide pSVVGTPAYLAPEVLR following FGF1 treatment (A) Time profile of endogenous peptides; (B) Time profile of IS peptides. Three transitions shown in the figure are neutral loss ion (precursor-98, blue), b3 (purple) and y10 (dark red).

6.2.5 Response of multi-site phosphopeptides

6.2.5.1 Fibroblast growth factor receptor 2

Figure 6.10 shows the temporal phosphorylation profile of two isobaric phosphopeptides (Tyr656 and Tyr657) following the addition of FGF1 and the absolute abundance of phosphopeptides present at each time point is quantified. For DINNIDpYYKK, the phosphorylation level showed a time-dependent increase following the addition of FGF1, and

at 60 min the maximum phosphorylation level was reached. For DINNIDYpYKK, FGF1 induced a quick reduction in phosphorylation level and the phosphorylation level tended to be stable after 1 min of FGF1 stimulation.

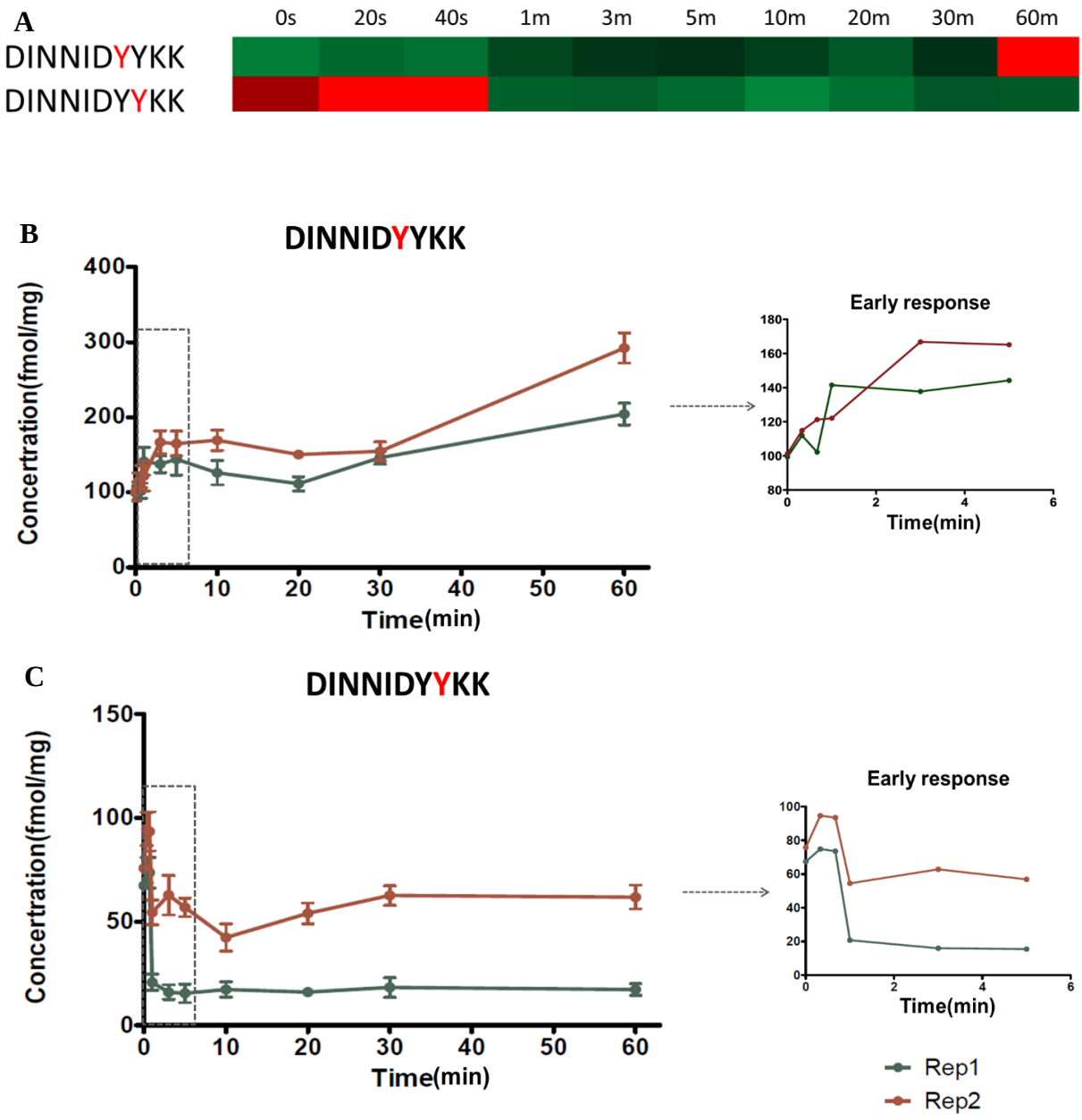

Figure 6.10 Phosphorylation profile of 2 isobaric phosphopeptides of FGFR2
(A): Clustering presentation of phosphopeptides from FGFR2. (B) Phosphorylation profile of peptide DINNIDpYYKK (Tyr656) following addition of FGF1. (C) Phosphorylation profile of peptide DINNIDYpYKK (Tyr657) following addition of FGF1. Early response profile was shown on the right of the figure. Results from two biological replicates are shown in green and red.

6.2.5.2 Ribosomal protein S6 kinase alpha-1

Figure 6.11 shows the temporal phosphorylation profile of three isobaric phosphopeptides (Ser363, Ser369 and both) following addition of FGF1 and the absolute abundance of phosphopeptides present at each time point is quantified. For all three peptides, up-regulated phosphorylation levels were observed from 20 s after the addition of FGF1 and the phosphorylation level reached a maximum around 40 s to 1 min. After 10 min stimulation, the response was slowly tuned back to initiation level. The phosphorylation of Ser359 of RSK1 and Ser369 of RSK3 (homologous to Ser363 of RSK1) exhibited a similar profile, displayed in Figure 6.12 and 6.13.

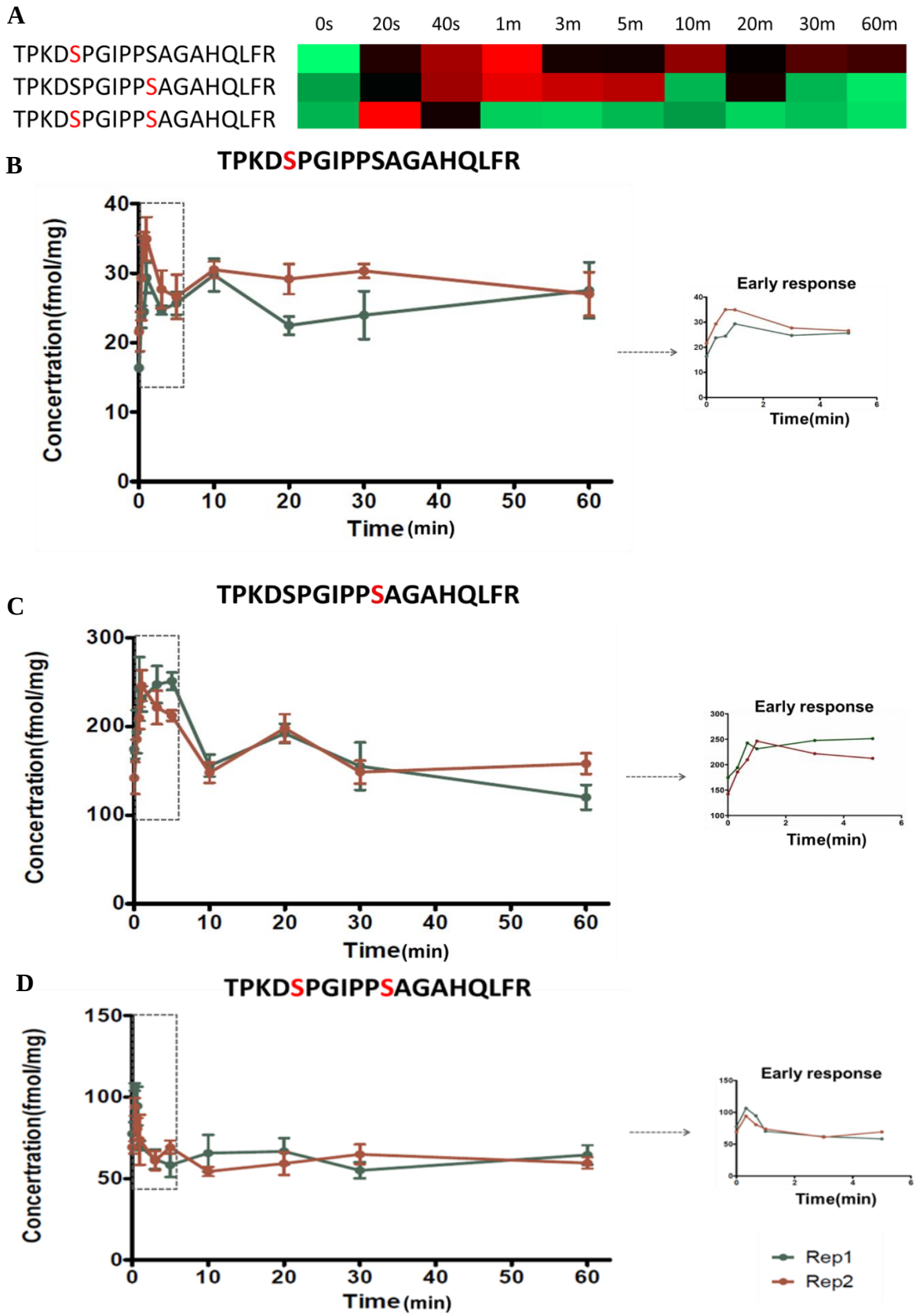

Figure 6.11 Phosphorylation profile of a group phosphopeptides of RSK1
(A) Clustering presentation of phosphopeptides from RSK1. (B) Phosphorylation profile of peptide TPKDpSPGIPPSAGAHQLFR (Ser363) following addition of FGF1. (C) Phosphorylation profile of peptide TPKDSPGIPPpSAGAHQLFR (Ser369) following addition of FGF1. (D) Phosphorylation profile of peptide TPKDpSPGIPPpSAGAHQLFR (Ser363 and Ser369) following addition of FGF1. Early response profile was shown on the right of the figure. Results from two biological replicates are shown in green and red.

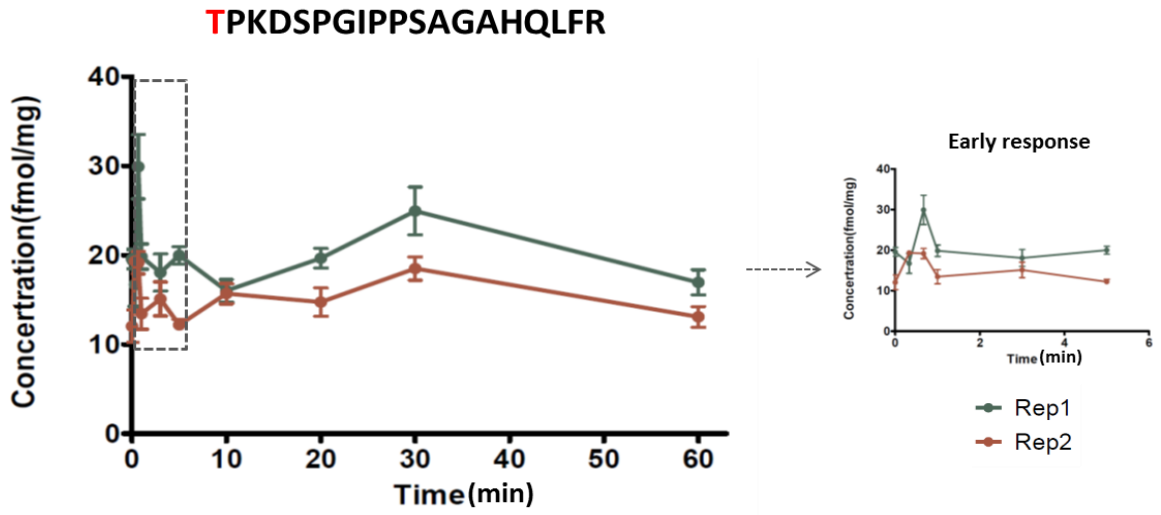

Figure 6.12 Phosphorylation profile of peptide pTPKDSPGIPPSAGAHQLFR (Ser359) of RSK1
Early response profile was shown on the right of the figure. Results from two biological replicates are shown in green and red.

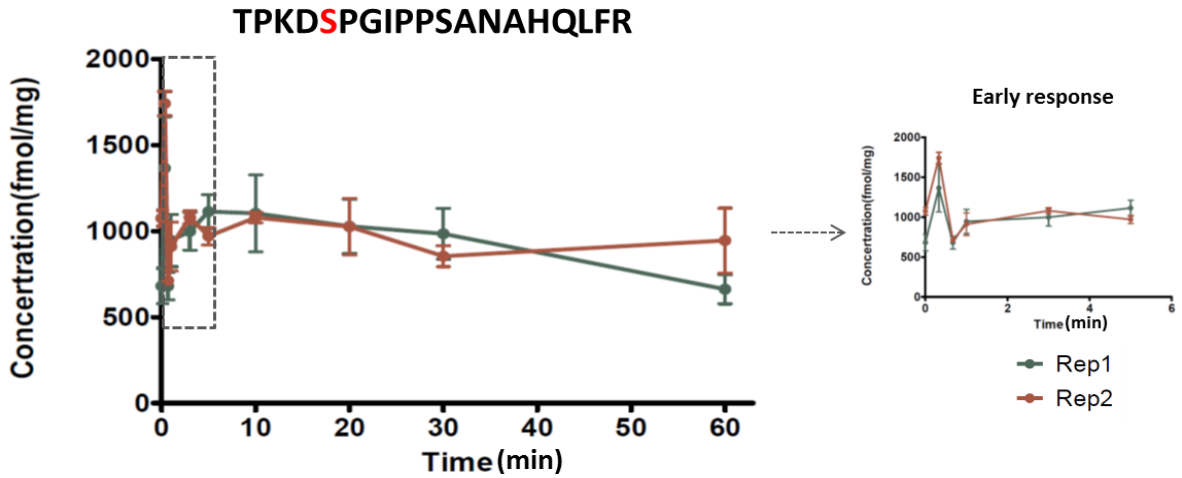

Figure 6.13 Phosphorylation profile of peptide TPKDpSPGIPPSANAHQLFR (Ser369) of RSK3
Early response profile was shown on the right of the figure. Results from two biological replicates are shown in green and red.

6.2.5.3 Extracellular signal-regulated kinase 1

Figure 6.14 shows the temporal phosphorylation profile of three isobaric phosphopeptides (Thr202, Tyr204 and both) following addition of FGF1 and the absolute abundance of phosphopeptides present at each time point is quantified. The expression level of singly phosphorylated peptide (Thr202) was up-regulated after the addition of FGF1 and continued to increase after 20 min of stimulation. For the Tyr204 phosphopeptide, a similar response was

revealed and a rapid increase in phosphorylation was observed at 1 min of FGF1 stimulation. For the doubly-phosphorylated peptide (Thr202 and Tyr204), the phosphorylation level was increased at 40 s and 20 min of stimulation and decreased after 20 min. From the analysis of the three isobaric peptides, it is likely that upon FGF1 stimulation, Thr202 and Tyr204 are both activated. Dephosphorylation of these two sites is initiated after 20 min, therefore a decrease was observed.

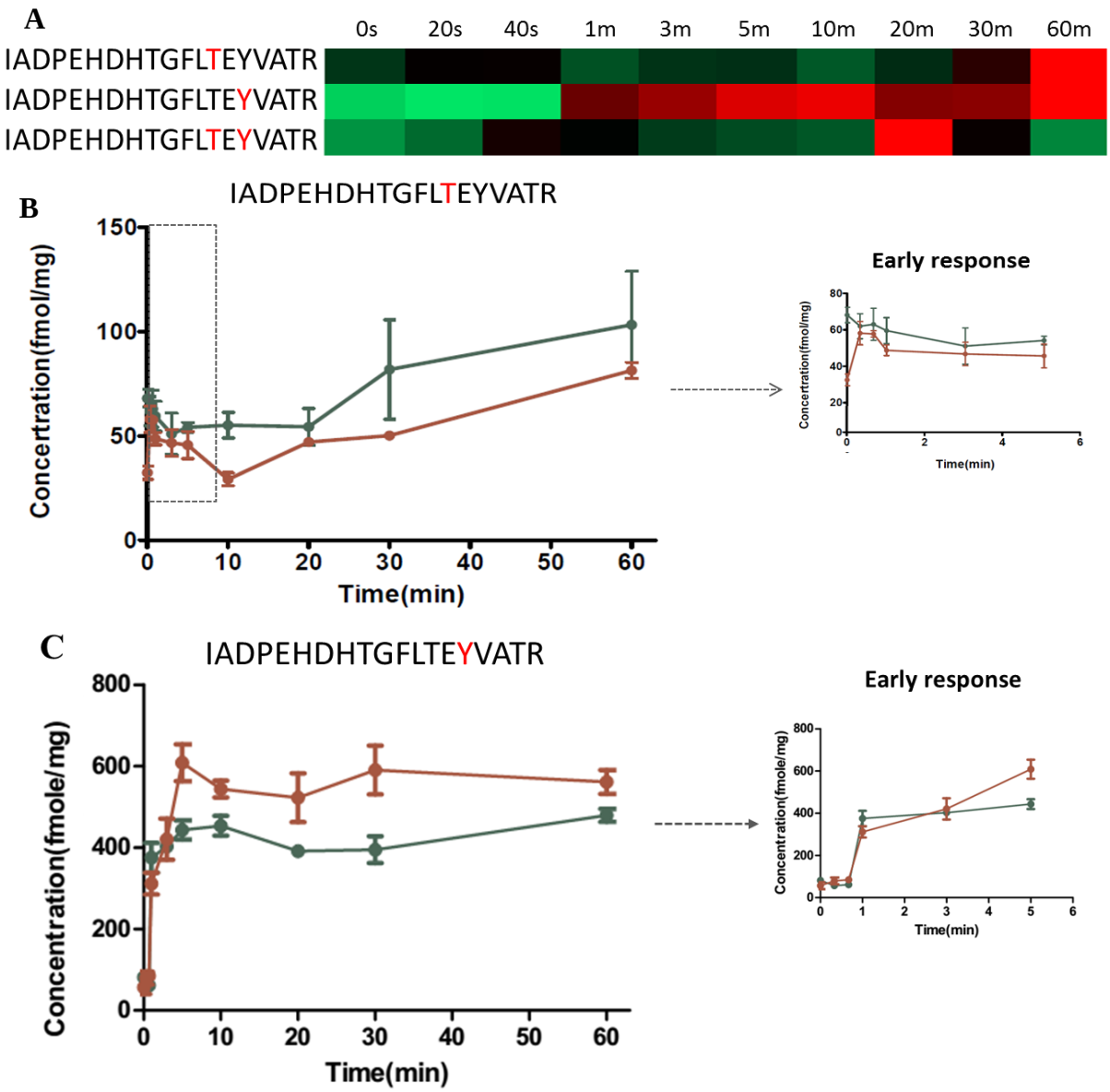

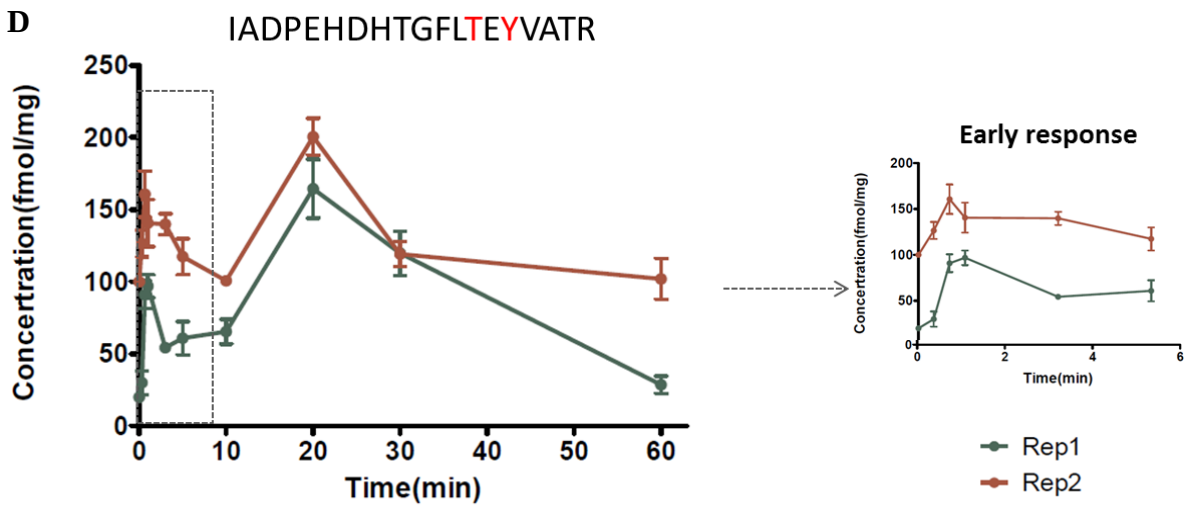

Figure 6.14 Phosphorylation profile of a group of isobaric phosphopeptides of ERK1
(A): Clustering presentation of phosphopeptides from ERK1. (B) Phosphorylation profile of peptide IADPEHDHTGFLpTEYVATR (Thr202) following addition of FGF1. (C) Phosphorylation profile of peptide IADPEHDHTGFLTEpYVATR (Tyr204) following addition of FGF1. (D) Phosphorylation profile of peptide IADPEHDHTGFLpTEpYVATR (Thr202 and Tyr204) following addition of FGF1.Early response profile was shown on the right of the figure. Results from two biological replicates are shown in green and red.

6.2.5.4 Extracellular signal-regulated kinase 2

Figure 6.15 shows the temporal phosphorylation profile of three phosphopeptides (Thr185, Tyr187 and both) following addition of FGF1 and the absolute abundance of phosphopeptides present at each time point is quantified. The response of the three phosphopeptides is different in response to FGF1. Singly-phosphorylated peptide Thr185 showed an increase following addition of FGF1 and the phosphorylation level kept increasing until 60 min of treatment. For peptide with Tyr187 phosphorylation, no obvious response was observed. In contrast, the phosphorylation level of the doubly phosphorylated peptide showed a reduction immediately after treatment.

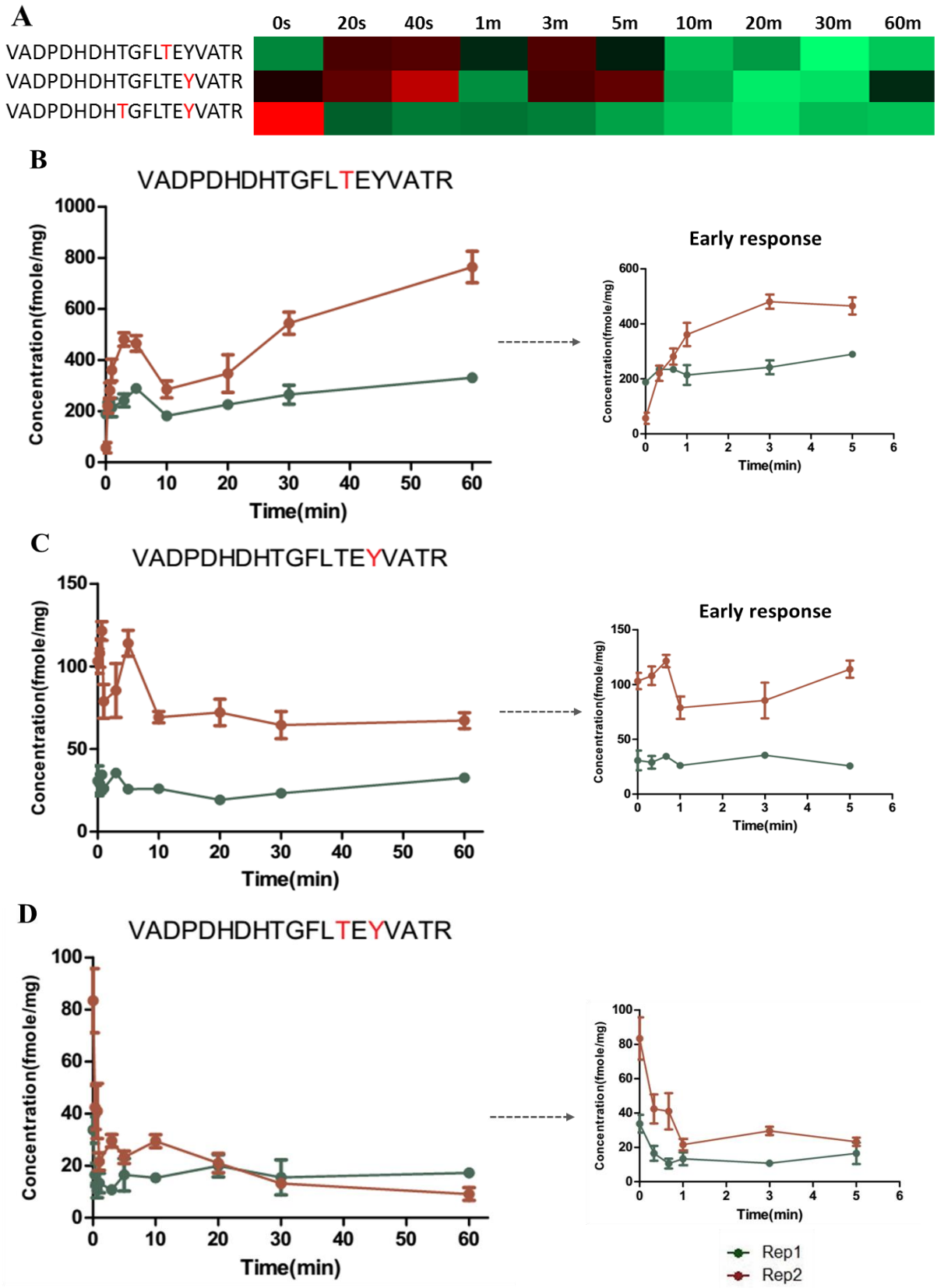

Figure 6.15 Phosphorylation profile of a group of phosphopeptides of MAPK2
(A): Clustering presentation of phosphopeptides from ERK2. (B) Phosphorylation profile of peptide VADPDHDHTGFLpTEYVATR (Tyr185) following addition of FGF1. (C) Phosphorylation profile of peptide VADPDHDHTGFLTEpYVATR (Thr187) following addition of FGF1. (D) Phosphorylation profile of peptide VADPDHDHTGFLpTEpYVATR (Thr185 and Tyr187) following addition of FGF1. Early response profile was shown on the right of the figure. Results from two biological replicates are shown in green and red.

6.2.6 Trouble shooting

A total of 75 phosphosites were submitted for SRM quantitation, 38 of which were reproducibly quantified. The other 37 phosphopeptides were not successfully quantified due to a number of reasons, as summarised in Table 6.5. In order to ensure reproducible quantitation, a peak area cut-off of 5000 was selected to exclude low-abundance ions. A total of 21 phosphopeptides were removed from further analyses as a result of low MS response. Five phosphopeptides showed sufficient MS signal but fell partially outside of the retention time window, therefore the data could not be used for quantitation. Peptides EHIEIIAPpSPQR, EKFpSFEPK and pSGGGDLTLGLEPSEEEAPR were successfully identified in only one set of biological replicates. Six phosphopeptides did not show good correlation between the two biological replicates, therefore they were excluded from further analysis.

Table 6.5 Summary of identification results

Peptide sequence	Identification results	Peptide sequence	Identification results
ATDSFSGRFEDVYQLQEDVLGEGAHAR	Low signal	RLNSSPRAPVSPLK	Low signal
DINNIDYYKK	Low signal	RLSSTSLASGHSVR	Low signal
EHIEIIAPSPQR	One repeat	RNSFTPLSSSNTIR	Low signal
EKFSFEPK	One repeat	RPHFPQFSYSASGRE	Outside of RT window
EYGSPLKAYTPVVVTQWYR	Low signal	RPHFPQFSYSASGRE	Poor reproducibility
GAILTTM(ox)LVSR	Low signal	RPPGMEYSYDINR	Outside of RT window
GAQASSGSPALPR	Low signal	RSDSASSEPVGIYQGFEK	Low signal
GFSFVATGLM(ox)EDDGKPR	Outside of RT window	RVSLSEIGFGK	Low signal
GLCTSPAEHQYFMTEYVATR	Low signal	SGGGDLTLGLEPSEEEAPR	One repeat
GRNSATSADEQPHIGNYR	Low signal	SGSPSDNSGAEEMEVSLAKPK	Low signal
HFM(ox)HQIITGMLYLHSHGILHR	Outside of RT window	SHNDFVAILDLPEGEHQYK	Outside of RT window
KLPSTTL	Poor reproducibility	STVASMMHR	Low signal
LQPFHSTELEDDAIYSVHVPAGLYR	Low signal	THFPQFSYSASIRE	No calibration data
NFSAAKSLLNKK	Poor reproducibility	TPKDSPGIPPSANAHQLFR	Low signal
NFSAAKSLLNKK	Poor reproducibility	TTSFAESCKPVQQPSAFGSM(o	No calibration data
NFSAAKSLLNKK	Poor reproducibility	TTSFAESCKPVQQPSAFGSMK	Poor reproducibility
NLQSPTQFQTPR	Low signal	VADPDHDHTGFLTEYVATR	Low signal
NYSVGSRPLKPLSPLR	Low signal	VTSGGVSESPSGFSK	Low signal
NYSVGSRPLKPLSPLR	Low signal		

6.3 Discussion

6.3.1 Initial assessment of SRM assay

To measure the biological reproducibility of the SRM assay, a histogram was used to assess the overall performance between the two datasets. Approximately 39.8% of peptides showed a variance above 20%. This results is due, firstly, to the variance in instrumental performance. The samples from the two biological replicates were analysed on different days, therefore a certain level of instrumental error was expected. Secondly, for each phosphopeptide, the ratio of absolute measurements used in the evaluation of biological reproducibility is the average expression across the time expression profile, where different phosphorylation levels are expected within a time-dependent profile. Although high variances were observed between biological replicates, in some cases, a similar response pattern was found in the two replicates. To further optimize the reproducibility, inclusion of an internal standard (*i.e.* a peptide of a known amount) was thought to be advisable.

6.3.2 Phosphopeptides response to FGF1 treatment

In the initial stage of FGF activation, a number of conserved tyrosine residues in the intracellular domain of the FGFR will undergo phosphorylation. The activated FGFR kinases, in turn, phosphorylate downstream signalling protein for signal transduction. The trafficking of FGF signalling is mediated by the diverse downstream responses. Dissecting their expression patterns and subjecting them to pathway analysis may yield deeper insights into the mechanisms of FGF activation and trafficking.

The SRM assay identified differences in the phosphorylation response after the activation of FGF signalling. The clustering of phosphopeptide expression patterns allowed the peptides that

play different roles in FGF signalling to be distinguished. Previously published data demonstrated that immediate phosphorylation of the receptor and tyrosine phosphorylation of FGFR was observed to occur within 30 seconds of FGF stimulation *in vitro*[18]. FGF1 induced intra-cellular signalling is time-dependent and the induction can be sustained until 24 hours after FGF1 stimulation. In order to study the immediate and transient activation of FGF signalling, in this assay, the expression profile of key phosphorylation events within one hour of FGF1 stimulation was monitored.

6.3.3 Calibration curve

The calibration curve was generated from three independent calibration analyses performed on different days. Certain types of data, *e.g.* gene expression data or protein expression data, are heavily skewed in linear scale[229]. It is arbitrary simply to take the average for data analysis. When interpreting SRM data, the value of peak area over 6 concentrations can differ by up to 1,000 fold. Thus, using the mean of three inter-day results could potentially bias the calibration curve. To reduce the data skewness in linear scale, a log-transform approach was used to calculate the calibration curve, as described by Irizarry *et al*[230]. After log2 transformation, parameters of linear regression were calculated. To identify the linearity of calibration data, an empirical R-squared value of 0.9 was selected as the cut-off.

6.3.4 Response of multi-site phosphopeptides

6.3.4.1 Fibroblast growth factor receptor 2

FGFR2 is a key protein in FGF signalling and predominantly expressed in epithelium cells[16]. FGFR2 isoforms, both FGFR2IIIb and FGFR2IIIc have been shown to interact with FGF1 to

initiate the signalling[231]. The crystal structure revealed that the interaction between FGFR2 and FGF1 was formed by linking the two ligands into the dimeric receptors chains[232]. The direct result of this interaction is the conformation change in the cytoplasmic domain of the receptor, which will lead to the autophosphorylation of two tyrosine site Y656 and Y657.

A mechanism of FGFR1 activation has been described by Furdui *et al*[21]. They hypothesised a two-step activation mechanism by using rapid chemical quench method and time-resolved ESI-TOF-MS. In the first step, the autophosphorylation of Y653 (homologous to Y656 of FGFR2) in the activation loop will result in approximately 50 to 100 fold increase in kinase activity, whereas the catalyse activity is further enhanced by 500 to 1000 fold after the auto-phosphorylation of Y654 (homologous to Y657 of FGFR2). The auto-phosphorylation of FGFR1 is not a homogenous process, but a sequential, strictly ordered reaction. Next, Y463 in juxtamembrane region, Y586 and Y588 in kinase insert, and Y769 in C-terminal region are also phosphorylated to enhance the signal propagation or serve as recruitment sites for downstream signalling proteins.

The results here provide temporal evidence in support of this hypothesis. In the first step, FGF1 stimulation enhances kinase activity by phosphorylating of Y656 of FGFR2, which was evidenced by the increased phosphorylation level of DINNIDpYYKK (Figure 6.9B). The subsequent phosphorylation of Y657 will further promote catalytic activity of FGFR2, resulting in a decreased phosphorylation level of the singly phosphorylated peptide and an increased level of the doubly phosphorylated peptide. Unfortunately, the doubly phosphorylated version was too low abundance to establish a temporal phosphorylation profile. The results presented here support the theory that the catalytic activity of FGFR during signal initiation stage is activated and mediated by a sequential tyrosine autophosphorylation process. Moreover, this process is likely to be a conserved mechanism of FGFR family members.

6.3.4.2 Ribosomal protein S6 kinase alpha-1

Ribosomal protein S6 kinase (RSK) represents an important family of serine-threonine kinases that acts downstream of the Ras-MAPK cascade[233]. RSKs comprise two distinct kinase domain (N- and C-terminal kinase domain) and this family has four isoforms (RSK1-4) in humans. Phosphorylation of RSKs occurs at multiple Ser and Thr sites through sequential reactions by various kinases, *e.g*. Erk1/2 in response to growth factors[234]. RSKs have been extensively implicated in mitotic phosphorylation events and the regulation of cell cycle[235]. There is increasing evidence pointing to RSKs as the potential therapeutic targets for a number of cancers, including breast cancer[236,237].

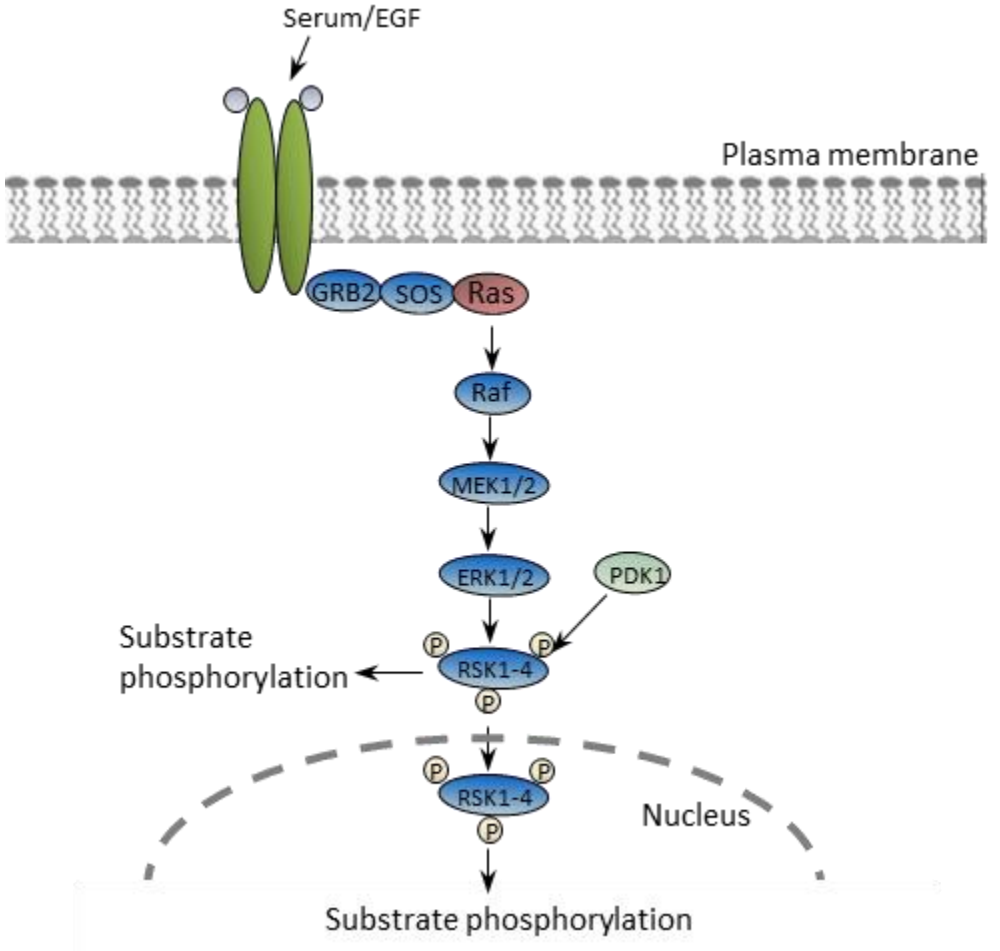

Figure 6.16 A schematic model for RSK activation (Adapted from Anjum and Blenis[234])

RSKs can be activated via canonical MAPK cascade upon treatment with growth factors and other extracellular signals. As shown in Figure 6.16, activation of cell surface receptor leads to

auto-phosphorylation of receptor and creates recruitment sites for scaffolding proteins such as growth factor receptor-bound protein-2 (GRB2). Upon activation of GRB2, downstream signalling protein, such as SOS, Ras and Raf, are recruited subsequently, leading to the activation of MEK1/2. Next, ERK1/2 directly phosphorylates and activates RSKs (e.g. Ser363 and Ser380 of RSK1). Alternatively, RSK is modulated by 3'-phosphoinositide-dependent kinase-1 (PDK) by phosphorylation of Ser221 of RSK1.

Ser363 of RSK1 (TPKDpSPGIPPSAGAHQLFR, homologous to other members of RSK family) is located within sequences that are conserved in the most AGC kinases and is phosphorylated by ERK1/2[238]. It has been demonstrated that the phosphorylation of Ser363 and Ser380 is critical for activation of the N-terminal kinase domain. Together with Ser359 (pTPKDSPGIPPSAGAHQLFR), these two sites has been termed the 'turn-motif', which is primarily involved in modulating structure of the kinase in order to influence kinase activity. Our findings showed FGF1 stimulation induced immediate response and increase of Ser359, Ser363 and the doubly-phosphorylated version. It was previously reported the phosphorylation of doubly-phosphorylated version was involved in stabilizing the kinase core[239]. Whether the phosphorylation of Ser359 is required for activation is unclear so far, but the low level of the Ser359 peptide may indicate it is not a specific target of ERK1/2.

In addition, absolute quantitation results revealed that the phosphorylation level of Ser369 of RSK3 was much higher than the homologous site of RSK1 (see Figure 6.13), which suggests the basal level of RSK3-associate phosphorylation is more abundant than other members of RSK family. There is evidence demonstrating, upon mitogen stimulation, RSK3 is able to maintain interaction with ERK1/2 longer than RSK1 and RSK2 in 293T cells[240]. Therefore, it is likely that the high level of RSK3 phosphorylation is associated with the preference of ERK1/2 to bind with RSK3 than other members of RSK family.

6.3.4.3 Extracellular signal-regulated kinase 1

Extracellular signal-regulated kinase, also known as mitogen-activated protein kinase 3 (MAPK3), is one of the central regulators in cellular response to extracellular stimuli, such as oxidative stress, DNA damage and infection *etc*[241]. The ERK1/ERK2 pathway is known to be the best-characterized MAPK cascade. ERK1 was found to be phosphorylated on Tyr and Thr residues in response to a wide variety of stimuli, such as growth factor, Ca^{2+}, neurotransmitters[242]. Thr202 and Tyr204 of ERK1 were shown to be further phosphorylated by MEK1/2 to fully active kinase activity and Thr202 and Tyr204 are the only substrates of MEK1/2 known so far[243]. Crystal structure revealed the mono-phosphorylated form at Tyr204 and dual-phosphorylated form possess distinct conformations, which contribute to the huge difference in kinase activity[244]. Some proteins have been identified to regulate ERK1 activity in multiple levels. Upstream of ERK1, the phosphorylation status of Ser298 outside of activation loop of MEK could regulate ERK1 activity in positive or negative manner. Dual Specificity Phosphatases (DUSPs) interact directly with ERK1 to dephosphorylate both sites of Thr202 and Tyr204 to regulate its kinase activity[245]. Downstream of ERK1, negative regulation also occurs through feedback of a variety of substrates and its subcellular localization.

Currently, antibody in the market is only able to target Thr202 and Tyr204 at the same time. However, our results showed a different effect on three isobaric phosphopeptides upon FGF1 treatment. An increase in the singly phosphorylated form while a decrease in the doubly phosphorylated form was observed after 20 min stimulation. This is likely to be a negative feedback in response to the activated MAPK pathway. It is unclear which mechanism is responsible for this negative regulation. However, it is obvious that the addition of ligand is able to induce an immediate response of ERK1 through phosphorylation of Thr202 and Tyr204, and a negative feedback is initiated around 20 min after the stimulation.

6.3.4.4 Extracellular signal-regulated kinase 2

ERK2 (also known as mitogen-activated protein kinase 1, MAPK1) is a member of MAP kinase family. Together with ERK1, they participate in MAP kinase signal transduction pathway and regulate a variety of biological processes. The Thr185 and Tyr187 of ERK2 are homologous to Thr202 and Tyr204 of ERK1, as shown in Figure 6.17. Similar to ERK1, activity of ERK2 is regulated through the dual-phosphorylation mechanism of Thr185 and Tyr187[246]. Thr185 and Tyr187 have been reported to be phosphorylated by a number of upstream kinases, *e.g.* PLC-γ[247], MEK1 and MEK2[248]. All known cellular stimuli of the ERK1/2 pathway are able to induce the parallel activation of ERK1 and ERK2. On the other hand, a number of downstream substrates can regulate ERK2 kinase activity, *e.g.* DUSP5, a mitogen-activated protein kinase dephosphorylates ERK2 at Thr185 and Tyr187 to prevent it from leaving nucleus, therefore deactivating the kinase[249].

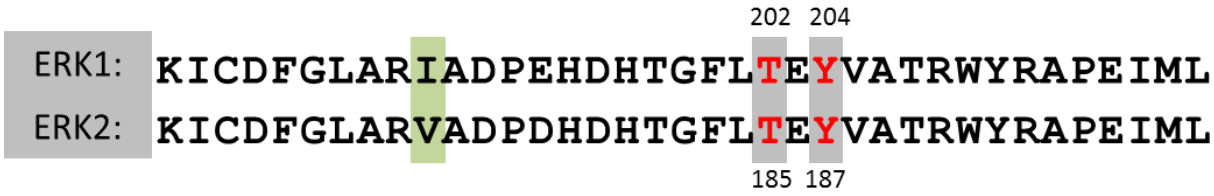

Figure 6.17 Alignment of amino acid sequence in active site of ERK1 and ERK2

The dual phosphorylation sites are shown in red. Numbers indicate the site of amino acid in ERK1 or ERK2. The unconserved amino acid between ERK1/2 is shown in green.

ERK1 and ERK2 are 82% identical in amino acid sequence and they share the same substrates specificity under most circumstances[250]. Also, they are co-expressed ubiquitously but with a remarkably variable relative abundance[251]. Recent evidence suggests ERK1 and ERK2 are not always interchangeable and some differences between their regulation and function have been elucidated under specific conditions. Fischer *et al*,. showed ERK2 was indispensable in multiple stages of T-cell development in mice, while ERK1-deficient mice was still viable through the development[252]. Also, ERK2 but not ERK1 is necessary for Ras-induced epithelial-

to-mesenchymal transformation (EMT)[253]. Moreover, a number of research points that quantitative differences in ERK1 and ERK2 dynamics could have a significant role in their regulation. Pages *et al,*. have shown an elevated level of ERK1 protein was capable of compensating the lack of ERK2 during the proliferation and differentiation of positive thymocytes[254]. It indicates ERK1 and ERK2 might compete with each other for upstream MEK activation. Last, alternatively spliced isoforms of ERK1 and ERK2 have been reported to determine signalling specificity[255,256].

Thr185 (ERK1) and Thr 202 (ERK2) showed a similar phosphorylation profile in response to FGF1. Their phosphorylation was gradually increased until 60 min of stimulation. Tyr187 (ERK1) showed in increase while Tyr204 (ERK2) showed a decrease following addition of FGF1. For doubly phosphorylated peptides, ERK2 peptide showed a sharp decrease while ERK1 peptide exhibited a peak of phosphorylation aound 20 min of stimulation. ERK2 showed higher absolute abundance than ERK1 in general. Our data suggests, in SUM52 cells, the activation of FGF signalling does not induce equivalent activation of ERK1 and ERK2, as their dual-phosphorylation response are different. It may suggest there is regulation either in the specificity of ERK isoform or in the quantitative difference.

6.3.5 Trouble shooting

The SRM assay reproducibly quantified 38 of 75 phosphopeptides. The method used in this assay presents a substantial room for optimization. A total of 28.0% of phosphopeptides were not successfully quantified due to a low MS signal. The MS response in SRM analysis is determined by the abundance of target peptide in the sample, the compatibility with LC separation and the intensity of the specified transitions[257]. The phosphopeptides selected for these assay are all from related kinases, which are usually low-abundant proteins compared

with the majority of cellular proteins. Selective prefractionation techniques are available to enrich phosphopeptides, however, additional sample handling places more risk in interfering with the quantitation results.

The scheduled SRM approach decreases the number of concurrent transitions monitored simultaneously. In this assay, most of the peptides are scheduled in a 6-minute window (from 13 min to 19 min) and 50 peptides (25 IS peptide and 25 endogenous peptides) are monitored within one run. The congestion of scheduled transitions potentially decrease the dwell time for each transition, therefore decrease the signal[258]. A certain number of peptide was not successfully quantified because the specified retention time window did not cover the whole peak of transitions. A more relaxed schedule method or a method with fewer transitions can be established in the future. Compromise choices will need to be made between the amount of sample, the number of instrument hours and the signal in order to obtain data for analysis. Combined with western blot, the establishment of the phosphorylation site analysis can also be applied as a standard platform for further quantitation investigations.

6.4 Conclusion

In this chapter, a quantitative and time-resolved phosphorylation site analysis was performed to study the phosphorylation responses following FGF1 stimulation. A total of 38 phosphopeptides were reproducibly quantified. The clustering of relative phosphorylation profile showed distinct associations towards FGF1 stimulation. The phosphorylation response was classified as early, mid and late response type. With a special focus on peptide of differentially phosphorylated versions, results showed a sequential phosphorylation pattern was observed for phosphorylation sites in the activation loop of FGFR2 and ERK1. A similar phosphorylation response was observed for isobaric phosphorylated peptides of RSK1. As

shown in this study, evidence for the previously proposed mechanisms of FGF signal transduction was provided. Following the proteome-scale studies, this assay provided a more detailed insight into the central regulators involved in the signal transduction process.

CHAPTER 7

CONCLUSIONS AND FUTURE WORK

FGF signalling is a highly complex growth factor signalling pathway, reflecting a wide range of biological processes regulated through phosphorylation and dephosphorylation events. The deregulation of FGF signalling is closely linked to many human diseases, including cancer. The aim of the work presented in this thesis was to investigate the key phosphorylation events and dynamics of FGF signalling using mass spectrometry tools, including the development of those tools. To address this aim, the method of LC-FAIMS-MS/MS analyses was established (Chapter 3), the phosphorylation response to signalling inhibitors was investigated by LC-MS/MS and LC-FAIMS-MS/MS (Chapter 4); the performance of a novel FAIMS interface was evaluated for further proteomic analyses (Chapter 5); a targeted quantitation assay was performed to profile the dynamics of the key phosphorylation events in FGF signalling (Chapter 6).

7.1 Optimization of phosphoproteomic analysis by LC-FAIMS-MS/MS

In order to establish the method for quantitative analysis, the performance of LC-FAIMS-MS/MS was evaluated. The use of calibration standards with isotopic labels showed FAIMS did not alter quantitation results compared with the LC-MS/MS method. The method for quantitative LC-FAIMS-MS/MS analysis was optimized using 293T cells and SUM52 cells. A CV range from -22.5 V to -50 V (with 2.5 V intervals) was selected for future experiments.

7.2 FAIMS and phosphoproteomics of FGF signalling

In Chapter 4, the LC-MS/MS and LC-FAIMS-MS/MS analyses have combined SILAC labelling with SCX pre-fractionation and phosphoenrichment. This approach allowed the investigation of the regulated phosphorylation events involved in FGF signalling. The two

techniques showed complementarity. An enhancement in the identification of multiply phosphorylated peptides and a preference for peptides with high charge states (3+ and above) was observed in the LC-FAIMS-MS/MS dataset. It was also observed that ~20% of the phosphosites identified via FAIMS have not been reported previously.

The LC-FAIMS-MS/MS analyses also revealed a substantial number of phosphosites regulated upon inhibitor treatments, especially sites from multiply-phosphorylated peptides. An attractive application of FAIMS is the targeted analysis of peptides, thus enabling the direct quantitation of peptide candidates in the future. Together, these observations open new possibilities for in-depth characterisation of interesting candidates for their roles in FGF signalling and trafficking.

7.3 Evaluation of modified FAIMS interface

In Chapter 5, the performance of a novel FAIMS interface was evaluated and compared with the commercial standard FAIMS device, from direct infusion of peptide standards and peptide mixtures to LC-FAIMS-MS/MS analysis of peptide mixture and whole cell lysates. The modified FAIMS interface showed a CV shift of approximately 10 V and nearly 3-fold increase in peak capacity. In the analyses of whole cell lysate, an increase in the proteome coverage of 69.4% was observed in the modified FAIMS dataset. The increase in proteome coverage can be attributed to the reduced redundancy in identifications between CV steps when using the modified FAIMS, in turn result in improved resolution.

The elimination of He in the modified FAIMS device is advantageous in terms of cost reduction and laboratory automation. Therefore, these results demonstrate the modified FAIMS interface

as a powerful tool for proteomic study that provides high resolution and low redundancy identifications.

7.4 Investigation of dynamics of the key phosphorylation events in FGF signalling by selected reaction monitoring

A number of phosphoproteomic studies have attempted to understand FGF signalling on a wide scale. Chapter 6 was aimed at exploring the site-specific response during the activation FGF signalling using a targeted mass spectrometry approach. A quantitative and time-resolved SRM assay of 38 phosphorylation sites was successfully performed. The hierarchy clustering of their relative phosphorylation profiles showed distinct associations towards FGF1 stimulation. The phosphorylation response was classified as early, mid and late response type.

Following the proteome-scale studies, this assay provided a more detailed insight into the central regulators involved in the signal transduction process. For future study, the SRM workflow could be optimized to obtain the desired data. The detailed specific phosphorylation profile of individual phosphorylation site need to be investigated, ideally compared with biochemistry evidence, to fully understand the potential mechanisms of the activation FGF signalling.

Reference

(1) Armelin, H. A. Pituitary Extracts and Steroid Hormones in the Control of 3T3 Cell Growth. *Proc. Natl. Acad. Sci.* **1973**, *70* (9), 2702–2706.

(2) Ornitz, D. M.; Itoh, N. Fibroblast growth factors. *Genome Biol.* **2001**, *2* (3), REVIEWS3005.

(3) Powers, C. J.; McLeskey, S. W.; Wellstein, a. Fibroblast growth factors, their receptors and signaling. *Endocr. Relat. Cancer* **2000**, *7* (3), 165–197.

(4) Greenman, C.; Stephens, P.; Smith, R.; Dalgliesh, G. L.; Hunter, C.; Bignell, G.; Davies, H.; Teague, J.; Butler, A.; Stevens, C.; et al. Patterns of somatic mutation in human cancer genomes. *Nature* **2007**, *446* (7132), 153–158.

(5) Imel, E. A.; Econs, M. J. Fibroblast growth factor 23: roles in health and disease. *J. Am. Soc. Nephrol.* **2005**, *16* (9), 2565–2575.

(6) Burgess, W. H.; Maciag, T. The heparin-binding (fibroblast) growth factor family of proteins. *Annu. Rev. Biochem.* **1989**, *58*, 575–606.

(7) Wiedłocha, A.; Sørensen, V. Signaling, internalization, and intracellular activity of fibroblast growth factor. *Curr. Top. Microbiol. Immunol.* **2004**, *286*, 45–79.

(8) Sheng, Z.; Lewis, J. A.; Chirico, W. J. Nuclear and nucleolar localization of 18-kDa fibroblast growth factor-2 is controlled by C-terminal signals. *J. Biol. Chem.* **2004**, *279* (38), 40153–40160.

(9) Stachowiak, M. K.; Maher, P. A.; Joy, A.; Mordechai, E.; Stachowiak, E. K. Nuclear localization of functional FGF receptor 1 in human astrocytes suggests a novel mechanism for growth factor action. *Mol. Brain Res.* **1996**, *38* (1), 161–165.

(10) Beenken, A.; Mohammadi, M. The FGF family: biology, pathophysiology and therapy. *Nat. Rev. Drug Discov.* **2009**, *8* (3), 235–253.

(11) Schlessinger, J. Cell Signaling by Receptor Tyrosine Kinases. *Cell* **2000**, *103* (2), 211–225.

(12) Turner, N.; Grose, R. Fibroblast growth factor signalling: from development to cancer. *Nat. Rev. Cancer* **2010**, *10* (2), 116–129.

(13) Mohammadi, M.; Olsen, S. K.; Ibrahimi, O. A. Structural basis for fibroblast growth factor receptor activation. *Cytokine Growth Factor Rev.* **2005**, *16* (2), 107–137.

(14) Cha, J. Y.; Maddileti, S.; Mitin, N.; Harden, T. K.; Der, C. J. Aberrant receptor internalization and enhanced FRS2-dependent signaling contribute to the transforming activity of the fibroblast growth factor receptor 2 IIIb C3 isoform. *J. Biol. Chem.* **2009**, *284* (10), 6227–6240.

(15) Zhang, X.; Ibrahimi, O. A.; Olsen, S. K.; Umemori, H.; Mohammadi, M.; Ornitz, D. M. Receptor specificity of the fibroblast growth factor family. The complete mammalian FGF family. *J. Biol. Chem.* **2006**, *281* (23), 15694–15700.

(16) Orr-Urtreger, A.; Bedford, M. T.; Burakova, T.; Arman, E.; Zimmer, Y.; Yayon, A.; Givol, D.; Lonai, P. Developmental localization of the splicing alternatives of fibroblast growth factor receptor-2 (FGFR2). *Dev. Biol.* **1993**, *158* (2), 475–486.

(17) Sahni, M.; Ambrosetti, D.-C.; Mansukhani, A.; Gertner, R.; Levy, D.; Basilico, C. FGF signaling inhibits chondrocyte proliferation and regulates bone development through the STAT-1 pathway. *Genes Dev.* **1999**, *13* (11), 1361–1366.

(18) Coughlin, S. R.; Barr, P. J.; Cousens, L. S.; Fretto, L. J.; Williams, L. T. Acidic and basic fibroblast growth factors stimulate tyrosine kinase activity in vivo. *J. Biol. Chem.* **1988**, *263* (2), 988–993.

(19) Mohammadi, M.; Dikic, I.; Sorokin, A.; Burgess, W. H.; Jaye, M.; Schlessinger, J. Identification of six novel autophosphorylation sites on fibroblast growth factor receptor 1 and elucidation of their importance in receptor activation and signal transduction. *Mol. Cell. Biol.* **1996**, *16* (3), 977–989.

(20) Mohammadi, M.; Honegger, A. M.; Rotin, D.; Fischer, R.; Bellot, F.; Li, W.; Dionne, C. A.; Jaye, M.; Rubinstein, M.; Schlessinger, J. A tyrosine-phosphorylated carboxy-terminal peptide of the fibroblast growth factor receptor (Flg) is a binding site for the SH2 domain of phospholipase C-gamma 1. *Mol. Cell. Biol.* **1991**, *11* (10), 5068–5078.

(21) Furdui, C. M.; Lew, E. D.; Schlessinger, J.; Anderson, K. S. Autophosphorylation of FGFR1 kinase is mediated by a sequential and precisely ordered reaction. *Mol. Cell* **2006**, *21* (5), 711–717.

(22) Ornitz, D. M.; Itoh, N. The Fibroblast Growth Factor signaling pathway. *Wiley Interdiscip. Rev. Dev. Biol.* **2015**, *4* (3), 215–266.

(23) Gotoh, N. Regulation of growth factor signaling by FRS2 family docking/scaffold adaptor proteins. *Cancer Sci.* **2008**, *99* (7), 1319–1325.

(24) Ubersax, J. a; Ferrell, J. E. Mechanisms of specificity in protein phosphorylation. *Nat. Rev. Mol. Cell Biol.* **2007**, *8* (7), 530–541.

(25) Pinna, L. A.; Ruzzene, M. How do protein kinases recognize their substrates? *Biochim. Biophys. Acta - Mol. Cell Res.* **1996**, *1314* (3), 191–225.

(26) Fantl, W. J.; Johnson, D. E.; Williams, L. T. Signalling by receptor tyrosine kinases. *Annu. Rev. Biochem.* **1993**, *62*, 453–481.

(27) Sarabipour, S.; Hristova, K. Mechanism of FGF receptor dimerization and activation. *Nat. Commun.* **2016**, *7*, 10262.

(28) Zhan, X.; Plourde, C.; Hu, X.; Friesel, R.; Maciag, T. Association of fibroblast growth factor receptor-1 with c-Src correlates with association between c-Src and cortactin. *J. Biol. Chem.* **1994**, *269* (32), 20221–20224.

(29) Altomare, D. A.; Testa, J. R. Perturbations of the AKT signaling pathway in human cancer. *Oncogene* **2005**, *24* (50), 7455–7464.

(30) Kouhara, H.; Hadari, Y. R.; Spivak-Kroizman, T.; Schilling, J.; Bar-Sagi, D.; Lax, I.; Schlessinger, J. A lipid-anchored Grb2-binding protein that links FGF-receptor activation to the Ras/MAPK signaling pathway. *Cell* **1997**, *89* (5), 693–702.

(31) Hers, I.; Vincent, E. E.; Tavaré, J. M. Akt signalling in health and disease. *Cell. Signal.* **2011**, *23* (10), 1515–1527.

(32) Manning, B. D.; Cantley, L. C. AKT/PKB signaling: navigating downstream. *Cell* **2007**, *129* (7), 1261–1274.

(33) Parsons, S. J.; Parsons, J. T. Src family kinases, key regulators of signal transduction. *Oncogene* **2004**, *23* (48), 7906–7909.

(34) Twamley-Stein, G. M.; Pepperkok, R.; Ansorge, W.; Courtneidge, S. A. The Src family tyrosine kinases are required for platelet-derived growth factor-mediated signal transduction in NIH 3T3 cells. *Proc. Natl. Acad. Sci. U. S. A.* **1993**, *90* (16), 7696–7700.

(35) Biscardi, J. S.; Maa, M.-C.; Tice, D. A.; Cox, M. E.; Leu, T.-H.; Parsons, S. J. c-Src-mediated Phosphorylation of the Epidermal Growth Factor Receptor on Tyr845 and Tyr1101 Is Associated with Modulation of Receptor Function. *J. Biol. Chem.* **1999**, *274* (12), 8335–8343.

(36) Bromann, P. A.; Korkaya, H.; Courtneidge, S. A. The interplay between Src family kinases and receptor tyrosine kinases. *Oncogene* **2004**, *23* (48), 7957–7968.

(37) Dorey, K.; Amaya, E. FGF signalling: diverse roles during early vertebrate embryogenesis. *Development* **2010**, *137* (22), 3731–3742.

(38) Raffioni, S.; Thomas, D.; Foehr, E. D.; Thompson, L. M.; Bradshaw, R. A. Comparison of the intracellular signaling responses by three chimeric fibroblast growth factor receptors in PC12 cells. *Proc. Natl. Acad. Sci.* **1999**, *96* (13), 7178–7183.

(39) Sharpe, R.; Pearson, A.; Herrera-Abreu, M. T.; Johnson, D.; Mackay, A.; Welti, J. C.; Natrajan, R.; Reynolds, A. R.; Reis-Filho, J. S.; Ashworth, A.; et al. FGFR signaling promotes the growth of triple-negative and basal-like breast cancer cell lines both in vitro and in vivo. *Clin. Cancer Res.* **2011**, *17* (16), 5275–5286.

(40) Adnane, J.; Gaudray, P.; Dionne, C. A.; Crumley, G.; Jaye, M.; Schlessinger, J.; Jeanteur, P.; Birnbaum, D.; Theillet, C. BEK and FLG, two receptors to members of the FGF family, are amplified in subsets of human breast cancers. *Oncogene* **1991**, *6* (4), 659–663.

(41) Tannheimer, S. L.; Rehemtulla, A.; Ethier, S. P. Characterization of fibroblast growth factor receptor 2 overexpression in the human breast cancer cell line SUM-52PE. *Breast Cancer Res.* **2000**, *2* (4), 311–320.

(42) Vercoutter-Edouart, A. S.; Czeszak, X.; Crépin, M.; Lemoine, J.; Boilly, B.; Le Bourhis, X.; Peyrat, J. P.; Hondermarck, H. Proteomic detection of changes in protein synthesis induced by fibroblast growth factor-2 in MCF-7 human breast cancer cells. *Exp. Cell Res.* **2001**, *262* (1), 59–68.

(43) Kunii, K.; Davis, L.; Gorenstein, J.; Hatch, H.; Yashiro, M.; Di Bacco, A.; Elbi, C.; Lutterbach, B. FGFR2-amplified gastric cancer cell lines require FGFR2 and Erbb3 signaling for growth and survival. *Cancer Res.* **2008**, *68* (7), 2340–2348.

(44) Turner, N. C.; Reis-Filho, J. S. Tackling the diversity of triple-negative breast cancer. *Clin. Cancer Res.* **2013**, *19* (23), 6380–6388.

(45) Ricol, D.; Cappellen, D.; El Marjou, A.; Gil-Diez-de-Medina, S.; Girault, J. M.; Yoshida, T.; Ferry, G.; Tucker, G.; Poupon, M. F.; Chopin, D.; et al. Tumour suppressive properties of fibroblast growth factor receptor 2-IIIb in human bladder cancer. *Oncogene* **1999**, *18* (51), 7234–7243.

(46) Easton, D. F.; Pooley, K. A.; Dunning, A. M.; Pharoah, P. D. P.; Thompson, D.; Ballinger, D. G.; Struewing, J. P.; Morrison, J.; Field, H.; Luben, R.; et al. Genome-wide association study identifies novel breast cancer susceptibility loci. *Nature* **2007**, *447* (7148), 1087–1093.

(47) Garcia-Closas, M.; Hall, P.; Nevanlinna, H.; Pooley, K.; Morrison, J.; Richesson, D. A.; Bojesen, S. E.; Nordestgaard, B. G.; Axelsson, C. K.; Arias, J. I.; et al. Heterogeneity of breast cancer associations with five susceptibility loci by clinical and pathological characteristics. *PLoS Genet.* **2008**, *4* (4), e1000054.

(48) Serra S, Zheng L, Hassan M, Phan AT, Woodhouse LJ, Yao JC, Ezzat S, A. S. The FGFR4-G388R single-nucleotide polymorphism alters pancreatic neuroendocrine tumor progression and response to mTOR inhibition therapy. *Cancer Res.* **2012**, *72* (22), 5683–5691.

(49) Baird, K.; Davis, S.; Antonescu, C. R.; Harper, U. L.; Walker, R. L.; Chen, Y.; Glatfelter, A. A.; Duray, P. H.; Meltzer, P. S. Gene expression profiling of human sarcomas: insights into sarcoma biology. *Cancer Res.* **2005**, *65* (20), 9226–9235.

(50) Pollock, P. M.; Gartside, M. G.; Dejeza, L. C.; Powell, M. A.; Mallon, M. A.; Davies, H.; Mohammadi, M.; Futreal, P. A.; Stratton, M. R.; Trent, J. M.; et al. Frequent activating FGFR2 mutations in endometrial carcinomas parallel germline mutations associated with craniosynostosis and skeletal dysplasia syndromes. *Oncogene* **2007**, *26* (50), 7158–7162.

(51) Turner, N.; Pearson, A.; Sharpe, R.; Lambros, M.; Geyer, F.; Lopez-Garcia, M. A.; Natrajan, R.; Marchio, C.; Iorns, E.; Mackay, A.; et al. FGFR1 amplification drives endocrine therapy resistance and is a therapeutic target in breast cancer. *Cancer Res.* **2010**, *70* (5), 2085–2094.

(52) Heiskanen, M.; Kononen, J.; Bärlund, M.; Torhorst, J.; Sauter, G.; Kallioniemi, A.; Kallioniemi, O. CGH, cDNA and tissue microarray analyses implicate FGFR2 amplification in a small subset of breast tumors. *Anal. Cell. Pathol.* **2001**, *22* (4), 229–234.

(53) Marshall, M. E.; Hinz, T. K.; Kono, S. A.; Singleton, K. R.; Bichon, B.; Ware, K. E.; Marek, L.; Frederick, B. A.; Raben, D.; Heasley, L. E. Fibroblast growth factor receptors are components of autocrine signaling networks in head and neck squamous cell carcinoma cells. *Clin. Cancer Res.* **2011**, *17* (15), 5016–5025.

(54) Flemming, A. Cancer: Small-molecule FGF trap shrinks tumours. *Nat. Rev. Drug Discov.* **2015**, *14* (10), 680.

(55) Gavine, P. R.; Mooney, L.; Kilgour, E.; Thomas, A. P.; Al-Kadhimi, K.; Beck, S.; Rooney, C.; Coleman, T.; Baker, D.; Mellor, M. J.; et al. AZD4547: an orally

bioavailable, potent, and selective inhibitor of the fibroblast growth factor receptor tyrosine kinase family. *Cancer Res.* **2012**, *72* (8), 2045–2056.

(56) Mohammadi, M.; McMahon, G.; Sun, L.; Tang, C.; Hirth, P.; Yeh, B. K.; Hubbard, S. R.; Schlessinger, J. Structures of the tyrosine kinase domain of fibroblast growth factor receptor in complex with inhibitors. *Science* **1997**, *276* (5314), 955–960.

(57) Katoh, M.; Nakagama, H. FGF receptors: cancer biology and therapeutics. *Med. Res. Rev.* **2014**, *34* (2), 280–300.

(58) Siu, J. L. and L. L. Development of Fibroblast Growth Factor Receptor Inhibitors: Kissing Frogs to Find a Prince? *Am. Soc. Clin. Oncol.* **2015**, *33* (30), 3372–3374.

(59) Das, J.; Chen, P.; Norris, D.; Padmanabha, R.; Lin, J.; Moquin, R. V; Shen, Z.; Cook, L. S.; Doweyko, A. M.; Pitt, S.; et al. 2-aminothiazole as a novel kinase inhibitor template. Structure-activity relationship studies toward the discovery of N-(2-chloro-6-methylphenyl)-2-[[6-[4-(2-hydroxyethyl)-1- piperazinyl)]-2-methyl-4-pyrimidinyl]amino)]-1,3-thiazole-5-carboxamide (Dasatin. *J. Med. Chem.* **2006**, *49* (23), 6819–6832.

(60) Dieci, M. V.; Arnedos, M.; Andre, F.; Soria, J. C. Fibroblast growth factor receptor inhibitors as a cancer treatment: from a biologic rationale to medical perspectives. *Cancer Discov.* **2013**, *3* (3), 264–279.

(61) Mann, M.; Ong, S.-E.; Grønborg, M.; Steen, H.; Jensen, O. N.; Pandey, A. Analysis of protein phosphorylation using mass spectrometry: deciphering the phosphoproteome. *Trends Biotechnol.* **2002**, *20* (6), 261–268.

(62) Glish, G. L.; Vachet, R. W. The basics of mass spectrometry in the twenty-first century. *Nat. Rev. Drug Discov.* **2003**, *2* (2), 140–150.

(63) Nilsson, T.; Mann, M.; Aebersold, R.; Yates, J. R.; Bairoch, A.; Bergeron, J. J. M. Mass spectrometry in high-throughput proteomics: ready for the big time. *Nat. Methods* **2010**, *7* (9), 681–685.

(64) Tost, J.; Gut, I. G. DNA analysis by mass spectrometry-past, present and future. *J. Mass Spectrom.* **2006**, *41* (8), 981–995.

(65) Harvey, D. J. Matrix-assisted laser desorption/ionization mass spectrometry of carbohydrates. *Mass Spectrom. Rev.* **1999**, *18* (6), 349–450.

(66) Mueller, C. A.; Weinmann, W.; Dresen, S.; Schreiber, A.; Gergov, M. Development of a multi-target screening analysis for 301 drugs using a QTrap liquid chromatography/tandem mass spectrometry system and automated library searching. *Rapid Commun. Mass Spectrom.* **2005**, *19* (10), 1332–1338.

(67) Dempster, A. J. A new Method of Positive Ray Analysis. *Phys. Rev.* **1918**, *11* (4), 316–325.

(68) Munson, M. S. B.; Field, F. H. Chemical Ionization Mass Spectrometry. I. General Introduction. *J. Am. Chem. Soc.* **1966**, *88* (12), 2621–2630.

(69) Morris, H. R.; Panico, M.; Barber, M.; Bordoli, R. S.; Sedgwick, R. D.; Tyler, A. Fast atom bombardment: A new mass spectrometric method for peptide sequence analysis. *Biochem. Biophys. Res. Commun.* **1981**, *101* (2), 623–631.

(70) De Pauw, E.; Agnello, A.; Derwa, F. Liquid matrices for liquid secondary ion mass spectrometry-fast atom bombardment: An update. *Mass Spectrom. Rev.* **1991**, *10* (4), 283–301.

(71) Tanaka, K.; Waki, H.; Ido, Y.; Akita, S.; Yoshida, Y.; Yoshida, T.; Matsuo, T. Protein and polymer analyses up tom/z 100 000 by laser ionization time-of-flight mass spectrometry. *Rapid Commun. Mass Spectrom.* **1988**, *2* (8), 151–153.

(72) Fenn, J. B.; Mann, M.; Meng, C. K.; Wong, S. F.; Whitehouse, C. M. Electrospray ionization for mass spectrometry of large biomolecules. *Science* **1989**, *246* (4926), 64–71.

(73) Seeley, E. H.; Caprioli, R. M. Molecular imaging of proteins in tissues by mass spectrometry. *Proc. Natl. Acad. Sci. U. S. A.* **2008**, *105* (47), 18126–18131.

(74) Dole, M. Molecular Beams of Macroions. *J. Chem. Phys.* **1968**, *49* (5), 2240.

(75) Iribarne, J. V. On the evaporation of small ions from charged droplets. *J. Chem. Phys.* **1976**, *64* (6), 2287.

(76) Wolff, M. M.; Stephens, W. E. A Pulsed Mass Spectrometer with Time Dispersion. *Rev. Sci. Instrum.* **1953**, *24* (8), 616.

(77) Paul, W.; Reinhard, H. P.; von Zahn, U. Das elektrische Massenfilter als Massenspektrometer und Isotopentrenner. *Zeitschrift für Phys.* **1958**, *152* (2), 143–182.

(78) Prestage, J. D.; Dick, G. J.; Maleki, L. New ion trap for frequency standard applications. *J. Appl. Phys.* **1989**, *66* (3), 1013.

(79) Wolfgang, P.; Helmut, S. Apparatus for separating charged particles of different specific charges. December 21, 1954.

(80) Comisarow, M. B.; Marshall, A. G. Fourier transform ion cyclotron resonance spectroscopy. *Chem. Phys. Lett.* **1974**, *25* (2), 282–283.

(81) Makarov, A. Electrostatic Axially Harmonic Orbital Trapping: A High-Performance Technique of Mass Analysis. *Anal. Chem.* **2000**, *72* (6), 1156–1162.

(82) Jennings, K. R. Collision-induced decompositions of aromatic molecular ions. *Int. J. Mass Spectrom. Ion Phys.* **1968**, *1* (3), 227–235.

(83) Haddon, W. F.; McLafferty, F. W. Metastable ion characteristics. VII. Collision-induced metastables. *J. Am. Chem. Soc.* **1968**, *90* (17), 4745–4746.

(84) ZUBAREV, R. A.; KELLEHER, N. L.; MCLAFFERTY, F. W. ELECTRON CAPTURE DISSOCIATION OF MULTIPLY CHARGED PROTEIN CATIONS. A NONERGODIC PROCESS . *J. Am. Chem. Soc. 120* (13), 3265–3266.

(85) Syka, J. E. P.; Coon, J. J.; Schroeder, M. J.; Shabanowitz, J.; Hunt, D. F. Peptide and protein sequence analysis by electron transfer dissociation mass spectrometry. *Proc. Natl. Acad. Sci. U. S. A.* **2004**, *101* (26), 9528–9533.

(86) Tsaprailis, G.; Nair, H.; Somogyi, Á.; Wysocki, V. H.; Zhong, W.; Futrell, J. H.; Summerfield, S. G.; Gaskell, S. J. Influence of Secondary Structure on the Fragmentation of Protonated Peptides. *J. Am. Chem. Soc.* **1999**, *121* (22), 5142–5154.

(87) McCormack, A. L.; Somogyi, A.; Dongre, A. R.; Wysocki, V. H. Fragmentation of protonated peptides: surface-induced dissociation in conjunction with a quantum mechanical approach. *Anal. Chem.* **1993**, *65* (20), 2859–2872.

(88) Wells, J. M.; McLuckey, S. A. Collision-induced dissociation (CID) of peptides and proteins. *Methods Enzymol.* **2005**, *402*, 148–185.

(89) Roepstorff, P.; Fohlman, J. Proposal for a common nomenclature for sequence ions in mass spectra of peptides. *Biomed. Mass Spectrom.* **1984**, *11* (11), 601.

(90) Kim, M.-S.; Pandey, A. Electron transfer dissociation mass spectrometry in proteomics. *Proteomics* **2012**, *12* (4-5), 530–542.

(91) Sobczyk M, Anusiewicz I, Berdys-Kochanska J, Sawicka A, Skurski P, S. J. Coulomb-Assisted Dissociative Electron Attachment: Application to a Model Peptide. *J. Phys. Chem. A* **2005**, *109* (1), 250–258.

(92) Syrstad, E. A.; Turecek, F. Toward a general mechanism of electron capture dissociation. *J. Am. Soc. Mass Spectrom.* **2005**, *16* (2), 208–224.

(93) Kim, M.-S.; Zhong, J.; Kandasamy, K.; Delanghe, B.; Pandey, A. Systematic evaluation of alternating CID and ETD fragmentation for phosphorylated peptides. *Proteomics* **2011**, *11* (12), 2568–2572.

(94) Olsen, J. V; Schwartz, J. C.; Griep-Raming, J.; Nielsen, M. L.; Damoc, E.; Denisov, E.; Lange, O.; Remes, P.; Taylor, D.; Splendore, M.; et al. A dual pressure linear ion trap Orbitrap instrument with very high sequencing speed. *Mol. Cell. Proteomics* **2009**, *8* (12), 2759–2769.

(95) Schwartz, J. C.; Senko, M. W.; Syka, J. E. P. A two-dimensional quadrupole ion trap mass spectrometer. *J. Am. Soc. Mass Spectrom.* **2002**, *13* (6), 659–669.

(96) Lesur, A.; Domon, B. Advances in high-resolution accurate mass spectrometry application to targeted proteomics. *Proteomics* **2015**, *15* (5-6), 880–890.

(97) Yost, R. A.; Enke, C. G. Selected ion fragmentation with a tandem quadrupole mass spectrometer. *J. Am. Chem. Soc.* **1978**, *100* (7), 2274–2275.

(98) Paul, Wolfgang; Steinwedel, H. Ein neues Massenspektrometer ohne Magnetfeld. *Zeitschrift für Naturforsch. A* **1953**, *8* (7), 448–450.

(99) Anderson, L.; Hunter, C. L. Quantitative mass spectrometric multiple reaction monitoring assays for major plasma proteins. *Mol. Cell. Proteomics* **2006**, *5* (4), 573–588.

(100) Johnson, J. V.; Yost, R. A.; Kelley, P. E.; Bradford, D. C. Tandem-in-space and tandem-in-time mass spectrometry: triple quadrupoles and quadrupole ion traps. *Anal. Chem.* **1990**, *62* (20), 2162–2172.

(101) Ariel Bensimon, Albert J.R. Heck, and R. A. Mass Spectrometry–Based Proteomics and Network Biology. *Annu. Rev. Biochem.* **2012**, *81* (10), 379–405.

(102) Zhang, H.; Ge, Y. Comprehensive Analysis of Protein Modifications by Top-down Mass Spectrometry. *Circ Cardiovasc Genet* **2011**, *4* (6), 711–726.

(103) Chang, C.-Y.; Picotti, P.; Hüttenhain, R.; Heinzelmann-Schwarz, V.; Jovanovic, M.; Aebersold, R.; Vitek, O. Protein significance analysis in selected reaction monitoring (SRM) measurements. *Mol. Cell. Proteomics* **2012**, *11* (4), M111.014662.

(104) Duncan, M. W.; Yergey, A. L.; Patterson, S. D. Quantifying proteins by mass spectrometry: The selectivity of SRM is only part of the problem. *Proteomics* **2009**, *9* (5), 1124–1127.

(105) Egertson, J. D.; Kuehn, A.; Merrihew, G. E.; Bateman, N. W.; MacLean, B. X.; Ting, Y. S.; Canterbury, J. D.; Marsh, D. M.; Kellmann, M.; Zabrouskov, V.; et al. Multiplexed MS/MS for improved data-independent acquisition. *Nat. Methods* **2013**, *10* (8), 744–746.

(106) Song, C.; Ye, M.; Liu, Z.; Cheng, H.; Jiang, X.; Han, G.; Songyang, Z.; Tan, Y.; Wang, H.; Ren, J.; et al. Systematic analysis of protein phosphorylation networks from phosphoproteomic data. *Mol. Cell. Proteomics* **2012**, *11* (10), 1070–1083.

(107) Olsen, J. V; Blagoev, B.; Gnad, F.; Macek, B.; Kumar, C.; Mortensen, P.; Mann, M. Global, in vivo, and site-specific phosphorylation dynamics in signaling networks. *Cell* **2006**, *127* (3), 635–648.

(108) Thingholm TE, Jensen ON, L. M. Analytical strategies for phosphoproteomics. *Proteomics* **2009**, *9* (6), 1451–1468.

(109) Zhao, X.; Wang, Q.; Wang, S.; Zou, X.; An, M.; Zhang, X.; Ji, J. Citric acid-assisted two-step enrichment with TiO2 enhances the separation of multi- and monophosphorylated peptides and increases phosphoprotein profiling. *J. Proteome Res.* **2013**, *12* (6), 2467–2476.

(110) Sugiyama, N.; Masuda, T.; Shinoda, K.; Nakamura, A.; Tomita, M.; Ishihama, Y. Phosphopeptide enrichment by aliphatic hydroxy acid-modified metal oxide chromatography for nano-LC-MS/MS in proteomics applications. *Mol. Cell. Proteomics* **2007**, *6* (6), 1103–1109.

(111) Lu, J.; Qi, D.; Deng, C.; Zhang, X.; Yang, P. Hydrothermal synthesis of α-Fe(2)O(3)@SnO(2) core-shell nanotubes for highly selective enrichment of phosphopeptides for mass spectrometry analysis. *Nanoscale* **2010**, *2* (10), 1892–1900.

(112) He, X.-M.; Zhu, G.-T.; Li, X.-S.; Yuan, B.-F.; Shi, Z.-G.; Feng, Y.-Q. Rapid enrichment of phosphopeptides by SiO2-TiO2 composite fibers. *Analyst* **2013**, *138* (18), 5495–5502.

(113) Grønborg, M.; Kristiansen, T. Z.; Stensballe, A.; Andersen, J. S.; Ohara, O.; Mann, M.; Jensen, O. N.; Pandey, A. A mass spectrometry-based proteomic approach for

identification of serine/threonine-phosphorylated proteins by enrichment with phospho-specific antibodies: identification of a novel protein, Frigg, as a protein kinase A substrate. *Mol. Cell. Proteomics* **2002**, *1* (7), 517–527.

(114) Neville, D. C.; Rozanas, C. R.; Price, E. M.; Gruis, D. B.; Verkman, A. S.; Townsend, R. R. Evidence for phosphorylation of serine 753 in CFTR using a novel metal-ion affinity resin and matrix-assisted laser desorption mass spectrometry. *Protein Sci.* **1997**, *6* (11), 2436–2445.

(115) Thingholm, T. E.; Larsen, M. R.; Ingrell, C. R.; Kassem, M.; Jensen, O. N. TiO(2)-based phosphoproteomic analysis of the plasma membrane and the effects of phosphatase inhibitor treatment. *J. Proteome Res.* **2008**, *7* (8), 3304–3313.

(116) Thingholm, T. E.; Jensen, O. N.; Robinson, P. J.; Larsen, M. R. SIMAC (sequential elution from IMAC), a phosphoproteomics strategy for the rapid separation of monophosphorylated from multiply phosphorylated peptides. *Mol. Cell. Proteomics* **2008**, *7* (4), 661–671.

(117) Oda, Y.; Nagasu, T.; Chait, B. T. Enrichment analysis of phosphorylated proteins as a tool for probing the phosphoproteome. *Nat. Biotechnol.* **2001**, *19* (4), 379–382.

(118) Moore, L. J.; Machlan, L. A. High-accuracy determination of calcium in blood serum by isotope dilution mass spectrometry. *Anal. Chem.* **1972**, *44* (14), 2291–2296.

(119) Cohen, A.; Hertz, H. S.; Mandel, J.; Paule, R. C.; Schaffer, R.; Sniegoski, L. T.; Sun, T.; Welch, M. J.; White, E. Total serum cholesterol by isotope dilution/mass spectrometry: a candidate definitive method. *Clin. Chem.* **1980**, *26* (7), 854–860.

(120) White, E.; Welch, V. M.; Sun, T.; Sniegoski, L. T.; Schaffer, R.; Hertz, H. S.; Cohen, A. The accurate determination of serum glucose by isotope dilution mass spectrometry--two methods. *Biomed. Mass Spectrom.* **1982**, *9* (9), 395–405.

(121) Gygi, S. P.; Rist, B.; Gerber, S. A.; Turecek, F.; Gelb, M. H.; Aebersold, R. Quantitative analysis of complex protein mixtures using isotope-coded affinity tags. *Nat. Biotechnol.* **1999**, *17* (10), 994–999.

(122) Schmidt, A.; Kellermann, J.; Lottspeich, F. A novel strategy for quantitative proteomics using isotope-coded protein labels. *Proteomics* **2005**, *5* (1), 4–15.

(123) Wiese, S.; Reidegeld, K. A.; Meyer, H. E.; Warscheid, B. Protein labeling by iTRAQ: a new tool for quantitative mass spectrometry in proteome research. *Proteomics* **2007**, *7* (3), 340–350.

(124) Thompson, A.; Schäfer, J.; Kuhn, K.; Kienle, S.; Schwarz, J.; Schmidt, G.; Neumann, T.; Hamon, C. Tandem Mass Tags: A Novel Quantification Strategy for Comparative Analysis of Complex Protein Mixtures by MS/MS. *Anal. Chem.* **2003**, *75* (8), 1895–1904.

(125) Ong, S.-E.; Blagoev, B.; Kratchmarova, I.; Kristensen, D. B.; Steen, H.; Pandey, A.; Mann, M. Stable isotope labeling by amino acids in cell culture, SILAC, as a simple and accurate approach to expression proteomics. *Mol. Cell. Proteomics* **2002**, *1*, 376–386.

(126) Olsen, J. V; Vermeulen, M.; Santamaria, A.; Kumar, C.; Miller, M. L.; Jensen, L. J.; Gnad, F.; Cox, J.; Jensen, T. S.; Nigg, E. A.; et al. Quantitative phosphoproteomics reveals widespread full phosphorylation site occupancy during mitosis. *Sci. Signal.* **2010**, *3* (104), ra3.

(127) Hinsby, A. M.; Olsen, J. V; Mann, M. Tyrosine phosphoproteomics of fibroblast growth factor signaling: a role for insulin receptor substrate-4. *J. Biol. Chem.* **2004**, *279* (45), 46438–46447.

(128) Krüger, M.; Moser, M.; Ussar, S.; Thievessen, I.; Luber, C. A.; Forner, F.; Schmidt, S.; Zanivan, S.; Fässler, R.; Mann, M. SILAC mouse for quantitative proteomics uncovers kindlin-3 as an essential factor for red blood cell function. *Cell* **2008**, *134* (2), 353–364.

(129) Kosako, H.; Nagano, K. Quantitative phosphoproteomics strategies for understanding protein kinase-mediated signal transduction pathways. *Expert Rev. Proteomics* **2011**, *8* (1), 81–94.

(130) Griffin, N. M.; Yu, J.; Long, F.; Oh, P.; Shore, S.; Li, Y.; Koziol, J. A.; Schnitzer, J. E. Label-free, normalized quantification of complex mass spectrometry data for proteomic analysis. *Nat. Biotechnol.* **2010**, *28* (1), 83–89.

(131) Langlais, P.; Mandarino, L. J.; Yi, Z. Label-free relative quantification of co-eluting isobaric phosphopeptides of insulin receptor substrate-1 by HPLC-ESI-MS/MS. *J. Am. Soc. Mass Spectrom.* **2010**, *21* (9), 1490–1499.

(132) Old, W. M.; Shabb, J. B.; Houel, S.; Wang, H.; Couts, K. L.; Yen, C.-Y.; Litman, E. S.; Croy, C. H.; Meyer-Arendt, K.; Miranda, J. G.; et al. Functional proteomics identifies targets of phosphorylation by B-Raf signaling in melanoma. *Mol. Cell* **2009**, *34* (1), 115–131.

(133) Boersema, P. J.; Mohammed, S.; Heck, A. J. R. Phosphopeptide fragmentation and analysis by mass spectrometry. *J. Mass Spectrom.* **2009**, *44* (6), 861–878.

(134) Wiesner, J.; Premsler, T.; Sickmann, A. Application of electron transfer dissociation (ETD) for the analysis of posttranslational modifications. *Proteomics* **2008**, *8* (21), 4466–4483.

(135) Sweet, S. M. M.; Bailey, C. M.; Cunningham, D. L.; Heath, J. K.; Cooper, H. J. Large scale localization of protein phosphorylation by use of electron capture dissociation mass spectrometry. *Mol. Cell. Proteomics* **2009**, *8* (5), 904–912.

(136) Zhang, Y.; Ficarro, S. B.; Li, S.; Marto, J. A. Optimized Orbitrap HCD for quantitative analysis of phosphopeptides. *J. Am. Soc. Mass Spectrom.* **2009**, *20* (8), 1425–1434.

(137) Carr, S. A.; Huddleston, M. J.; Annan, R. S. Selective detection and sequencing of phosphopeptides at the femtomole level by mass spectrometry. *Anal. Biochem.* **1996**, *239* (2), 180–192.

(138) Nardiello, D.; Palermo, C.; Natale, A.; Quinto, M.; Centonze, D. Strategies in protein sequencing and characterization: multi-enzyme digestion coupled with alternate CID/ETD tandem mass spectrometry. *Anal. Chim. Acta* **2015**, *854*, 106–117.

(139) Linding, R.; Jensen, L. J.; Ostheimer, G. J.; van Vugt, M. A. T. M.; Jørgensen, C.; Miron, I. M.; Diella, F.; Colwill, K.; Taylor, L.; Elder, K.; et al. Systematic discovery of in vivo phosphorylation networks. *Cell* **2007**, *129* (7), 1415–1426.

(140) Steen, H.; Jebanathirajah, J. A.; Rush, J.; Morrice, N.; Kirschner, M. W. Phosphorylation analysis by mass spectrometry: myths, facts, and the consequences for qualitative and quantitative measurements. *Mol. Cell. Proteomics* **2006**, *5* (1), 172–181.

(141) Yates, J. R. The revolution and evolution of shotgun proteomics for large-scale proteome analysis. *J. Am. Chem. Soc.* **2013**, *135* (5), 1629–1640.

(142) Brun, V.; Dupuis, A.; Adrait, A.; Marcellin, M.; Thomas, D.; Court, M.; Vandenesch, F.; Garin, J. Isotope-labeled protein standards: toward absolute quantitative proteomics. *Mol. Cell. Proteomics* **2007**, *6* (12), 2139–2149.

(143) Addona, T. A.; Abbatiello, S. E.; Schilling, B.; Skates, S. J.; Mani, D. R.; Bunk, D. M.; Spiegelman, C. H.; Zimmerman, L. J.; Ham, A.-J. L.; Keshishian, H.; et al. Multi-site assessment of the precision and reproducibility of multiple reaction monitoring-based measurements of proteins in plasma. *Nat. Biotechnol.* **2009**, *27* (7), 633–641.

(144) Sherman, J.; McKay, M. J.; Ashman, K.; Molloy, M. P. How specific is my SRM?: The issue of precursor and product ion redundancy. *Proteomics* **2009**, *9* (5), 1120–1123.

(145) Nesvizhskii, A. I.; Vitek, O.; Aebersold, R. Analysis and validation of proteomic data generated by tandem mass spectrometry. *Nat. Methods* **2007**, *4* (10), 787–797.

(146) Mallick, P.; Schirle, M.; Chen, S. S.; Flory, M. R.; Lee, H.; Martin, D.; Ranish, J.; Raught, B.; Schmitt, R.; Werner, T.; et al. Computational prediction of proteotypic peptides for quantitative proteomics. *Nat. Biotechnol.* **2007**, *25* (1), 125–131.

(147) Picotti, P.; Aebersold, R.; Domon, B. The implications of proteolytic background for shotgun proteomics. *Mol. Cell. Proteomics* **2007**, *6* (9), 1589–1598.

(148) Fusaro, V. A.; Mani, D. R.; Mesirov, J. P.; Carr, S. A. Prediction of high-responding peptides for targeted protein assays by mass spectrometry. *Nat. Biotechnol.* **2009**, *27* (2), 190–198.

(149) Deutsch, E. W.; Lam, H.; Aebersold, R. PeptideAtlas: a resource for target selection for emerging targeted proteomics workflows. *EMBO Rep.* **2008**, *9* (5), 429–434.

(150) Craig, R.; Cortens, J. P.; Beavis, R. C. Open source system for analyzing, validating, and storing protein identification data. *J. Proteome Res. 3* (6), 1234–1242.

(151) Picotti, P.; Lam, H.; Campbell, D.; Deutsch, E. W.; Mirzaei, H.; Ranish, J.; Domon, B.; Aebersold, R. A database of mass spectrometric assays for the yeast proteome. *Nat. Methods* **2008**, *5* (11), 913–914.

(152) Picotti, P.; Bodenmiller, B.; Mueller, L. N.; Domon, B.; Aebersold, R. Full dynamic range proteome analysis of S. cerevisiae by targeted proteomics. *Cell* **2009**, *138* (4), 795–806.

(153) Jemal, M.; Xia, Y.-Q. The need for adequate chromatographic separation in the quantitative determination of drugs in biological samples by high performance liquid chromatography with tandem mass spectrometry. *Rapid Commun. Mass Spectrom.* **1999**, *13* (2), 97–106.

(154) Gerber, S. A.; Rush, J.; Stemman, O.; Kirschner, M. W.; Gygi, S. P. Absolute quantification of proteins and phosphoproteins from cell lysates by tandem MS. *Proc. Natl. Acad. Sci. U. S. A.* **2003**, *100* (12), 6940–6945.

(155) Berna, M.; Ackermann, B. Increased throughput for low-abundance protein biomarker verification by liquid chromatography/tandem mass spectrometry. *Anal. Chem.* **2009**, *81* (10), 3950–3956.

(156) Barnett, D. a; Ding, L.; Ells, B.; Purves, R. W.; Guevremont, R. Tandem mass spectra of tryptic peptides at signal-to-background ratios approaching unity using electrospray ionization high-field asymmetric waveform ion mobility spectrometry/hybrid quadrupole time-of-flight mass spectrometry. *Rapid Commun. Mass Spectrom.* **2002**, *16* (7), 676–680.

(157) Ong, S.-E.; Mann, M. Mass spectrometry-based proteomics turns quantitative. *Nat. Chem. Biol.* **2005**, *1* (5), 252–262.

(158) Zhang, H.; Liu, Q.; Zimmerman, L. J.; Ham, A.-J. L.; Slebos, R. J. C.; Rahman, J.; Kikuchi, T.; Massion, P. P.; Carbone, D. P.; Billheimer, D.; et al. Methods for peptide and protein quantitation by liquid chromatography-multiple reaction monitoring mass spectrometry. *Mol. Cell. Proteomics* **2011**, *10* (6), M110.006593.

(159) Beynon, R. J.; Doherty, M. K.; Pratt, J. M.; Gaskell, S. J. Multiplexed absolute quantification in proteomics using artificial QCAT proteins of concatenated signature peptides. *Nat. Methods* **2005**, *2* (8), 587–589.

(160) Holzmann, J.; Pichler, P.; Madalinski, M.; Kurzbauer, R.; Mechtler, K. Stoichiometry determination of the MP1-p14 complex using a novel and cost-efficient method to produce an equimolar mixture of standard peptides. *Anal. Chem.* **2009**, *81* (24), 10254–10261.

(161) Wang, Q.; Chaerkady, R.; Wu, J.; Hwang, H. J.; Papadopoulos, N.; Kopelovich, L.; Maitra, A.; Matthaei, H.; Eshleman, J. R.; Hruban, R. H.; et al. Mutant proteins as cancer-specific biomarkers. *Proc. Natl. Acad. Sci. U. S. A.* **2011**, *108* (6), 2444–2449.

(162) Jovanovic, M.; Reiter, L.; Picotti, P.; Lange, V.; Bogan, E.; Hurschler, B. A.; Blenkiron, C.; Lehrbach, N. J.; Ding, X. C.; Weiss, M.; et al. A quantitative targeted proteomics approach to validate predicted microRNA targets in C. elegans. *Nat. Methods* **2010**, *7* (10), 837–842.

(163) Wolf-Yadlin, A.; Hautaniemi, S.; Lauffenburger, D. A.; White, F. M. Multiple reaction monitoring for robust quantitative proteomic analysis of cellular signaling networks. *Proc. Natl. Acad. Sci. U. S. A.* **2007**, *104* (14), 5860–5865.

(164) Picotti, P.; Aebersold, R. Selected reaction monitoring-based proteomics: workflows, potential, pitfalls and future directions. *Nat. Methods* **2012**, *9* (6), 555–566.

(165) Keshishian, H.; Addona, T.; Burgess, M.; Kuhn, E.; Carr, S. A. Quantitative, multiplexed assays for low abundance proteins in plasma by targeted mass spectrometry and stable isotope dilution. *Mol. Cell. Proteomics* **2007**, *6* (12), 2212–2229.

(166) Cima, I.; Schiess, R.; Wild, P.; Kaelin, M.; Schüffler, P.; Lange, V.; Picotti, P.; Ossola, R.; Templeton, A.; Schubert, O.; et al. Cancer genetics-guided discovery of serum biomarker signatures for diagnosis and prognosis of prostate cancer. *Proc. Natl. Acad. Sci. U. S. A.* **2011**, *108* (8), 3342–3347.

(167) Guevremont, R. High-field asymmetric waveform ion mobility spectrometry: A new tool for mass spectrometry. *J. Chromatogr. A* **2004**, *1058* (1-2), 3–19.

(168) McDaniel, E. W.; Martin, D. W.; Barnes, W. S. Drift Tube-Mass Spectrometer for Studies of Low-Energy Ion-Molecule Reactions. *Rev. Sci. Instrum.* **1962**, *33* (1), 2.

(169) Buryakov, I. A.; Krylov, E. V.; Nazarov, E. G.; Rasulev, U. K. A new method of separation of multi-atomic ions by mobility at atmospheric pressure using a high-frequency amplitude-asymmetric strong electric field. *Int. J. Mass Spectrom. Ion Process.* **1993**, *128* (3), 143–148.

(170) Kolakowski, B. M.; Mester, Z. Review of applications of high-field asymmetric waveform ion mobility spectrometry (FAIMS) and differential mobility spectrometry (DMS). *Analyst* **2007**, *132* (9), 842–864.

(171) Mason, E. A.; Schamp, H. W. Mobility of gaseous lons in weak electric fields. *Ann. Phys. (N. Y).* **1958**, *4* (3), 233–270.

(172) Giles, K.; Pringle, S. D.; Worthington, K. R.; Little, D.; Wildgoose, J. L.; Bateman, R. H. Applications of a travelling wave-based radio-frequency-only stacked ring ion guide. *Rapid Commun. Mass Spectrom.* **2004**, *18* (20), 2401–2414.

(173) Pringle, S. D.; Giles, K.; Wildgoose, J. L.; Williams, J. P.; Slade, S. E.; Thalassinos, K.; Bateman, R. H.; Bowers, M. T.; Scrivens, J. H. An investigation of the mobility separation of some peptide and protein ions using a new hybrid quadrupole/travelling wave IMS/oa-ToF instrument. *Int. J. Mass Spectrom.* **2007**, *261* (1), 1–12.

(174) Guevremont, R.; Purves, R. W. Atmospheric pressure ion focusing in a high-field asymmetric waveform ion mobility spectrometer. *Rev. Sci. Instrum.* **1999**, *70* (2), 1370.

(175) Shvartsburg, A. A.; Li, F.; Tang, K.; Smith, R. D. High-resolution field asymmetric waveform ion mobility spectrometry using new planar geometry analyzers. *Anal. Chem.* **2006**, *78* (11), 3706–3714.

(176) Barnett, D. A.; Ells, B.; Guevremont, R.; Purves, R. W. Separation of leucine and isoleucine by electrospray ionization-high field asymmetric waveform ion mobility spectrometry-mass spectrometry. *J. Am. Soc. Mass Spectrom.* **1999**, *10* (12), 1279–1284.

(177) Krylov, E. V. Comparison of the planar and coaxial field asymmetrical waveform ion mobility spectrometer (FAIMS). *Int. J. Mass Spectrom.* **2003**, *225* (1), 39–51.

(178) Krylov, E. V. A method of reducing diffusion losses in a drift spectrometer. *Tech. Phys.* **1999**, *44* (1), 113–116.

(179) Swearingen, K. E.; Hoopmann, M. R.; Johnson, R. S.; Saleem, R. a.; Aitchison, J. D.; Moritz, R. L. Nanospray FAIMS Fractionation Provides Significant Increases in Proteome Coverage of Unfractionated Complex Protein Digests. *Mol. Cell. Proteomics* **2012**, *11* (4), M111.014985–M111.014985.

(180) Shvartsburg, A. A.; Smith, R. D.; Wilks, A.; Koehl, A.; Ruiz-Alonso, D.; Boyle, B. Ultrafast differential ion mobility spectrometry at extreme electric fields in multichannel microchips. *Anal. Chem.* **2009**, *81* (15), 6489–6495.

(181) Prasad, S.; Belford, M. W.; Dunyach, J.-J.; Purves, R. W. On an Aerodynamic Mechanism to Enhance Ion Transmission and Sensitivity of FAIMS for Nano-Electrospray Ionization-Mass Spectrometry. *J. Am. Soc. Mass Spectrom.* **2014**.

(182) Beach, D. G.; Gabryelski, W. Nontarget analysis of urine by electrospray ionization-high field asymmetric waveform ion mobility-tandem mass spectrometry. *Anal. Chem.* **2011**, *83* (23), 9107–9113.

(183) Xia, Y.-Q.; Wu, S. T.; Jemal, M. LC-FAIMS-MS/MS for quantification of a peptide in plasma and evaluation of FAIMS global selectivity from plasma components. *Anal. Chem.* **2008**, *80* (18), 7137–7143.

(184) Shvartsburg, A. A.; Creese, A. J.; Smith, R. D.; Cooper, H. J. Separation of a set of peptide sequence isomers using differential ion mobility spectrometry. *Anal. Chem.* **2011**, *83* (18), 6918–6923.

(185) Venne, K.; Bonneil, E.; Eng, K.; Thibault, P. Improvement in Peptide Detection for Proteomics Analyses Using NanoLC - MS and High-Field Spectrometry. **2005**, *77* (7), 2176–2186.

(186) Canterbury, J. D.; Yi, X.; Hoopmann, M. R.; MacCoss, M. J. Assessing the dynamic range and peak capacity of nanoflow LC-FAIMS-MS on an ion trap mass spectrometer for proteomics. *Anal. Chem.* **2008**, *80* (18), 6888–6897.

(187) Saba, J.; Bonneil, E.; Pomie, C.; Eng, K.; Thibault, P. Enhanced Sensitivity in Proteomics Experiments Using FAIMS Coupled with a Hybrid Linear Ion Trap / Orbitrap Mass Spectrometer † research articles. **2009**, No. Cv, 3355–3366.

(188) Shvartsburg, A. A.; Tang, K.; Smith, R. D. Understanding and designing field asymmetric waveform ion mobility spectrometry separations in gas mixtures. *Anal. Chem.* **2004**, *76* (24), 7366–7374.

(189) Shvartsburg, A. A.; Danielson, W. F.; Smith, R. D. High-resolution differential ion mobility separations using helium-rich gases. *Anal. Chem.* **2010**, *82* (6), 2456–2462.

(190) Angel, T. E.; Aryal, U. K.; Hengel, S. M.; Baker, E. S.; Kelly, R. T.; Robinson, E. W.; Smith, R. D. Mass spectrometry-based proteomics: existing capabilities and future directions. *Chem. Soc. Rev.* **2012**, *41* (10), 3912–3928.

(191) Creese, A. J.; Smart, J.; Cooper, H. J. Large-scale analysis of peptide sequence variants: the case for high-field asymmetric waveform ion mobility spectrometry. *Anal. Chem.* **2013**, *85* (10), 4836–4843.

(192) Cunningham, D. L.; Sweet, S. M. M.; Cooper, H. J.; Heath, J. K. Differential Phosphoproteomics of Fibroblast Growth Factor Signaling : Identification of Src Family Kinase-Mediated Phosphorylation Events research articles. **2010**, 2317–2328.

(193) Cox, J.; Mann, M. MaxQuant enables high peptide identification rates, individualized p.p.b.-range mass accuracies and proteome-wide protein quantification. *Nat. Biotechnol.* **2008**, *26* (12), 1367–1372.

(194) MacLean, B.; Tomazela, D. M.; Shulman, N.; Chambers, M.; Finney, G. L.; Frewen, B.; Kern, R.; Tabb, D. L.; Liebler, D. C.; MacCoss, M. J. Skyline: an open source document editor for creating and analyzing targeted proteomics experiments. *Bioinformatics* **2010**, *26* (7), 966–968.

(195) Shvartsburg, A. A.; Smith, R. D. Fundamentals of traveling wave ion mobility spectrometry. *Anal. Chem.* **2008**, *80* (24), 9689–9699.

(196) Villén J, G. S. The SCX/IMAC enrichment approach for global phosphorylation analysis by mass spectrometry. *Nat. Protoc.* **2008**, *3* (10), 1630–1638.

(197) Hornbeck, P. V; Kornhauser, J. M.; Tkachev, S.; Zhang, B.; Skrzypek, E.; Murray, B.; Latham, V.; Sullivan, M. PhosphoSitePlus: a comprehensive resource for investigating the structure and function of experimentally determined post-translational modifications in man and mouse. *Nucleic Acids Res.* **2012**, *40* (Database issue), D261–D270.

(198) Chou, M. F.; Schwartz, D. Using the scan-x Web site to predict protein post-translational modifications. *Curr. Protoc. Bioinformatics* **2011**, *Chapter 13*, Unit 13.16.

(199) Mansour, S. J.; Matten, W. T.; Hermann, A. S.; Candia, J. M.; Rong, S.; Fukasawa, K.; Vande Woude, G. F.; Ahn, N. G. Transformation of mammalian cells by constitutively active MAP kinase kinase. *Science* **1994**, *265* (5174), 966–970.

(200) Huang, D. W.; Sherman, B. T.; Lempicki, R. A. Systematic and integrative analysis of large gene lists using DAVID bioinformatics resources. *Nat. Protoc.* **2009**, *4* (1), 44–57.

(201) Hashiguchi, M.; Kobori, H.; Ritprajak, P.; Kamimura, Y.; Kozono, H.; Azuma, M. Triggering receptor expressed on myeloid cell-like transcript 2 (TLT-2) is a counter-receptor for B7-H3 and enhances T cell responses. *Proc. Natl. Acad. Sci. U. S. A.* **2008**, *105* (30), 10495–10500.

(202) Roy, R.; Durie, D.; Li, H.; Liu, B.-Q.; Skehel, J. M.; Mauri, F.; Cuorvo, L. V.; Barbareschi, M.; Guo, L.; Holcik, M.; et al. hnRNPA1 couples nuclear export and translation of specific mRNAs downstream of FGF-2/S6K2 signalling. *Nucleic Acids Res.* **2014**, *42* (20), 12483–12497.

(203) van Agthoven, T.; van Agthoven, T. L.; Dekker, A.; van der Spek, P. J.; Vreede, L.; Dorssers, L. C. Identification of BCAR3 by a random search for genes involved in antiestrogen resistance of human breast cancer cells. *EMBO J.* **1998**, *17* (10), 2799–2808.

(204) Makkinje, A.; Vanden Borre, P.; Near, R. I.; Patel, P. S.; Lerner, A. Breast cancer anti-estrogen resistance 3 (BCAR3) protein augments binding of the c-Src SH3 domain to Crk-associated substrate (p130cas). *J. Biol. Chem.* **2012**, *287* (33), 27703–27714.

(205) Crooks, G. E.; Hon, G.; Chandonia, J.-M.; Brenner, S. E. WebLogo: a sequence logo generator. *Genome Res.* **2004**, *14* (6), 1188–1190.

(206) Shannon, P.; Markiel, A.; Ozier, O.; Baliga, N. S.; Wang, J. T.; Ramage, D.; Amin, N.; Schwikowski, B.; Ideker, T. Cytoscape: a software environment for integrated models of biomolecular interaction networks. *Genome Res.* **2003**, *13* (11), 2498–2504.

(207) Pearson, G.; Robinson, F.; Beers Gibson, T.; Xu, B. E.; Karandikar, M.; Berman, K.; Cobb, M. H. Mitogen-activated protein (MAP) kinase pathways: regulation and physiological functions. *Endocr. Rev.* **2001**, *22* (2), 153–183.

(208) Helling, S.; Shinde, S.; Brosseron, F.; Schnabel, A.; Müller, T.; Meyer, H. E.; Marcus, K.; Sellergren, B. Ultratrace enrichment of tyrosine phosphorylated peptides on an imprinted polymer. *Anal. Chem.* **2011**, *83* (5), 1862–1865.

(209) Edelmann, M. J. Strong cation exchange chromatography in analysis of posttranslational modifications: innovations and perspectives. *J. Biomed. Biotechnol.* **2011**, *2011*, 936508.

(210) Dailey, L.; Ambrosetti, D.; Mansukhani, A.; Basilico, C. Mechanisms underlying differential responses to FGF signaling. *Cytokine Growth Factor Rev.* **2005**, *16* (2), 233–247.

(211) Zakrzewska, M.; Haugsten, E. M.; Nadratowska-Wesolowska, B.; Oppelt, A.; Hausott, B.; Jin, Y.; Otlewski, J.; Wesche, J.; Wiedlocha, A. ERK-mediated phosphorylation of fibroblast growth factor receptor 1 on Ser777 inhibits signaling. *Sci. Signal.* **2013**, *6* (262), ra11.

(212) Varedi K, S. M.; Ventura, A. C.; Merajver, S. D.; Lin, X. N. Multisite phosphorylation provides an effective and flexible mechanism for switch-like protein degradation. *PLoS One* **2010**, *5* (12), e14029.

(213) Valk, E.; Venta, R.; Ord, M.; Faustova, I.; Kõivomägi, M.; Loog, M. Multistep phosphorylation systems: tunable components of biological signaling circuits. *Mol. Biol. Cell* **2014**, *25* (22), 3456–3460.

(214) Gunawardena, J. Distributivity and processivity in multisite phosphorylation can be distinguished through steady-state invariants. *Biophys. J.* **2007**, *93* (11), 3828–3834.

(215) Jin, J.; Pawson, T. Modular evolution of phosphorylation-based signalling systems. *Philos. Trans. R. Soc. B Biol. Sci.* **2012**, *367* (1602), 2540–2555.

(216) Lee, J. Y.; Chiu, Y.-H.; Asara, J.; Cantley, L. C. Inhibition of PI3K binding to activators by serine phosphorylation of PI3K regulatory subunit p85alpha Src homology-2 domains. *Proc. Natl. Acad. Sci. U. S. A.* **2011**, *108* (34), 14157–14162.

(217) Swearingen, K. E.; Winget, J. M.; Hoopmann, M. R.; Kusebauch, U.; Moritz, R. L. Decreased Gap Width in a Cylindrical High-Field Asymmetric Waveform Ion Mobility Spectrometry Device Improves Protein Discovery. *Anal. Chem.* **2015**, *87* (24), 12230–12237.

(218) Shvartsburg, A. A.; Tang, K.; Smith, R. D. Optimization of the design and operation of FAIMS analyzers. *J. Am. Soc. Mass Spectrom.* **2005**, *16* (1), 2–12.

(219) Shvartsburg, A. A.; Tang, K.; Smith, R. D. FAIMS operation for realistic gas flow profile and asymmetric waveforms including electronic noise and ripple. *J. Am. Soc. Mass Spectrom.* **2005**, *16* (9), 1447–1455.

(220) Barnett, D. A.; Belford, M.; Dunyach, J.-J.; Purves, R. W. Characterization of a temperature-controlled FAIMS system. *J. Am. Soc. Mass Spectrom.* **2007**, *18* (9), 1653–1663.

(221) Shvartsburg, A. A.; Tang, K.; Smith, R. D. Differential ion mobility separations of peptides with resolving power exceeding 50. *Anal. Chem.* **2010**, *82* (1), 32–35.

(222) Barnett, D. A.; Ouellette, R. J. Elimination of the helium requirement in high-field asymmetric waveform ion mobility spectrometry (FAIMS): beneficial effects of decreasing the analyzer gap width on peptide analysis. *Rapid Commun. Mass Spectrom.* **2011**, *25* (14), 1959–1971.

(223) Nesvizhskii, A. I.; Aebersold, R. Interpretation of shotgun proteomic data: the protein inference problem. *Mol. Cell. Proteomics* **2005**, *4* (10), 1419–1440.

(224) Richards, A. L.; Merrill, A. E.; Coon, J. J. Proteome sequencing goes deep. *Curr. Opin. Chem. Biol.* **2015**, *24*, 11–17.

(225) Kearney, R.; Blondeau, F.; McPherson, P.; Bell, A.; Servant, F.; Drapeau, M.; de Grandpre, S.; Jm Bergeron, J. Elimination of redundant protein identifications in high throughput proteomics. *Conf. Proc. ... Annu. Int. Conf. IEEE Eng. Med. Biol. Soc. IEEE Eng. Med. Biol. Soc. Annu. Conf.* **2005**, *5*, 4803–4806.

(226) Frimpong, A. K.; Abzalimov, R. R.; Uversky, V. N.; Kaltashov, I. A. Characterization of intrinsically disordered proteins with electrospray ionization mass spectrometry: conformational heterogeneity of alpha-synuclein. *Proteins* **2010**, *78* (3), 714–722.

(227) Sandilands, E.; Akbarzadeh, S.; Vecchione, A.; McEwan, D. G.; Frame, M. C.; Heath, J. K. Src kinase modulates the activation, transport and signalling dynamics of fibroblast growth factor receptors. *EMBO Rep.* **2007**, *8* (12), 1162–1169.

(228) Mani, D. R.; Abbatiello, S. E.; Carr, S. A. Statistical characterization of multiple-reaction monitoring mass spectrometry (MRM-MS) assays for quantitative proteomics. *BMC Bioinformatics* **2012**, *13 Suppl 1* (Suppl 16), S9.

(229) Durbin, B. P.; Hardin, J. S.; Hawkins, D. M.; Rocke, D. M. A variance-stabilizing transformation for gene-expression microarray data. *Bioinformatics* **2002**, *18* (Suppl 1), S105–S110.

(230) Irizarry, R. A.; Hobbs, B.; Collin, F.; Beazer-Barclay, Y. D.; Antonellis, K. J.; Scherf, U.; Speed, T. P. Exploration, normalization, and summaries of high density oligonucleotide array probe level data. *Biostatistics* **2003**, *4* (2), 249–264.

(231) Stauber, D. J.; DiGabriele, A. D.; Hendrickson, W. A. Structural interactions of fibroblast growth factor receptor with its ligands. *Proc. Natl. Acad. Sci. U. S. A.* **2000**, *97* (1), 49–54.

(232) Pellegrini, L.; Burke, D. F.; von Delft, F.; Mulloy, B.; Blundell, T. L. Crystal structure of fibroblast growth factor receptor ectodomain bound to ligand and heparin. *Nature* **2000**, *407* (6807), 1029–1034.

(233) Doehn, U.; Hauge, C.; Frank, S. R.; Jensen, C. J.; Duda, K.; Nielsen, J. V; Cohen, M. S.; Johansen, J. V; Winther, B. R.; Lund, L. R.; et al. RSK is a principal effector of the RAS-ERK pathway for eliciting a coordinate promotile/invasive gene program and phenotype in epithelial cells. *Mol. Cell* **2009**, *35* (4), 511–522.

(234) Anjum, R.; Blenis, J. The RSK family of kinases: emerging roles in cellular signalling. *Nat. Rev. Mol. Cell Biol.* **2008**, *9* (10), 747–758.

(235) Dephoure, N.; Zhou, C.; Villen, J.; Beausoleil, S. A.; Bakalarski, C. E.; Elledge, S. J.; Gygi, S. P. A quantitative atlas of mitotic phosphorylation. *Proc. Natl. Acad. Sci.* **2008**, *105* (31), 10762–10767.

(236) Cho, Y.-Y.; Yao, K.; Kim, H.-G.; Kang, B. S.; Zheng, D.; Bode, A. M.; Dong, Z. Ribosomal S6 kinase 2 is a key regulator in tumor promoter induced cell transformation. *Cancer Res.* **2007**, *67* (17), 8104–8112.

(237) Stratford, A. L.; Reipas, K.; Hu, K.; Fotovati, A.; Brough, R.; Frankum, J.; Takhar, M.; Watson, P.; Ashworth, A.; Lord, C. J.; et al. Targeting p90 ribosomal S6 kinase eliminates tumor-initiating cells by inactivating Y-box binding protein-1 in triple-negative breast cancers. *Stem Cells* **2012**, *30* (7), 1338–1348.

(238) Dalby, K. N.; Morrice, N.; Caudwell, F. B.; Avruch, J.; Cohen, P. Identification of regulatory phosphorylation sites in mitogen-activated protein kinase (MAPK)-activated protein kinase-1a/p90rsk that are inducible by MAPK. *J. Biol. Chem.* **1998**, *273* (3), 1496–1505.

(239) Newton, A. C. Regulation of the ABC kinases by phosphorylation: protein kinase C as a paradigm. *Biochem. J.* **2003**, *370* (Pt 2), 361–371.

(240) Roux, P. P.; Richards, S. A.; Blenis, J. Phosphorylation of p90 ribosomal S6 kinase (RSK) regulates extracellular signal-regulated kinase docking and RSK activity. *Mol. Cell. Biol.* **2003**, *23* (14), 4796–4804.

(241) Cargnello, M.; Roux, P. P. Activation and function of the MAPKs and their substrates, the MAPK-activated protein kinases. *Microbiol. Mol. Biol. Rev.* **2011**, *75* (1), 50–83.

(242) Cooper, J. A.; Bowen-Pope, D. F.; Raines, E.; Ross, R.; Hunter, T. Similar effects of platelet-derived growth factor and epidermal growth factor on the phosphorylation of tyrosine in cellular proteins. *Cell* **1982**, *31* (1), 263–273.

(243) Roskoski, R. MEK1/2 dual-specificity protein kinases: structure and regulation. *Biochem. Biophys. Res. Commun.* **2012**, *417* (1), 5–10.

(244) Kinoshita, T.; Yoshida, I.; Nakae, S.; Okita, K.; Gouda, M.; Matsubara, M.; Yokota, K.; Ishiguro, H.; Tada, T. Crystal structure of human mono-phosphorylated ERK1 at Tyr204. *Biochem. Biophys. Res. Commun.* **2008**, *377* (4), 1123–1127.

(245) Jeffrey, K. L.; Camps, M.; Rommel, C.; Mackay, C. R. Targeting dual-specificity phosphatases: manipulating MAP kinase signalling and immune responses. *Nat. Rev. Drug Discov.* **2007**, *6* (5), 391–403.

(246) Canagarajah, B. J.; Khokhlatchev, A.; Cobb, M. H.; Goldsmith, E. J. Activation Mechanism of the MAP Kinase ERK2 by Dual Phosphorylation. *Cell* **1997**, *90* (5), 859–869.

(247) Sözeri, O.; Vollmer, K.; Liyanage, M.; Frith, D.; Kour, G.; Mark, G. E.; Stabel, S. Activation of the c-Raf protein kinase by protein kinase C phosphorylation. *Oncogene* **1992**, *7* (11), 2259–2262.

(248) Robbins, D.; Zhen, E.; Owaki, H.; Vanderbilt, C.; Ebert, D.; Geppert, T.; Cobb, M. Regulation and properties of extracellular signal-regulated protein kinases 1 and 2 in vitro. *J. Biol. Chem.* **1993**, *268* (7), 5097–5106.

(249) Bellou, S.; Hink, M. A.; Bagli, E.; Panopoulou, E.; Bastiaens, P. I. H.; Murphy, C.; Fotsis, T. VEGF autoregulates its proliferative and migratory ERK1/2 and p38 cascades by enhancing the expression of DUSP1 and DUSP5 phosphatases in endothelial cells. *Am. J. Physiol. Cell Physiol.* **2009**, *297* (6), C1477–C1489.

(250) Roskoski, R. ERK1/2 MAP kinases: structure, function, and regulation. *Pharmacol. Res.* **2012**, *66* (2), 105–143.

(251) Vantaggiato, C.; Formentini, I.; Bondanza, A.; Bonini, C.; Naldini, L.; Brambilla, R. ERK1 and ERK2 mitogen-activated protein kinases affect Ras-dependent cell signaling differentially. *J. Biol.* **2006**, *5* (5), 14.

(252) Fischer, A. M.; Katayama, C. D.; Pagès, G.; Pouysségur, J.; Hedrick, S. M. The role of erk1 and erk2 in multiple stages of T cell development. *Immunity* **2005**, *23* (4), 431–443.

(253) Shin, S.; Dimitri, C. A.; Yoon, S.-O.; Dowdle, W.; Blenis, J. ERK2 but not ERK1 induces epithelial-to-mesenchymal transformation via DEF motif-dependent signaling events. *Mol. Cell* **2010**, *38* (1), 114–127.

(254) Pagès, G. Defective Thymocyte Maturation in p44 MAP Kinase (Erk 1) Knockout Mice. *Science (80-.).* **1999**, *286* (5443), 1374–1377.

(255) Lefloch, R.; Pouysségur, J.; Lenormand, P. Single and combined silencing of ERK1 and ERK2 reveals their positive contribution to growth signaling depending on their expression levels. *Mol. Cell. Biol.* **2008**, *28* (1), 511–527.

(256) Wortzel, I.; Seger, R. The ERK Cascade: Distinct Functions within Various Subcellular Organelles. *Genes Cancer* **2011**, *2* (3), 195–209.

(257) Lange, V.; Picotti, P.; Domon, B.; Aebersold, R. Selected reaction monitoring for quantitative proteomics: a tutorial. *Mol. Syst. Biol.* **2008**, *4*, 222.

(258) Wissing, J.; Jänsch, L.; Nimtz, M.; Dieterich, G.; Hornberger, R.; Kéri, G.; Wehland, J.; Daub, H. Proteomics analysis of protein kinases by target class-selective prefractionation and tandem mass spectrometry. *Mol. Cell. Proteomics* **2007**, *6* (3), 537–547.

(259) Stasyk, T.; Morandell, S.; Bakry, R.; Feuerstein, I.; Huck, C. W.; Stecher, G.; Bonn, G. K.; Huber, L. A. Quantitative detection of phosphoproteins by combination of two-dimensional difference gel electrophoresis and phosphospecific fluorescent staining. *Electrophoresis* **2005**, *26* (14), 2850–2854.

(260) McNulty, D. E.; Annan, R. S. Hydrophilic interaction chromatography reduces the complexity of the phosphoproteome and improves global phosphopeptide isolation and detection. *Mol. Cell. Proteomics* **2008**, *7* (5), 971–980.

Appendix

Appendix 1 Information of novel phosphorylation sites

Peptide sequence	Position	Ratio SU5402/ FGF1	Ratio dasatinib/ FGF1	Amino acid	No of phosphosites	Charge	Localization prob	Sensitive to treatments
(ac)AEQVLPQALY(ph)LSNM(ox)R	10	0	0	Y	1	3	0.764266	
(ac)ATPAAVNPPEMAS(ph)DIPGSVTLPVAPM(ox)AAT(ph)GQVR	29	2.4473	0.69875	T	2	4	0.957397	+
(ac)EETMKLAT(ph)M(ox)EDT(ph)VEYCLFLIPDESR	12	2.3208	0.94942	T	2	3	0.758026	+
(ac)GQHNLTVLTEFILM(ox)ELT(ph)R	17	0.65406	0.54629	T	1	3	0.999583	
(ac)M(ox)DLNNMNQSLTLELNT(ph)MKQAMK	16	0	0	T	1	3	0.99976	
(ac)M(ox)S(ph)S(ph)NSDTGDLQES(ph)LK	3	2.2934	1.4706	S	3	3	0.899368	+
(ac)M(ox)TTAHFYCQYCT(ph)ASLLGK	12	9.2525	2.6136	T	1	3	0.832268	+
(ac)MAS(ph)LS(ph)AAAIT(ph)VPPSVPSR	3	0.36143	0.43905	S	3	3	0.999828	+
(ac)PNVPAPLAQSQQLS(ph)S(ph)HTPVS(ph)R	20	0	0	S	3	3	0.999446	
(ac)RALAVLS(ph)VTLVMACT(ph)EAFFPFIS(ph)R	23	0	0	S	3	3	0.999818	
(ac)RALAVLS(ph)VTLVMACT(ph)EAFFPFIS(ph)R	15	0	0	T	3	3	0.947686	
(ac)RALAVLS(ph)VTLVMACT(ph)EAFFPFIS(ph)R	7	0	0	S	3	3	0.754244	
(ac)RPGLAPEPLSAPPGS(ph)PPPS(ph)AAPTSATSNSSNGGGPSK	15	0	0	S	2	3	0.899589	
(ac)USEVDVLVFVVDS(ph)ADRLR	13	0.96865	1.0219	S	1	3	0.99902	
(ac)VALAGLLM(ox)T(ph)LPHFISEPYR	9	0.20042	0.91782	T	1	3	0.984761	+
(ac)VSLPPPQS(ph)DVTLPGPTR	8	1.0517	0.8099	S	1	3	0.825843	
AADVWSLGVM(ox)LY(ph)TM(ox)LVGR	12	0.58929	0.69977	Y	1	3	0.840918	
AMQEKAQDY(ph)QAEQDALR	9	1.6691	1.031	Y	1	3	1	+
AS(ph)SPHQAGLGLS(ph)LTPS(ph)PES(ph)PPLPDVSAFS(ph)RGRGGGEGR	2	0.2513	0.25375	S	5	4	0.825627	+
AS(ph)SPHQAGLGLS(ph)LTPS(ph)PES(ph)PPLPDVSAFS(ph)RGRGGGEGR	29	0.2513	0.25375	S	5	4	0.786732	+
ASLY(ph)VGDLHPEVT(ph)EAM(ox)LY(ph)EK	13	0.43994	0.24746	T	3	3	0.999923	+
AT(ph)LM(ox)GGQVYFCY(ph)DGSPYR	2	0.65888	0.86031	T	2	3	0.999993	
AT(ph)PLS(ph)STVTLS(ph)M(ox)S(ph)ADVPLVVEY(ph)K	22	0.17484	0.19655	Y	5	3	0.986773	+
AT(ph)PLS(ph)STVTLS(ph)M(ox)S(ph)ADVPLVVEY(ph)K	11	0.17484	0.19655	S	5	3	0.781149	+
AT(ph)PLS(ph)STVTLS(ph)M(ox)S(ph)ADVPLVVEY(ph)K	13	0.17484	0.19655	S	5	3	0.781149	+
AY(ph)PGY(ph)YFT(ph)GDGAYR	8	0.69665	0.79007	T	3	2	0.978978	
DGKLVPM(ox)T(ph)VFHK	8	0	0	T	1	3	1	

Peptide sequence	Position	Ratio SU5402/ FGF1	Ratio dasatinib/ FGF1	Amino acid	No of phosphosites	Charge	Localization prob	Sensitive to treatments
DS(ph)GQVIPLIVES(ph)CIR	2	4.697	0.78668	S	2	2	1	+
DS(ph)GQVIPLIVES(ph)CIR	12	4.697	0.78668	S	2	2	1	+
DSEDS(ph)LY(ph)NDYVDVFY(ph)NTK	7	4.0314	2.1864	Y	3	3	0.988714	+
DSEDS(ph)LY(ph)NDYVDVFY(ph)NTK	5	4.0314	2.1864	S	3	3	0.941579	+
DT(ph)LSNS(ph)TLT(ph)EFVK	2	0.6235	0.66507	T	3	3	0.961756	
DT(ph)LSNS(ph)TLT(ph)EFVK	9	0.6235	0.66507	T	3	3	0.880026	
EFGSQS(ph)IAIHEPQCLQK	6	0.78923	0.68849	S	1	3	0.826564	
ENTICLLSQHQFMSGYSQDILM(ox)PLWT(ph)S(ph)YT(ph)VDR	29	0.95505	1.0024	T	3	4	0.87502	
ENTICLLSQHQFMSGYSQDILM(ox)PLWT(ph)S(ph)YT(ph)VDR	26	0.95505	1.0024	T	3	4	0.805635	
EVM(ox)LENY(ph)GNVVS(ph)LGILLR	12	1.7859	0.53794	S	2	3	1	+
EVM(ox)LENY(ph)GNVVS(ph)LGILLR	7	1.7859	0.53794	Y	2	3	1	+
EVMLENYGNLVSVGCQLS(ph)K	18	0.65302	0.63587	S	1	3	0.973629	
FPGGSCM(ox)AALTVT(ph)LM(ox)VLSS(ph)PLALAGDTR	13	4.082	2.0966	T	2	3	0.953492	+
FVSIVT(ph)EEEGVY(ph)S(ph)VDYS(ph)K	12	0	0	Y	4	3	0.989888	
FVSIVT(ph)EEEGVY(ph)S(ph)VDYS(ph)K	13	0	0	S	4	3	0.972152	
FVSIVT(ph)EEEGVY(ph)S(ph)VDYS(ph)K	6	0	0	T	4	3	0.777465	
GLLYDS(ph)DEEDEERPAR	6	0.80199	0.71766	S	1	2	1	
GLS(ph)LDSFLR	3	1.0269	0.84621	S	1	2	1	
GS(ph)FIITLVKIPRMILM(ox)Y(ph)IHS(ph)QLK	2	0.28389	0.34202	S	3	3	0.867587	+
GS(ph)T(ph)VHT(ph)AY(ph)LVLSSLAMFT(ph)CLCGM(ox)AGNSM	18	0.23937	0.23771	T	5	4	0.924398	+
GS(ph)T(ph)VHT(ph)AY(ph)LVLSSLAMFT(ph)CLCGM(ox)AGNSM	8	0.23937	0.23771	Y	5	4	0.814082	+
GY(ph)LSETVS(ph)NALGPQGR	2	0.84249	0.94568	Y	2	2	0.865648	
GY(ph)QEVIQS(ph)IVQGPGT(ph)LGR	2	0.95576	0.57832	Y	3	3	1	
HLPSPPTLDS(ph)IIT(ph)EY(ph)LR	15	0	0	Y	3	3	0.999796	
HLPSPPTLDS(ph)IIT(ph)EY(ph)LR	13	0	0	T	3	3	0.999252	
HSGLY(ph)LVVTTSENVS(ph)PFS(ph)LLELLSR	18	0	0	S	3	3	0.789984	
HSGLY(ph)LVVTTSENVS(ph)PFS(ph)LLELLSR	5	0	0	Y	3	3	0.784338	
IAESHLQSIS(ph)NLNENQASEEEDELGELR	10	0.47153	0.41918	S	1	4	0.837253	

Peptide sequence	Position	Ratio SU5402/ FGF1	Ratio dasatinib/ FGF1	Amino acid	No of phosphosites	Charge	Localization prob	Sensitive to treatments
IAFLFDS(ph)T(ph)LTAFLM(ox)M(ox)GNLSPNLK	7	0.93878	0.98284	S	1	3	0.999834	
IAFLFDS(ph)T(ph)LTAFLM(ox)M(ox)GNLSPNLK	8	0.93878	0.98284	T	1	3	0.999641	
IAQFLS(ph)DIPETVPLSTVNR	6	0.91981	0.80601	S	1	3	0.999994	
IIFHENYNAGT(ph)YQNDIALIEMK	11	0.90388	0.7692	T	2	3	0.787359	
IIFSTLGVCT(ph)FFAVGY(ph)MLLPLFAY(ph)FIR	24	0	0	Y	2	3	0.997899	
IIFSTLGVCT(ph)FFAVGY(ph)MLLPLFAY(ph)FIR	16	0	0	Y	2	3	0.994484	
IIFSTLGVCT(ph)FFAVGY(ph)MLLPLFAY(ph)FIR	10	0	0	T	1	3	0.902139	
ILQQLGLDST(ph)CEDSIVVK	10	0.64662	0.76701	T	2	3	0.753397	
IRS(ph)S(ph)LAVLHLENAS(ph)LS(ph)GRP	3	1.0031	1.0551	S	1	3	1	
IRS(ph)S(ph)LAVLHLENAS(ph)LS(ph)GRP	4	1.0031	1.0551	S	1	3	1	
IS(ph)LDSAQSSRSTSYSPR	2	0.66952	0.79173	S	1	3	0.997764	
ITDT(ph)GLS(ph)Y(ph)LS(ph)TM(ox)SSLR	10	0.25479	0.1748	S	1	3	0.972387	+
ITDT(ph)GLS(ph)Y(ph)LS(ph)TM(ox)SSLR	8	0.25479	0.1748	Y	1	3	0.963579	+
ITDT(ph)GLS(ph)Y(ph)LS(ph)TM(ox)SSLR	4	0.25479	0.1748	T	1	3	0.878893	+
ITDT(ph)GLS(ph)Y(ph)LS(ph)TM(ox)SSLR	7	0.25479	0.1748	S	1	3	0.87763	+
IWALKNAFDY(ph)FNNM(ox)R	10	0	0	Y	1	3	1	
IYS(ph)GTIK	3	0.80176	0.88136	S	3	2	0.863251	
KDYLT(ph)GT(ph)GQDSS(ph)HLVLVTFK	7	0	0	T	2	3	0.758531	
KDYLT(ph)GT(ph)GQDSS(ph)HLVLVTFK	12	0	0	S	1	3	0.877501	
KY(ph)QM(ox)T(ph)GVEEVT(ph)QIPQEEHAANGPELLR	2	0	0	Y	2	3	1	
KY(ph)QM(ox)T(ph)GVEEVT(ph)QIPQEEHAANGPELLR	5	0	0	T	1	3	1	
KY(ph)QM(ox)T(ph)GVEEVT(ph)QIPQEEHAANGPELLR	11	0	0	T	1	3	1	
LES(ph)Y(ph)LDLM(ox)PNPSLAQVK	3	0.38154	0.3069	S	2	3	0.999889	+
LES(ph)Y(ph)LDLM(ox)PNPSLAQVK	4	0.38154	0.3069	Y	1	3	0.999882	+
LGLLLLS(ph)LS(ph)QGQECGEY(ph)PVT(ph)IPSDLPADFQDFLK	9	1.3789	7.3773	S	1	4	0.999434	+
LGLLLLS(ph)LS(ph)QGQECGEY(ph)PVT(ph)IPSDLPADFQDFLK	7	1.3789	7.3773	S	1	4	0.99942	+
LHT(ph)PMYFFISQLALM(ox)DLMY(ph)LCVTVPK	19	0	0	Y	4	3	0.950056	
LIMIPVELLLCY(ph)LLLHPVDAT(ph)S(ph)Y(ph)GK	21	0	0	T	2	3	1	

Peptide sequence	Position	Ratio SU5402/ FGF1	Ratio dasatinib/ FGF1	Amino acid	No of phosphosites	Charge	Localization prob	Sensitive to treatments
LIMIPVELLLCY(ph)LLLHPVDAT(ph)S(ph)Y(ph)GK	12	0	0	Y	2	3	1	
LIMIPVELLLCY(ph)LLLHPVDAT(ph)S(ph)Y(ph)GK	22	0	0	S	1	3	1	
LIMIPVELLLCY(ph)LLLHPVDAT(ph)S(ph)Y(ph)GK	23	0	0	Y	1	3	1	
LLEPGTHQFAS(ph)VPVR	11	0.51573	3.4313	S	3	3	0.999999	+
LLQT(ph)IS(ph)DLM(ox)MS(ph)LPSGSSLQQM(ox)ALR	4	0	0	T	2	3	0.817507	
LLQT(ph)IS(ph)DLM(ox)MS(ph)LPSGSSLQQM(ox)ALR	6	0	0	S	1	3	0.820288	
LLS(ph)HPFLS(ph)THLGSS(ph)M(ox)AR	3	0.40429	0.19312	S	2	3	0.95699	+
LLS(ph)HPFLS(ph)THLGSS(ph)M(ox)AR	8	0.40429	0.19312	S	1	3	0.95699	+
LLS(ph)HPFLS(ph)THLGSS(ph)M(ox)AR	14	0.40429	0.19312	S	1	3	0.788614	+
LNDCS(ph)CLAS(ph)QAILLGILLK	5	0.23268	0.60836	S	1	3	1	+
LNDCS(ph)CLAS(ph)QAILLGILLK	9	0.23268	0.60836	S	1	3	1	+
LPAPLIS(ph)KQQFLS(ph)NS(ph)S(ph)R	7	1.3606	1.6391	S	4	3	1	+
LPAPLIS(ph)KQQFLS(ph)NS(ph)S(ph)R	13	1.3606	1.6391	S	4	3	1	+
LPEFLS(ph)LGNT(ph)FNS(ph)ITLQDEIHDDQGT(ph)TVIFQER	6	0.72807	2.9788	S	1	4	0.930955	+
LPEFLS(ph)LGNT(ph)FNS(ph)ITLQDEIHDDQGT(ph)TVIFQER	13	0.72807	2.9788	S	1	4	0.805934	+
LPEFLS(ph)LGNT(ph)FNS(ph)ITLQDEIHDDQGT(ph)TVIFQER	10	0.72807	2.9788	T	1	4	0.805934	+
LPVAT(ph)IFTT(ph)HAT(ph)LLGR	5	0.33658	0.75037	T	2	3	0.999966	+
LS(ph)ENAT(ph)IQLDVVEAET(ph)EEIT(ph)QGNT(ph)LLR	2	0	0	S	3	3	1	
LS(ph)ENAT(ph)IQLDVVEAET(ph)EEIT(ph)QGNT(ph)LLR	6	0	0	T	3	3	1	
LS(ph)ENAT(ph)IQLDVVEAET(ph)EEIT(ph)QGNT(ph)LLR	16	0	0	T	3	3	1	
LS(ph)ENAT(ph)IQLDVVEAET(ph)EEIT(ph)QGNT(ph)LLR	24	0	0	T	2	3	1	
LS(ph)ENAT(ph)IQLDVVEAET(ph)EEIT(ph)QGNT(ph)LLR	20	0	0	T	1	3	1	
LS(ph)VLSALQDTFFAKLHR	2	0.83668	0.74408	S	1	3	0.99507	
LSCHVLS(ph)ASVGSSAVMS(ph)T(ph)AIM(ox)AT(ph)LLLFK	23	0	0	T	1	3	0.982996	
LSCHVLS(ph)ASVGSSAVMS(ph)T(ph)AIM(ox)AT(ph)LLLFK	18	0	0	T	1	3	0.864788	
M(ox)DIGTLIWDGGPVPNT(ph)HINKCKNY(ph)Y(ph)EVLGVTK	25	0.3768	0.17034	Y	2	4	0.914605	+
M(ox)FFIQNYVVSEGQLEDS(ph)S(ph)LLEVDGPAM(ox)K	18	0	0	S	2	3	0.938655	
M(ox)FFIQNYVVSEGQLEDS(ph)S(ph)LLEVDGPAM(ox)K	17	0	0	S	2	3	0.794356	

Peptide sequence	Position	Ratio SU5402/ FGF1	Ratio dasatinib/ FGF1	Amino acid	No of phosphosites	Charge	Localization prob	Sensitive to treatments
M(ox)GRTPT(ph)AVQVKS(ph)FTK	12	3.7885	1.5436	S	4	3	0.990097	+
M(ox)S(ph)GEFPSPVS(ph)IS(ph)IISSTSGGS(ph)GYGFR	2	0	0	S	3	3	0.772995	
M(ox)SM(ox)PEALAAAT(ph)INAAYALGK	11	0.85343	0.63642	T	1	3	0.986677	
M(ox)T(ph)CT(ph)AFGNPKPIVT(ph)WLK	14	0.67662	2.7014	T	4	2	1	+
M(ox)T(ph)VFQT(ph)TMCSILTR	2	1.0903	0.794	T	4	2	0.966739	
MAPAFLLLLLWPQGCVSGPS(ph)ADS(ph)VY(ph)T(ph)K	27	0.18958	1.0006	T	3	3	0.999335	+
MAPAFLLLLLWPQGCVSGPS(ph)ADS(ph)VY(ph)T(ph)K	26	0.18958	1.0006	Y	3	3	0.999285	+
MAPAFLLLLLWPQGCVSGPS(ph)ADS(ph)VY(ph)T(ph)K	24	0.18958	1.0006	S	3	3	0.997649	+
MAPAFLLLLLWPQGCVSGPS(ph)ADS(ph)VY(ph)T(ph)K	21	0.18958	1.0006	S	3	3	0.839079	+
MS(ph)NQT(ph)DLLALGT(ph)AVGSILLYSTVK	12	0.91468	0.80016	T	4	4	0.966186	
MS(ph)NQTDLLALGT(ph)AVGS(ph)ILLYSTVK	16	0.90513	0.84099	S	4	3	0.780623	
NNS(ph)M(ox)NS(ph)NM(ox)GTGTFGPVGNGVHTGPES(ph)R	3	1.2943	0.56317	S	1	4	0.947038	
NNS(ph)M(ox)NS(ph)NM(ox)GTGTFGPVGNGVHTGPES(ph)R	6	1.2943	0.56317	S	1	4	0.897224	
NNS(ph)M(ox)NS(ph)NM(ox)GTGTFGPVGNGVHTGPES(ph)R	26	1.2943	0.56317	S	1	4	0.894947	
NS(ph)QNPALEWNMASSIR	2	1.0189	0.75327	S	1	3	0.999726	
PLAPPPQPPASPTHS(ph)PS(ph)FPIPDR	17	0.71038	2.2022	S	2	3	0.999956	+
PLAPPPQPPASPTHS(ph)PS(ph)FPIPDR	15	0.71038	2.2022	S	2	3	0.998423	+
PPALLT(ph)LYPAPDEDEAVERCS(ph)R	21	0	0	S	2	3	1	
PPALLT(ph)LYPAPDEDEAVERCS(ph)R	6	0	0	T	2	3	0.84134	
PPS(ph)VT(ph)PIFLEPPPK	3	0	0	S	2	2	1	
PPS(ph)VT(ph)PIFLEPPPK	5	0	0	T	2	2	1	
PRLELMDIIAENVLS(ph)EDR	15	11.696	2.7661	S	1	3	1	
PS(ph)T(ph)GLLM(ox)YTLATR	2	0.85225	0.71016	S	5	3	0.996922	
PS(ph)T(ph)GLLM(ox)YTLATR	3	0.85225	0.71016	T	1	3	0.996923	
PT(ph)S(ph)S(ph)Y(ph)S(ph)MEQDK	2	0	0	T	2	2	1	
PT(ph)S(ph)S(ph)Y(ph)S(ph)MEQDK	5	0	0	Y	2	2	1	
PT(ph)S(ph)S(ph)Y(ph)S(ph)MEQDK	3	0	0	S	1	2	1	
PT(ph)S(ph)S(ph)Y(ph)S(ph)MEQDK	4	0	0	S	1	2	1	

Peptide sequence	Position	Ratio SU5402/ FGF1	Ratio dasatinib/ FGF1	Amino acid	No of phosphosites	Charge	Localization prob	Sensitive to treatments
PT(ph)S(ph)S(ph)Y(ph)S(ph)MEQDK	6	0	0	S	1	2	1	
PVVCATQM(ox)LESMIT(ph)KPR	14	0.68123	0.82517	T	3	3	0.973748	
QFIT(ph)ILEAT(ph)HR	4	9.2751	1.7877	T	1	3	1	+
QFIT(ph)ILEAT(ph)HR	9	9.2751	1.7877	T	1	3	1	+
QGQY(ph)S(ph)PM(ox)AIEEQVAVIY(ph)AGVR	17	0.3762	0.6444	Y	2	3	1	+
QGQY(ph)S(ph)PM(ox)AIEEQVAVIY(ph)AGVR	5	0.3762	0.6444	S	1	3	1	+
QGQY(ph)S(ph)PM(ox)AIEEQVAVIY(ph)AGVR	4	0.3762	0.6444	Y	1	3	1	+
QIHDIVQS(ph)CQPGEVVIR	8	1.4595	0.70571	S	1	3	1	
QIVSAVAY(ph)VHS(ph)QGYAHR	11	8.4832	5.4356	S	1	3	0.997785	+
QIVSAVAY(ph)VHS(ph)QGYAHR	8	11.233	6.9786	Y	1	3	0.979815	+
QLEPT(ph)VQSLEMKSKT(ph)AR	15	0.11109	0.11454	T	2	3	0.907779	+
QLEPT(ph)VQSLEMKSKT(ph)AR	5	0.11109	0.11454	T	2	3	0.907754	+
QT(ph)LAQELSLNES(ph)QIK	12	0	0	S	1	3	0.999865	
QT(ph)LAQELSLNES(ph)QIK	2	0	0	T	1	3	0.999741	
QYEQMHKELT(ph)DKLEHLEQEK	10	0.72529	0.74974	T	1	3	0.999971	
RAT(ph)KELLST(ph)ITDPSVIVM(ox)ADWLK	9	0.61388	0.60149	T	1	3	0.870452	
RLIAEGDAS(ph)PGEDR	9	0.74168	0.73998	S	3	3	1	
S(ph)FTQNYDLLRHERLHMK	1	0.63816	0.19704	S	1	3	0.855715	+
S(ph)KTEADMEEY(ph)IWENSSSERNILET(ph)LLQMK	24	0.65116	0.52321	T	1	4	0.925526	
S(ph)KTEADMEEY(ph)IWENSSSERNILET(ph)LLQMK	10	0.65116	0.52321	Y	1	4	0.924293	
S(ph)LS(ph)TSHLPGLTT(ph)HS(ph)NKTFTQR	14	0.73791	0.54414	S	1	3	0.784995	
S(ph)LS(ph)TSHLPGLTT(ph)HS(ph)NKTFTQR	12	0.73791	0.54414	T	1	3	0.784995	
S(ph)LSQSFENLLDEPAYGLIQK	1	1.1582	0.89334	S	5	3	0.995734	
S(ph)PEWQVVTQDGT(ph)GALHT(ph)T(ph)Y(ph)LQCK	17	0.82352	0.85004	T	1	3	0.998854	
S(ph)PEWQVVTQDGT(ph)GALHT(ph)T(ph)Y(ph)LQCK	18	0.82352	0.85004	T	1	3	0.998854	
S(ph)PEWQVVTQDGT(ph)GALHT(ph)T(ph)Y(ph)LQCK	19	0.82352	0.85004	Y	1	3	0.997419	
S(ph)PEWQVVTQDGT(ph)GALHT(ph)T(ph)Y(ph)LQCK	12	0.82352	0.85004	T	1	3	0.98088	
S(ph)PT(ph)S(ph)SVATPS(ph)STIST(ph)PT(ph)KR	15	0	0	T	2	3	0.833694	

Peptide sequence	Position	Ratio SU5402/ FGF1	Ratio dasatinib/ FGF1	Amino acid	No of phosphosites	Charge	Localization prob	Sensitive to treatments
S(ph)PT(ph)S(ph)SVATPS(ph)STIST(ph)PT(ph)KR	17	0	0	T	1	3	0.96545	
S(ph)PT(ph)S(ph)SVATPS(ph)STIST(ph)PT(ph)KR	1	0	0	S	1	3	0.858673	
S(ph)SHETLNIVEEK	1	1.3562	1.0807	S	1	3	0.848773	
SHLS(ph)T(ph)AGGLAVPSLPT(ph)AGPYY(ph)S(ph)PYALYGQR	5	2.509	1.2208	T	1	3	0.851058	+
SHLS(ph)T(ph)AGGLAVPSLPT(ph)AGPYY(ph)S(ph)PYALYGQR	4	2.509	1.2208	S	1	3	0.766145	+
SHLS(ph)T(ph)AGGLAVPSLPT(ph)AGPYY(ph)S(ph)PYALYGQR	16	2.509	1.2208	T	1	3	0.752798	+
STAPLLDVFS(ph)S(ph)MLKDTTS(ph)QHR	11	0.70068	0.61142	S	2	3	0.946406	+
STAPLLDVFS(ph)S(ph)MLKDTTS(ph)QHR	10	0.70068	0.61142	S	2	3	0.941476	+
T(ph)EEEIEM(ox)M(ox)KLMGFASFDSTK	1	0.7057	0.97952	T	4	3	0.997829	+
T(ph)EFLM(ox)QLDT(ph)VLT(ph)SAEDQIVVICATSK	1	0	0	T	4	3	0.990126	+
T(ph)EFLM(ox)QLDT(ph)VLT(ph)SAEDQIVVICATSK	9	0	0	T	1	3	0.884717	+
T(ph)FLHPEGDHFTLISIYK	1	1.1585	0.88084	T	3	3	0.999385	+
T(ph)GT(ph)PAVT(ph)STS(ph)SASSSLGEK	1	0.64191	0.71316	T	3	3	0.998091	+
T(ph)GT(ph)PAVT(ph)STS(ph)SASSSLGEK	3	0.64191	0.71316	T	3	3	0.923683	+
T(ph)GT(ph)PAVT(ph)STS(ph)SASSSLGEK	7	0.64191	0.71316	T	2	3	0.784398	+
T(ph)KSPTDDEVTPSAVVR	1	0.52839	0.61456	T	2	2	0.98241	+
T(ph)LAHGALAQLGS(ph)LQPLS(ph)VGCVEIR	12	0	0	S	1	3	1	+
T(ph)LAHGALAQLGS(ph)LQPLS(ph)VGCVEIR	17	0	0	S	1	3	1	+
T(ph)TEELNEALSAK	1	0.90643	0.75699	T	5	3	0.857802	+
T(ph)Y(ph)T(ph)VNHETS(ph)HPPPS(ph)K	3	0	0	T	1	2	0.997149	+
T(ph)Y(ph)T(ph)VNHETS(ph)HPPPS(ph)K	14	0	0	S	1	2	0.988568	+
T(ph)Y(ph)T(ph)VNHETS(ph)HPPPS(ph)K	1	0	0	T	1	2	0.987583	+
T(ph)Y(ph)T(ph)VNHETS(ph)HPPPS(ph)K	2	0	0	Y	1	2	0.986485	
TFLTPS(ph)IFIIM(ox)VWY(ph)WR	6	0.4843	0.93855	S	1	3	0.775677	
THNYSM(ox)AIT(ph)Y(ph)Y(ph)EAALK	10	0.67136	2.9971	Y	3	3	0.978973	+
THNYSM(ox)AIT(ph)Y(ph)Y(ph)EAALK	11	0.67136	2.9971	Y	1	3	0.978973	+
THNYSM(ox)AIT(ph)Y(ph)Y(ph)EAALK	9	0.67136	2.9971	T	1	3	0.975938	+
TLLTPHT(ph)GVT(ph)S(ph)QVLGVAAAVM(ox)TPLPGGHAAGR	7	0.14675	0.30174	T	2	5	0.788483	+

Peptide sequence	Position	Ratio SU5402/ FGF1	Ratio dasatinib/ FGF1	Amino acid	No of phosphosites	Charge	Localization prob	Sensitive to treatments
TLLTPHT(ph)GVT(ph)S(ph)QVLGVAAAVM(ox)TPLPGGHAAGR	10	0.14675	0.30174	T	1	5	0.788483	+
TLLTPHT(ph)GVT(ph)S(ph)QVLGVAAAVM(ox)TPLPGGHAAGR	11	0.14675	0.30174	S	1	5	0.788208	+
TSIIDAVELAKDHS(ph)DLSR	14	0.6999	0.83091	S	2	3	0.918179	
TT(ph)LNQGS(ph)CLHNPPRLGEIFM(ox)LK	7	0.674	0.72307	S	1	3	0.808808	
TVLFGVQPKFT(ph)NVDIR	11	0.85867	0.89044	T	2	3	0.998902	
TVTGT(ph)T(ph)M(ox)T(ph)LIPSEMPTPPK	8	0.25593	0.24376	T	2	3	0.865637	+
VS(ph)PVIINT(ph)MITITSALY(ph)T(ph)T(ph)K	19	0.51028	1.0429	T	4	3	0.990055	
VS(ph)PVIINT(ph)MITITSALY(ph)T(ph)T(ph)K	17	0.51028	1.0429	Y	4	3	0.986243	
VS(ph)PVIINT(ph)MITITSALY(ph)T(ph)T(ph)K	18	0.51028	1.0429	T	2	3	0.990058	
VT(ph)VNYYDEEGS(ph)IPIDQAGLFLT(ph)AIEIS(ph)LDVDADR	2	0.51581	10.971	T	3	4	0.841158	+
VT(ph)VNYYDEEGS(ph)IPIDQAGLFLT(ph)AIEIS(ph)LDVDADR	27	0.52948	7.0426	S	2	4	0.999879	+
VT(ph)VNYYDEEGS(ph)IPIDQAGLFLT(ph)AIEIS(ph)LDVDADR	11	0.51581	10.971	S	2	4	0.966652	+
VT(ph)VNYYDEEGS(ph)IPIDQAGLFLT(ph)AIEIS(ph)LDVDADR	22	0.52948	7.0426	T	1	4	0.999921	+
VTIS(ph)VHEKGFIEIK	4	0.76744	0.54445	S	3	3	0.999196	
VVLAAASHFFNLM(ox)FT(ph)T(ph)NM(ox)LES(ph)K	16	0.48894	0.36648	T	2	3	0.995543	+
VVLAAASHFFNLM(ox)FT(ph)T(ph)NM(ox)LES(ph)K	21	0.48894	0.36648	S	2	3	0.990395	+
VVLAAASHFFNLM(ox)FT(ph)T(ph)NM(ox)LES(ph)K	15	0.48894	0.36648	T	1	3	0.995543	+
WLIGGPNPNS(ph)LS(ph)GIRTSK	10	0.65487	1.3571	S	5	3	0.996741	
WLIGGPNPNS(ph)LS(ph)GIRTSK	12	0.65487	1.3571	S	5	3	0.971689	
WPDLLT(ph)EM(ox)VNRFQSGDFHVINGVLR	6	0.83567	0.74258	T	5	3	0.999331	
WY(ph)LAT(ph)GDDIY(ph)DVPHIR	5	0	0	T	4	3	1	
WY(ph)LAT(ph)GDDIY(ph)DVPHIR	2	0	0	Y	4	3	1	
WY(ph)LAT(ph)GDDIY(ph)DVPHIR	10	0	0	Y	1	3	1	
Y(ph)ILQGVT(ph)SWGLGCARPNKPGVY(ph)AR	1	0.56516	0.73067	Y	2	4	0.899308	
Y(ph)IWGGFAY(ph)LQDM(ox)VEQGIT(ph)R	18	0.70745	2.8826	T	2	3	1	+
Y(ph)IWGGFAY(ph)LQDM(ox)VEQGIT(ph)R	1	0.70745	2.8826	Y	2	3	1	+
Y(ph)IWGGFAY(ph)LQDM(ox)VEQGIT(ph)R	8	0.70745	2.8826	Y	2	3	1	+
Y(ph)VM(ox)T(ph)FLNVLNFGDQGVYDIVNNLGSLVAR	1	0	0	Y	1	3	0.998426	
Y(ph)VM(ox)T(ph)FLNVLNFGDQGVYDIVNNLGSLVAR	4	0	0	T	1	3	0.995058	
YILQGVT(ph)S(ph)WGLGCARPNKPGVY(ph)AR	7	0.97795	0.48898	T	1	4	0.836514	

Appendix 2 DAVID analysis of the regulated phosphopeptides in LC-FAIMS-MS/MS

Category	Term
KEGG_PATHWAY	Insulin signalling pathway
KEGG_PATHWAY	Endocytosis
KEGG_PATHWAY	Regulation of actin cytoskeleton
KEGG_PATHWAY	Fc gamma R-mediated phagocytosis
KEGG_PATHWAY	Tight junction
KEGG_PATHWAY	G protein coupled receptors
KEGG_PATHWAY	ErbB signalling pathway
KEGG_PATHWAY	Base excision repair
KEGG_PATHWAY	mTOR signalling pathway
KEGG_PATHWAY	Thyroid cancer

Appendix 3 Peptide details of the SRM assay

Set 1

Peptide sequence	Precursor ion (m/z)	Transition ion (m/z)	Ion type	Collision energy (eV)	RT window(min)
RLS(ph)STSLASGHSVR	513.254	437.19	b3	26	12.8 - 14.2
RLS(ph)STSLASGHSVR	513.254	480.595	precursor-98	26	12.8 - 14.2
RLS(ph)STSLASGHSVR	513.254	1268.563	y12	23	12.8 - 14.2
RLNSS(ph)PRAPVSPLK	534.622	501.963	precursor-98	27	13.6 - 14.7
RLNSS(ph)PRAPVSPLK	534.622	964.593	y9	27	13.6 - 14.7
RLNSS(ph)PRAPVSPLK	534.622	1131.592	y10	26	13.6 - 14.7
GAQASSGS(ph)PALPR	639.795	553.345	y5	25	13.8 - 15.1
GAQASSGS(ph)PALPR	639.795	590.807	precursor-98	25	13.8 - 15.1
GAQASSGS(ph)PALPR	639.795	777.365	y7	25	13.8 - 15.1
DINNIDY(ph)Y(ph)KK	723.291	761.266	y4	28	14.2 - 15.5
DINNIDY(ph)Y(ph)KK	723.291	876.293	y5	28	14.2 - 15.5
DINNIDY(ph)Y(ph)KK	723.291	989.378	y6	28	14.2 - 15.5
NFSAAKS(ph)LLNKK	467.583	434.923	precursor-98	24	14.5 - 16.3
NFSAAKS(ph)LLNKK	467.583	782.417	y6	24	14.5 - 16.3
NFSAAKS(ph)LLNKK	467.583	910.512	y7	24	14.5 - 16.3
STS(ph)WHTALR	569.756	520.767	precursor-98	23	14.7 - 15.7
STS(ph)WHTALR	569.756	783.426	y6	23	14.7 - 15.7
STS(ph)WHTALR	569.756	950.424	y7	23	14.7 - 15.7
RPHFPQFSY(ph)SASGRE	615.942	849.313	y7	30	14.7 - 16.2
RPHFPQFSY(ph)SASGRE	615.942	936.345	y8	30	14.7 - 16.2
RPHFPQFSY(ph)SASGRE	615.942	1240.529	b9	28	14.7 - 16.2
VTS(ph)GGVSESPSGFSK	753.33	704.341	precursor-98	29	14.7 - 16.2
VTS(ph)GGVSESPSGFSK	753.33	925.426	y9	29	14.7 - 16.2
VTS(ph)GGVSESPSGFSK	753.33	1305.535	y13	26	14.7 - 16.2
TPKDS(ph)PGIPPSANAHQLFR	705.012	442.229	b4	34	14.9 - 17.2
TPKDS(ph)PGIPPSANAHQLFR	705.012	609.227	b5	34	14.9 - 17.2
TPKDS(ph)PGIPPSANAHQLFR	705.012	672.354	precursor-98	34	14.9 - 17.2
RES(ph)VVNLENFRK	524.263	491.604	precursor-98	26	15 - 16.2
RES(ph)VVNLENFRK	524.263	552.217	b4	26	15 - 16.2
RES(ph)VVNLENFRK	524.263	920.494	y7	26	15 - 16.2
TPKDS(ph)PGIPPSAGAHQLFR	686.007	442.229	b4	33	15 - 17.2
TPKDS(ph)PGIPPSAGAHQLFR	686.007	609.227	b5	33	15 - 17.2
TPKDS(ph)PGIPPSAGAHQLFR	686.007	653.346	precursor-98	33	15 - 17.2
RNS(ph)FTPLSSSNTIR	553.933	521.274	precursor-98	28	15.1 - 16.5
RNS(ph)FTPLSSSNTIR	553.933	585.217	b4	28	15.1 - 16.5
RNS(ph)FTPLSSSNTIR	553.933	1222.642	y11	25	15.1 - 16.5
NYSVGSRPLKPLS(ph)PLR	622.001	589.341	precursor-98	31	15.5 - 16.7
NYSVGSRPLKPLS(ph)PLR	622.001	665.338	y5	31	15.5 - 16.7
NYSVGSRPLKPLS(ph)PLR	622.001	762.39	y6	31	15.5 - 16.7
EHIEIIAPS(ph)PQR	735.361	664.281	y5	28	15.6 - 16.8
EHIEIIAPS(ph)PQR	735.361	686.373	precursor-98	28	15.6 - 16.8
EHIEIIAPS(ph)PQR	735.361	961.486	y8	28	15.6 - 16.8
RYS(ph)DHAGPAIPSVVAYPK	669.994	487.17	b3	33	15.7 - 17
RYS(ph)DHAGPAIPSVVAYPK	669.994	602.197	b4	33	15.7 - 17

Set 1 continued

Peptide sequence	Precursor ion (m/z)	Transition ion (m/z)	Ion type	Collision energy (eV)	RT window(min)
RYS(ph)DHAGPAIPSVVAYPK	669.994	637.336	precursor-98	33	15.7 - 17
NFS(ph)AAKS(ph)LLNKK	494.237	461.578	precursor-98	25	16 - 17.3
NFS(ph)AAKS(ph)LLNKK	494.237	782.417	y6	25	16 - 17.3
NFS(ph)AAKS(ph)LLNKK	494.237	1219.584	y10	23	16 - 17.3
HFM(ox)HQIITGMLYLHS(ph)HGILHR	879.765	732.426	y6	35	16.1 - 17.7
HFM(ox)HQIITGMLYLHS(ph)HGILHR	879.765	847.104	precursor-98	35	16.1 - 17.7
HFM(ox)HQIITGMLYLHS(ph)HGILHR	879.765	1036.483	y8	35	16.1 - 17.7
TTS(ph)FAESCKPVQQPSAFGSMK	771.009	203.102	b2	35	16.3 - 17.6
TTS(ph)FAESCKPVQQPSAFGSMK	771.009	370.1	b3	35	16.3 - 17.6
TTS(ph)FAESCKPVQQPSAFGSMK	771.009	738.35	precursor-98	35	16.3 - 17.6
RSDS(ph)ASSEPVGIYQGFEK	679.639	526.165	b4	33	16.4 - 18
RSDS(ph)ASSEPVGIYQGFEK	679.639	597.202	b5	33	16.4 - 18
RSDS(ph)ASSEPVGIYQGFEK	679.639	646.978	precursor-98	33	16.4 - 18
T(ph)TSFAESCKPVQQPSAFGSM(ox)K	776.341	182.021	b1	35	16.5 - 18
T(ph)TSFAESCKPVQQPSAFGSM(ox)K	776.341	743.682	precursor-98	35	16.5 - 18
T(ph)TSFAESCKPVQQPSAFGSM(ox)K	776.341	840.391	y8	35	16.5 - 18
VADPDHDHT(ph)GFLTEY(ph)VATR	768.65	689.301	y5	35	16.9 - 18.1
VADPDHDHT(ph)GFLTEY(ph)VATR	768.65	735.991	precursor-98	35	16.9 - 18.1
VADPDHDHT(ph)GFLTEY(ph)VATR	768.65	1068.378	b9	35	16.9 - 18.1
THFPQFS(ph)YSASIRE	583.926	551.267	y7	29	17.3 - 18.4
THFPQFS(ph)YSASIRE	583.926	825.409	y9	29	17.3 - 18.4
THFPQFS(ph)YSASIRE	583.926	1139.476	precursor-98	28	17.3 - 18.4
ALGERVS(ph)IL	519.273	470.285	precursor-98	21	18.2 - 19.4
ALGERVS(ph)IL	519.273	667.353	y5	21	18.2 - 19.4
ALGERVS(ph)IL	519.273	796.396	y6	21	18.2 - 19.4
S(ph)HNDFVAILDLPEGEHQYK	764.683	419.107	b3	35	18.6 - 19.9
S(ph)HNDFVAILDLPEGEHQYK	764.683	732.024	precursor-98	35	18.6 - 19.9
S(ph)HNDFVAILDLPEGEHQYK	764.683	1328.648	y11	34	18.6 - 19.9
DALDLSDINSEPPRGS(ph)FPSFEPR	876.066	843.407	precursor-98	35	19.7 - 22
DALDLSDINSEPPRGS(ph)FPSFEPR	876.066	879.435	y7	35	19.7 - 22
DALDLSDINSEPPRGS(ph)FPSFEPR	876.066	1356.609	y11	35	19.7 - 22

Set 2

Peptide sequence	Precursor ion (m/z)	Transition ion (m/z)	Ion type	Collision energy (eV)	RT window(min)
RLSS(ph)TSLASGHSVR	513.256	357.224	y7	26	12.7 - 14
RLSS(ph)TSLASGHSVR	513.256	480.595	precursor-98	26	12.7 - 14
RLSS(ph)TSLASGHSVR	513.256	1181.531	y11	24	12.7 - 14
RLNSSPRAPVS(ph)PLK	534.624	501.963	precursor-98	27	13.9 - 14.7
RLNSSPRAPVS(ph)PLK	534.624	623.316	y5	27	13.9 - 14.7
RLNSSPRAPVS(ph)PLK	534.624	720.369	y6	27	13.9 - 14.7
LSEEAECPNPST(ph)PSK	834.845	512.211	y4	32	14.1 - 15.5
LSEEAECPNPST(ph)PSK	834.845	696.296	y6	32	14.1 - 15.5
LSEEAECPNPST(ph)PSK	834.845	785.856	precursor-98	32	14.1 - 15.5
RRSIQDLT(ph)VTGTEPGQVSSR	756.376	723.717	precursor-98	35	14.1 - 15.7
RRSIQDLT(ph)VTGTEPGQVSSR	756.376	1050.509	b8	35	14.1 - 15.7
RRSIQDLT(ph)VTGTEPGQVSSR	756.376	1149.577	b9	35	14.1 - 15.7
RLNSS(ph)PRAPVS(ph)PLK	561.278	524.247		28	14.4 - 15.6
RLNSS(ph)PRAPVS(ph)PLK	561.278	528.619		28	14.4 - 15.6
RLNSS(ph)PRAPVS(ph)PLK	561.278	1211.558		26	14.4 - 15.6
DINNIDY(ph)YKK	683.308	438.271	y3	27	14.4 - 15.8
DINNIDY(ph)YKK	683.308	909.411	y6	27	14.4 - 15.8
DINNIDY(ph)YKK	683.308	928.344	b7	27	14.4 - 15.8
T(ph)TSQCKSEPPLLR	513.913	182.021	b1	26	14.7 - 16.1
T(ph)TSQCKSEPPLLR	513.913	481.254	precursor-98	26	14.7 - 16.1
T(ph)TSQCKSEPPLLR	513.913	1358.709	y12	22	14.7 - 16.1
RPPGMEY(ph)SYDINR	559.908	533.252	y6	28	15 - 16.2
RPPGMEY(ph)SYDINR	559.908	767.368	y8	28	15 - 16.2
RPPGMEY(ph)SYDINR	559.908	1139.44	y10	27	15 - 16.2
TPKDSPGIPPS(ph)AGAHQLFR	686.009	653.346	precursor-98	33	15.1 - 16.9
TPKDSPGIPPS(ph)AGAHQLFR	686.009	1163.535	y10	32	15.1 - 16.9
TPKDSPGIPPS(ph)AGAHQLFR	686.009	1260.588	y11	31	15.1 - 16.9
LGS(ph)YSGPTSVSR	645.79	501.174	b4	25	15.2 - 16.3
LGS(ph)YSGPTSVSR	645.79	588.206	b5	25	15.2 - 16.3
LGS(ph)YSGPTSVSR	645.79	596.802	precursor-98	25	15.2 - 16.3
KLPS(ph)TTL	420.217	371.229	precursor-98	18	15.3 - 17.3
KLPS(ph)TTL	420.217	501.195	y3	18	15.3 - 17.3
KLPS(ph)TTL	420.217	598.248	y5	18	15.3 - 17.3
RNSFT(ph)PLSSSNTIR	553.935	521.274	precursor-98	28	15.4 - 16.8
RNSFT(ph)PLSSSNTIR	553.935	686.265	b5	28	15.4 - 16.8
RNSFT(ph)PLSSSNTIR	553.935	1155.54	y10	26	15.4 - 16.8
RIS(ph)LSDMPR	577.773	518.239	y4	23	15.8 - 16.9
RIS(ph)LSDMPR	577.773	605.271	y5	23	15.8 - 16.9
RIS(ph)LSDMPR	577.773	718.355	y6	23	15.8 - 16.9
NLQS(ph)PTQFQTPR	748.848	699.86	precursor-98	29	15.9 - 17.2
NLQS(ph)PTQFQTPR	748.848	974.505	y8	29	15.9 - 17.2
NLQS(ph)PTQFQTPR	748.848	1141.503	y9	27	15.9 - 17.2
RPHFPQFS(ph)Y(ph)SASGRE	642.596	609.937	precursor-98	32	16 - 17.5
RPHFPQFS(ph)Y(ph)SASGRE	642.596	849.313	y7	32	16 - 17.5
RPHFPQFS(ph)Y(ph)SASGRE	642.596	1016.312	y8	31	16 - 17.5
VADPDHDHTGFLT(ph)EYVATR	741.995	709.336	precursor-98	35	16.1 - 18.5

Set 2 continued

Peptide sequence	Precursor ion (m/z)	Transition ion (m/z)	Ion type	Collision energy (eV)	RT window(min)
VADPDHDHTGFLT(ph)EYVATR	741.995	738.378	y6	35	16.1 - 18.5
VADPDHDHTGFLT(ph)EYVATR	741.995	919.391	y7	35	16.1 - 18.5
IADPEHDHTGFLT(ph)EYVATR	751.339	718.68	precursor-98	35	16.4 - 18.8
IADPEHDHTGFLT(ph)EYVATR	751.339	738.378	y6	35	16.4 - 18.8
IADPEHDHTGFLT(ph)EYVATR	751.339	1032.476	y8	35	16.4 - 18.8
NYS(ph)VGSRPLKPLS(ph)PLR	648.655	544.18	y4	32	16.7 - 17.7
NYS(ph)VGSRPLKPLS(ph)PLR	648.655	615.996	precursor-98	32	16.7 - 17.7
NYS(ph)VGSRPLKPLS(ph)PLR	648.655	665.338	b5	32	16.7 - 17.7
RPHFPQFS(ph)YSASGTA	866.878	656.288	y7	33	16.7 - 17.8
RPHFPQFS(ph)YSASGTA	866.878	817.889	precursor-98	33	16.7 - 17.8
RPHFPQFS(ph)YSASGTA	866.878	1098.413	y10	32	16.7 - 17.8
IADPEHDHT(ph)GFLTEY(ph)VATR	777.994	751.339	precursor-98	35	16.9 - 18.4
IADPEHDHT(ph)GFLTEY(ph)VATR	777.994	818.344	y6	35	16.9 - 18.4
IADPEHDHT(ph)GFLTEY(ph)VATR	777.994	1153.43	b10	35	16.9 - 18.4
VADPDHDHTGFLT(ph)EY(ph)VATR	768.653	689.301	y5	35	17 - 18.2
VADPDHDHTGFLT(ph)EY(ph)VATR	768.653	741.995	y6	35	17 - 18.2
VADPDHDHTGFLT(ph)EY(ph)VATR	768.653	1316.532	y10	34	17 - 18.2
RVS(ph)LSEIGFGK	636.821	423.175	b3	25	17.4 - 18.3
RVS(ph)LSEIGFGK	636.821	587.833	precursor-98	25	17.4 - 18.3
RVS(ph)LSEIGFGK	636.821	1017.465	y9	25	17.4 - 18.3
S(ph)GGGDLTLGLEPSEEEAPR	997.441	282.048	b3	35	18.3 - 19.5
S(ph)GGGDLTLGLEPSEEEAPR	997.441	948.453	precursor-98	35	18.3 - 19.5
S(ph)GGGDLTLGLEPSEEEAPR	997.441	1156.547	y10	35	18.3 - 19.5
AVLS(ph)PGSVFSPGR	677.332	628.343	precursor-98	26	19.1 - 20.3
AVLS(ph)PGSVFSPGR	677.332	806.415	y8	26	19.1 - 20.3
AVLS(ph)PGSVFSPGR	677.332	903.468	y9	26	19.1 - 20.3
ATDSFS(ph)GRFEDVYQLQEDVLGEGAHAR	1026.459	522.219	precursor-98	35	20 - 21.6
ATDSFS(ph)GRFEDVYQLQEDVLGEGAHAR	1026.459	746.239	y6	35	20 - 21.6
ATDSFS(ph)GRFEDVYQLQEDVLGEGAHAR	1026.459	993.8	b10	35	20 - 21.6

Set 3

Peptide sequence	Precursor ion (m/z)	Transition ion (m/z)	Ion type	Collision energy (eV)	RT window(min)
GRNS(ph)ATSADEQPHIGNYR	684.968	566.208	b5	33	12.9 - 14.4
GRNS(ph)ATSADEQPHIGNYR	684.968	652.309	precursor-98	33	12.9 - 14.4
GRNS(ph)ATSADEQPHIGNYR	684.968	667.255	b6	33	12.9 - 14.4
RLS(ph)S(ph)TSLASGHSVR	539.91	507.251	precursor-98	27	13.4 - 14.8
RLS(ph)S(ph)TSLASGHSVR	539.91	705.236	b5	27	13.4 - 14.8
RLS(ph)S(ph)TSLASGHSVR	539.91	1014.532	y10	27	13.4 - 14.8
S(ph)TVASMMHR	550.225	269.053	b2	22	14.1 - 15.4
S(ph)TVASMMHR	550.225	501.236	precursor-98	22	14.1 - 15.4
S(ph)TVASMMHR	550.225	932.443	y8	22	14.1 - 15.4
DINNIDYY(ph)KK	683.31	518.237	y3	27	14.1 - 15.6
DINNIDYY(ph)KK	683.31	848.378	b7	27	14.1 - 15.6
DINNIDYY(ph)KK	683.31	909.411	y6	27	14.1 - 15.6
NFS(ph)AAKSLLNKK	467.581	429.116	precursor-98	24	14.4 - 16.3
NFS(ph)AAKSLLNKK	467.581	434.923	b3	24	14.4 - 16.3
NFS(ph)AAKSLLNKK	467.581	500.154	b4	24	14.4 - 16.3
S(ph)GEQITSSPVSPK	698.821	354.069	b3	27	14.6 - 15.8
S(ph)GEQITSSPVSPK	698.821	649.833	precursor-98	27	14.6 - 15.8
S(ph)GEQITSSPVSPK	698.821	802.43	y8	27	14.6 - 15.8
RPHFPQFS(ph)YSASGRE	615.94	583.282	precursor-98	30	14.7 - 16.4
RPHFPQFS(ph)YSASGRE	615.94	1077.466	b8	30	14.7 - 16.4
RPHFPQFS(ph)YSASGRE	615.94	1083.414	y9	30	14.7 - 16.4
RPPGMEYS(ph)YDINR	559.91	527.249	precursor-98	28	14.8 - 16.6
RPPGMEYS(ph)YDINR	559.91	680.336	y5	28	14.8 - 16.6
RPPGMEYS(ph)YDINR	559.91	1010.397	y7	28	14.8 - 16.6
T(ph)PKDSPGIPPSAGAHQLFR	686.005	279.074	b2	33	14.9 - 17
T(ph)PKDSPGIPPSAGAHQLFR	686.005	407.168	b3	33	14.9 - 17
T(ph)PKDSPGIPPSAGAHQLFR	686.005	653.346	precursor-98	33	14.9 - 17
EKFS(ph)FEPK	546.244	497.256	precursor-98	22	15 - 16.3
EKFS(ph)FEPK	546.244	687.274	y5	22	15 - 16.3
EKFS(ph)FEPK	546.244	834.343	y6	22	15 - 16.3
KLPST(ph)TL	420.219	371.229	precursor-98	18	15.3 - 17.1
KLPST(ph)TL	420.219	414.163	y3	18	15.3 - 17.1
KLPST(ph)TL	420.219	598.248	y5	18	15.3 - 17.1
SGS(ph)PSDNSGAEEMEVSLAKPK	733.987	312.059	b3	35	15.6 - 16.9
SGS(ph)PSDNSGAEEMEVSLAKPK	733.987	409.111	b4	35	15.6 - 16.9
SGS(ph)PSDNSGAEEMEVSLAKPK	733.987	701.328	precursor-98	35	15.6 - 16.9
TPKDS(ph)PGIPPS(ph)ANAHQLFR	731.668	609.227	b5	35	15.6 - 18
TPKDS(ph)PGIPPS(ph)ANAHQLFR	731.668	699.009	precursor-98	35	15.6 - 18
TPKDS(ph)PGIPPS(ph)ANAHQLFR	731.668	1220.557	y10	33	15.6 - 18
NYS(ph)VGSRPLKPLSPLR	622	544.18	b4	31	15.7 - 16.9
NYS(ph)VGSRPLKPLSPLR	622	589.341	precursor-98	31	15.7 - 16.9
NYS(ph)VGSRPLKPLSPLR	622	601.201	b5	31	15.7 - 16.9
TPKDS(ph)PGIPPS(ph)AGAHQLFR	712.661	680.002	precursor-98	35	15.9 - 18
TPKDS(ph)PGIPPS(ph)AGAHQLFR	712.661	706.28	b6	35	15.9 - 18
TPKDS(ph)PGIPPS(ph)AGAHQLFR	712.661	1163.535	y10	33	15.9 - 18

Set 3 continued

Peptide sequence	Precursor ion (m/z)	Transition ion (m/z)	Ion type	Collision energy (eV)	RT window(min)
VADPDHDHTGFLTEY(ph)VATR	741.997	446.272	y4	35	16 - 18.4
VADPDHDHTGFLTEY(ph)VATR	741.997	689.301	y5	35	16 - 18.4
VADPDHDHTGFLTEY(ph)VATR	741.997	715.34	y7	35	16 - 18.4
IADPEHDHTGFLTEY(ph)VATR	751.341	689.301	y5	35	16.3 - 17.3
IADPEHDHTGFLTEY(ph)VATR	751.341	724.683	y6	35	16.3 - 17.3
IADPEHDHTGFLTEY(ph)VATR	751.341	818.344	y7	35	16.3 - 17.3
RS(ph)DSASSEPVGIYQGFEK	679.637	324.106	b2	33	16.4 - 17.8
RS(ph)DSASSEPVGIYQGFEK	679.637	439.133	b3	33	16.4 - 17.8
RS(ph)DSASSEPVGIYQGFEK	679.637	646.978	precursor-98	33	16.4 - 17.8
IADPEHDHTGFLT(ph)EY(ph)VATR	777.996	751.339	y6	35	16.8 - 18.3
IADPEHDHTGFLT(ph)EY(ph)VATR	777.996	818.344	y7	35	16.8 - 18.3
IADPEHDHTGFLT(ph)EY(ph)VATR	777.996	1112.442	y8	35	16.8 - 18.3
GLCTSPAEHQYFMTEY(ph)VATR	795.341	689.301	y5	35	16.9 - 18.4
GLCTSPAEHQYFMTEY(ph)VATR	795.341	768.686	precursor-98	35	16.9 - 18.4
GLCTSPAEHQYFMTEY(ph)VATR	795.341	818.344	y6	35	16.9 - 18.4
GAILTTM(ox)LVS(ph)R	629.317	580.329	precursor-98	25	17.4 - 18.5
GAILTTM(ox)LVS(ph)R	629.317	701.305	y5	25	17.4 - 18.5
GAILTTM(ox)LVS(ph)R	629.317	802.352	y6	25	17.4 - 18.5
GFS(ph)FVATGLM(ox)EDDGKPR	641.617	608.958	precursor-98	32	18.5 - 19.8
GFS(ph)FVATGLM(ox)EDDGKPR	641.617	618.232	b5	32	18.5 - 19.8
GFS(ph)FVATGLM(ox)EDDGKPR	641.617	1076.504	y9	31	18.5 - 19.8
LQPFHST(ph)ELEDDAIYSVHVPAGLYR	979.799	710.361	b6	35	19.4 - 20.6
LQPFHST(ph)ELEDDAIYSVHVPAGLYR	979.799	947.14	precursor-98	35	19.4 - 20.6
LQPFHST(ph)ELEDDAIYSVHVPAGLYR	979.799	1020.418	b8	35	19.4 - 20.6
S(ph)VVGTPAYLAPEVLR	826.426	366.142	b3	31	19.7 - 21
S(ph)VVGTPAYLAPEVLR	826.426	777.438	precursor-98	31	19.7 - 21
S(ph)VVGTPAYLAPEVLR	826.426	1128.641	y10	30	19.7 - 21
EYGS(ph)PLKAYT(ph)PVVVTQWYR	806.371	614.185	b5	35	20.3 - 22
EYGS(ph)PLKAYT(ph)PVVVTQWYR	806.371	773.712	precursor-98	35	20.3 - 22
EYGS(ph)PLKAYT(ph)PVVVTQWYR	806.371	1328.639	y10	35	20.3 - 22

Appendix 4 Quantitation results of SRM assay

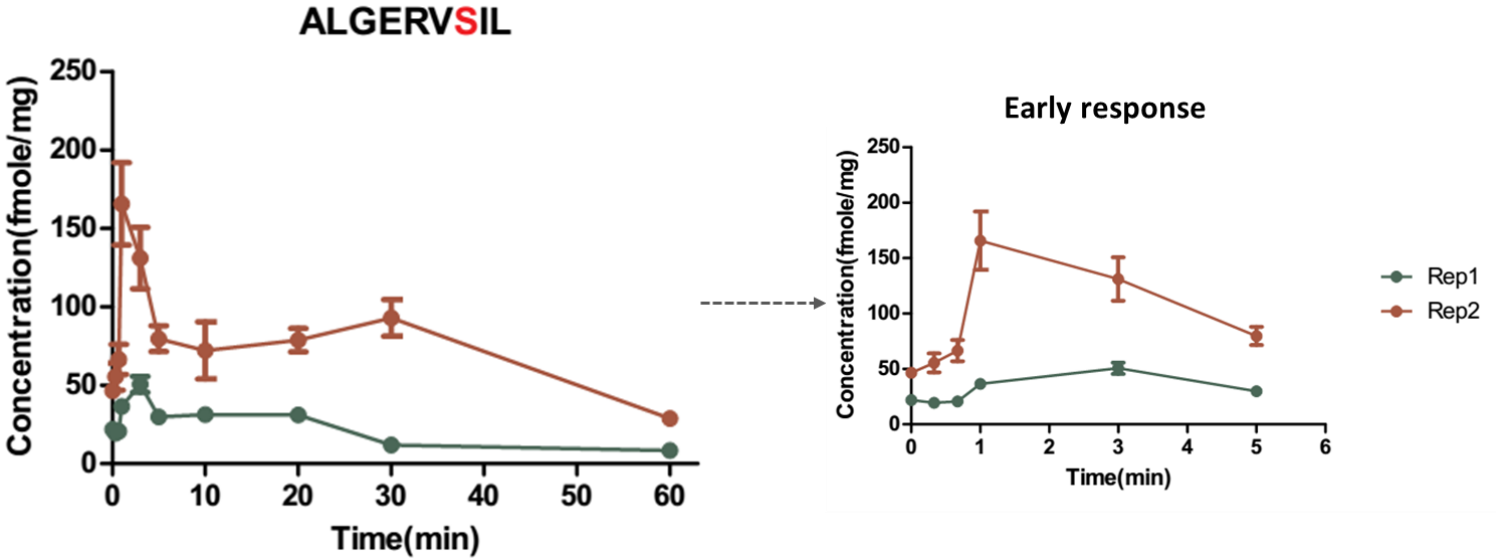

Figure 1 Phosphorylation profile of ALGERVpSIL in response to FGF1

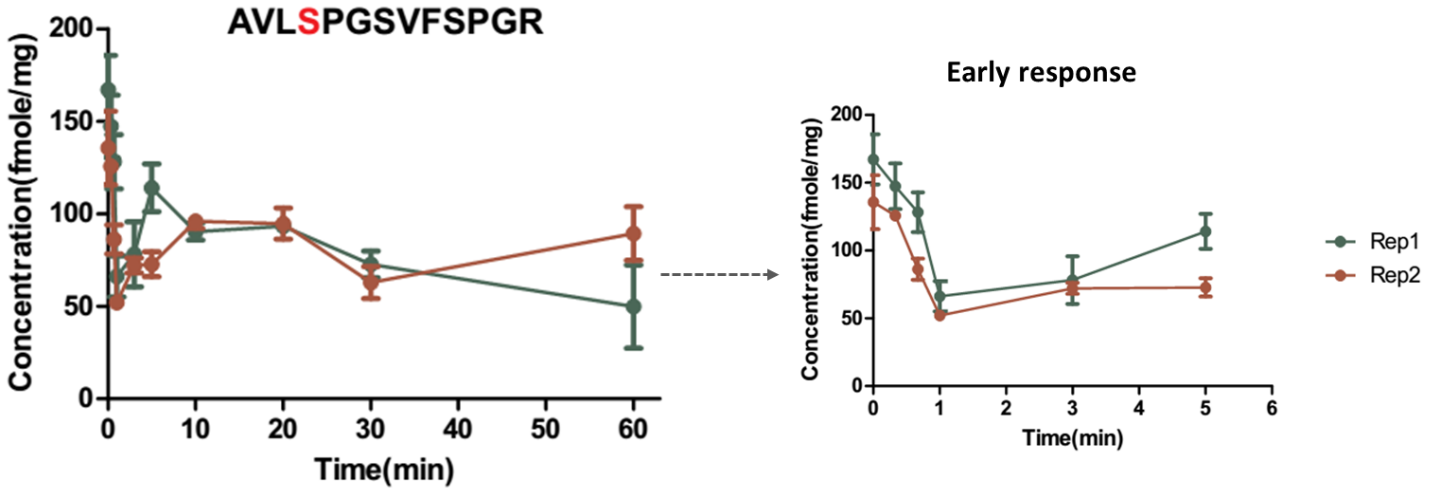

Figure 2 Phosphorylation profile of AVLpSPGSVFSPGR in response to FGF1

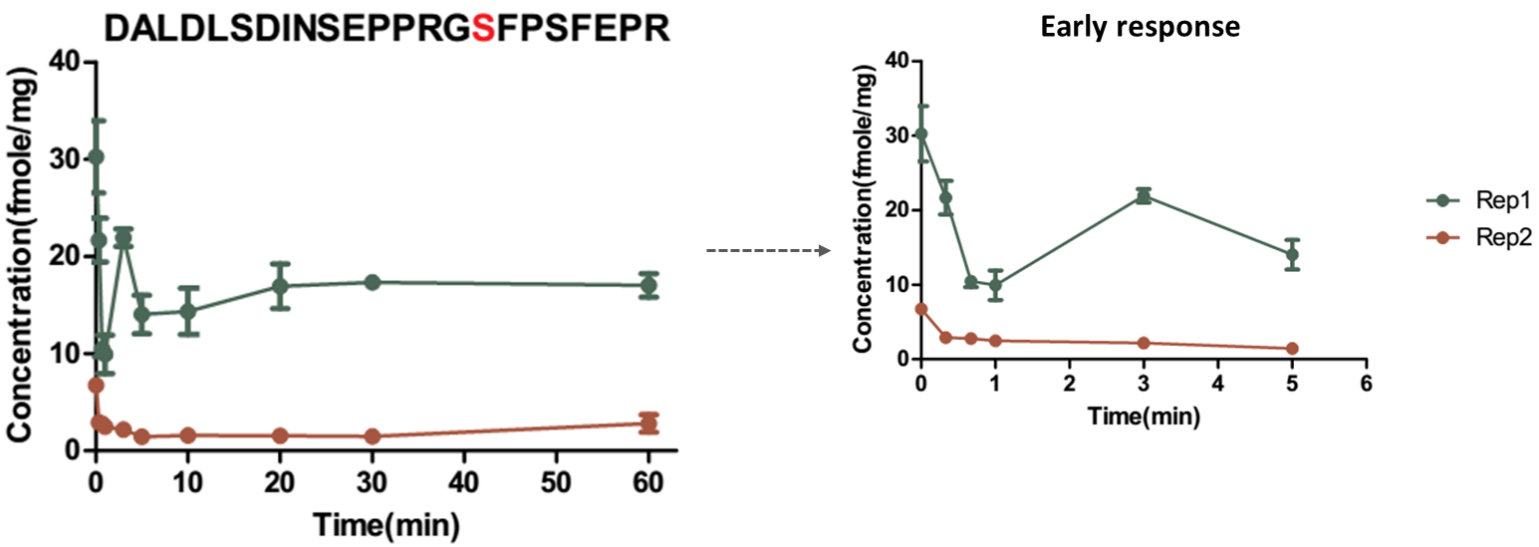

Figure 3 Phosphorylation profile of DALDLSDINSEPPRGpSFPSFEPR in response to FGF1

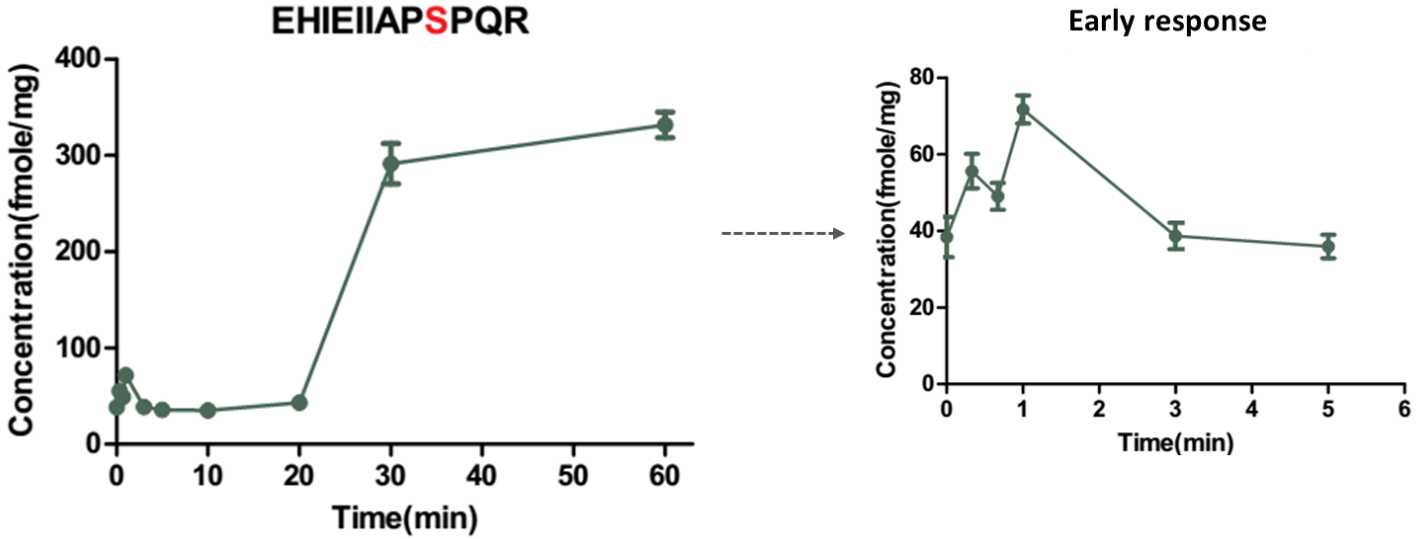

Figure 4 Phosphorylation profile of EHIEIIAPpSPQR in response to FGF1

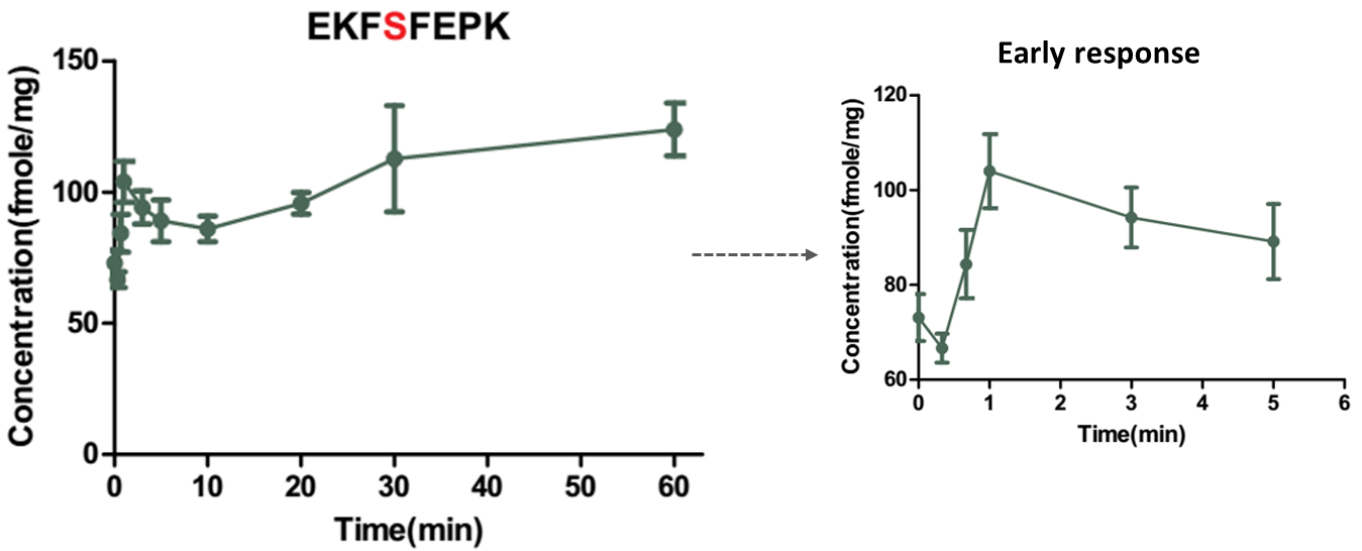

Figure 5 Phosphorylation profile of EKFpSFEPK in response to FGF1

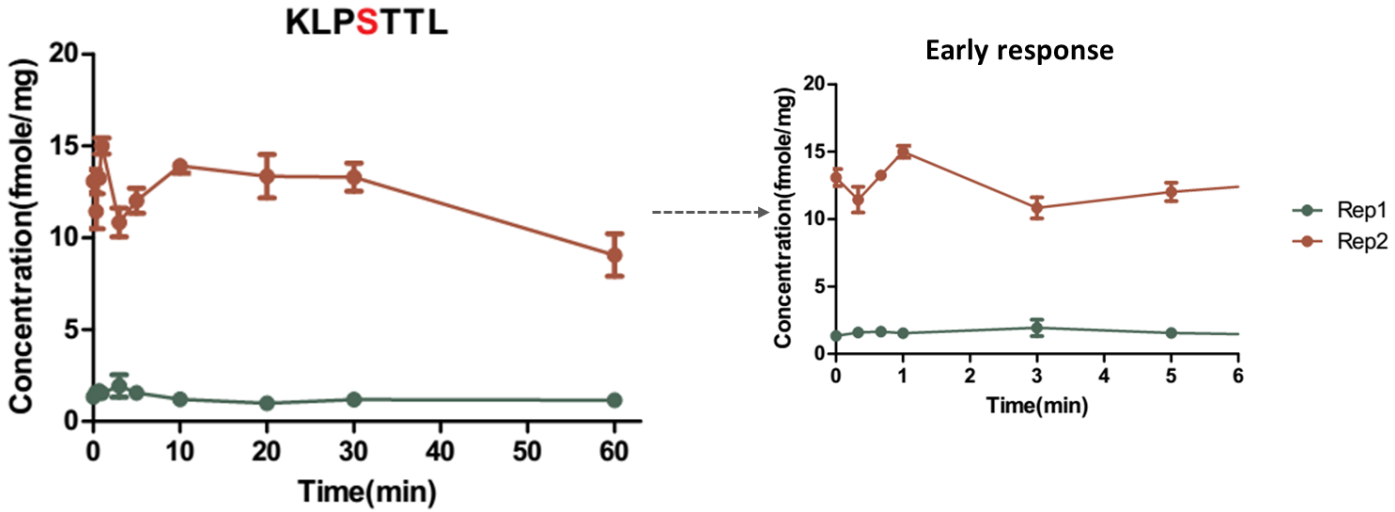

Figure 6 Phosphorylation profile of KLPpSTTL in response to FGF1

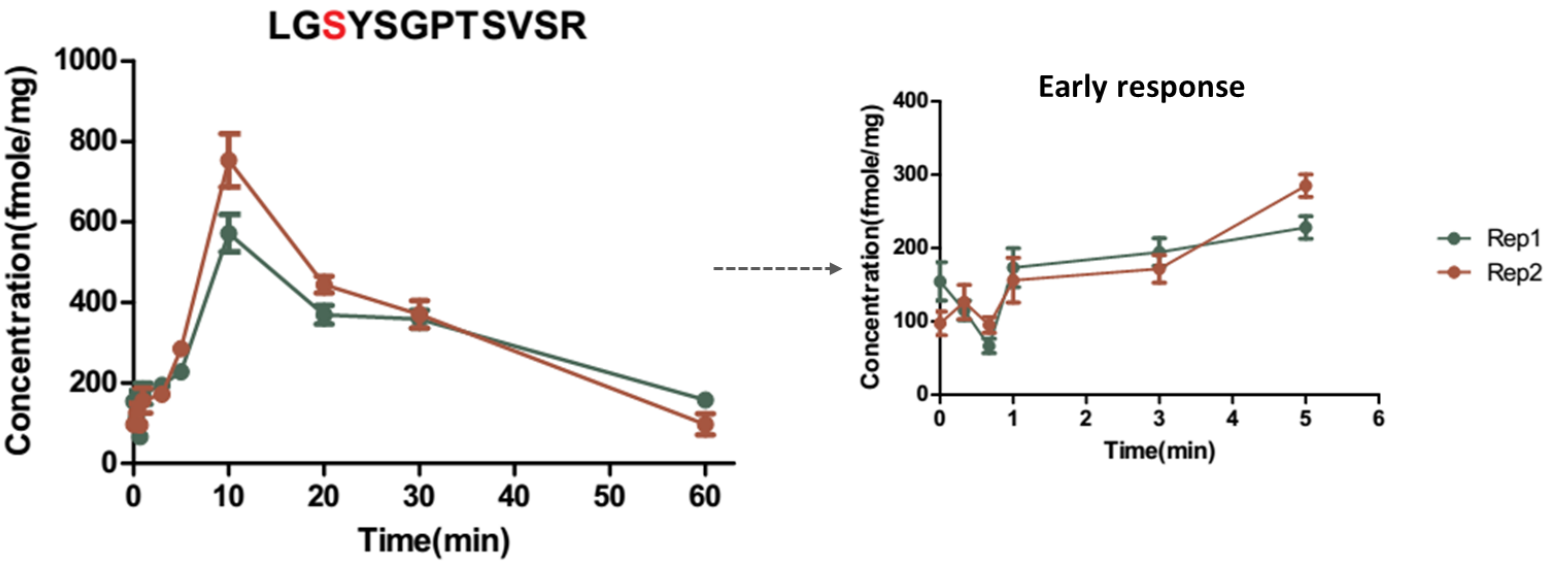

Figure 7 Phosphorylation profile of LGpSYSGPTSVSR in response to FGF1

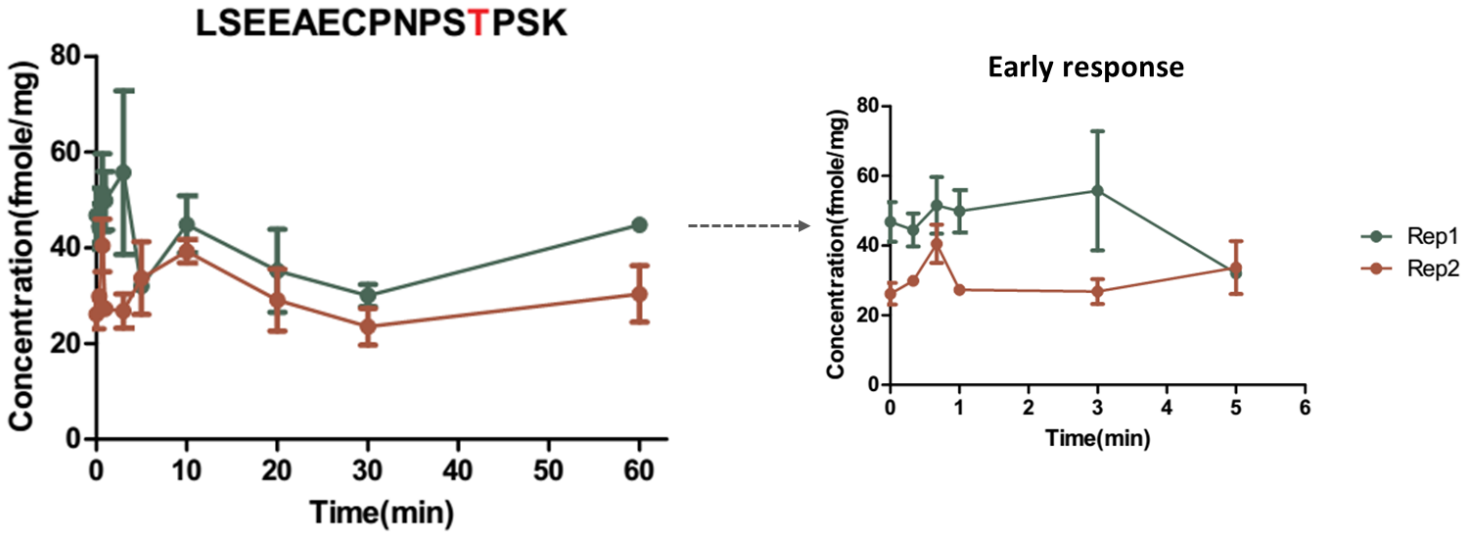

Figure 8 Phosphorylation profile of LSEEAECPNPSpTPSK in response to FGF1

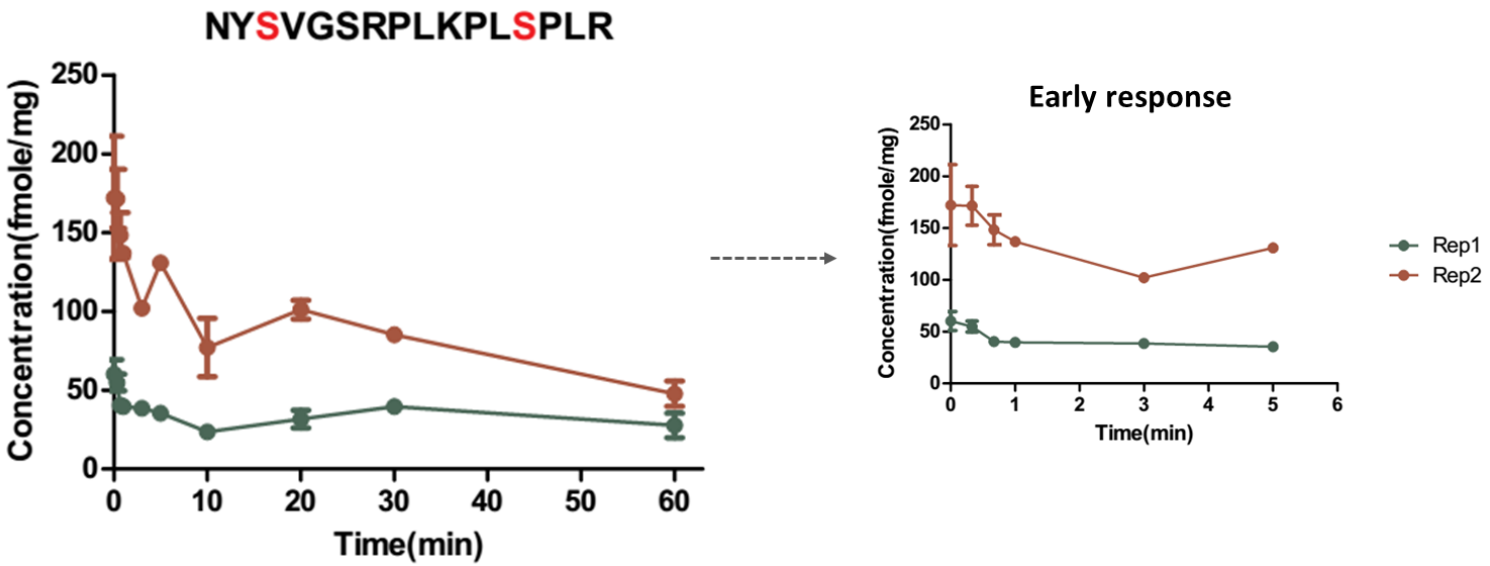

Figure 9 Phosphorylation profile of NYpSVGSRPLKPLpSPLR in response to FGF1

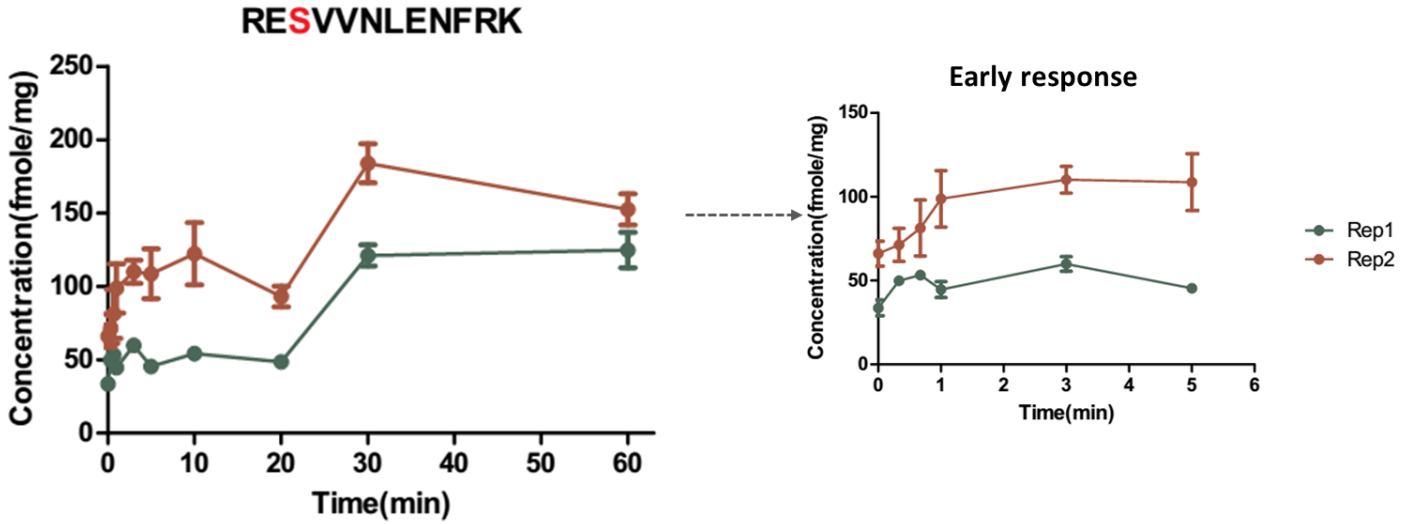

Figure 10 Phosphorylation profile of REpSVVNLENFRK in response to FGF1

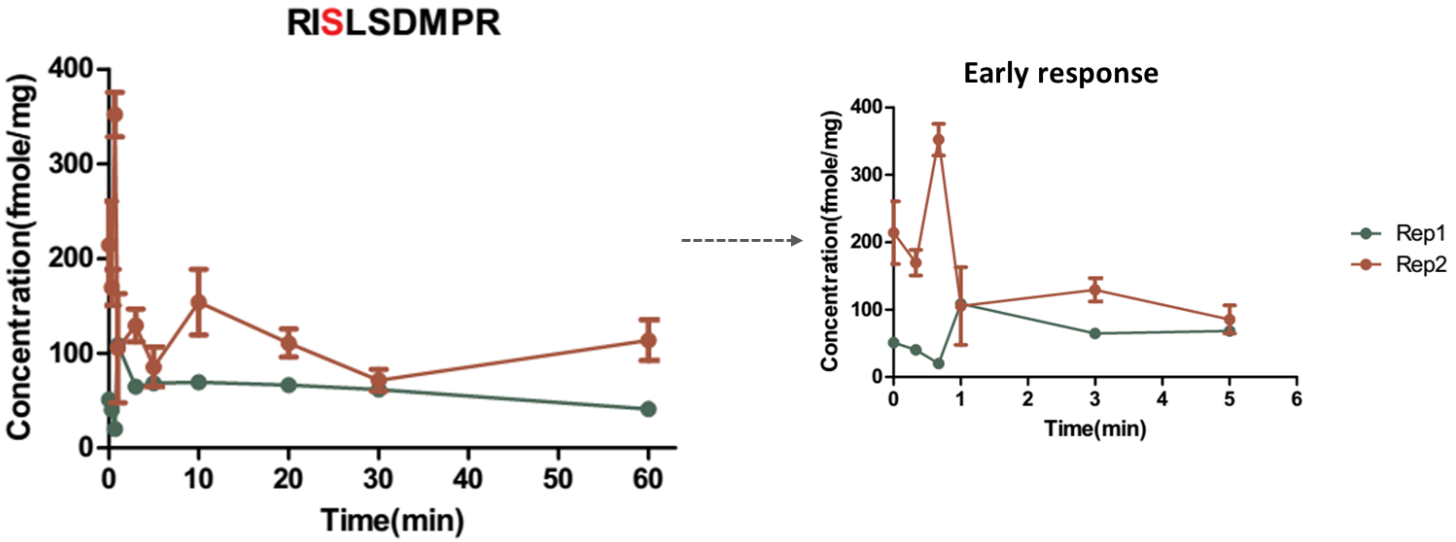

Figure 11 Phosphorylation profile of RIpSLSDMPR in response to FGF1

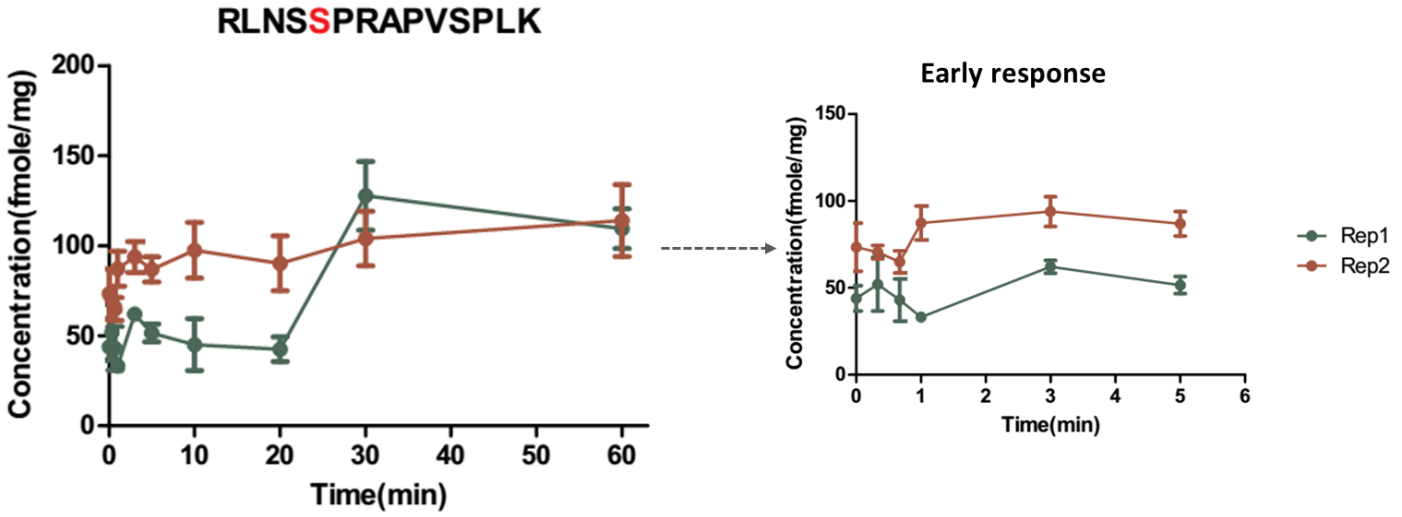

Figure 12 Phosphorylation profile of RLNSpSPRAPVSPLK in response to FGF1

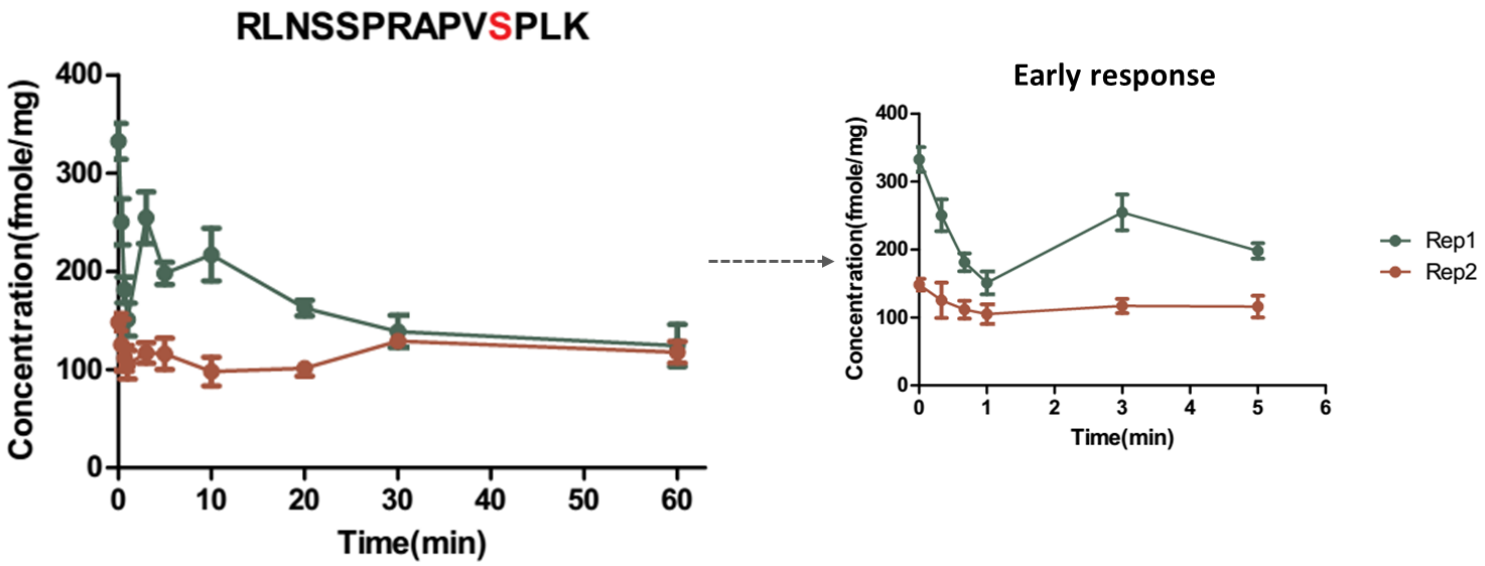

Figure 13 Phosphorylation profile of RLNSSPRAPVpSPLK in response to FGF1

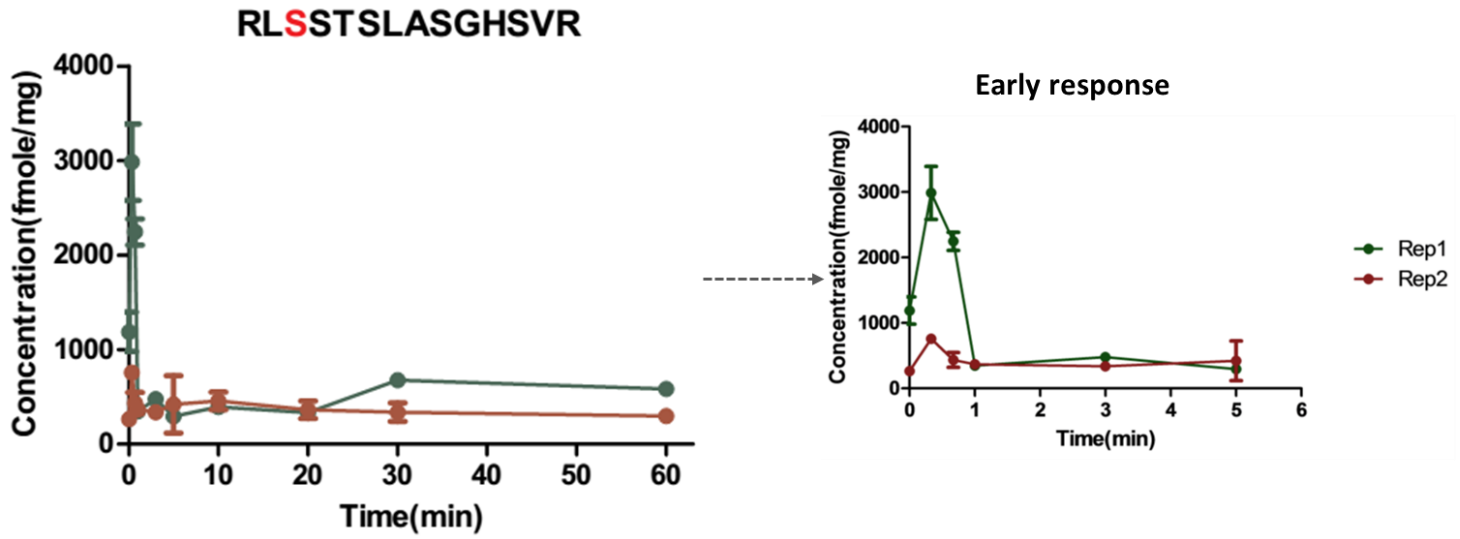

Figure 14 Phosphorylation profile of RLpSSTSLASGHSVR in response to FGF1

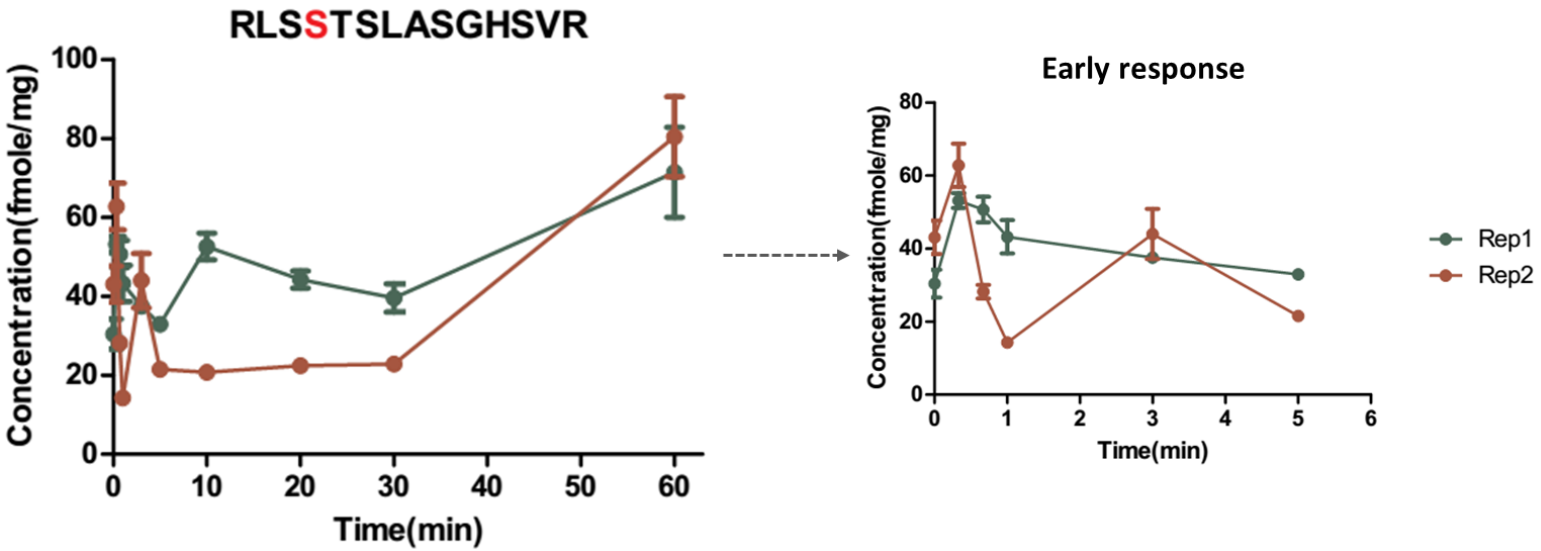

Figure 15 Phosphorylation profile of RLSpSTSLASGHSVR in response to FGF1

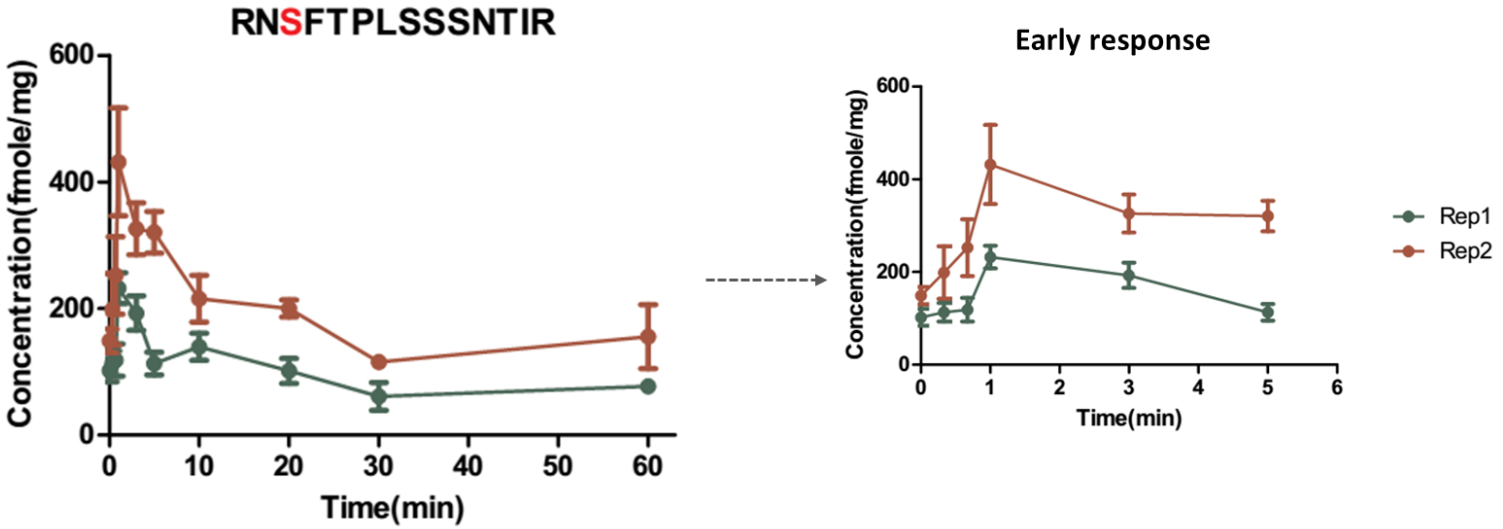

Figure 16 Phosphorylation profile of RNpSFTPLSSSNTIR in response to FGF1

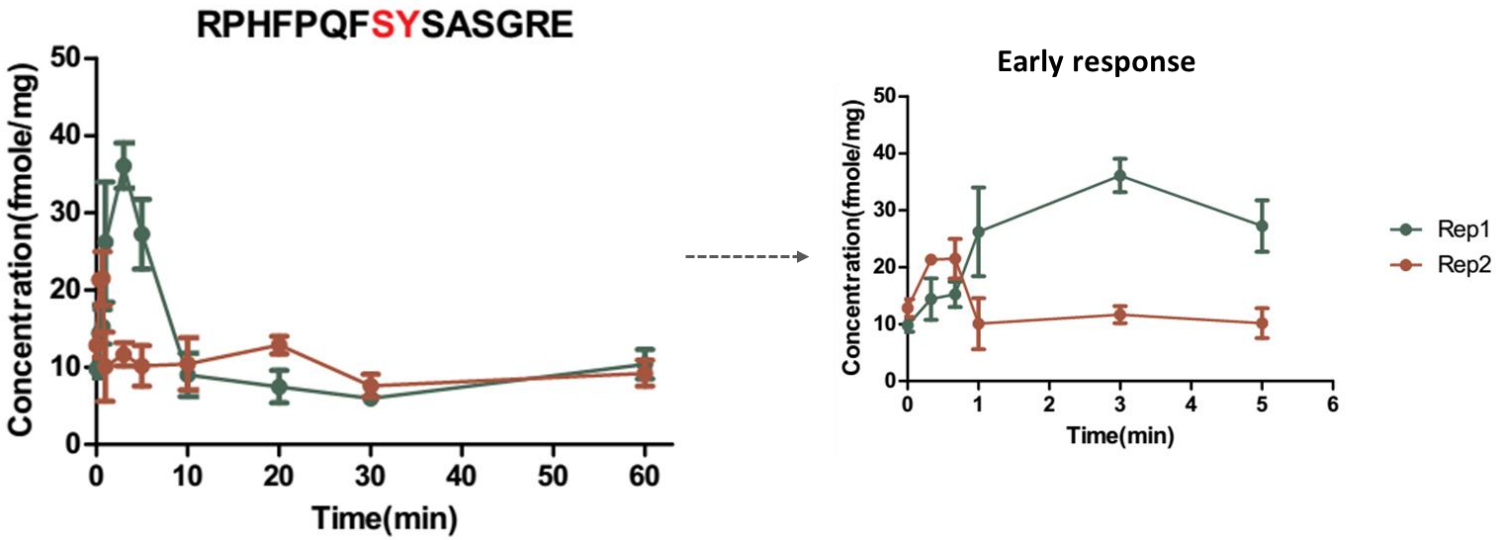

Figure 17 Phosphorylation profile of RPHFPQFpSpYSASGRE in response to FGF1

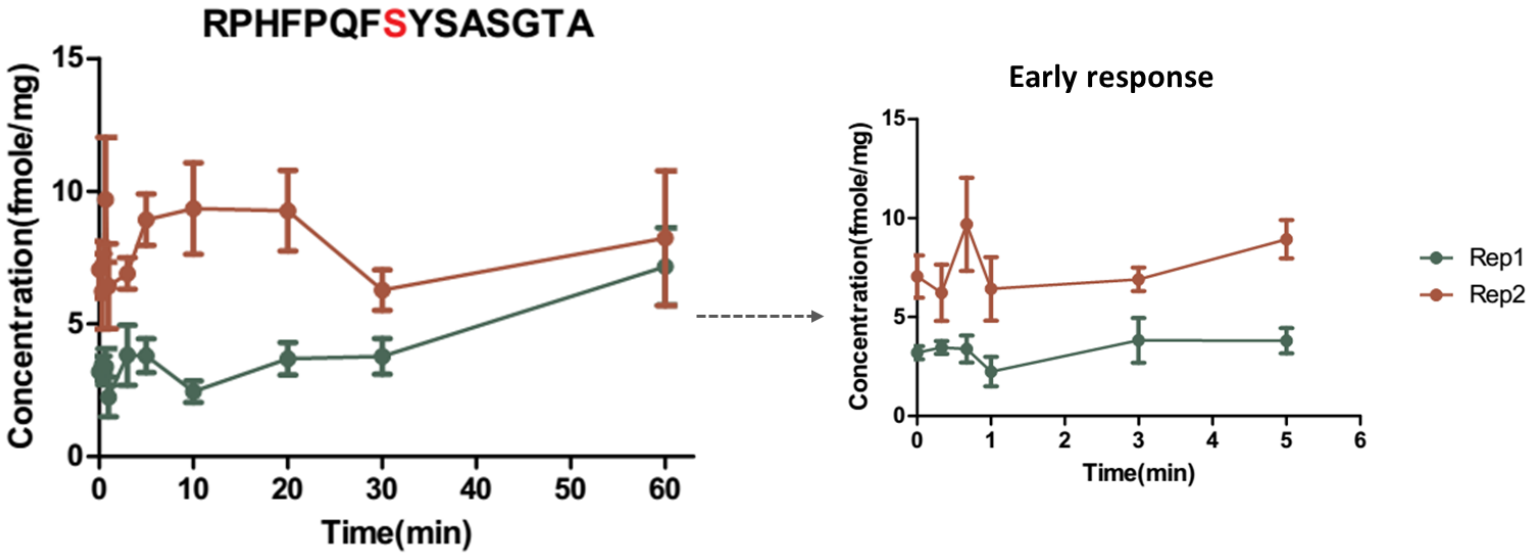

Figure 18 Phosphorylation profile of RPHFPQFpSYSASGTA in response to FGF1

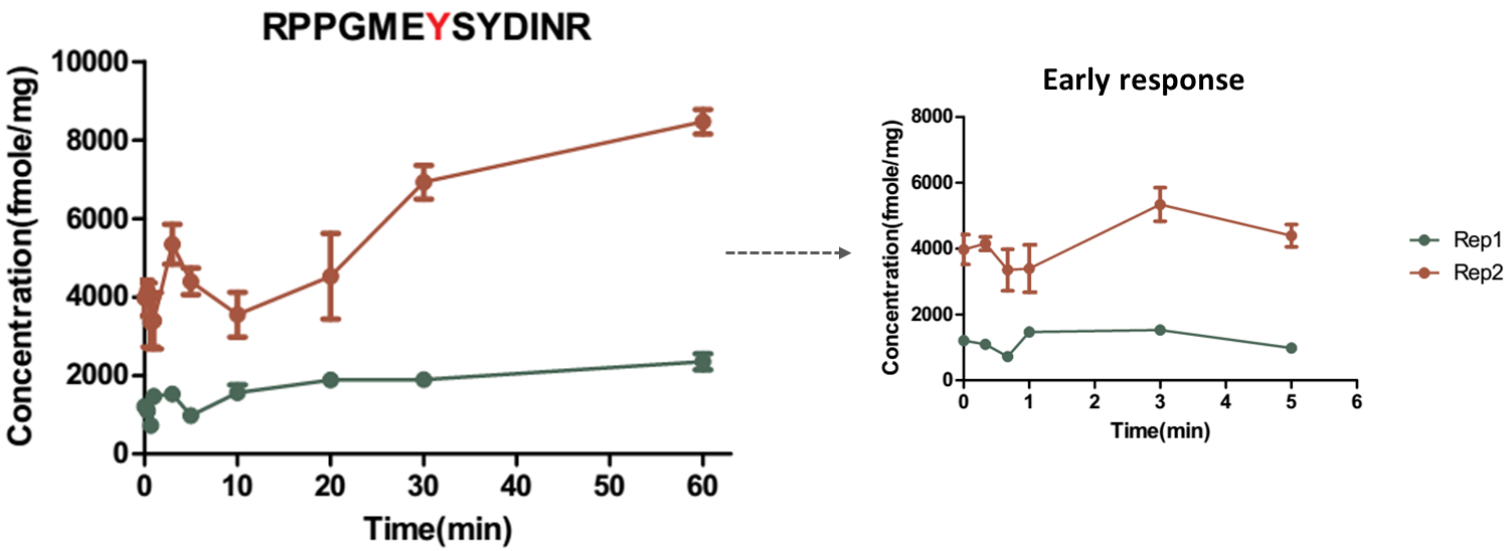

Figure 19 Phosphorylation profile of RPPGMEpYSYDINR in response to FGF1

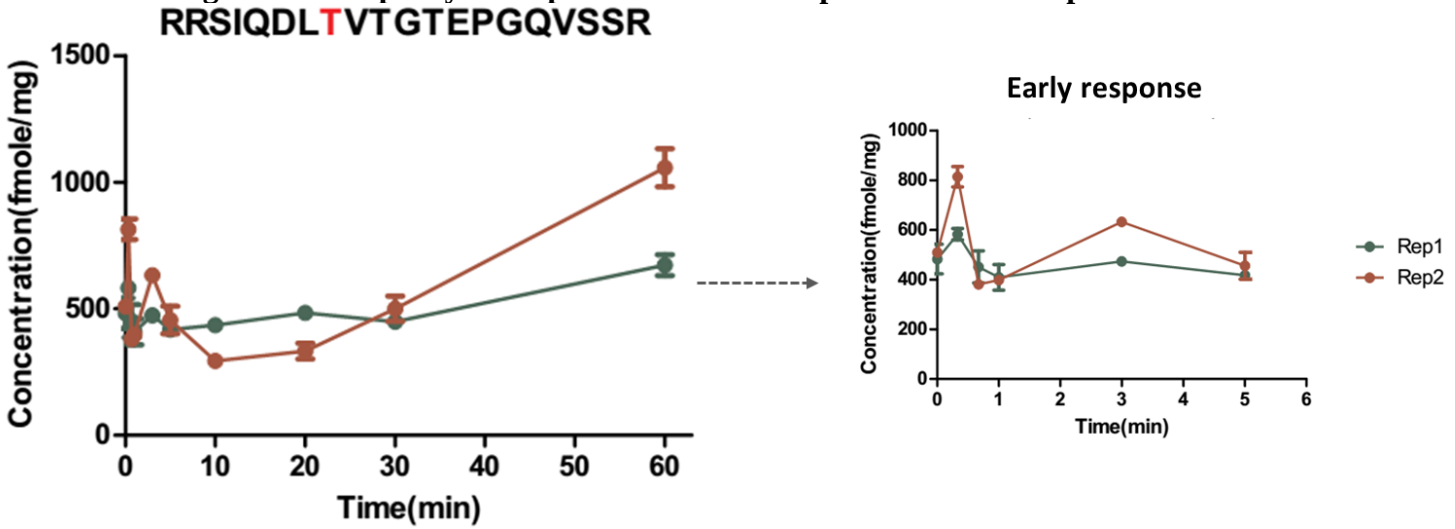

Figure 20 Phosphorylation profile of RRSIQDLpTVTGTEPGQVSSR in response to FGF1

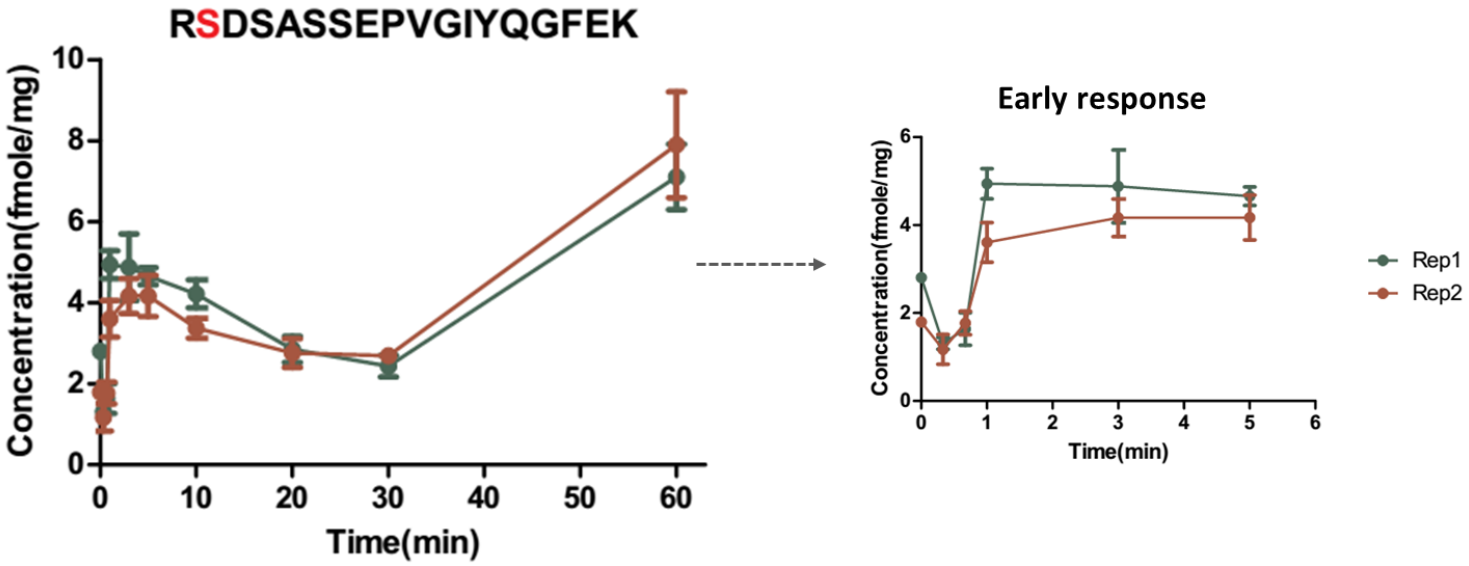

Figure 21 Phosphorylation profile of RpSDSASSEPVGIYQGFEK in response to FGF1

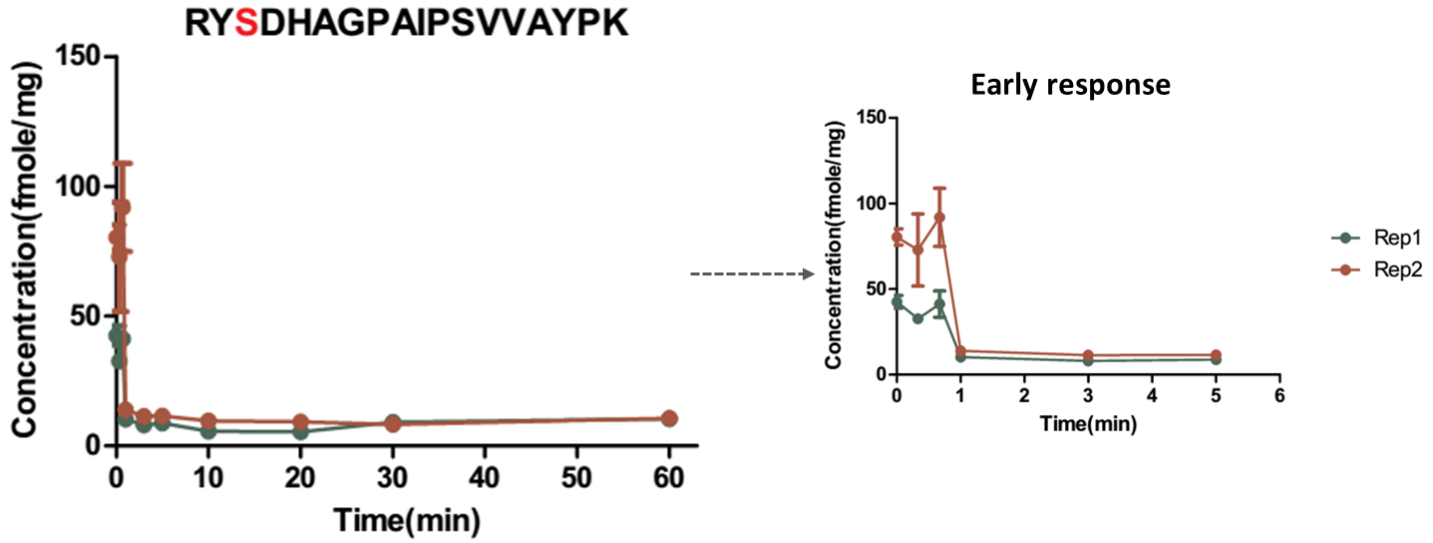

Figure 22 Phosphorylation profile of RYpSDHAGPAIPSVVAYPK in response to FGF1

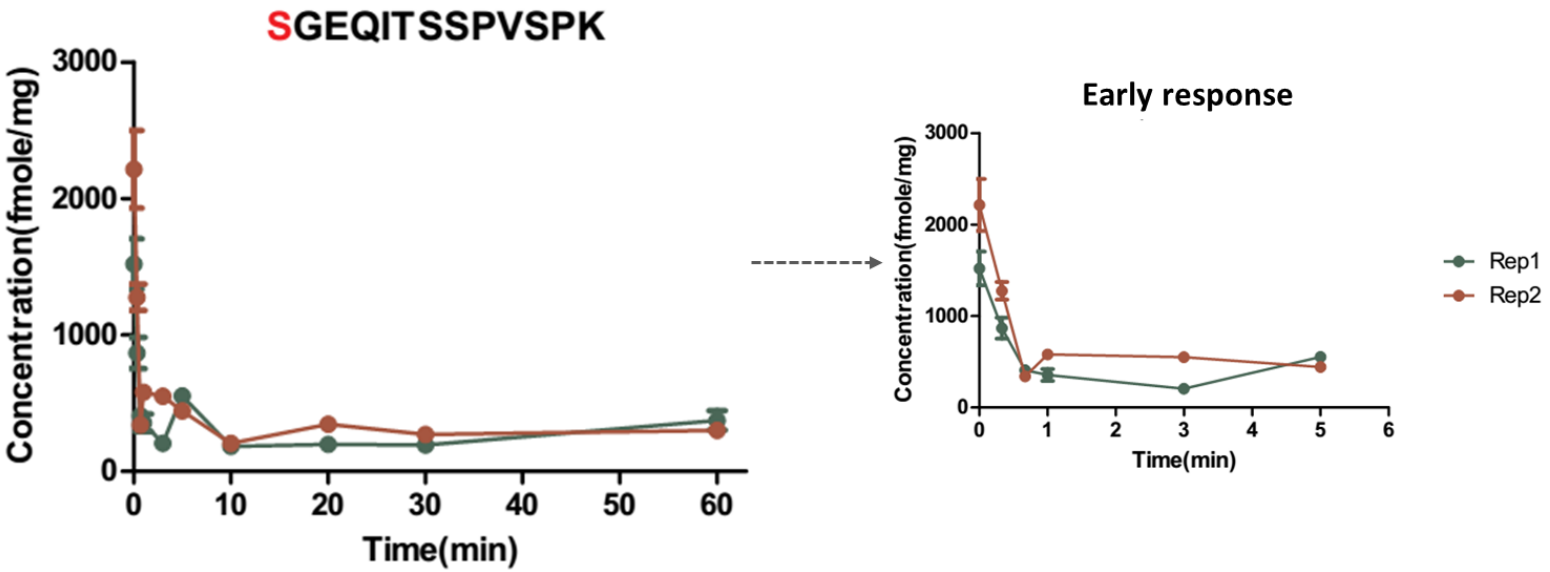

Figure 23 Phosphorylation profile of pSGEQITSSPVSPK in response to FGF1

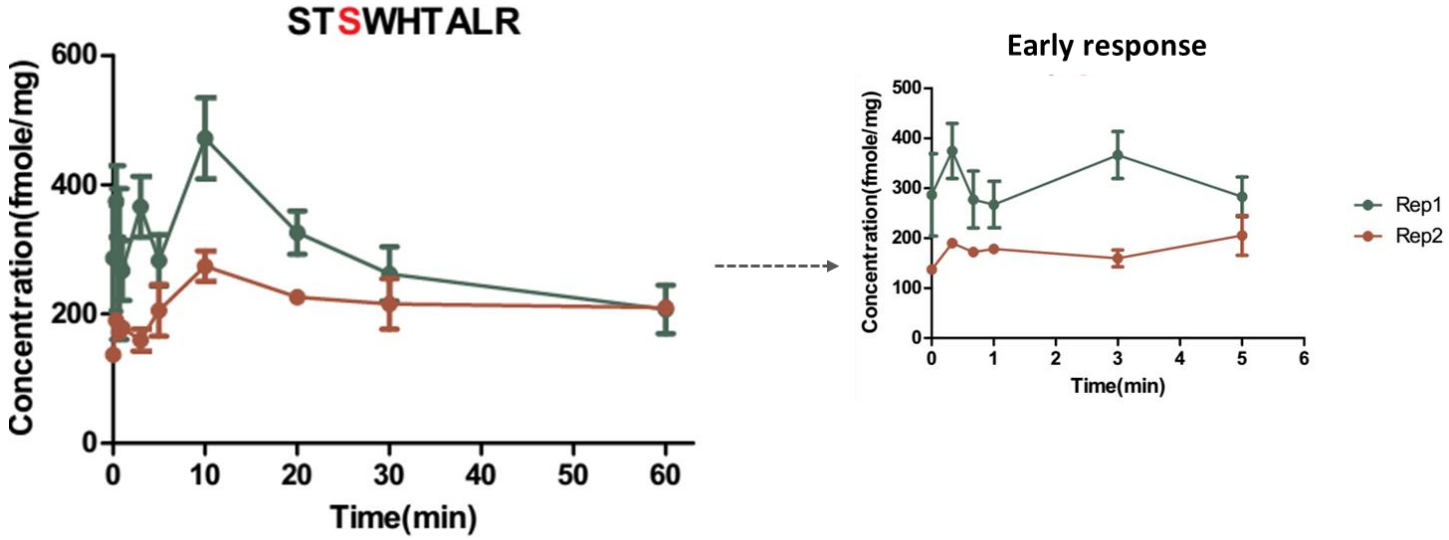

Figure 24 Phosphorylation profile of STpSWHTALR in response to FGF1

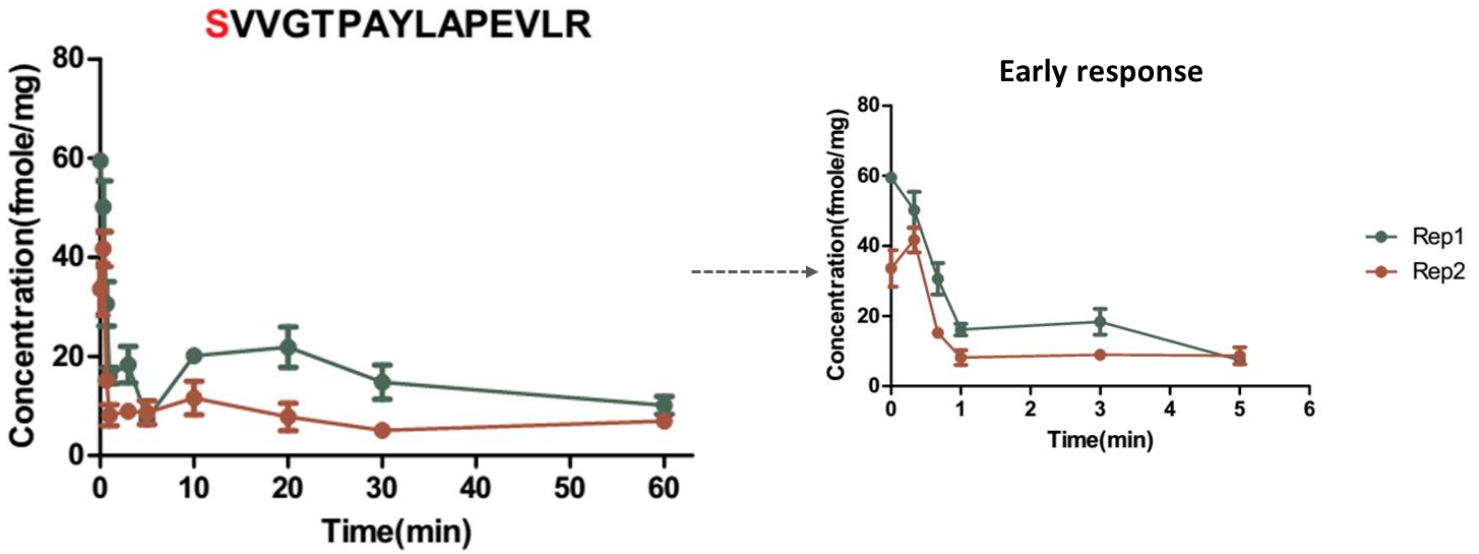

Figure 25 Phosphorylation profile of pSVVGTPAYLAPEVLR in response to FGF1

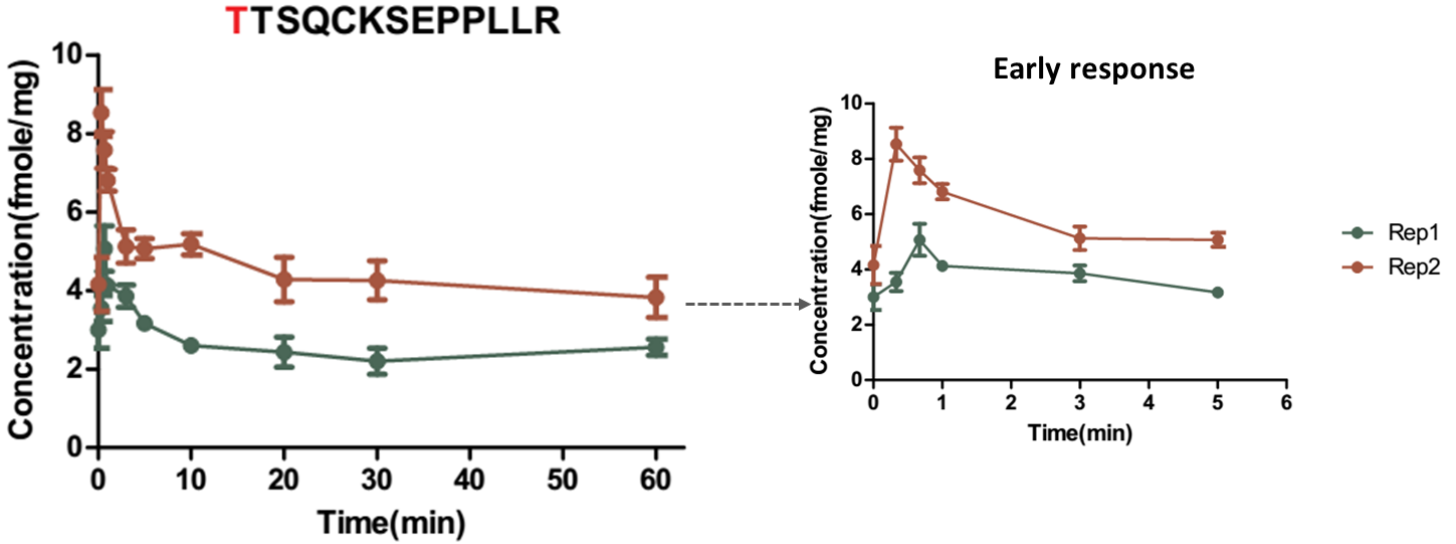

Figure 26 Phosphorylation profile of pTTSQCKSEPPLLR in response to FGF1

Appendix 5 Publications

Zhao H, Cunningham DL, Creese AJ, Heath JK, Cooper HJ. FAIMS and Phosphoproteomics of Fibroblast Growth Factor Signaling: Enhanced Identification of Multiply Phosphorylated Peptides. 2015, *14*(12), 5077-87